DESIGNING NOVEL MODULATORS SELECTIVE FOR THE INTERMEDIATE CONDUCTANCE CALCIUM ACTIVATED POTASSIUM CHANNEL

Christopher S. Delaforce

St Cross College

Thesis submitted for the degree of

Doctor of Philosophy in Cardiovascular Medicinal Chemistry

Under the Supervision of

Professor Stuart J. Conway, Dept of Chemistry

Professor Timothy J. Donohoe, Dept of Chemistry

Professor Christopher J. Garland, Dept of Pharmacology

Funded by

Oxford British Heart Foundation Centre of Research Excellence

Thesis submitted for the degree of: *Doctor of Philosophy in Cardiovascular Medicinal Chemistry*

Title: Designing Novel Modulators Selective for the Intermediate Conductance Calcium Activated Potassium Channel

I. Abstract

Reduction of systemic vascular resistance by dilation of resistance arteries, is a powerful method of blood pressure reduction.[1] Endothelium derived hyperpolarisation is a major vasorelaxant pathway in resistance arteries, dependant on the activation of endothelium Ca^{2+} activated K^+ (K_{Ca}) channels.[2] Existing positive modulators of K_{Ca} channels act by stabilising the protein-protein interaction of the K_{Ca} channel gating complex, involving the Ca^{2+} sensing protein, calmodulin (CaM).[3] Herein describes an investigation of the K_{Ca} channel positive modulator binding cavity, the rational design of next generation positive modulators, and developments towards a biophysical screening assay.

A homology model of the intermediate conductance ($IK_{Ca}3.1$) channel positive modulator binding cavity was generated, docked with existing positive modulators and scrutinised for the rational design of novel next generation analogues. A set of modulator analogues, capable of hydrogen bonding to an $IK_{Ca}3.1$ specific serine residue, were designed and synthesised. These analogues were tested for K_{Ca} channel modulation *via* their vasorelaxant activities by *ex vivo* artery wire myography. During this assessment, a novel and unknown vasorelaxant effect, unrelated to K_{Ca} channels, was discovered.

The $IK_{Ca}3.1$ gating complex proteins, CaM and the channel CaM binding domain (CaMBD), were expressed for biophysical investigation. Several techniques were designed, developed and evaluated as a modulator screening assay. In differential scanning fluorimetry (DSF), existing K_{Ca} channel positive modulators produced a significant effect, potentially enabling the observation of direct gating complex stabilisation. Native protein mass spectrometry observed oligomerisation of the gating complex in solution and could be used in future to confirm modulator binding and so the DSF results. This would be the first biophysical assay able to identify K_{Ca} channel ligands; a powerful tool for the development of increasingly potent and selective positive modulators.

1. Cohn, J. N., McInnes, G. T. & Shepherd, A. M. Direct-acting vasodilators. *J. Clin. Hypertens.* **13,** 690–692 (2011).
2. Félétou, M. & Vanhoutte, P. M. Endothelium-Derived Hyperpolarizing Factor. *Clin. Exp. Pharmacol. Physiol.* **23,** 1082–1090 (1996).
3. Zhang, M., Pascal, J. M., Schumann, M., Armen, R. S. & Zhang, J.-F. Identification of the functional binding pocket for compounds targeting small-conductance Ca2+-activated potassium channels. *Nat. Commun.* **3,** 1021 (2012).

II. ACKNOWLEDGEMENTS

I would like to begin with my three supervisors: Professor Stuart Conway, Professor Timothy Donohoe and Professor Christopher Garland, or as I call them; my holy trinity. Without your help I would not have been able to navigate so complicated a project with so many learning curves. Your guidance has enabled me to develop from a guy with interest and a little knowledge in science and research, until now, handing in my own DPhil thesis. An impressive feat of supervision if ever there was one. For all your help, guidance, wisdom and patience, you have my sincerest gratitude and thanks.

Of those who are or have been slaving away in the laboratories, there are a few of whom I should also like to make note. Actually, as a member of not one, not two, but three different research groups, there are a multitude of people who have helped to shape me as a practical chemist, a biochemist and even something close to a pharmacologist. This may stretch on a bit…

Of the Conways

Whilst everyone in the lab imparted some wisdom during my brief visits and sojourns, I should start with those who more specifically supervised my misadventures therein. First supervisor I had in the lab was *Doctor Michael Brand*, thankyou for muddling through. I know you were not prepared to take on yet another charge, one who could barely integrate an NMR without your assistance, for longer than I care to admit. However, we got through it more or less together. I hope the rest of your supervising positions of the future are easier for you. *Doctor James Clayton*, lord of the manor. I must say your ability to teach and to go the extra mile to help train the rest of us was very fatherly and well done. I look forward to seeing your own well led research group. *Doctor Anthony Chan* the whirlwind of G12. I have never known anyone or thing to move as quickly and efficiently about a lab, performing several tasks at once, while being in the office writing papers and still have time for absolutely anybody. Seriously, how are you still alive? You should take more time to rest, but thanks for always being there for me and my pestering. Doctor Matthias Schiedel and Doctor Ewen Calder, the founts of so much technical knowledge and ability. Thank you for your respective advice over the years and sorry Maze for stealing so much of your precious fluorescein. Doctor Amelie Joffrin, Doctor Alex Saunders, old hands in the lab when I started, and always there with an invaluable lab tip, thanks. My fellow Candidates, Charles Evans, Sarah Collins, Catherine ‘cat lady’ Haslam, Corentine Laurin, Larissa See, what a time we

had. You know all my pains and tribulations during this journey and I know yours. It was a pleasure to share your comradery against the peril that is medicinal chemistry research, I hope you all achieve in your respective projects and continue on. To those that follow, Mustafa Moroglu, Amy Scorah, Holly Bunce, Joe Bluck and Jess Reynolds, keep on trucking. It all ends, and quicker than you might suppose, so try to enjoy your time as part of such a close family of researchers while you can. Others, there are more rotation students and part IIs than I can list on these few pages, all high fliers and off to other bigger better things. Although I would like to keep Jesse Moses in memory, he was a kind and cool Part II.

Of the Donohoes

Specifically, the F7s

Really the only lab to be in, and I count myself extremely lucky to have been placed in F-heaven with the rest of you. Everyone made my time working in the lab so enjoyable, I almost forgot the ever-present danger of the chemicals we bandied around there. Technically my lab supervisor was *Doctor Johannes Walker*. What a guy. I am seriously thankful to have met such a good friend and one whom I shall hope to keep till the day I die. Thanks for all of it, advice, friendship and the rest. *Doctor James 'Frosty', 'Frosty the snowman', 'the Frosteneggar' Frost*, oh captain, my captain. A man who did not suffer fools and wasted little time on them. No idea why I passed that internal test, but I appreciate all your help, both technical and with more explode-y situations too. I'm certain you'll get wherever you're going, a big ol' brain like that can't and won't be wasted, I'm sure. *Doctor Roland 'Rolly' Armstrong* and Doctor Simon Wuebbolt, although we didn't spend a long time together you were always very approachable and quick to give no-fuss help and advice. True gentlemen. Doctor Wasim 'Waz' Akhtar, Doctor Sandra 'Sandy' Balcells Garcia and good ol' Melodie 'Smellodie-(sorry)' Richardson. We definitely shared something magic in that lab, and I know the like of it will not grace that building again. What songs, what games, what fun we had. And then there's Oskar 'the' Hoff, Timothy 'little Tim' Kwok and Christopher 'the second-best Chris in the village' Hall. In your hands are the keys to a kingdom, look after it well and it shall whisk you to your respective projects' speedy conclusions, through hard times and good. This was less of a thankyou note, more of a love letter. But still, thanks and love to you all.

And the rest… F8

Choon Boon 'Choon Boon I want you in my room', 'CB' Cheong, a special guy. You're a unique chap and you needn't worry about finding your place in the world, because it wouldn't be the same without you. To me, you were always an F heaven-er. There have been many doctors of F8, all have been good guys and treated us F7-ers fairly and kindly when we stole as much as we could from your lab; Doctor Harish Kumar Potukuchi, Doctor Simon Werrel, Doctor Henrique Esteves, Doctor Hamish Hepburn and Doctor Harry Shirley, thanks for your help from afar. My counterparts of F8; Alexandru Grozavu, Anna Chamberlain, Maxwell Haughey and Yuxiang 'Daniel' Zhu. While we didn't share a lab, we'll always have brew, I'll miss you all. There are so many more names who have passed those hallowed labs, F7 and F8, I can't name all of you now. I won't miss anyone either, most of you were brilliant characters keeping us on our toes.

Of the Garlands

Pharmacology was and is a new and confounding beast to me. You all did your best to take me in hand and try to illuminate what you could for me. Professor Kim Dora, thanks for taking the time to help me get a better understanding of the results I generated and how they truly fit together. My laboratory supervisor, *Doctor Alice Pinkney*, you taught strict lessons which seemed hard at the time but that I came to realize were the best I have come across and have made me a better scientist. Doctor Lyudmyla Borysova, Doctor Xi Ye, Doctor Chloe Lim and Doctor Harrison Davis thanks for your help on my mundane questions that you put up with. *Hamish Lemmey* and Joshua Smith, a likely couple of rogues, thanks for all your help writing up and deciphering my own work and assays, it was fun.

Of my Family, Close and Extended

At the risk of dragging these acknowledgements out further, I could not conclude them without mentioning the family which always supported and guided me through all the most difficult and confusing times of my DPhil. I may have inhabited another world of baffling long words and abstract nonsense for 4 years, but I finally made it and hopefully it will all hold me in good stead. It saddens me that my Grandpa could not be around to watch me graduate from Oxford because, like the rest of my family, I would have liked to have seen him proud.

To my supervisor of life, my wife, Rebecca ‘Becci’ ‘Becks’ ‘Speckles’ ‘Toots’ Delaforce. I could write another page thanking you for everything I have ever done at Oxford or before. Without you, there would be no thesis. Without you, there would be no Oxford, no DPhil. Without you, I’d have no future.

I dedicate this thesis to you.

III. LIST OF ABBREVIATIONS

%ID	percentage of identical residues
×g	relative centrifugal force
°C	degrees Celsius
^{13}C	carbon nuclei
^{1}H	proton nuclei
2× TY	tryptone yeast extract media
Å	Angstrom
ACE	angiotensin converting enzyme
ACh	acetylcholine
Ala	alanine
ANOVA	analysis of variance
aph	aminoglycoside-3'-phosphotransferase gene
aq.	aqueous
ARB	angiotensin II receptor blocker (antagonist)
ATP	adenosine triphosphate
ATR	angiotensin II receptor
$BK_{Ca}1.1$	big conductance Ca^{2+} activated K^{+} channel
Boc	*tert*-butyloxycarbonyl protecting group
bp	base pairs
BP	blood pressure
br	broad signal
$Ca^{2+}{}_{ATP}$	Ca^{2+} ATPase
CaM	calmodulin
cam	calmodulin gene
CaMBD	calmodulin binding domain (coloured blue in figures throughout)
cambd	calmodulin binding domain gene
CCB	Ca^{2+} channel blocker (antagonist)
$(CD_3)CO$	deuterated acetone
CD_3OD	deuterated methanol
$(CD_3)SO$	deuterated dimethyl sulfoxide

$CDCl_3$	deuterated chloroform
CI	chemical ionisation
CK2	casein kinase 2
CO	cardiac output
COSY	2D correlation spectroscopy
CV	column volumes
$_C\delta$	carbon chemical shift
d	day
d (*NMR*)	doublet
Da	Dalton
DCEBIO	dichloro-N-ethyl benzimidazolone
DELTA-BLAST	domain enhanced lookup time accelerated basic local alignment search tool
DLS	dynamic light scattering
DMI	dimethyl isoxazole
DMSO	dimethyl sulfoxide
DNA	deoxyribonucleic acid
DSF	differential scanning fluorimetry
E. coli	*Escherichia coli*
EBIO	*N*-ethyl benzimidazolone
EC_{50}	half maximal effective concentration
EDH	endothelium derived hyperpolarisation
EDTA	ethylenediaminetetraacetic acid
EGTA	ethylene glycol-bis(β-aminoethyl ether)-*N,N,N′,N′*-tetraacetic acid
EI	electron ionisation
eNOS	endothelial nitric oxide synthase
eq.	equivalents
ER	endoplasmic reticulum
ESI	electro spray ionisation
FP	fluorescence polarisation
FTIR	fourier transform infra-red spectroscopy
g/L	grammes per litre

GC	guanylyl cyclase
GTP	guanosine triphosphate
h	hour
H_6	hexahistadine tag
H-bond	hydrogen bond
HEPES	4-(2-hydroxyethyl)-1-piperazineethanesulfonic acid
HIC	hydrophobic interaction chromatography
HMBC	heteronuclear multiple bond correlation spectroscopy
HPLC	high performance liquid chromatography
HS	*Homo sapiens*
HRMS	high resolution mass spectrometry
HSQC	heteronuclear single quantum coherence spectroscopy
$_H\delta$	proton chemical shift
$IK_{Ca}3.1$	intermediate conductance Ca^{2+} activated K^+ channel (coloured purple in figures throughout)
IMAC	immobilised metal affinity chromatography
IP_3	inositol triphosphate
IP_3R	inositol triphosphate receptor
IPTG	isopropyl β-D-1-thiogalactopyranoside
ITC	isothermal titration calorimetry
J	scalar coupling
K^+_{ATP}	K^+ ATPase
KCa	Ca^{2+} activated K^+ channel
K_d	Dissociation constant
L	Litre
LacI	lactose repressor
LacO	lactose operon
L-NAME	N(ω)-nitro-L-arginine methyl ester
LogDx	distribution coefficient at x pH
LogP	partition coefficient
LRMS	low resolution mass spectrometry
Lx	lane x
Lys	lysine

m	medium strength signal
M	molar
m (NMR)	multiplet
m.p.	melting point
m/z	mass to charge ratio
M_3	muscarinic receptor
MALS	multi angle laser scattering
mAU	milli-absorbance units
MeCN	acetonitrile
meGJ	myo-endothelial gap junction
Met	methionine
min	minutes
MLCK	myosin light chain kinase
mmHg	milli-metre of mercury
MOPS	3-(N-morpholino)propanesulfonic acid
mP	milli-polarisation unit
MS	mass spectrometry
MW	molecular weight
MWCO	molecular weight cut off
n	number of repeats
N.E.	no effect
NEB	New England Biolabs
NMR	nuclear magnetic resonance
NO	nitric oxide
No.	number
NOESY	nuclear Overhauser effect spectroscopy
p	pentet
P	probability value
pCaM	cam gene plamid construct
pCaM/CaMBD	cam-cambd gene plasmid construct
pCaMBD	cambd gene plasmid construct
PCR	polymerase chain reaction
PDB	Protein Data Base

pDNA	plasmid DNA
PE	phenylephrine
pH	−Log[H^+]
PIP_2	phosphatidylinositol 4,5-bisphosphate
PKG	protein kinase G
PLC	phospholipase C
PP2A	protein phosphatase 2
PPI	protein-protein interaction
ppm	parts per million
q	quartet
r	rat (*Rattus norvegicus*)
RAAS	renin-angiotensin-aldosterone-system
R_f	retention factor
RMSD	random mean squared deviation
RT	room temperature
RyR	ryanodine receptor
s (*NMR*)	singlet
s	strong signal
sacB	bacillus subtilis levansucrase gene
Sarkosyl	sodium lauroyl sarcosinate
sat.	saturated
SDS-PAGE	sodium dodecyl sulphate polymerase agarose gel electrophoresis
SEC	size exclusion chromatography
Ser	serine
SERCA	sarcoplasmic/endoplasmic reticulum Ca^{2+} ATPase
$SK_{Ca}2.x$	small conductance Ca^{2+} activated K^+ channels (2.1-3) (coloured orange in figure throughout)
SMC	smooth muscle cell
S_NAr	nucleophilic aromatic substitution
SR	sarcoplasmic reticulum
SVR	systemic vascular resistance
T	temperature

t	triplet
TFA	trifluoroacetic acid
TLC	thin layer chromatography
T_m	melting temperature
U	enzyme unit
U.V.	ultraviolet light
V	volt
v/v	volume per volume
Val	valine
VGCC	voltage gated Ca^{2+} channel
w	weak signal
α-R	α-adrenoreceptor
(α/β) blocker	(α/β)-adrenoreceptor antagonist
ΔG	difference in free energy
ΔH	difference in enthalpy
ΔS	difference in entropy
ΔT_m	difference in melting temperature (thermal)
λ_{max}	wave length
ν_{max}	Absorption maxima

IV. TABLE OF CONTENTS

I. Abstract I

II. Acknowledgements II

III. List of abbreviations VI

CHAPTER 1 INTRODUCTION **1**

1.1 Blood Pressure and Disease 1

1.1.1 Current Antihypertension Drugs and their Mechanism of Action 2

1.1.2 Continuing Need for Novel Hypertension Treatments 7

1.2 Project Themes and Aims 9

1.2.1 Smooth Muscle Contraction and Relaxation 10

1.2.2 Endothelium Dependant Smooth Muscle Relaxation 14

1.3 Assay Starting Points 16

1.3.1 $IK_{Ca}3.1$ Channel Structure and Gating Mechanism 18

1.3.2 Biological Assays Based on the $IK_{Ca}3.1$ Channel and Resulting Leads 19

1.3.3 Potential Biochemical Assays Based on the $IK_{Ca}3.1$ Channel 23

Chapter 1 References 25

CHAPTER 2 MODELLING, DESIGN & SYNTHESIS **30**

2.1 Homology Modelling of the $IK_{Ca}3.1$ Modulator Binding Cavity 30

2.1.1 Identifying and Investigating the $IK_{Ca}3.1$ Calmodulin Binding Domain Primary Sequence 31

2.1.2 Modelling the $IK_{Ca}3.1$ Modulator Binding Cavity 34

2.2. Docking Experiments & Rational Design of Novel $IK_{Ca}3.1$ Selective Small Molecule Modulators 38

2.2.1 Docking Validation Experiments 39

2.2.2 Binding cavity Assessment & Novel $IK_{Ca}3.1$ Selective Ligand Design 53

2.3 Synthetic Work 64

2.3.1 Synthesis of Published $IK_{Ca}3.1$ Naphthothiazole Modulators 66

2.3.2 Synthesis of Novel Naphthothiazole Analogues 67

2.3.3 Synthesis of Published K_{Ca} Channel Modulators: EBIO, DCEBIO and NS309 79

2.4 Summary 81

Chapter 2 References ... 85

CHAPTER 3 CELLULAR BIOLOGY, BIOPHYSICS & ASSAYS ... **89**

3.1 Production and Characterisation of K_{Ca} Channel Gating Proteins ... 91

3.1.1 Molecular Cloning ... 91

3.1.2 Protein Expression and Purification ... 93

3.1.3 Protein Characterisation ... 98

3.2 Developing a K_{Ca} Gating Complex Binding Biophysical Screening Platform ... 105

3.2.1 Differential Scanning Fluorimetry as a Biophysical Binding Assay ... 107

3.2.2 Fluorescence Polarisation as a Biophysical Binding Assay ... 121

3.2.3 Towards Isothermal Titration Calorimetry as a Biophysical Binding Assay ... 124

3.2.4 Towards Native Protein Mass Spectrometry as a Biophysical Binding Assay ... 128

3.2.5 Protein Crystallography ... 130

3.3 Summary ... 132

Chapter 3 References ... 136

CHAPTER 4 PHARMACOLOGY ... **141**

4.1 Modulation of Endothelium Derived Hyperpolarisation ... 142

4.2 Investigating Direct K_{Ca} Channel Modulator Induced Vasorelaxation ... 149

4.2.1 Vasorelaxation Assay Format Based on Direct Response to K_{Ca} Channel Modulators ... 150

4.2.2 Proving the Mechanism of Naphthothiazole K_{Ca} Modulator Action ... 157

4.3 Summary ... 164

Chapter 4 References ... 165

CHAPTER 5 FINAL CONCLUSION & FUTURE WORK 158 ... **168**

5.1 Rational Design and Evaluation of Existing and Novel K_{Ca} Channel Modulators ... 168

5.2 Investigating the Biophysics of the K_{Ca} Channel Gating Complex ... 175

Chapter 5 References ... *180*

CHAPTER 6 EXPERIMENTAL SECTION ... **182**

6.1 Computational Modelling and Docking Details ... 182

6.1.1 Molecular Homology Modelling ... 182

6.1.2 Docking Assessment ... 183

6.1.3 Dock Screening 184

6.3.4 Rational Ligand Design 184

6.2 Experimental Biochemistry Details 185

6.2.1 Molecular Cloning 185

6.2.2 Protein Expression 189

6.2.3 Protein Purification 189

6.2.4 Protein Characterisation 191

6.2.5 Differential Scanning Fluorimetry (DSF) 192

6.2.6 Isothermal Titration Calorimetry (ITC) 194

6.2.8 Crystallography 196

6.2.9 Expressed Proteins Primary Sequences 197

6.3 Chemistry Experimental Details 198

6.3.1 General Experimental 198

6.3.2 Procedures 200

6.4 Experimental Pharmacology Details 232

6.4.1 Animal Procedures and Isolated Tissue Preparation 232

6.4.2 Assessment of Vasodilation to Novel and Published Small Molecule KCa Channel Modulators 234

6.4.3 Drugs and Solutions 234

6.4.4 Data Analysis 235

Chapter 6 References 236

CHAPTER 1 INTRODUCTION

Blood pressure reduction has been a target for pharmaceutical treatment for decades and has led to the development of several block buster drug classes. Despite these drugs, blood pressure remains a critical threat to global modern-day health with resistant hypertension and poor control in aging and black populations. [1,2] This is a continuing and significantly growing issue. The presented research herein, investigates the potential control of blood pressure *via* novel pharmacological methods, and aimed to identify novel antihypertensive small molecule leads.

1.1 Blood Pressure and Disease

Far from being just a modern disease, high blood pressure as hypertension was identified as a health risk as far back as 2600 BCE, in the ancient city of Nineveh.[3] This indicator of mortality is very complicated and now known to correlate to an increasing list of cardiovascular related diseases: stroke, heart failure, ventricular hypertrophy, coronary artery disease, kidney disease, peripheral vascular disease, atrial fibrillation, vision loss and dementia.[1,4–8] Afflicting around a third of the entire global population and set to continue to rise, it is unsurprising that hypertension is the greatest burden to global health, and a contributing factor to 50% of all global deaths.[9–13]

The measurement of blood pressure is vital in hypertension diagnosis and treatment.[4] Blood pressure varies throughout the cardiac cycle. The process of heart pumping consists of two main stages; systole, where the heart is fully contracted, pumping blood to the lungs and body; diastole, where the heart fully relaxes refiling with returning blood.[14] Healthy blood pressure is measured as around 120/80 mmHg, that is 120 mmHg during systole and 80 mmHg during diastole. Hypertensive blood pressure

is considered mild at 140/90 mmHg and severe at 180/110 mmHg.[15] The importance of these numbers is denoted by their effect on patient outcome and mortality. Starting as low as 115/75 mmHg, each 20 mmHg increase of systolic pressure, or 10 mmHg diastolic pressure, doubles the chance of death by stroke.[1]

1.1.1 Current Antihypertension Drugs and their Mechanism of Action

Understanding the risks of hypertension has led to great human effort dedicated to alleviate it, from bloodletting and leeches to more sophisticated pharmaceutical treatments.[3,4] Several medications have been developed to help combat hypertension and other related cardiovascular diseases, many are listed by the World Health Organisation's list of essential medicines.[16]

Blood pressure can be reduced in several ways by adjusting the parameters of Equation 1.1: lowering cardiac output through slowing heart rate or contractile force and lowering systemic vascular resistance *via* arterial vasorelaxation. Lowering the volume of blood or increasing the capacity of the cardiovascular system will also lower blood pressure because the cardiovascular system is a closed system. A number of antihypertensive drug classes have been developed to lower blood pressure by targeting each of these mechanisms.

$$BP = CO \times SVR \qquad \text{Equation 1.1}$$

Where *BP* is blood pressure, *CO* is cardiac output determined by heart rate and pumping strength, and *SVR* is the systemic vascular resistance, the resistance to blood flow.

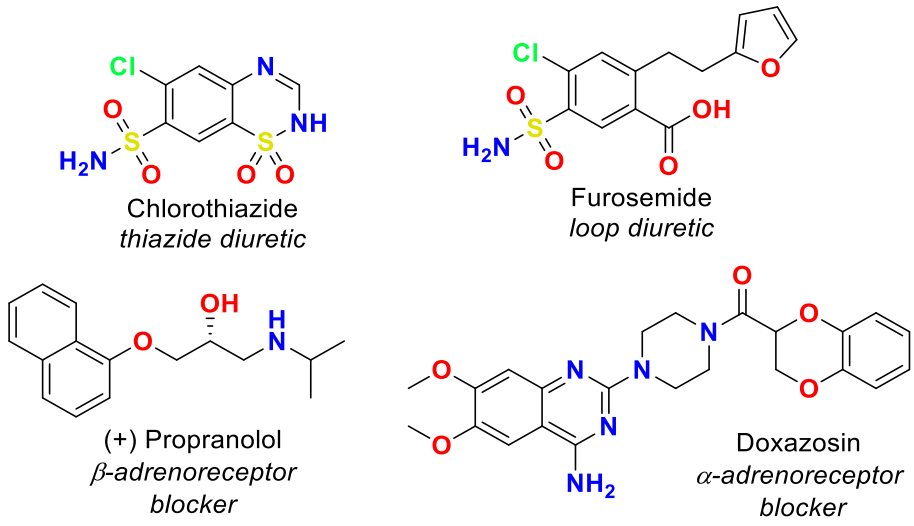


Figure 1.1; Skeletal structures of hypertensive drugs: a thiazide diuretic (top left), a loop diuretic (top right), adrenergic system blockers including a β-blocker (bottom left) and an α-blocker (bottom right).

One of the first antihypertensive treatments available were the thiazide diuretics, such as chlorothiazide, developed in the 1950s, Figure 1.1.[17] These drugs promote water loss by altering kidney function, reducing blood volume. The kidneys function by removing all components of blood, smaller than a protein, and then reabsorbing the necessary components of blood plasma: water, inorganic ions and sugar. Thiazide diuretics block the action of the kidney nephron distal convoluted tubule Na^+-Cl^- co-transporter, responsible for reabsorption of both ions in plasma filtrate. By blocking the reabsorption of Na^+ ions, they are lost to the body. Increased Na^+ concentration in blood filtrate causes a greater loss of water by osmosis. Loop diuretics, such as furosemide, were developed in the early 1960s and act on the Na^+-K^+-$2Cl^-$ co-transporter of the nephron loop of Henley, Figure 1.1.[18] Thiazide diuretics and, to a lesser extent, loop diuretics, are still a recommended first line treatment of hypertension.

The second hypertension treatment class of drugs developed were β-blockers, such as propranolol, discovered by James Black's chemical alteration of adrenaline at ICI in

1964, Figure 1.1.[19,20] The autonomic system comprises the sympathetic (adrenergic) and parasympathetic (muscarinic) systems, which control the balance between the physiological responses: flight or fight (stress) vs rest and digest (relaxation).[7] Stimulation of the sympathetic system, by the hormones adrenaline and noradrenaline, causes an increase in blood pressure and cardiac output *via* stimulation of adrenergic receptors, subcategorised as β (expressed in the heart) and α (expressed in the vasculature).[21] The first adrenergic antagonists were β-blockers, which bind β-receptors without activation, blocking the positive inotropic and chronotropic effects of adrenaline and noradrenaline. Later α-blockers, such as doxazosin, were developed to target the vasculature, blocking adrenergic vasoconstriction, resulting in vasorelaxation, Figure 1.1.[7]

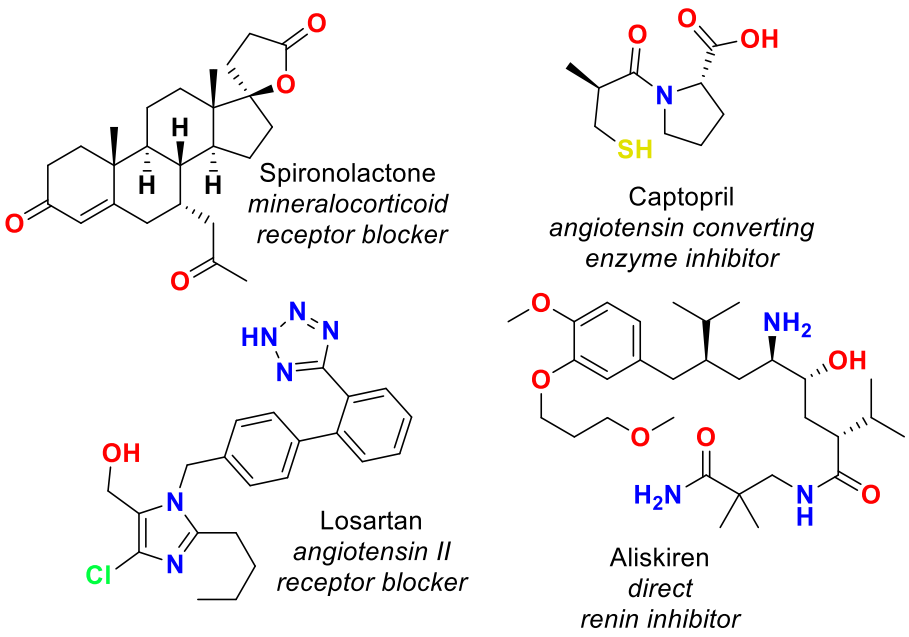


Figure 1.2; Skeletal structures of RAAS inhibitor drugs, including a mineralocorticoid receptor blocker (top left), an ACE inhibitor (top right), an angiotensin II receptor blocker (bottom left) and a direct renin inhibitor (bottom right).

The most important class of hypertensive treatments inhibit a homeostatic blood pressure increasing system, the renin-angiotensin-aldosterone-system (RAAS).[22] The

RAAS is a cascade system, which increases the release of the enzyme renin from the kidney.[23] Renin cleaves the protein hormone angiotensinogen to the activated form, angiotensin I. This is further cleaved by dedicated enzymes, being converted into angiotensin II, then III and finally IV.[7] Angiotensin II has several blood pressure increasing activities: causing arteriole vasoconstriction, increasing cardiac output *via* increasing noradrenaline, Na^+ retention, and inducing the release of aldosterone from the adrenal gland.[7,24,25] Aldosterone is a corticosteroid that binds a mineralocorticoid receptor in the kidney, stimulating the retention of Na^+ ions and thus water.

There have been serval pharmaceutical attempts to reduce blood pressure by blocking the action of the RAAS at different levels: the first were mineralocorticoid receptor blockers, such as spironolactone, Figure 1.2. Spironolactone was developed in 1959 as an aldosterone antagonist diuretic. Aldosterone's involvement in the RAAS was determined later.[26] Blockade of the RAAS cascade further upstream, was first attempted with captopril, an angiotensin I converting enzyme (ACE) inhibitor developed in 1975 at Squibb, Figure 1.2.[27] Later, it was found that the action of ACE inhibitors was surmounted by increased renin release, leading to 'RAAS escape'. The angiotensin II receptor blocker (ARB), losartan, was developed in 1995 at Merck, combating RAAS escape, Figure 1.2.[25,28] Ultimately, the first RAAS enzyme renin was subsequently targeted by Novartis and Speedel to better block the RAAS system, giving rise to aliskiren in 2007, Figure 1.2.[29] This class of hypertension treatments are so effective because of the pluripotency of controlling the RAAS system: lowering blood volume, cardiac output and causing vasorelaxation.

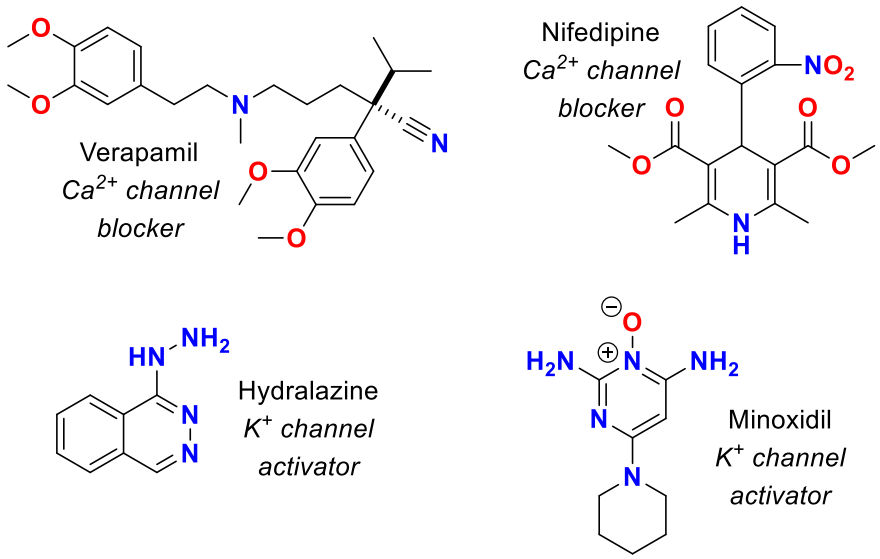


Figure 1.3; Skeletal structures of direct vasodilators: Ca^{2+} channel blockers (top) and K^+ channel activators (bottom).

Unlike the previous signalling, based RAAS and β-blocker hypertensive drug classes, direct vasorelaxants control vasomotor mechanisms of vascular smooth muscle, powerfully promoting vasorelaxation. Such direct vasodilators most commonly affect smooth muscle Ca^{2+} and K^+ ion channels.[30–35] These ion channels are fundamental to the control and operation of smooth muscle cells (SMCs) contractile machinery.

The importance of Ca^{2+} signalling in cardiac and smooth muscle was first identified in the 1950s by Albrecht Fleckenstein.[36] It wasn't until 1981 that Fleckenstein's development of Ca^{2+} antagonists produced the first marketed Ca^{2+} channel blocker (CCB), verapamil, followed by the more potent dihydropyridine, nifedipine, Figure 1.3.[34,37] Voltage gated Ca^{2+} channels (VGCCs), such as the L-type channel, are important in excitable tissues: their inward current in smooth muscle cells directly causes the contractile machinery of the cell to activate.[38] CCB blockade of VGCCs leads to a decreasing inotropic effect of the heart and vasorelaxation of the peripheral vasculature.[35,37] These CCB effects correspond to a decrease in cardiac output, decrease in systemic vascular resistance and effectively increase in the capacity of the

cardiovascular system, powerfully lowering blood pressure. Thus, CCBs are important in the treatment of resistant forms of hypertension and are employed as 1st and 2nd line treatments (mono- and co-therapies).[39]

Activation of SMC K^+ channels allows for K^+ efflux, hyperpolarising the SMC cell membrane below −55 mV, inhibiting VGCCs.[31,32,40] Thus, K^+ channel activators, such as hydralazine and minoxidil, prevent VGCC activation by blocking Ca^{2+} influx and arterial vasocontraction, Figure 1.3.[30,33] The K^+ channel activator class of direct vasodilators are very potent: the use of hydralazine and others are therefore reserved for very acute, or the most resistant forms of hypertension.[30,41]

1.1.2 Continuing Need for Novel Hypertension Treatments

Hypertension is a complex symptom resulting from many possible underlying causes, and each class of treatment has limits. While inhibition of the RAAS and adrenoreceptor systems are generally very effective, RAAS inhibitors and β-blockers rely on these respective systems to be responsive in the patient. Increasing age, co-morbidities such as diabetes, and even race, can all limit the extent to which blood pressure is reduced by treatments reliant on these systems.

Blood pressure measurements of >140/<90 mmHg indicate isolated systolic hypertension.[42] Systolic blood pressure has been observed to increase by as much as 40 mmHg with age: where each 10 mmHg represents a 16% increase in all-cause mortality.[1,43] Systolic pressure increase in elderly patients is due to decreasing responsivity to RAAS and adrenoreceptor inhibition, as well as the stiffening of arteries as the elastin fibres in the media tunica degrade over time. Constricted peripheral conductance arteries cause faster wave reflection and prolonged high mean arterial pressure, putting increased stress on the heart, leading to heart failure.[42] A suggested solution is peripheral artery vasorelaxation with CCBs, or blood volume reduction with

diuretics. However, in elderly patients, usage of CCBs can lead to cardiac ischemia if coronary artery vasorelaxation produces a drop in perfusion pressure.[44] Diuretics in the elderly, can lead to hypokalaemia resulting in heart arrythmias and sudden death.[45] Hypertension in the elderly thus remains difficult, and with and aging global population, systolic hypertension represents a major ongoing challenge.

For unknown reasons the control of hypertension in black patients is often inadequate.[2] This demographic problem is compounded by lower nephron numbers, a higher hypertension prevalence, more sensitivity to systolic blood pressure and greater risk of stroke than in other ethnicities.[1,2,41,46] There may be a more active polymorphism of renal salt transporters in black ethnicities, leading to greater Na^+ retention sensitivity.[2] Currently, CCBs and diuretics are preferred first line treatments in black patients, yet overall blood pressure control still remains insufficient.[47] RAAS inhibition has been considered less effective in black populations due to inferior blood pressure reductions by comparison with diuretics or CCBs. However, this is not necessarily true and RAAS inhibition becomes equally effective as in other ethnicities, when given as secondary treatment co-therapies: highlighting the complexity of the biological causes of hypertension.[2,41]

Generally, β-blockers and α-blockers have both been shown to be inferior to other treatment modes as first line antihypertensive therapies, and their outcomes such as stroke can be much worse.[39,48,49] Often, one treatment class does not to lower blood pressure enough to reach a safer target pressure and so combinatorial co-treatments are common.[41,50,51] With co-therapy, however, comes more complications of drug-drug interactions. Even with co-therapy, blood pressure may still remain too high, this is termed resistant hypertension (when three or more treatments are not enough to reach a desired goal blood pressure).[41,50,52,53] Unfortunately, resistant hypertension has been

observed in 28% of US, and 8% of UK patients and is expected to rise in the future by 10% by 2025.[52,53] Thus, more hypertension treatments are as necessary today as they have ever been.

1.2 Project Themes and Aims

CCBs and K^+ channel activators have been shown to be effective in patients with resistant hypertension, or impaired vasculature function, due to advanced age or co-morbidity.[30,52,53] These drug classes successfully lower blood pressure in these patients by targeting the vasomotor biochemical processes of arteries and reducing systemic vascular resistance. Systemic vascular resistance is largely generated and controlled by the lumen diameter of resistance arteries. These arteries increase blood pressure by reducing their lumen size *via* vasoconstriction, increasing their internal surface area to lumen volume, and producing greater resistance to blood flow.[54] Collectively, constricted resistance arteries decrease the effective volume capacity of the entire cardiovascular system, increasing pressure on the contained volume of blood, and *vice versa*.

Pharmaceutically manipulating novel hypertension alleviating cellular targets continues to provide therapeutic benefits by widening therapeutic choice. New drug classes allow physicians to better tailor prescribed treatments to individual patients based on their specific medical history. With the increased pharmaceutical dexterity provided by these novel drugs, physicians are better equipped to manage the potential complications of a patient's genetics, co-morbidities or age.

This project was therefore focused on targeting artery vasomotor biochemical pathways as a means of developing a novel therapy for hypertensive patients not currently managed by existing drugs.

1.2.1 Smooth Muscle Contraction and Relaxation

Resistance arteries are finely branched arterioles, much smaller than the preceding conductance arteries, which circulate blood across the body to the limbs and organs. Resistance arteries contain smooth muscle, retaining vasomotor function (vasoconstriction and vasorelaxation), unlike capillaries, which are made only of the single layer of endothelial cells, Figure 1.4 A.[54]

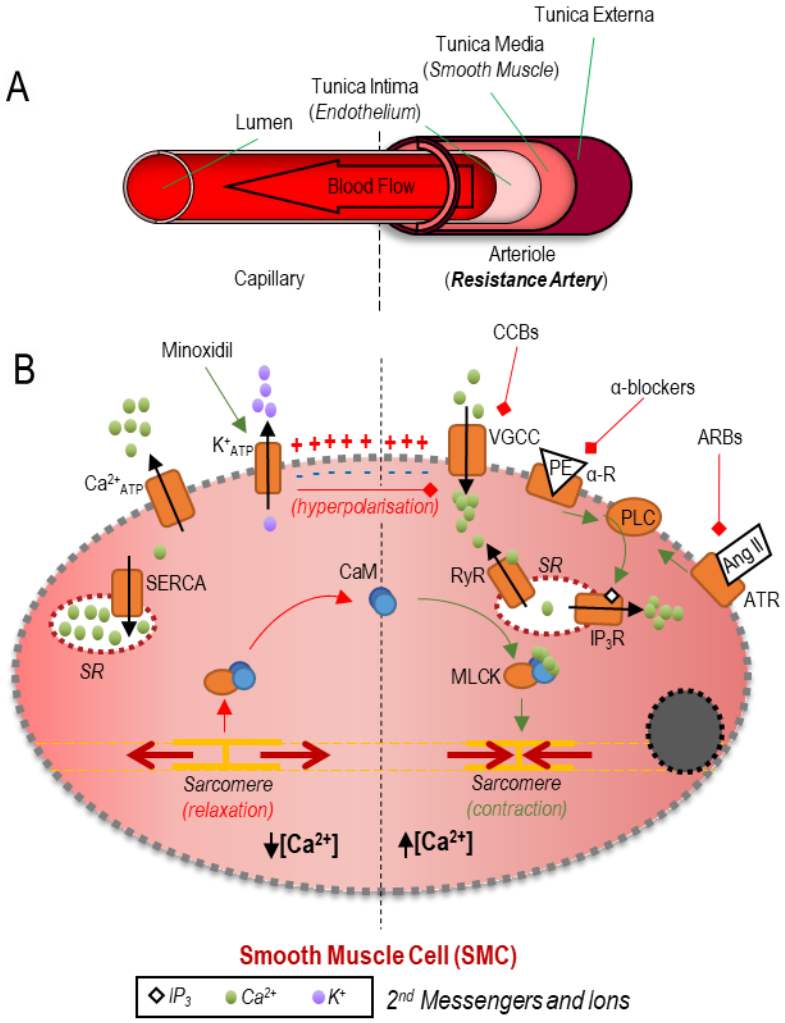


Figure 1.4; Resistance artery anatomy and diagram of the relaxant and contractive biochemical pathways and mechanisms of smooth muscle cells (SMCs). A) The tissue layers which make up a resistance artery, including the difference between artery and capillary. B) Biochemical vasomotor pathways of artery smooth muscle. Relaxant pathways, left, with red arrows and contractive pathways, right, with green arrows. Hyperpolarisation voltage, less than the resting potential of −55 mV across the cell membrane, shown with $^+$ and – signs. General proteins shown in orange: α-adrenoreceptor (α-R), angiotensin II receptor (ATR), ATP sensitive K^+ channel (K^+_{ATP}), Ca^{2+} ATPase (Ca^{2+}_{ATP}), inositol triphosphate receptor (IP_3R), myosin light chain kinase (MLCK), phospholipase C (PLC), ryanodine receptor (RyR), sarco-endoplasmic reticulum Ca^{2+} ATPase (SERCA) and voltage gated Ca^{2+} channel (VGCC). Calmodulin (CaM) shown in blue. Contractile machinery proteins of the sarcomere presented as yellow, for actin filaments, red for myosin chains; movement of which is shown by arrow direction under each condition. Intracellular Ca^{2+} store, the sarcoplasmic reticulum (SR), shown in white with red dashed outline. Targets of inhibitor antihypertension drug classes shown with red square arrows and activator drug target shown in green arrow. Please see key for chemical 2nd messenger and ion labels (bottom).

SMCs contain contractile machinery, made of interlocked actin filaments and myosin proteins called the sarcomere. This is linked to the cell's actin cytoskeleton, enabling changes to cell shape.[55] As the SMC cytosolic [Ca^{2+}] increases, myosin filaments of the sarcomere are phosphorylated by myosin light chain kinase (MLCK); itself activated by the Ca^{2+} sensing protein Calmodulin (CaM), Figure 1.4 B. Phosphorylated myosin proteins are able to bind and contract the actin filaments of the sarcomere, producing cellular and arterial contraction.[54] Thus, arterial tone is ultimately controlled by the cytosolic [Ca^{2+}] of SMCs, modulated by balanced adrenergic and muscarinic stimulation.[38]

Adrenergic stimulation of SMC α-adrenoreceptors (α-R) and angiotensin II receptors (ATR) increases SMC cytosolic [Ca^{2+}]. Downstream activation of the inositol triphosphate (IP_3R) and ryanodine receptors (RyR) cause release of Ca^{2+} from the intracellular store, the sarcoplasmic reticulum (SR), Figure 1.4 B.[7,54,56] The inward Ca^{2+} current of VGCCs, open above a SMC membrane voltage of −55 mV, also increases SMC cytosolic [Ca^{2+}].[57,58] The vasorelaxant mechanisms of α-blockers and ARBs on the SMC receptors, or the blockade of VGCCs by CCBs, are all aimed at preventing the increase of the SMC cytosolic [Ca^{2+}].[21,25,34]

When the adrenergic systems are not in effect, the function of the Ca^{2+} pumps, including the sarco/endoplasmic reticulum Ca^{2+} ATPase (SERCA) and cell membrane bound Ca^{2+} ATPase ($Ca^{2+}{}_{ATP}$), are responsible for the reduction of the SMC cytosolic [Ca^{2+}].[38] SMC K^+ channels generate hyperpolarisation by active K^+ efflux.[30] SMC hyperpolarisation closes VGCCs, leading to [Ca^{2+}] reduction and resulting in sarcomere relaxation.[32,59,60] Inhibition of VGCCs is highly effective at reducing the SMC cytosolic [Ca^{2+}], and this is the aim of K^+ channel activators, such as hydralazine and minoxidil.[30,31,33] The K^+ channel activator class of antihypertensive drugs are

exceptionally effective vasorelaxants. While powerful, these drugs act ubiquitously through the body on all tissues containing their target ion channels, producing several side effects: K^+ channel activators are, therefore, held back for use in resistant forms of hypertension.[30,52] These direct vasorelaxants act throughout the vasculature on all types of artery smooth muscle, dramatically lowering blood pressure. Strong dilation of conductance arteries can counterproductively cause the activation of baroreceptors, inducing the adrenergic system activation, to increase cardiac output.[30] No current K^+ channel activator is known to specifically act on resistance arteries alone.

1.2.2 Endothelium Dependant Smooth Muscle Relaxation

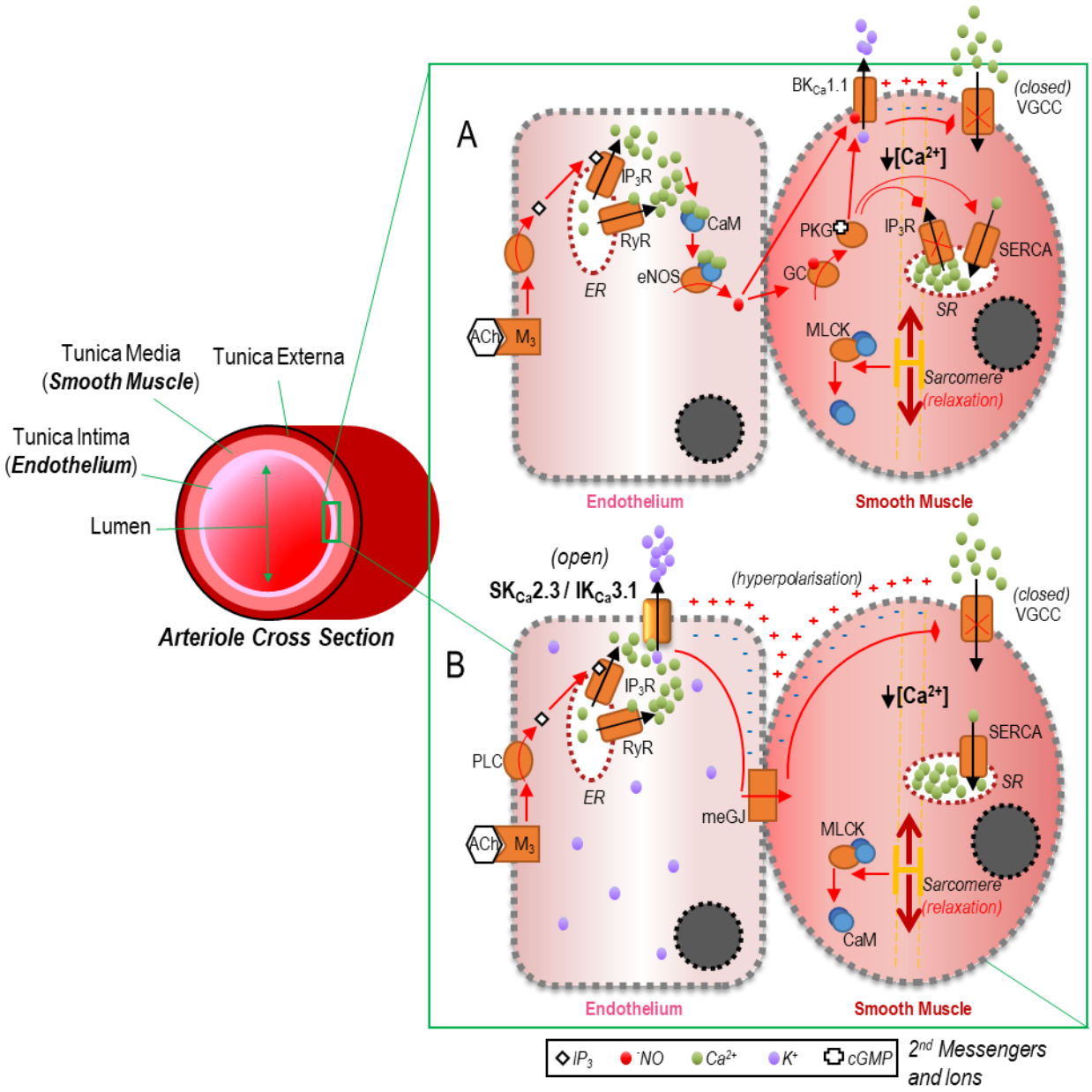


Figure 1.5; Endothelium dependant vasorelaxation nitric oxide (NO) and endothelium dependant hyperpolarisation (EDH), pathways. Expanded view of arteriole cross section shows cell interaction between endothelium and underlying smooth muscle. A) the NO pathway, B) the EDH pathway. Hyperpolarisation voltage, less than the resting potential of −55 mV across the cell membrane, shown with + and – signs. General proteins shown in orange: big Ca^{2+} activated K^+ channel ($BK_{Ca}1.1$), endothelial NO synthase (eNOS), guanylyl cyclase (GC), inositol triphosphate receptor (IP_3R), muscarinic receptor (M_3), myo-endothelial gap junction (meGJ), myosin light chain kinase (MLCK), phospholipase C (PLC), protein kinase G (PKG), ryanodine receptor (RyR), sarco-endoplasmic reticulum Ca^{2+} ATPase (SERCA) and voltage gated Ca^{2+} channel (VGCC). $SK_{Ca}2.3$ / $IK_{Ca}3.1$ channel shown in 3D. Calmodulin (CaM) shown in

blue. Intracellular Ca^{2+} stores, the sarcoplasmic reticulum (SR) and the endoplasmic reticulum (ER), shown in white with red dashed outlines. Contractile machinery proteins of the sarcomere presented as yellow for actin filaments and red for myosin chains, movement of which is shown by arrow direction under each condition. Please see key for chemical 2nd messenger and ion labels (bottom).

Additional to the SMC vasomotor pathways, discussed above, smooth muscle is controlled by several endothelium derived pathways. Two of these pathways, which operate in resistance arteries, are facilitated by nitric oxide (NO) and endothelium derived hyperpolarisation (EDH).[61,62] Unlike SMC contractile pathways, both the NO and EDH pathways begin with Ca^{2+} signalling. However, unlike in SMCs, increases in the endothelial cytosolic [Ca^{2+}] leads to artery vasorelaxation.[63]

The first endothelial vasorelaxant pathway, NO, is a universal mechanism of smooth muscle relaxation throughout the cardiovascular system. Acetylcholine (ACh) stimulation of the endothelium muscarinic receptor (M_3) leads to release of Ca^{2+} from the intracellular store, the endoplasmic reticulum (ER), *via* the IP_3R and RyR, Figure 1.5 A. Increases in the endothelium cytosolic [Ca^{2+}] are again sensed by CaM, yet in endothelial cells, CaM activates endothelium NO synthase (eNOS). eNOS produces the gaseous reactive radical, NO, which passively diffuses through cell membranes to the SMC layer.[62]

The effects of NO in SMCs are complex but all lead to vasorelaxation. NO causes guanylyl cyclase (GC) to produce guanyl monophosphate (cGMP), activating protein kinase G (PKG). PKG reduces the SMC cytosolic [Ca^{2+}] by phosphorylating several SMC protein targets: inhibiting the IP_3 receptor, activating the SERCA transporter and big Ca^{2+} activated K^+ channel ($BK_{Ca}1.1$).[62,64] The resulting $BK_{Ca}1.1$ cell hyperpolarisation closes VGCCs, Figure 1.5. As discussed above, reducing the SMC cytosolic [Ca^{2+}] leads to the relaxation of the sarcomere, cell and artery.[38]

The NO pathway has been an antihypertensive target for pharmaceutical activation with organic and inorganic NO yielding pro-drugs, such as nitroprusside, since the 1920s.[31,65] Some issues with the NO antihypertensive treatments have since been identified, especially in patients with co-morbidities, leading to endothelial dysfunction, such as diabetes mellitus or atherosclerosis. Endothelial dysfunction has been shown to reduce the vasorelaxant effect of the NO pathway, which is not greatly restored in the presence of NO yielding drugs.[66,67] In such cases, it has also been demonstrated that the second endothelium dependant vasorelaxant pathway, EDH, becomes more effective in resistance arteries.[68]

The EDH pathway begins with ACh induced Ca^{2+} release from the endoplasmic reticulum, as with the NO pathway.[69] The release of Ca^{2+} stimulates endothelium Ca^{2+} activated K^+ (K_{Ca}) channels; producing endothelium hyperpolarisation by enabling K^+ efflux, Figure 1.5.[61,70,71] Myo-endothelial gap junctions (meGJ) link the cytosols of the endothelium cells to the SMCs, and so hyperpolarisation of the endothelium is transferred to the SMCs.[60] As repeated above, SMC hyperpolarisation closes VGCCs and leads to SMC cytosolic [Ca^{2+}] reduction, causing vasorelaxation.[59] Unlike the NO pathway, the EDH pathway is more prevalent in resistance arteries than conductance arteries, presenting a novel opportunity as a target in treatment of hypertension.[72]

The main aim of this project was; to pharmacologically promote EDH type vasorelaxation of resistance arteries. To achieve this, a model of EDH vasorelaxation was required as an assay experiment, which could be probed with small molecules as potential vasorelaxants.

1.3 Assay Starting Points

The EDH mechanism of vasorelaxation is complicated by the necessary physical linkage, via gap junctions, between two different cell types. It is difficult to mimic the

EDH effect *in vitro,* unlike enzyme inhibition, because of the increased difficulty in culturing mixed mammalian cell types involving a physical linage. Fortunately, EDH is fundamentally produced by the activation of endothelium K_{Ca} channels, Figure 1.5.[69] The small conductance K_{Ca} channel ($SK_{Ca}2.3$) is widely expressed in excitable cells important to the function of the central nervous system, such as neurones.[73,74] Antihypertensive treatments altering the function of $SK_{Ca}2.3$ channels, known to be functionally important in the brain, may cause negative neurological side effects. The expression of the intermediate conductance K_{Ca} channel, $IK_{Ca}3.1$ however, is more commonly limited to non-excitable cell types, such as endothelial cells.[73] By targeting the $IK_{Ca}3.1$ channel, its function alone can be used to simplify and model EDH pathway initiation. An assay technique able to screen potential positive $IK_{Ca}3.1$ modulator candidates, was thus required.

1.3.1 $IK_{Ca}3.1$ Channel Structure and Gating Mechanism

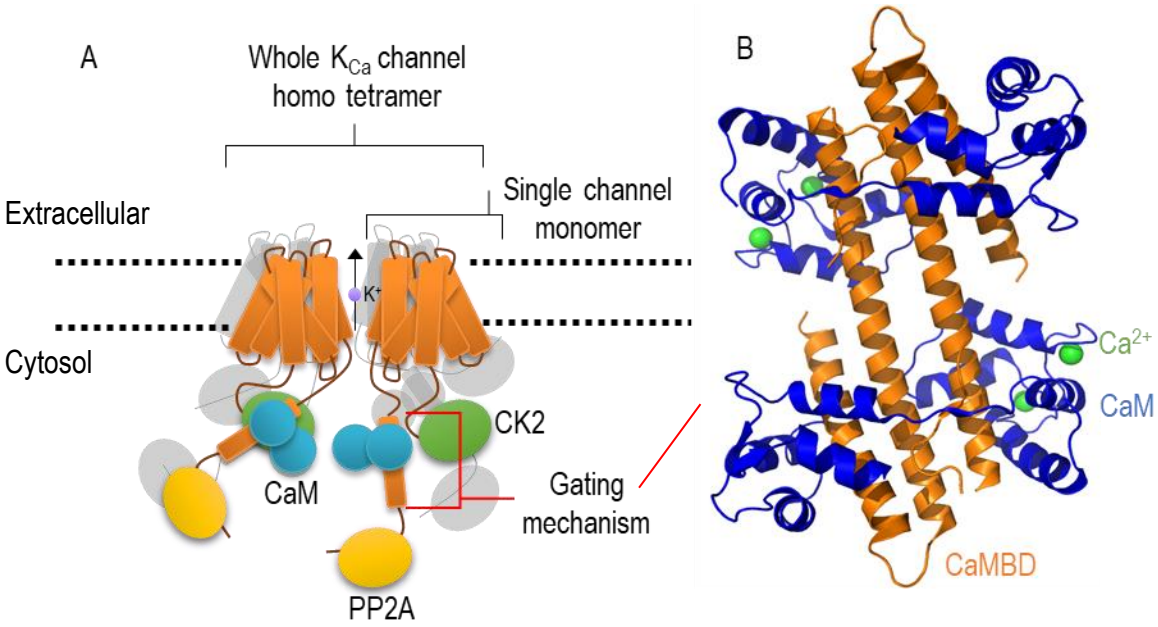


Figure 1.6; Representation of the K_{Ca} channel structure. A) Rendition of the full, membrane bound K_{Ca} channel structure. Channel protein shown in orange, with four subunits of seven transmembrane helices arranged in a homo-tetramer. Attached to the channel, on the cytosolic side of the membrane, are associated regulatory proteins required for Ca^{2+}, ATP and GTP sensing; calmodulin (CaM) in blue, protein phosphatase 2 (PP2A) in yellow, and casein kinase 2 (CK2) in green. The flux direction through the channel is indicated by the K^+ ion in purple, however, the channel gating complex is shown in a separated inactive (channel closed) form. CaM constitutively bound to the channel CaM-binding-domain (CaMBD), is highlighted in red as the canonical Ca^{2+} sensing gating complex, which gives the channels their name. B) Crystal structure of the activated and Ca^{2+} bound 2CaM:2CaMBD gating complex tetramer (PDB: 4G28).[75] Two CaM proteins, in blue, are shown to be wrapped around two CaMBD, in orange, with two Ca^{2+} ions bound to each.

K_{Ca} channels are made of four symmetrical membrane bound subunits arranged in a homo-tetramer, with a single K^+ ion selective pore, running down the centre. Each subunit of seven transmembrane helices has several associated regulatory proteins; conferring Ca^{2+} and ATP sensitivity to the channel, Figure 1.6 A.[76,77]

Associated CaM provides K_{Ca} channels their Ca^{2+} sensitivity, forming a gating complex, which activates the channel and opens the K^+ ion pore in the presence of Ca^{2+}.[78] CaM has two terminal lobes.[79] While the N-terminal lobe remains unbound in

the absence of Ca^{2+}, the C-terminal lobe is constitutively bound to each K_{Ca} channel subunit binding domain (CaMBD). Ca^{2+} causes the gating complex to further oligomerise, forming a hetero-tetrameric 2CaM:2CaMBD structure. This new tetramer joins two adjacent channel subunits, with two CaM bound symmetrically between two CaMBD, Figure 1.6 B.[77] A phosphatidylinositol bisphosphate (PIP_2) binding site has been suggested to form between the CaM and CaMBD of the tetrameric complex. Binding of PIP_2 to the activated gating complex may help physically associate it with the cell membrane, causing channel conformational change, opening the K^+ ion pore.[80,81] Casein kinase 2 (CK2) and protein phosphatase 2 (PP2A) are also both associated with each K_{Ca} channel subunit and modulate CaM's Ca^{2+} sensitivity. CK2 is activated by ATP and phosphorylates a tyrosine residue of CaM, lowering its Ca^{2+} sensitivity. PP2A is activated by GTP and dephosphorylates the CK2 modification to return CaM's original sensitivity.[77,80,82]

1.3.2 Biological Assays Based on the $IK_{Ca}3.1$ Channel and Resulting Leads

Despite simplifying the EDH response to the function of a single protein, the $IK_{Ca}3.1$ channel remained a difficult target to use in a typical medicinal chemistry screening assay because it is a membrane bound protein, Figure 1.6. It is notoriously difficult to isolate functionally active membrane proteins, such as ion channels, due to their large hydrophobic outer surfaces. Almost all protein purification techniques, largely chromatographic, rely on the protein of interest being soluble in aqueous media. Hydrophobic proteins must therefore be solubilised with detergents during the purification procedure and then reconstituted back into a phospholipid, or artificial, membrane. The folded secondary and tertiary structure of a hydrophobic protein is likely to be destabilised in the presence of a detergent and may not correctly re-fold upon detergent removal.[83]

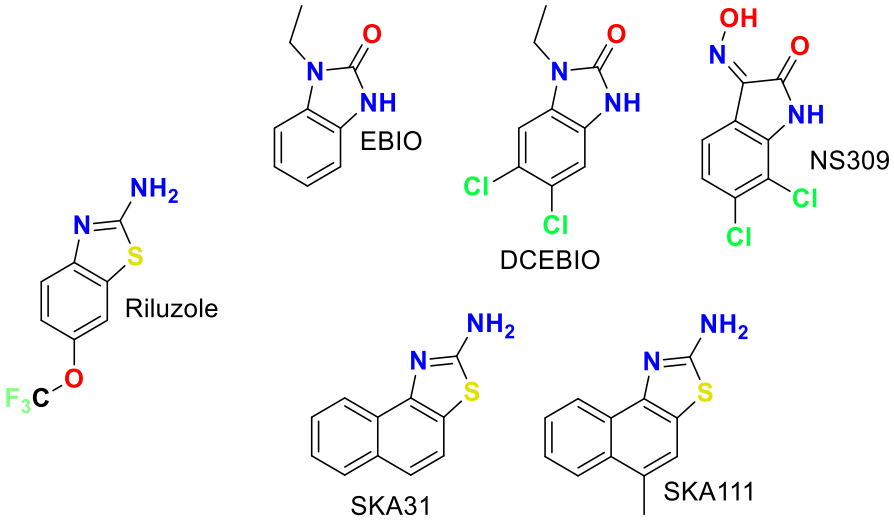


Figure 1.7; Chemical skeletal structures of known K_{Ca} channel small molecule modulators.

Fortunately, several small molecule K_{Ca} modulators have already been identified *via* screening campaigns based on cellular assays. Biological assays observe the action of the target protein *in vivo*. Small molecules which alter the target's canonical activity are then identified as biologically active. The greatest benefit of biological assays is that no purification of the target protein is required, leaving the target protein in a native environment, demonstrably active. This information is useful because it demonstrates biologically relevant small molecule activity under physiological conditions, a reliable reflection of the molecule's activity in living organisms.[84]

Riluzole is a drug originally developed as a muscle relaxant in the 1950s. Further research on riluzole's activity against a number of ion channels, led to it being the only drug approved for the general treatment of amyotrophic lateral sclerosis. [85] One notable effect of riluzole was the activation of K_{Ca} channels, especially $IK_{Ca}3.1$, making riluzole the first potential K_{Ca} channel activator lead.[86,87] Subsequently, several successful compound screening campaigns have been conducted, attempting to identify other molecule leads, similar to riluzole, which also act as K_{Ca} channel activators.

The K_{Ca} channel screening campaigns utilised patch clamp technology, in which a living cell membrane is electrostatically clamped onto a glass micro-pipette. The current of any embedded ion channels within the isolated cell membrane section can then be measured. The first K_{Ca} channel activator after riluzole, identified in patch clamp experiments, was *N*-ethyl benzimidazolone (EBIO), followed by the more potent derivative, dichloro-*N*-ethyl benzimidazolone (DCEBIO), Figure 1.7.[88,89] These new lead compounds were identified not to activate K_{Ca} channels alone, but at a lower activating concentration of Ca^{2+} than normal. Therefore, these molecules were not K_{Ca} channel activators, they increased the channels' Ca^{2+} sensitivity, acting instead as positive modulators. The next and more potent K_{Ca} channel modulator, dichloro-indoledione-3-oxime (NS309), was developed by NeuroSearch and is structurally similar to EBIO, Figure 1.7.[90] Finally, the most recent patch clamp screening campaign identified 2-amino-napthothiazole (SKA31), and then the 5-methyl substituted analogue (SKA111), which are the most potent and most $IK_{Ca}3.1$ channel selective positive modulators so far, Figure 1.7.[87,91]

As described above, the EDH effect is a physiological process between both endothelium and smooth muscle cell types. Creating a repeatable assay which models the interaction of two cell types is difficult, however, it is possible. Using *ex-vivo* artery preparations, it is possible to directly observe the interaction of endothelial and smooth muscle cells in their native environment. In these physiological artery assays, the translation of small molecule K_{Ca} channel modulation to the desired vasorelaxant activity can be observed. Channel modulation effects, observed under patch clamp assay conditions, may still not accurately reflect and predict the theoretical desired physiological outcome. In wire myography experiments where the NO pathway was blocked, SKA111 reduced the vasorelaxant EC_{50} of ACh.[91] This was because positive

modulation of $IK_{Ca}3.1$ by SKA111 enabled $IK_{Ca}3.1$ activation at lower concentrations of Ca^{2+}, liberated with less ACh stimulation. As such, SKA111 has been tested in rats to demonstrate a 30 mmHg drop in blood pressure.[91]

Biological assays reflect the intended and desired effects in whole organisms, such as vasorelaxation or blood pressure decrease. However, biological assays also suffer from several important disadvantages. Firstly, for biological assays based on living systems, *in vivo* conditions must be closely replicated, requiring lots of skill and attention to keep cells alive, making automation difficult. The limiting conditions of biological assays do not allow for high concentrations of test molecules or solubilising vehicle solvent, such as dimethyl sulfoxide, or even different pHs. These condition restrictions hamper small molecule development by limiting the molecular analogues experimentally assayable, reducing chemical space explored. Second, living cells are more complex than is currently understood. The inevitable slight changes in complex biological assay variables often causes a range of responses to the same molecule, which makes collecting consistent repeatable data difficult. Biological assays therefore require statistical analysis of time-consuming experimental repeats to give confidence to the results. Lastly, and foremost among biological assay disadvantages, is the high rate of false positives. Without isolating the target protein before conducting an assay, potential test molecule interactions with other proteins obfuscates the origin of an observed effect. Misleading small molecule interactions with non-target proteins that produce the same desired effect, such as vasorelaxation, confuse the development of small molecule structure activity relationships. This obfuscation makes it impossible to prove that the effect observed in biological assays is *via* modulation of the target alone.[84]

1.3.3 Potential Biophysical Assays Based on the $IK_{Ca}3.1$ Channel

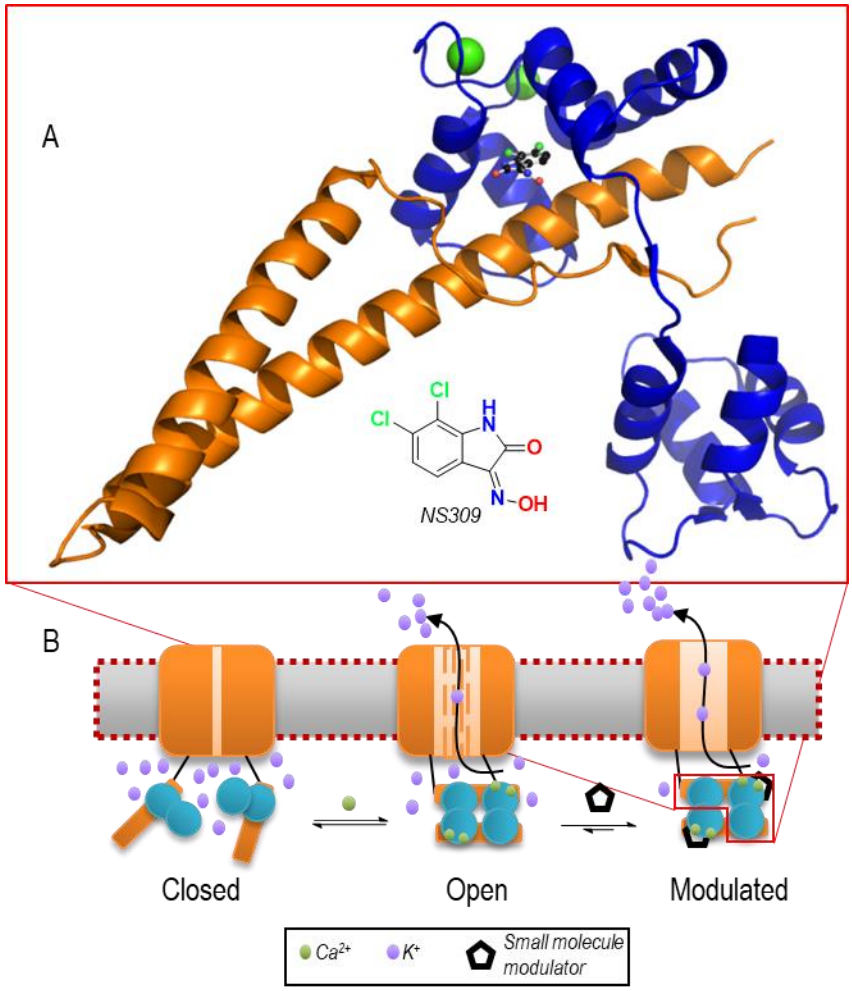


Figure 1.8; Co-Crystal structure of the K_{Ca} channel modulator, NS309, bound to the Ca^{2+} activated 2CaM:2CaMBD SK_{Ca} channel gating complex (PDB: 4J9Z) and proposed modulator mechanism.[75,92] A) Co-crystal structure of $SK_{Ca}2.2$ and modulator NS309. Only the secondary protein-protein interaction between CaM and the CaMBD of the Ca^{2+} activated 2CaM:2CaMBD tetramer is shown, for simplicity. (The constitutive interaction between CaM and the CaMBD is not shown). NS309 is presented as a ball and stick structure in elemental colours (skeletal structure also shown) seen bound at the interface between CaM, in blue, and the CaMBD, in orange. Ca^{2+} shown as green spheres. B) Schematic representation of small molecule modulation of the K_{Ca} channel gating complex. In the absence of Ca^{2+} the channel remains closed to K^+ ions. Ca^{2+} binds reversibly to CaM and causes the gating complex to reversibly oligomerise into the activating 2CaM:2CaMBD tetrameric structure increasing the open probability of the channel. Small molecule stabilisation pushes the oligomerisation equilibrium towards the active tetramer gating complex. Ion and modulator labels shown in key (bottom).

The binding site of K_{Ca} channel modulators has been identified in crystal structures of EBIO and NS309 with the K_{Ca} channel gating complex proteins (PDB: 4G28 and 4J9Z, respectively).[75] The NS309 binding site is shown to be at the Ca^{2+} induced interface between CaM and the K_{Ca} channel CaMBD, in the activated gating complex tetramer 2CaM:2CaMBD, Figure 1.8 A. An explanatory theory for the observed effect of these modulators on K_{Ca} channel Ca^{2+} sensitivity, suggests the molecules stabilise the activated, Ca^{2+} bound, gating complex, Figure 1.8 B.[93] Using this information, it was proposed to use the $IK_{Ca}3.1$ gating complex proteins to develop a biochemical assay capable of identifying K_{Ca} channel binders.

While crystallographic data provides invaluable structural information regarding the protein, binding site and ligand-protein molecular interactions, it still does not give molecular affinity.[94] As well as this, it can be difficult to produce protein crystals or ligand co-crystals, and more difficult to automate the process. By contrast, biophysical assays using isolated target protein(s) *in vitro* are quick, relatively simple to prepare, run and analyse. Biophysical assays are high throughput, and most importantly they prove target engagement while providing molecular affinity. Unlike cellular assays, however, biophysical assays do not provide information on efficacy. The effect of a ligand on the target protein's function, such as channel opening, is not indicated by biophysical assays. Consequently, many biophysical assays are unable to differentiate between agonists, antagonists or even strength of efficacy. Thus, only biological and biophysical assays, together, prove that small molecules may interact with the intended target protein *in vivo*.[84] Therefore, the constituent aims of the project were: to develop a biochemical assay for screening candidate ligand affinities for the $IK_{Ca}3.1$ channel, and to confirm identified $IK_{Ca}3.1$ channel ligands' potencies and effects using a biological assay. Using these assays, structural analogues of identified $IK_{Ca}3.1$ ligands could be

tested, and a selective modulator structure activity relationship elucidated. A developed $IK_{Ca}3.1$ modulator would promote EDH vasorelaxation of resistance arteries in whole organisms, lowering blood pressure.

Chapter 1 References

1. Gaciong, Z., Siński, M. & Lewandowski, J. Blood pressure control and primary prevention of stroke: Summary of the recent clinical trial data and meta-analyses. *Curr. Hypertens. Rep.* **15,** 559–574 (2013).
2. Flack, J. M. *et al.* Management of high blood pressure in blacks: An update of the International Society on hypertension in blacks consensus statement. *Hypertension* **56,** 780–800 (2010).
3. Esunge, P. M. From blood pressure to hypertension: the history of research. *J. R. Soc. Med.* **84,** 621 (1991).
4. Kotchen, T. A. Historical trends and milestones in hypertension research: A model of the process of translational research. *Hypertension* **58,** 522–538 (2011).
5. Rouch, L. *et al.* Antihypertensive drugs, prevention of cognitive decline and dementia: A systematic review of observational studies, randomized controlled trials and meta-analyses, with discussion of potential mechanisms. *CNS Drugs* **29,** 113–130 (2015).
6. Lackland, D. T. & Weber, M. A. Global burden of cardiovascular disease and stroke: Hypertension at the core. *Can. J. Cardiol.* **31,** 569–571 (2015).
7. Lymperopoulos, A., Rengo, G. & Koch, W. J. Adrenergic nervous system in heart failure: Pathophysiology and therapy. *Circ. Res.* **113,** 739–753 (2013).
8. Lau, D. H., Nattel, S., Kalman, J. M. & Sanders, P. Modifiable risk factors and atrial fibrillation. *Circulation* **136,** 583–596 (2017).
9. Mathers, C., Stevens, G. & Mascarenhas, M. *Global health risks: Mortality and burden of disease attributable to selected major risks*. (2009).
10. Campbell, N. R. C. *et al.* Using the global burden of disease study to assist development of nation-specific fact sheets to promote prevention and control of hypertension and reduction in dietary salt: a resource from the World Hypertension League. *J. Clin. Hypertens.* **17,** 165–167 (2015).
11. Mendis, S., Puska, P. & Norrving, B. *Global atlas on cardiovascular disease prevention and control*. (2011).
12. Benjamin, E. J. *et al. Heart disease and stroke statistics—2018 update: a report from the American Heart Association*. *Circulation* (2018). doi:10.1161/CIR.0000000000000558
13. Lloyd-Jones, D. *et al.* Executive summary: Heart disease and stroke statistics-2010 update: A report from the american heart association. *Circulation* **121,** 46–215 (2010).
14. Kim E. Barret, Susan M. Barman, Scott Boitano, H. L. B. The Heart as a Pump. in *Ganong's Review of Medical Physiology* (eds. Weitz, M. & Kearns, B.) 539–554 (McGraw-Hill, 2012).
15. Carretero, O. & Oparil, S. Essential hypertension Part I: definition and etiology. *Circulation* **101,** 329–335 (2000).
16. Organisation, W. H. *20th WHO model list of essential medicines*. (2017).
17. Moser, M. & Fieg, P. U. Fifty years of thiazide diuretic therapy for hypertension. *Arch. Intern. Med.* **169,** 1851–1856 (2009).
18. Malha, L. & Mann, S. J. Loop diuretics in the treatment of hypertension. *Curr. Hypertens. Rep.* **18,** (2016).

19. Black, J. Drugs from emasculated hormones: the principle of syntopic antagonism. *Biosci. Rep.* **24,** 302–22 (2005).
20. Quirke, V. Putting theory into practice: James Black, receptor theory and the development of the beta-blockers at ICI, 1958-1978. *Med. Hist.* **50,** 69–92 (2006).
21. Chapman, N. *et al.* Time to re-appraise the role of alpha-1 adrenoceptor antagonists in the management of hypertension? *J. Hypertens.* **28,** 1796–1803 (2010).
22. Orso, F., Fabbri, G., Baldasseroni, S. & Maggioni, A. P. Newest additions to heart failure treatment. *Expert Opin. Pharmacother.* **15,** 1849–61 (2014).
23. Van Epps, H. L. Harry Goldblatt and the discovery of renin. *J. Exp. Med.* **201,** 1351–1351 (2005).
24. Sumners, C. & Raizada, M. K. Angiotensin II stimulates norepinephrine uptake in hypothalamus-brain stem neuronal cultures. *Am. J. Physiol. Physiol.* **250,** C236–C244 (1986).
25. Burnier, M. & Brunner, H. R. Angiotensin II receptor antagonists. *Lancet* **355,** 637–645 (2000).
26. Kolkhof, P. & Bärfacker, L. Mineralocorticoid receptor antagonists: 60 years of research and development. *J. Endocrinol.* **234,** T125–T140 (2017).
27. Smith, C. G. & Vane, J. R. The Discovery of Captopril. *FASEB J.* 788–789 (2003).
28. Finnegan, P. M. & Gleason, B. L. Combination ACE inhibitors and angiotensin II receptor blockers for hypertension. *Ann. Pharmacother.* **37,** 886–889 (2003).
29. Krum, H. *et al.* Direct renin inhibition in addition to or as an alternative to angiotensin converting enzyme inhibition in patients with chronic systolic heart failure: rationale and design of the Aliskiren Trial to Minimize OutcomeS in Patients with HEart failuRE (ATMOS. *Eur. J. Heart Fail.* **13,** 107–14 (2011).
30. Sica, D. A. Minoxidil: an underused vasodilator for resistant or severe hypertension. *J. Clin. Hypertens. (Greenwich).* **6,** 283–287 (2004).
31. Cohn, J. N., McInnes, G. T. & Shepherd, A. M. Direct-acting vasodilators. *J. Clin. Hypertens.* **13,** 690–692 (2011).
32. Nielsen-Kudsk, J. E., Boesgaard, S. & Aldershvile, J. K + channel opening: A new drug principle in cardiovascular medicine. *Br. Heart J.* **76,** 109–116 (1996).
33. Kandler, M., Mah, G., Tejani, A., Stabler, S. & Salzwedel, D. Hydralazine for essential hypertension (Review). *Cochrane Database Syst Rev* 1–16 (2011). doi:10.1002/14651858.CD004934.pub4.www.cochranelibrary.com
34. Fleckenstein, A. Calcium antagonism in heart and smooth muscle. *Med. Res. Rev.* **5,** 395–425 (1985).
35. Eisenberg, M. J., Brox, A. & Bestawros, A. N. Calcium channel blockers: An update. *Am. J. Med.* **116,** 35–43 (2004).
36. Acierno, L. J. *et al.* Albrecht Fleckenstein: father of calcium antagonism. *Clin. Cardiol.* **27,** 710–1 (2004).
37. Fleckenstein, A., Frey, M. & Fleckenstein-grun, G. Antihypertensive and arterial anticalcinotic effects of calcium antagonists. *Am J Cardiol* **57,** 1D–10D (1986).
38. Karaki, H. *et al.* Calcium movements, distribution, and functions in smooth muscle. *Pharmacol. Rev.* **49,** 157–230 (1997).
39. Chen, N. *et al.* Calcium channel blockers versus other classes of drugs for hypertension. *Cochrane Database Syst Rev* 1–68 (2010). doi:10.1002/14651858.CD003654.pub4
40. Kuriyama, H. Mechanisms of vasodilatation induced by potassium-channel activators. 129–139 (1991).
41. Whelton, P. K. *et al. Guideline for the prevention, detection, evaluation, and management of high blood pressure in adults*. *Hypertension* (2018). doi:10.1161/HYP.0000000000000065
42. O'Rourke, M. F. & Nichols, W. W. Aortic diameter, aortic stiffness, and wave reflection increase with age and isolated systolic hypertension. *Hypertension* **45,** 652–658 (2005).

43. Vavricka, S. R., Himmelmann, A. & Schaffner, A. Age-specific relevance of usual blood pressure to vascular mortality a meta-analysis of individual data for one million adults in 61 prospective studies. *Lancet* **360,** 1903–1913 (2002).
44. Ishibashi, Y. *et al.* Sublingual nifedipine in elderly patients: Even a low dose induces myocardial ischaemia. *Clin. Exp. Pharmacol. Physiol.* **26,** 404–410 (1999).
45. Salvetti, A. & Ghiadoni, L. Thiazide diuretics in the treatment of hypertension: an update. *J. Am. Soc. Nephrol.* **17,** S25–S29 (2006).
46. Calhoun, D. A., Nishizaka, M. K., Zaman, M. A., Thakkar, R. B. & Weissmann, P. Hyperaldosteronism among black and white subjects with resistant hypertension. *Hypertension* **40,** 892–896 (2002).
47. Damasceno, A., Ferreira, B., Patel, S., Sevene, E. & Polonia, J. Efficacy of captopril and nifedipine in black and white patients with hypertensive crisis. *J. Hum. Hypertens.* **11,** 471–6 (1997).
48. Wiysonge, C., Bradley, H., Volmink, J., Mayosi, B. & Opie, L. Beta-blockers for hypertension (Review). *Cochrane Database Syst Rev* (2017). doi:10.1002/14651858.CD002003.pub5.www.cochranelibrary.com
49. Wright, J. M., Musini, V. M. & Gill, R. First-line drugs for hypertension (Review). *Cochrane Database Syst Rev* 1–149 (2018). doi:10.1002/14651858.CD001841.pub3.www.cochranelibrary.com
50. James, P. A. *et al. 2014 evidence-based guideline for the management of high blood pressure in adults*. *JAMA - Journal of the American Medical Association* **311,** (2014).
51. Evans, J. C. & Levy, D. Hypertension in adults across the age spectrum: current outcomes and control in the community. *JAMA - J. Am. Med. Assoc.* **294,** 466–472 (2005).
52. Vongpatanasin, W. Resistant hypertension: A review of diagnosis and management. *JAMA - J. Am. Med. Assoc.* **311,** 2216–2224 (2014).
53. Poulter, N. R., Prabhakaran, D. & Caulfield, M. Hypertension. *Lancet* **386,** 801–812 (2015).
54. Kim E. Barret, Susan M. Barman, Scott Boitano, H. L. B. Blood as a Circulatory Fluid & the Dynamics of Blood & Lymph Flow. in *Ganong's Review of Medical Physiology* (eds. Weitz, M. & Kearns, B.) 555–586 (McGraw-Hill, 2012).
55. Kim E. Barret, Susan M. Barman, Scott Boitano, H. L. B. Excitable Tissue: Muscle. in *Ganong's Review of Medical Physiology* (eds. Weitz, M. & Kearns, B.) 99–118 (McGraw-Hill, 2012).
56. Tamargo, J. & López-Sendón, J. Novel therapeutic targets for the treatment of heart failure. *Nat. Rev. Drug Discov.* **10,** 536–55 (2011).
57. Yamakage, M. & Namiki, A. Calcium channels - Basic aspects of their structure, function and gene encoding; anesthetic action on the channels - A review. *Can. J. Anesth.* **49,** 151–164 (2002).
58. Catterall, W. A., Perez-Reyes, E., Snutch, T. P. & Striessnig, J. Nomenclature and structure-function relationships of voltage-gated calcium channels. *Pharmacol. Rev.* **57,** 411–425 (2005).
59. Garland, C. J., Plane, F., Kemp, B. K. & Cocks, T. M. Endothelium-dependent hyperpolarization: A role in the control of vascular tone. *Trends Pharmacol. Sci.* **16,** 23–30 (1995).
60. Garland, C. J., Hiley, C. R. & Dora, K. a. EDHF: Spreading the influence of the endothelium. *Br. J. Pharmacol.* **164,** 839–852 (2011).
61. Goto, K., Ohtsubo, T. & Kitazono, T. Endothelium-dependent hyperpolarization (EDH) in hypertension: The role of endothelial ion channels. *Int. J. Mol. Sci.* **19,** 1–20 (2018).
62. Zhao, Y., Vanhoutte, P. M. & Leung, S. W. S. Vascular nitric oxide: Beyond eNOS. *J. Pharmacol. Sci.* **129,** 83–94 (2015).
63. Furchgott, R. F. & Jothianandan, D. Endothelium-dependent and -independent vasodilation involving cyclic GMP:

relaxation induced by nitric oxide, carbon monoxide and light. *Blood Vessels* **28,** 52–61 (1991).

64. Greenberg, H. Z. E. *et al.* Stimulation of calcium-sensing receptors induces endothelium-dependent vasorelaxations via nitric oxide production and activation of IKCa channels. *Vascul. Pharmacol.* **80,** 75–84 (2016).
65. Friederich, J. A. & Butterworth, J. F. Sodium Nitroprusside. *Anesth Analg* **81,** 152–162 (19995).
66. Ding, H. & Triggle, C. R. Endothelial dysfunction in diabetes : multiple targets for treatment. 977–994 (2010). doi:10.1007/s00424-010-0807-3
67. Williams, S. B., Cusco, J. A., Roddy, M. A., Johnstone, M. T. & Creager, M. A. Impaired nitric oxide-mediated vasodilation in patients with non-insulin-dependent diabetes mellitus. *J. Am. Coll. Cardiol.* **27,** 567–574 (1996).
68. M, S. S., Hanum, A. & Ghulam, R. Role of endothelium-dependent hyperpolarisation and prostacyclin in diabetes. **22,** 8–17 (2015).
69. Edwards, G., Dora, K. a, Gardener, M. J., Garland, C. J. & Weston, a H. K+ is an endothelium-derived hyperpolarizing factor in rat arteries. *Nature* **396,** 269–272 (1998).
70. Rasmussen, K. M. B., Braunstein, T. H., Salomonsson, M., Brasen, J. C. & Sorensen, C. M. Contribution of K+ channels to endothelium-derived hypolarization-induced renal vasodilation in rats in vivo and in vitro. *Pflugers Arch. Eur. J. Physiol.* **468,** 1139–1149 (2016).
71. Félétou, M. & Vanhoutte, P. M. Endothelium-Derived Hyperpolarizing Factor. *Clin. Exp. Pharmacol. Physiol.* **23,** 1082–1090 (1996).
72. Quyyumi, A. A. & Ozkor, M. A. Endothelium-derived hyperpolarizing factor and vascular function. *Cardiol. Res. Pract.* **1,** (2011).
73. Wei, A. D. *et al.* Nomenclature and molecular relationships of calcium-activated potassium channels. *Pharmacol. Rev.* **57,** 463–472 (2005).
74. Wulff, H. & Köhler, R. Endothelial small- and intermediate-conductance KCa channels: an update on their pharmacology and usefulness as cardiovascular targets. *J. Cardiovasc Pharmacol.* **61,** 102–112 (2013).
75. Zhang, M., Pascal, J. M., Schumann, M., Armen, R. S. & Zhang, J.-F. Identification of the functional binding pocket for compounds targeting small-conductance Ca2+-activated potassium channels. *Nat. Commun.* **3,** 1021 (2012).
76. Guéguinou, M. *et al.* KCa and Ca2+channels: The complex thought. *Biochim. Biophys. Acta - Mol. Cell Res.* **1843,** 2322–2333 (2014).
77. Schumacher, M. a, Rivard, a F., Bächinger, H. P. & Adelman, J. P. Structure of the gating domain of a Ca2+-activated K+ channel complexed with Ca2+/calmodulin. *Nature* **410,** 1120–1124 (2001).
78. Saimi, Y. & Kung, C. Calmodulin as an ion channel subunit. *Annu. Rev. Physiol.* **64,** 289–311 (2002).
79. Zhang, M. *et al.* Structural basis for calmodulin as a dynamic calcium sensor. *Structure* **20,** 911–923 (2012).
80. Zhang, M. *et al.* Selective phosphorylation modulates the PIP2 sensitivity of the CaM-SK channel complex. *Nat Chem Biol* **10,** 753–759 (2014).
81. Zhang, M., Meng, X.-Y., Zhang, J.-F., Cui, M. & Logothetis, D. E. Molecular overlap in the regulation of SK channels by small molecules and phosphoinositides. *Sci. Adv.* **1,** e1500008 (2015).
82. Buchanan, K. A., Petrovic, M. M., Chamberlain, S. E. L., Marrion, N. V. & Mellor, J. R. Facilitation of long-term potentiation by muscarinic M1 receptors is mediated by inhibition of SK channels. *Neuron* **68,** 948–963 (2010).
83. Lin, S. H. & Guidotti, G. Chapter 35 Purification of Membrane Proteins. in *Methods in Enzymology* **463,** 619–629 (Elsevier Inc., 2009).
84. Cronk, D. High-Throughput Screening. in *Drug Discovery and Development: Technology in Transition* (eds. Hill, R. &

Rang, H.) 95–118 (Churchill Livingstone, 2012).

85. Bellingham, M. C. A review of the neural mechanisms of action and cinical efficiency of riluzole in treating amyotrophic lateral sclerosis: what have we Learned in the last decade? *CNS Neurosci. Ther.* **17,** 4–31 (2011).
86. Cao, Y. J., Dreixler, J. C., Couey, J. J. & Houamed, K. M. Modulation of recombinant and native neuronal SK channels by the neuroprotective drug riluzole. *Eur. J. Pharmacol.* **449,** 47–54 (2002).
87. Sankaranarayanan, A. *et al.* Naphtho[1,2-d]thiazol-2-ylamine (SKA-31), a new activator of KCa2 and KCa3.1 potassium channels, potentiates the endothelium-derived hyperpolarizing factor response and lowers blood pressure. *Mol. Pharmacol.* **75,** 281–95 (2009).
88. Devor, D. C., Singh, a K., Frizzell, R. a & Bridges, R. J. Modulation of Cl- secretion by benzimidazolones. I. Direct activation of a Ca(2+)-dependent K+ channel. *Am. J. Physiol.* **271,** L775-84 (1996).
89. Singh, S., Syme, C. a, Singh, a K., Devor, D. C. & Bridges, R. J. Benzimidazolone activators of chloride secretion: potential therapeutics for cystic fibrosis and chronic obstructive pulmonary disease. *J.Pharmacol.Exp.Ther.* **296,** 600–611 (2001).
90. Strøbæk, D. *et al.* Activation of human IK and SK Ca2+-activated K+ channels by NS309 (6,7-dichloro-1H-indole-2,3-dione 3-oxime). *Biochim. Biophys. Acta* **1665,** 1–5 (2004).
91. Coleman, N. *et al.* New positive Ca2+ -activated K+ channel gating modulators with selectivity for KCa3.1. *Mol. Pharmacol.* **86,** 342–357 (2014).
92. Cui, M., Qin, G., Yu, K., Bowers, M. S. & Zhang, M. Targeting the small- and intermediate-conductance Ca2+-activated potassium channels: the drug-binding pocket at the channel/calmodulin interface. *Neurosignals* **22,** 65–78 (2014).
93. Zhang, M., Pascal, J. M. & Zhang, J.-F. Unstructured to structured transition of an intrinsically disordered protein peptide in coupling Ca^{2+}-sensing and SK channel activation. *Proc. Natl. Acad. Sci. U. S. A.* **110,** 4828–33 (2013).
94. Mcnae, I. W. *et al.* Studying protein-ligand interactions using protein crystallography. *Crystallogr. Rev.* **11,** 61–71 (2005).

CHAPTER 2 MODELLING, DESIGN & SYNTHESIS

In this chapter, work is described to rationalise, design and synthesise novel ligands, selective for the target $IK_{Ca}3.1$ channel over the related SK_{Ca} channels, using homology models of the target, for which no crystal structure exists.

2.1 Homology Modelling of the $IK_{Ca}3.1$ Modulator Binding Cavity

The overall aim of this work was to discover novel small molecules ligands of the intermediate conductance Ca^{2+} activated K^+ channel ($IK_{Ca}3.1$). No experimentally determined structure of the $IK_{Ca}3.1$ channel has been solved. Instead a model was desired to achieve computational screening, aid ligand design and reduce the synthetic workload. Additionally, a K_{Ca} channel affinity probe, based on existing $IK_{Ca}3.1$ positive modulators, was required for later development of a fluorescence polarisation biophysical assay, described in Chapter 3. Structural information about the $IK_{Ca}3.1$ modulator binding cavity was desired to aid selection of the appropriate positive modulator, and design of a probe analogue.

To create a model of $IK_{Ca}3.1$, its primary sequence and a template structure of a homologous protein were required.[1] The full structures of $IK_{Ca}3.1$ and closely related small conductance Ca^{2+} activated K^+ channels ($SK_{Ca}2.1$–3), are also unknown. However, the sub-structure of the $SK_{Ca}2.2$ positive modulator binding cavity is known, identified in the channel's gating complex.[2] The K_{Ca} gating complex, formed by the Ca^{2+}-sensing regulator protein, calmodulin (CaM), and the channel's truncated calmodulin-binding domain (CaMBD), becomes a tetrameric 2CaM:2CaMBD structure when activated by Ca^{2+}.[2] K_{Ca} channel positive modulators stabilise the Ca^{2+} induced CaM-CaMBD protein-protein interaction of the activated gating complex tetramer.[3] Both

K_{Ca} channels are controlled by the same CaM based gating complex, and it was assumed that $IK_{Ca}3.1$ positive modulators bind to its corresponding cavity.[4] Thus, a facsimile of the target $IK_{Ca}3.1$ gating complex, and presumed binding cavity, was generated through homology modelling.

2.1.1 Identifying and Investigating the IKCa3.1 Calmodulin Binding Domain Primary Sequence

The primary structures, amino acid sequences, of the two proteins of the $IK_{Ca}3.1$ gating complex, CaM and truncated CaMBD, were required for homology modelling. CaM is a well-studied protein and its primary and secondary structures are known, so did not need to be identified.[5–9] Only the respective channel CaMBDs change between the template $SK_{Ca}2.2$ and target $IK_{Ca}3.1$ channels. Consequently, only the unknown $IK_{Ca}3.1$ CaMBD primary sequence remained to be identified for use with the known CaM sequence in modelling experiments.[10] The published $SK_{Ca}2.2$ co-crystal structure CaMBD-2 and CaM proteins were from *Rattus norvegicus*, however, both were found to be identical to the *Homo sapiens* (HS) protein sequences via BLAST analysis. The novel K_{Ca} channel modulators to be developed were ultimately designed to treat hypertension in humans, therefore, the homology modelling and rational drug design were conducted using the HS protein sequences.

The *Homo sapiens* $IK_{Ca}3.1$ CaMBD was identified by searching the National Centre for Biotechnical Information protein database using the DELTA-BLAST alignment tool.[11] The whole channel protein sequence alignment of $SK_{Ca}2.2$ and target $IK_{Ca}3.1$, from HS , is presented in Figure 2.1 A. The alignments of the HS CaMBDs from all the calmodulin gated K_{Ca} channels are presented in Figure 2.1 B. The CaMBDs from each channel are labelled numerically CaMBD-(1–4) corresponding to $SK_{Ca}2.1$–3, and $IK_{Ca}3.1$ being 4.

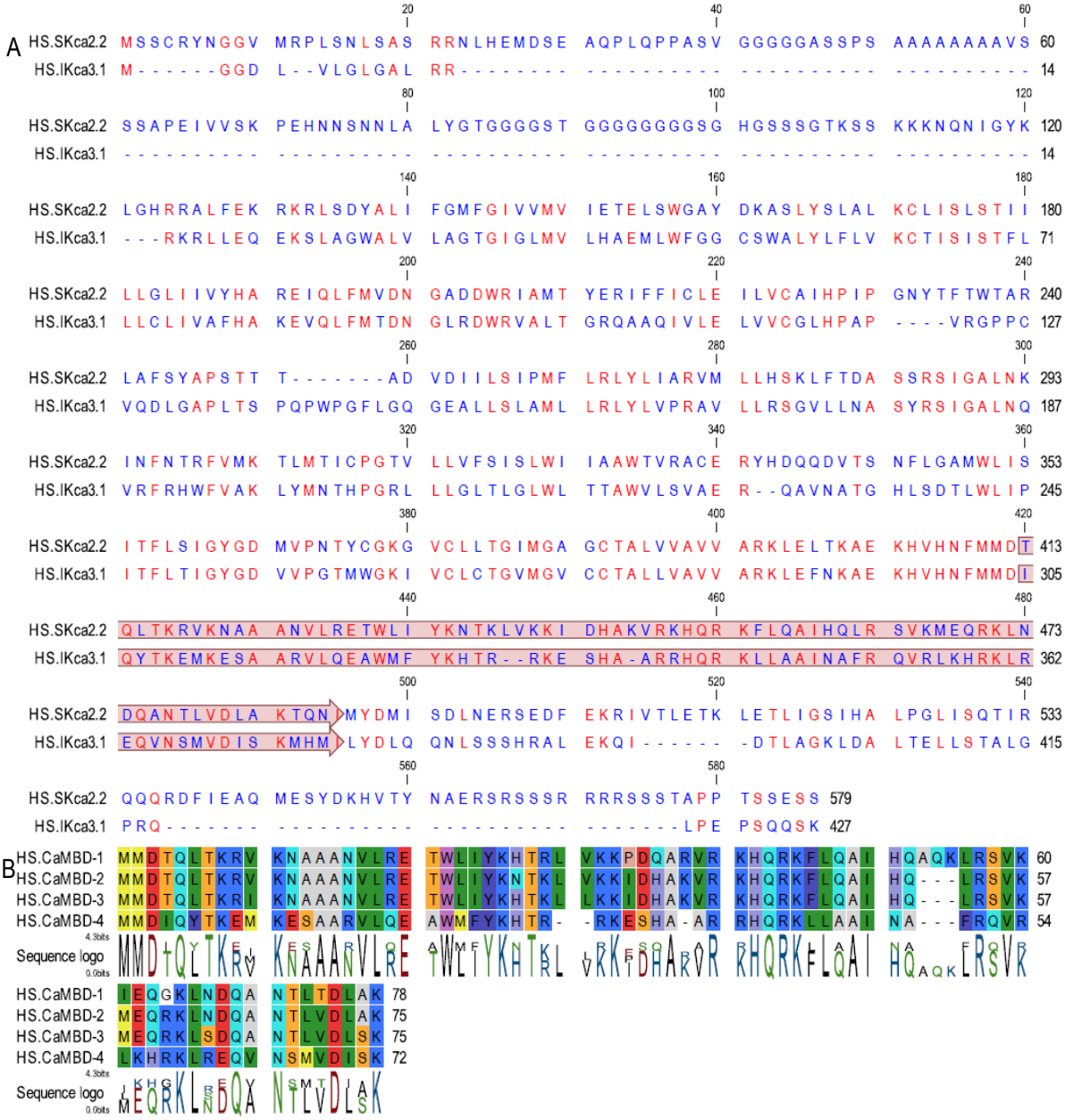


Figure 2.1; HS.K_{Ca} channel sequence alignments. A) SK_{Ca}2.2 and IK_{Ca}3.1 whole channel sequence alignment, conserved residues in blue and non-conserved residues in red, the CaMBD region of each channel highlighted with red arrows. B) Sequence alignments of all K_{Ca} channel CaMBDs: SK_{Ca}2.1 as CaMBD-1: SK_{Ca}2.2 as CaMBD-2: SK_{Ca}2.3 as CaMBD-3: IK_{Ca}3.1 as CaMBD-4, residues coloured with RasMol colour scheme, residue conservation presented as sequence logo where increasing letter size denotes increasing conservation.[12]*Table 2.1; Relationships of the HS.K_{Ca} CaMBDs; %ID is the*

percentage of identical residues (lower left values), %Coverage is the percentage of template sequence covered by the query (upper right values).

	CaMBD-1		CaMBD-2		CaMBD-3	
	%ID	%Coverage	%ID	%Coverage	%ID	%Coverage
CaMBD-2	88	93				
CaMBD-3	84	93	93	100		
CaMBD-4	49	93	52	97	54	97

The similarity between the whole channel protein sequences of the target, $IK_{Ca}3.1$, and template, $SK_{Ca}2.2$, was 46% identical (%ID). More importantly, the channels' CaMBDs had 52%ID, Table 2.1. This level of template-target sequence %ID was encouraging, because >50%ID is the confidence limit for producing the most accurate homology models.[13] While a higher %ID would have produced more confidence in subsequent homology models, the lower sequence %ID ensured more residue changes for possible exploitation when designing ligand selectivity for $IK_{Ca}3.1$.

Excluded from the sequence analysis was the big conductance K_{Ca} channel, $BK_{Ca}1.1$, which is the least structurally similar of the family. The $BK_{Ca}1.1$ channel does not require calmodulin because it has its own intrinsic Ca^{2+} sensing domain.[14,15] It was therefore unlikely $BK_{Ca}1.1$ would bind the modulator class of small molecules under investigation.

2.1.2 Modelling the IKCa3.1 Modulator Binding Cavity

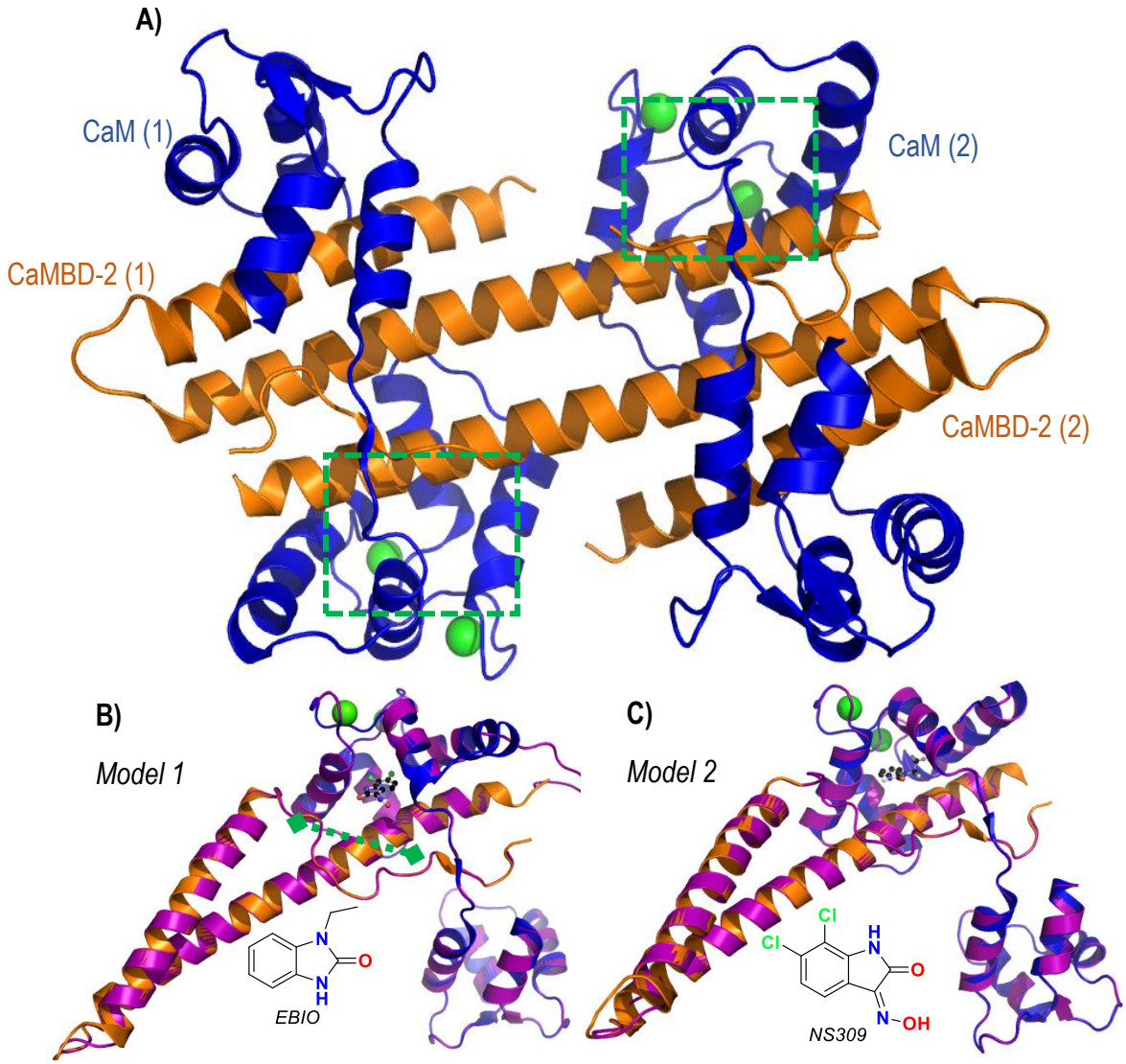


Figure 2.2; Overlay of HS.IK$_{Ca}$3.1 homology models onto r.SK$_{Ca}$2.2 co-crystal template structures; SK$_{Ca}$2.2 CaM in blue helices with bound activating Ca^{2+} as green spheres, CaMBD-2a in orange helices, homolog modelled IK$_{Ca}$3.1 CaM and CaMBD-4 in purple helices. A) Full SK$_{Ca}$2.2 gating complex in Ca^{2+} activated tetrameric form, constitutive CaM:CaMBD interactions highlighted in red dashed boxes, secondary Ca^{2+} induced CaM:CaMBD interactions and known modulator binding cavities highlighted in green dashed (PDB: 4G28). B) and C) (Only modulator binding cavity PPI shown), IK$_{Ca}$3.1 homology models 1 and 2 respectively overlaid in purple helices, SK$_{Ca}$2.2 co-crystal templates with ligands EBIO (PDB: 4G28) and NS309 (PDB: 4J9Z) presented as ball and sticks, undefined loop region highlighted with green dashed line.[16]

A known protein fold was required as a template structure to fit the identified CaMBD-4 sequence, thereby modelling the target IK$_{Ca}$3.1 half of the K$_{Ca}$ binding cavity. The

closely homologous $SK_{Ca}2.2$ 2CaM:2CaMBD-2 gating complex has been co-crystallised with the small molecule positive modulators NS309 (PDB: 4J9Z) and *N*-ethyl benzimidazolone (EBIO) (PDB: 4G28).[16] These $SK_{Ca}2.2$ structures thus served as templates to produce the target $IK_{Ca}3.1$ homology models, Figure 2.2 B and C.

It was important to simultaneously model the primary sequences of both $IK_{Ca}3.1$ CaMBD-4 and CaM to ensure their respective residues did not clash in the resulting model. The open access online server SWISSMODEL (ExPASy, Swiss Institute of Bioinformatics) was used to achieve this.[17,18] The raw protein sequences of CaMBD-4 and CaM were initially fitted to the $SK_{Ca}2.2$ backbones with the freeware DeepView (ExPASy, Swiss Institute of Bioinformatics) before being submitted to SWISSMODEL for modelling of the residue positions.[19] The resulting $IK_{Ca}3.1$ homology models overlaid on their parent template $SK_{Ca}2.2$ crystal structures, as presented in Figure 2.2.

Modelling $IK_{Ca}3.1$ using both $SK_{Ca}2.2$ crystals as templates was advantageous because this produced two homology model 'snapshots' of the target binding cavity for screening. The parent EBIO and NS309 template $SK_{Ca}2.2$ co-crystal structures generated the subsequent $IK_{Ca}3.1$ binding cavity conformers termed model 1 and 2, respectively. A significant difference between the $SK_{Ca}2.2$ co-crystal structures is the missing region of the CaMBD-2a backbone in the EBIO co-crystal shown by the green dashed line in Figure 2.2 B. The same region is observed in the NS309 co-crystal Figure 2.2 C.[20] The NS309 stabilised region is thought to be important in the channel activation mechanism, including a PIP2 binding site.[21,22]

SWISSMODEL provided a 'best guess' predicted conformation for the missing NS309-stabilised region in $IK_{Ca}3.1$ homology model 1, Figure 2.2 B. This homology modelled region may enable the structure-based design of ligands which potentially stabilise it. Designing ligands to purposely disrupt this region may have the effect of

producing negative modulators instead of positive modulators. Unfortunately, modelling of unknown loops is difficult and often flawed. Luckily the modelled loop can be compared to the known loop structure in $SK_{Ca}2.2$ NS309 co-crystal and $IK_{Ca}3.1$ homology model 2.[23] The loop in model 1 was similar to model 2 yet less rigid, thus it was imperative to fully validate the $IK_{Ca}3.1$ models, before they could be used in reliable docking experiments.

Root mean squared deviation (RMSD) analysis was used to validate the $IK_{Ca}3.1$ homology models. The RMSD between atomic positions of the protein backbones in the $IK_{Ca}3.1$ models and their template $SK_{Ca}2.2$ crystal structures was determined in PyMol, Equation 2.1.[24–26]

Equation 2.1

$$RMSD\ (\text{Å}) = \sqrt{\left(\frac{(SUM(d_{ii})^2)}{N}\right)}$$

Where d_{ii} is the distance between ith atom in the template structure and ith atom in the aligned query structure, and N is the number of matched atoms.[27]

The RMSDs of the $IK_{Ca}3.1$ homology models were 0.124 for model 1 and 0.072 for model 2. The RMSDs were not zero because the $IK_{Ca}3.1$ model backbones were necessarily adjusted by SWISSMODEL to accommodate the residue differences. However, both models' RMSDs were less than 1 Å which meant they closely mirrored the known $SK_{Ca}2.2$ protein fold giving confidence in their reliability.

An RMSD cannot be generated for the missing loop sections of homology model 1. Instead, an assessment of all the residue backbone dihedral angles, in model 1 and 2, was made to identify any impossible residue poses. A Ramachandran plot compares the dihedral torsion angles of each residue phi φ and psi ψ bonds in a protein structure to empirically observed residue propensities.[24,28–30] The empirical data indicates these

residue angles localise to 'preferred' regions of the graph, φ vs ψ. Residue angles of reliable protein structures remain within these preferred regions of the plot, whereas, residues with unrealistic orientations lie far outside these regions and are considered practicallyimpossible. Ramachandran plots of the template structures and target $IK_{Ca}3.1$ models were produced in UCSF Chimera, Figure 2.3.

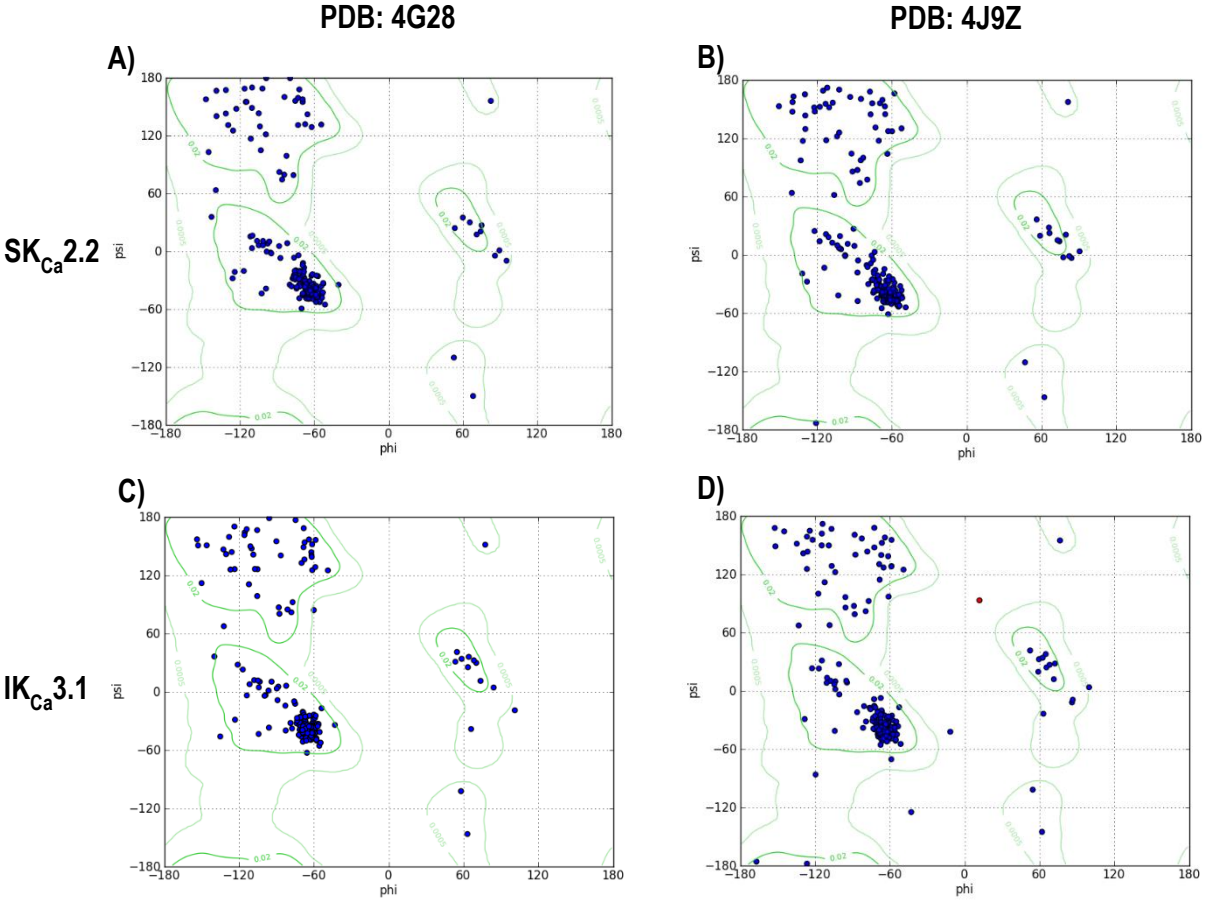


Figure 2.3; Ramachandran plots of $SK_{Ca}2.2$ co-crystal structures and $IK_{Ca}3.1$ homology models. Preferred regions presented within green lines, plots of residue φ and ψ angle relationships shown as blue points. A) and B) Ramachandran plots of the $SK_{Ca}2.2$ EBIO (PDB:4G28) and NS309 (PDB: 4J9Z) co-crystal templates, respectively. C) and D) Ramachandran plots of the $IK_{Ca}3.1$ models 1 and 2, respectively.

The Ramachandran plots of the $SK_{Ca}2.2$ structures, Figure 2.3 A and B, revealed the EBIO co-crystal had 98% preferred residue angles and the NS309 co-crystal had 97% preferred residue angles. This result showed the template structures were reliable for modelling, having very few unlikely residue angles. Despite the sequence residue gaps,

the target $IK_{Ca}3.1$ homology models had only slightly poorer preferred φ and ψ angle values: model 1 and model 2 had 97% and 95% preferred residue angles, respectively. Even though modelling software generates model residue angles to conform to expected Ramachandran propensities, the $IK_{Ca}3.1$ models could not have the same or better preferred residue percentages than their templates. SWISSMODEL necessarily adjusted the new residue angles to accommodate the different CaMBD-4 sidechains, ensuring no clashing occurred in the models due to the 51% sequence identity CaMBD-4 to the CaMBD-2a templates.[17,18]

The results showing the low percentage of unlikely dihedral angles in the $IK_{Ca}3.1$ models, as well as their above 50% sequence ID and low RMSD deviations, validated them as plausable structural approximations for docking.

2.2 Docking Experiments & Rational Design of Novel $IK_{Ca}3.1$ Selective Small Molecule Modulators

Before docking results could be used in design of novel $IK_{Ca}3.1$ ligands, it was necessary to validate them by showing they could reproduce known modulator binding poses. The published K_{Ca} channel modulators were docked against the validated homology models and their template structures. This investigation assessed the models' abilities to correctly dock known K_{Ca} channel binders, validating their ability to predict unknown binders. While quicker and more accessible than molecular dynamics, docking suffers from large errors in scoring function and rigid binding sites, both of which may not reflect the real dynamic biological state.[31–35] Assessment of the $IK_{Ca}3.1$ binding cavity highlighted key residue differences between $IK_{Ca}3.1$ and SK_{Ca} channels aiding development of selective ligand design rationale.

2.2.1 Docking Validation Experiments

Docking computationally models the interactions between a small molecule and the empirically known static structure of a macromolecule, often a protein.[36,37] There are millions of possible small molecule-protein interactions, each of which must be calculated. However, it is not possible to calculate every interaction state, or 'ligand pose', due to the unfeasible time such calculations would take. Therefore, docking experiment sample the total number of possible ligand poses, within a set time. Docking experiments generate random ligand poses, followed by their linear energetic minimisations, to reach the lowest energy minima.[32] Docking experiments predict program specific 'binding scores' for each ligand pose generated, ranking the ligands accordingly. Using docking rankings as an approximate guide, the ligands most likely to bind to the target protein can be prioritised for synthesis over less likely binders.[36] However, each docking program calculates docking scores differently, with different considerations and prioritisation of interactions modelled. Each docking program is therefore more or less suitable to model a particular system.[38–40] The K_{Ca} channel binding cavity is unusual due to its ability to dissociate into two halves, potentially enabling it to be much more or less accommodating than typical enzyme active sites. Thus, two docking software programs were compared for their suitability to model interactions of potential K_{Ca} channel ligands: the free online server SWISSDOCK (ExPASY, Swiss Institute of Bioinformatics) and the commercial software package CLC Drug Discovery Workbench 3 (Qiagen).[41]

Positive control docking experiments were performed to see if each docking software program could identify the crystal positions of NS309 and EBIO as their lowest energy binding poses. These control experiments were also used to validate the $IK_{Ca}3.1$ models' docking results, by comparison, validating their use in docking experiments

aimed at ligand design. Thus, both docking programs were used to dock EBIO and NS309 against their respective $SK_{Ca}2.2$ co-crystal structures and derived $IK_{Ca}3.1$ homology models. The results of the positive controls are presented in Figure 2.4 and Figure 2.5.

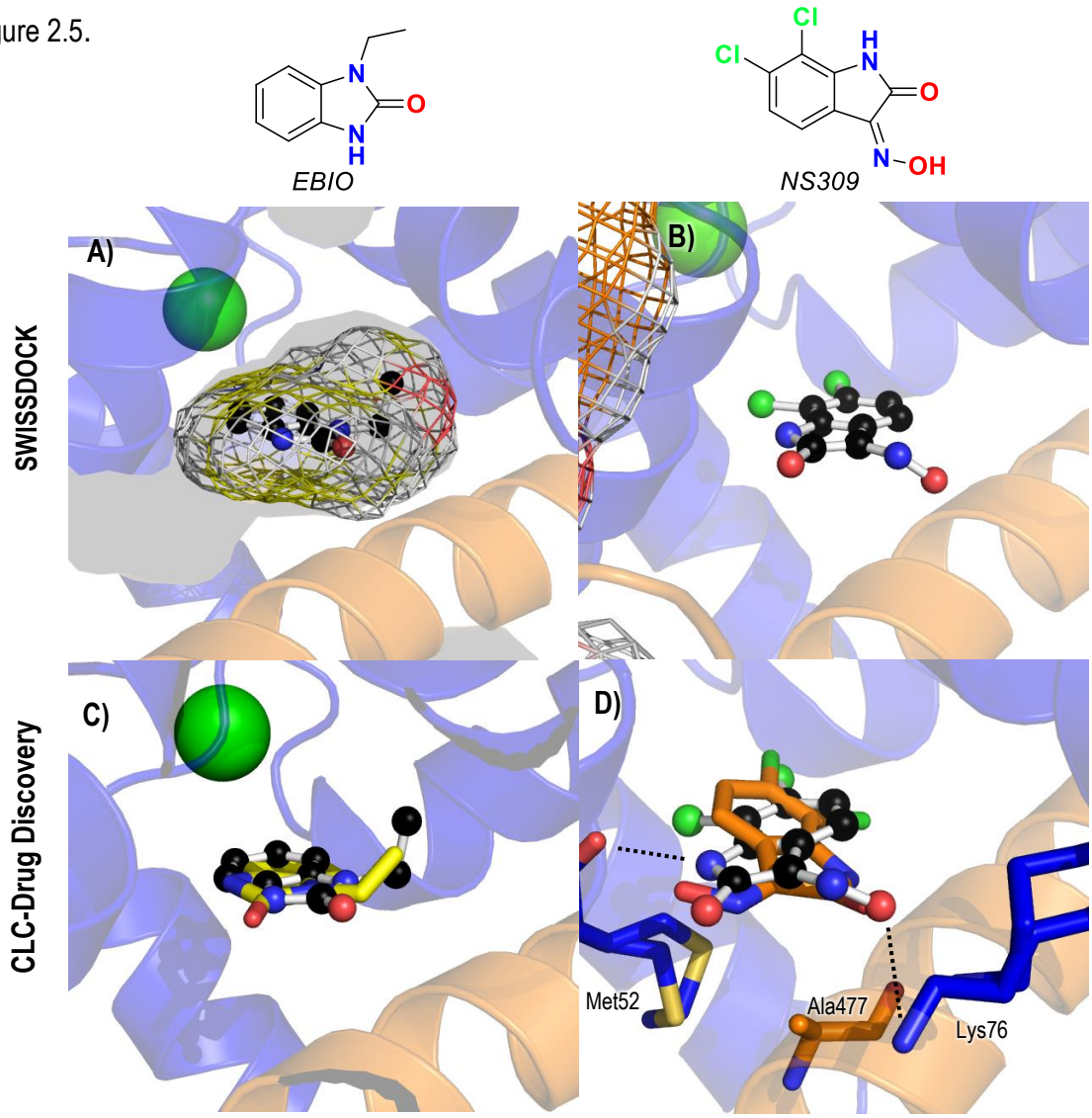


Figure 2.4; Positive control $SK_{Ca}2.2$ co-crystal ligand docking experiments. $SK_{Ca}2.2$ EBIO (PDB: 4G28) and NS309 (PDB: 4J9Z) co-crystals, CaM in blue helices with bound Ca^{2+} in green spheres, CaMBD-2a in orange helices, crystal ligand poses presented in ball and sticks. A) and C) EBIO docking results shown in yellow, SWISSDOCK multiple pose output shown as a density mesh amalgam in the former, CLC-Drug Discovery energy minimised pose output presented as sticks in the latter. B) and D) NS309 docking results shown in orange, SWISSDOCK multiple pose output as a density mesh amalgam in the former, CLC-Drug Discovery energy minimised pose output presented as sticks in the latter, CaM anchor residues Met52 and Lys76 shown as blue sticks, CaMBD-2a Ala477 shown as orange sticks, hydrogen bonds presented as dashed lines.[16]

The SWISSDOCK positive controls predicted EBIO to bind the expected cavity of its native $SK_{Ca}2.2$ co-crystal structure, Figure 2.4 A. The equivalent CLC-Drug Discovery positive controls were also able to dock EBIO close to its crystal position, Figure 2.4 C. However, both docking software programs were unable to correctly predict the binding of NS309 in its native $SK_{Ca}2.2$ co-crystal position. SWISSDOCK incorrectly predicted NS309 to not bind to the protein conformation observed in the crystal structure, Figure 2.4 B. The stabilised loop region in the NS309 $SK_{Ca}2.2$ co-crystal structure, absent from the EBIO co-crystal, may have obstructed ligand access to the binding cavity during SWISSDOCK calculations, Figure 2.2. Unlike SWISSDOCK, CLC-Drug Discovery has the ability to specify the binding cavity before docking, forcing the program to generate the lowest possible binding result within this restricted space, regardless of clashing interactions. CLC-Drug Discovery was, therefore, able to dock NS309 to its native co-crystal structure position, yet in the incorrect orientation, Figure 2.4 D.

The RMSD analysis of the $IK_{Ca}3.1$ homology models showed them to be very similar to their $SK_{Ca}2.2$ template structures. To further validate the $IK_{Ca}3.1$ homology models, the same positive control docking experiments were performed using them, Figure 2.5. While this experiment lacked known ligand crystal positions, compared to the $SK_{Ca}2.2$ controls, the abilities of the two models to bind the closest probable binding ligands were assessed. If the models were unable to dock the positive control ligands, they would be unlikely to accommodate other ligands in later docking experiments.

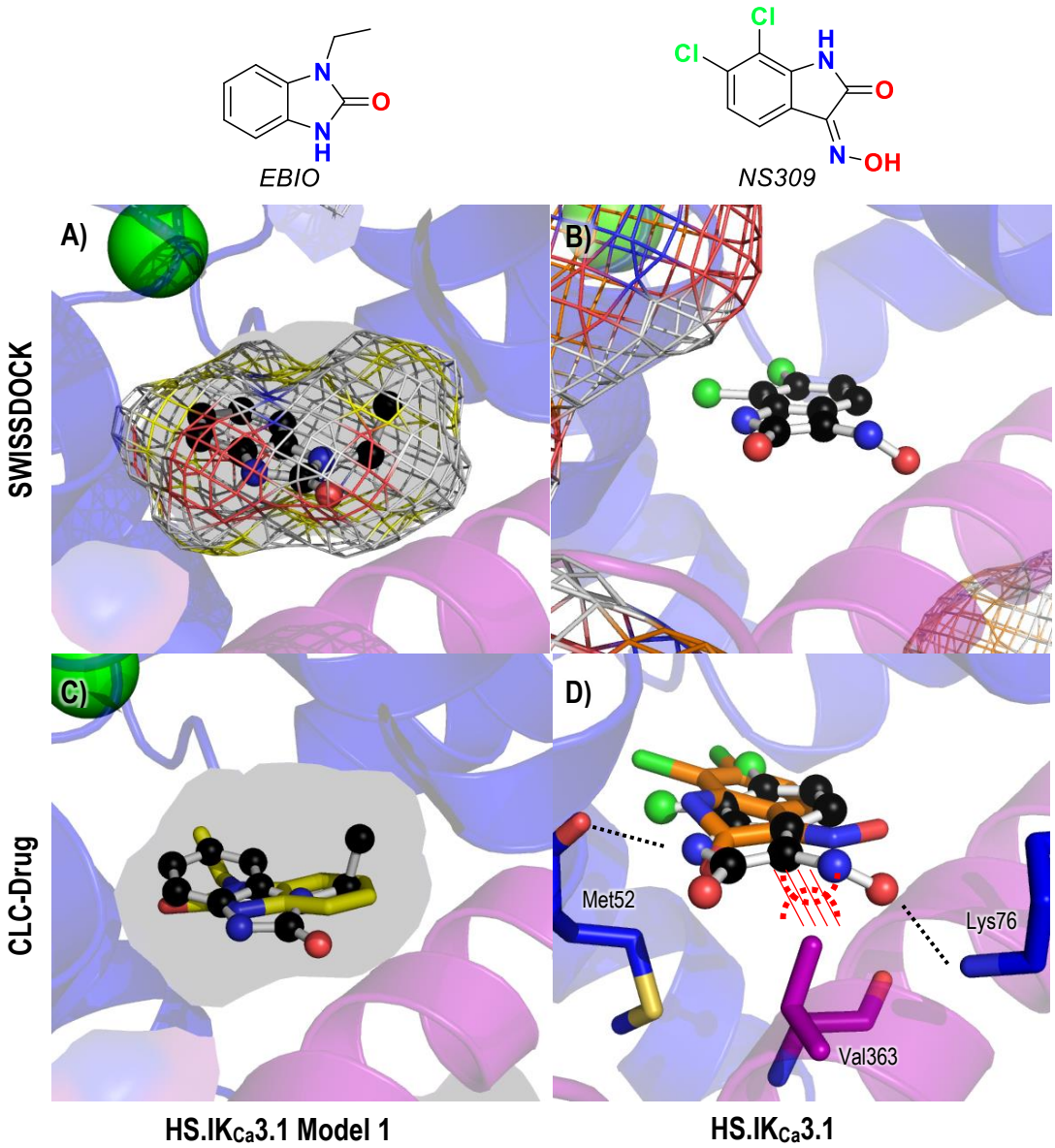


Figure 2.5; Positive control HS.IK$_{Ca}$3.1 docking experiments using putative ligands EBIO and NS309. Known SK$_{Ca}$2.2 ligand positions (EBIO in yellow sticks and NS309 in orange sticks) superimposed on related IK$_{Ca}$3.1 homology models (1 and 2) docking results for comparison. IK$_{Ca}$3.1 model 1, A) and C), from EBIO SK$_{Ca}$2.2 co-crystal template (PDB:4G28) and model 2, B) and D), from NS309 SK$_{Ca}$2.2 co-crystal template (PDB: 4J9Z), CaM in blue helices with bound Ca^{2+} in green spheres, CaMBD-4 in purple helices, imposed crystal ligand poses presented in ball and sticks. A) and C) EBIO docking results shown in yellow, SWISSDOCK multiple pose output as a density mesh amalgam in the former, CLC-Drug Discovery energy minimised pose output presented as sticks in the latter. B) and D) NS309 docking results shown in orange, SWISSDOCK multiple pose output as a density mesh amalgam in the former, CLC-Drug Discovery energy minimised pose output presented as sticks in the latter, CaM anchor residues Met52 and Lys76 shown as blue sticks, CaMBD-4 Val363 shown as purple sticks and potential clashing interaction with ligand highlighted in red, hydrogen bonds presented as black dashed lines.

The results for the $IK_{Ca}3.1$ homology model positive docking controls were very similar to those of the $SK_{Ca}2.2$ structures, providing further evidence that the $IK_{Ca}3.1$ models remained structurally similar to their templates. The SWISSDOCK homology model results mirrored the previous $SK_{Ca}2.2$ control results, where EBIO was correctly docked in the binding cavity yet NS309 was not, Figure 2.5 A and B.

The CLC-Drug Discovery results also mirrored the $SK_{Ca}2.2$ results, where both EBIO and NS309 were docked in the predicted $IK_{Ca}3.1$ binding cavity, Figure 2.5 C and F. Notably, NS309 was docked in the correct orientation in the $IK_{Ca}3.1$ model 2, however, it was unable to form the same hydrogen bonds (H-bonds) to CaM Met52 and Lys76 as in the template $SK_{Ca}2.2$ co-crystal. This result highlighted the first important difference between SK CaMBDs and $IK_{Ca}3.1$ CaMBD-4, a residue change of Ala in the former to Val363 in the latter. The larger Val363 of CaMBD-4 appears to close the entrance to the $IK_{Ca}3.1$ binding cavity pocket and clashes with the $SK_{Ca}2.2$ predicted ligand positions.

A second control docking experiment was conducted to determine the $IK_{Ca}3.1$ models' promiscuity to binding other ligands. The EBIO and NS309 modulators were docked with both docking programs against the opposite $IK_{Ca}3.1$ models, 1 and 2, respectively. Unsurprisingly, in SWISSDOCK, $IK_{Ca}3.1$ model 2 did not accommodate the EBIO ligand, yet fortunately model 1 accommodated NS309. This result showed model 1 had a larger binding cavity than model 2, making it more accommodating in docking. An accommodating binding cavity is important because ligand size generally increases throughout the optimisation process due to the addition of new functional groups, increasing affinity and specificity for the target protein.[42,43] Predictably, the CLC-Drug

Discovery docked both ligands into both $IK_{Ca}3.1$ homology models, due to the ability to specify the binding site.

CLC-Drug Discovery uses the docking algorithm PLANTS to score ligand interactions compared to SWISSDOCK which uses the algorithm EADock.[40,44,45] The algorithm PLANTS allows for some sidechain flexibility when accommodating a ligand and more realistically models ligand interactions than EADock, which does not.[33] Due to this flexibility and based on the control docking experiments, subsequent screening of ligand analogues was focused on the EBIO $SK_{Ca}2.2$ crystal structures and corresponding $IK_{Ca}3.1$ homology model 1 using CLC-Drug Discovery.

NS309 was still orientated incorrectly in the $IK_{Ca}3.1$ model 1 docking result, compared to the known ligand position of the $SK_{Ca}2.2$ co-crystal template. It is important to note: NS309 is over 10-fold more selective for $IK_{Ca}3.1$ than SK_{Ca} channels, and the most potent K_{Ca} modulator, with an $IK_{Ca}3.1$ EC_{50} of 20 nM.[46] The two $SK_{Ca}2.2$ conformations, represented by the two co-crystal structures, demonstrate the flexibility of the K_{Ca} channel modulator binding cavity. It could be surmised that CLC-Drug Discovery, while able to allow for side chain flexibility, cannot model the degree of protein flexibility needed to accurately predict ligand interactions.

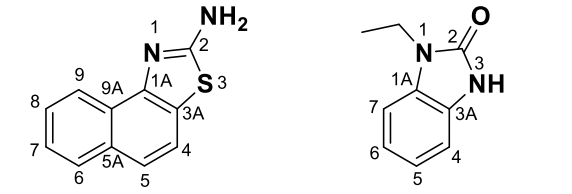


Figure 2.6; Primary hit naphthothiazole and secondary hit benzimidazolone cores.

The entire published naphthothiazole and benzimidazolone series of core analogues were docked against the EBIO $SK_{Ca}2.2$ crystal structure and its corresponding $IK_{Ca}3.1$

homology model 1, Figure 2.7 and Table 2.2 (page 45). This last control experiment aimed to expand on the second docking control experiment and give further evidence of the promiscuity of the $IK_{Ca}3.1$ binding cavity. The CLC-Drug Discovery docking scores versus screened ligand properties were plotted as scatter graphs to highlight any possible correlations, Figure 2.7. The published modulators' properties are all fragment-like: weights under 300 Da, fewer than 3 H-bond donors or acceptors, fewer than three rotatable bonds; yet many have LogP values above three.[47] This set of property restrictions may be due to the relatively small size of the $SK_{Ca}2.2$ or $IK_{Ca}3.1$ binding cavities. The cavities are largely hydrophobic with almost no polar residues and no static waters observed in the crystals. The ligand parameters plotted were, therefore, LogP and molecular weight, to see if these did affect docking scores.

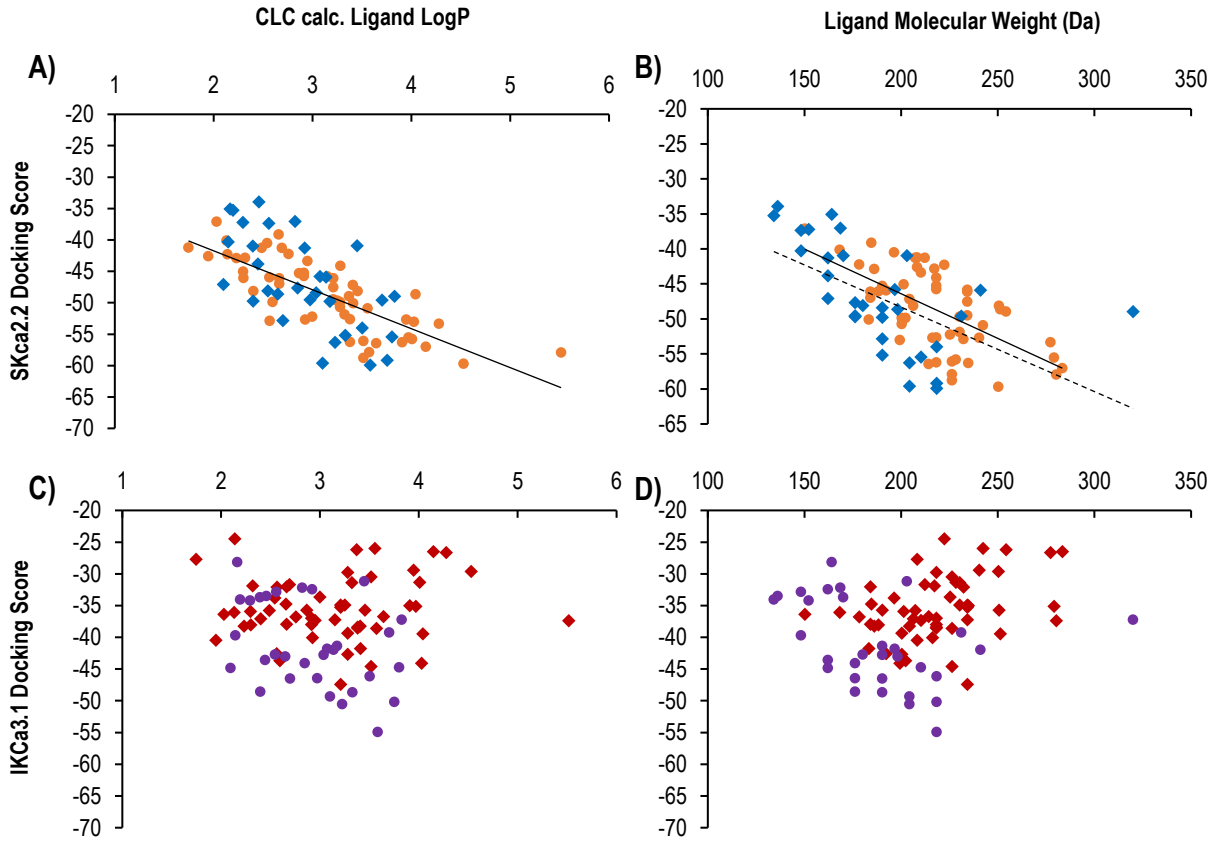


Figure 2.7; Correlation of ligand properties verses docking scores. Docking scores generated in CLC-Drug Discovery, increasingly negative scores predict increasing ligand binding potential. A), and B) $SK_{Ca}2.2$ docking scores (PDB: 4G28), benzimidazolone ligand scores presented in blue with dashed linear regressions and naphthothiazole ligand scores presented in orange with solid linear regressions. D) and C) $IK_{Ca}3.1$ docking scores (model 1), benzimidazolone ligand scores presented in purple, naphthothiazole ligand scores presented in red.

The predicted binding scores of the published benzimidazolone and naphthothiazole analogues, docked against the EBIO $SK_{Ca}2.2$ co-crystal structure, revealed positive correlations in ligand molecular weight and hydrophobicity with binding affinity, Figure 2.7 A and B. A larger lipophilic molecule may better fill a hydrophobic binding cavity and with increased affinity due to the greater entropic gain of a larger ligand's desolvation. By contrast, the corresponding $IK_{Ca}3.1$ model 1 docking results displayed almost no trends for either ligand series, Figure 2.7 C and D. The difference in ligand trends between $SK_{Ca}2.2$ and $IK_{Ca}3.1$, highlighted the effect of the CaMBD-4 residue changes in the

binding cavity. CaMBD-4 Val363 closes the binding cavity entrance and may remove the gain in predicted affinity through increased ligand size.

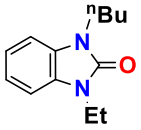
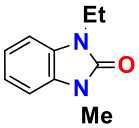
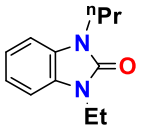
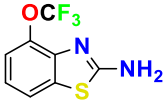
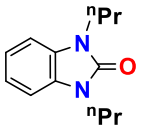
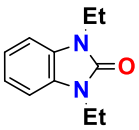
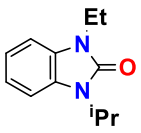
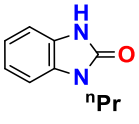
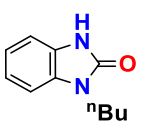
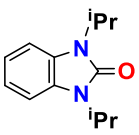
Both the benzimidazolone and naphthothiazole ligand series generally preferred the $SK_{Ca}2.2$ binding cavity compared to $IK_{Ca}3.1$, Figure 2.7 and Table 2.2. These results were unexpected as both ligand series display greater selectivity for the $IK_{Ca}3.1$ channel over the SK_{Ca} channels. The 100-fold $IK_{Ca}3.1$ selective published naphthothiazole SKA111 had a significantly higher potential binding score for $SK_{Ca}2.2$ compared with $IK_{Ca}3.1$.[48] Using docking to predict selectivity between $SK_{Ca}2.2$ vs $IK_{Ca}3.1$ was, therefore, not demonstrated in the last control experiment.

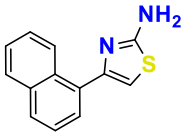
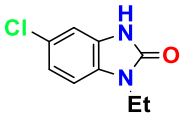
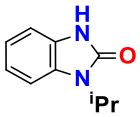
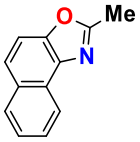
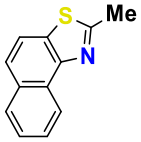
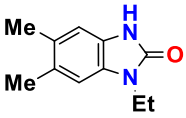
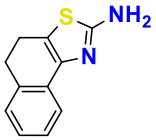
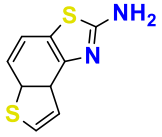
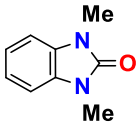
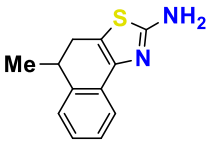
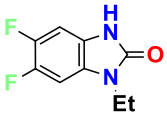
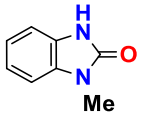
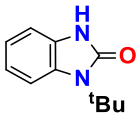
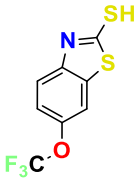
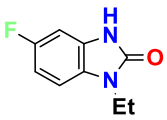
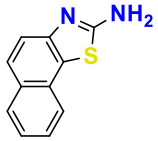
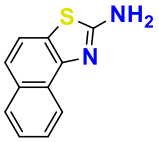
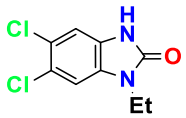
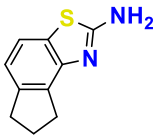
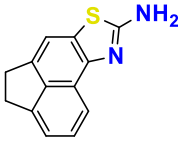
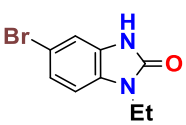
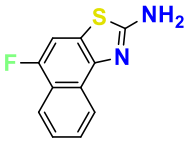
Out of the published analogues of both the benzimidazolone and naphthothiazole cores, those empirically determined to be biologically inactive, were unexpectedly predicted by docking to have some of the highest binding scores, and *vice versa.* Docking only calculates the interaction between ligand and protein, not the effectiveness of a ligand on protein function. All of the published data for the modulator molecules is given in half maximal effective concentrations (EC_{50}s) generated in biological assays. Additionally, only positive channel modulation was observed, not negative modulation. The lack of docking score differentiation between modulators like SKA111 and EBIO did not reflect their reported EC_{50} values, suggesting that the scoring function does not accurately model the $IK_{Ca}3.1$ native *in vivo* binding state.

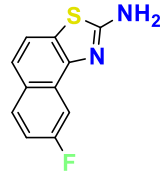
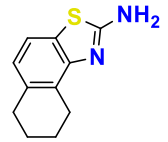
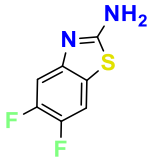
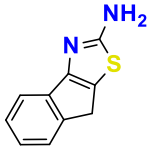
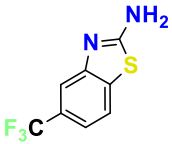
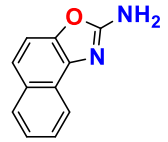
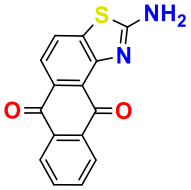
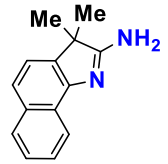
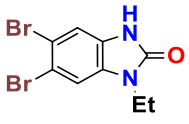
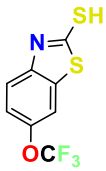
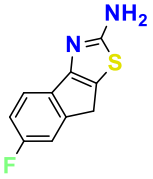
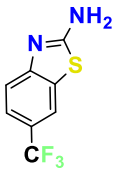
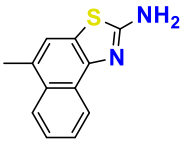
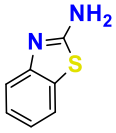
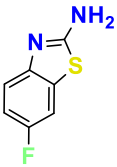
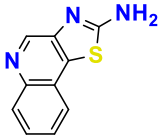
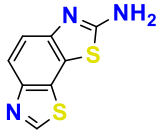
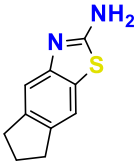
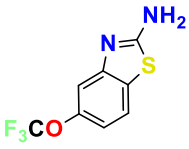
It is possible that the energetic contribution of ligand displacement of unstructured waters in the lipophilic binding cavity, not revealed by crystallography, may also be the cause for the failure of the docking experiments to accurately predict known ligand interaction. As trapped waters are displaced they are able to hydrogen bond with other solution waters and so stabilise their polar bonds. Docking of $IK_{Ca}3.1$ modulators could have failed due to the modelled clashing of CaMBD-4 Val363, which may suggest the

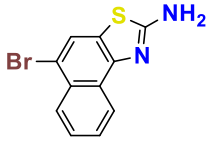
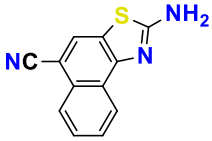
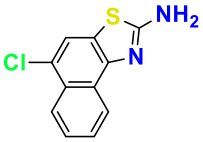
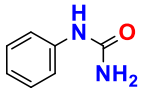
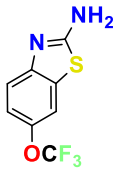
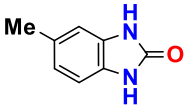
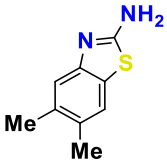
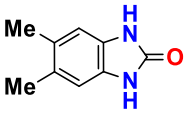
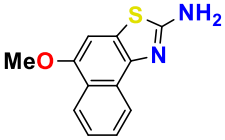
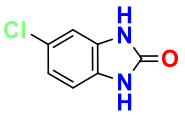
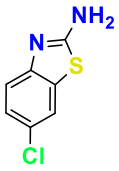
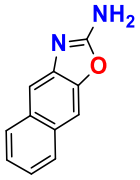
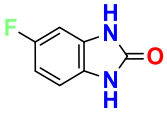
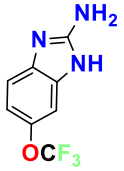
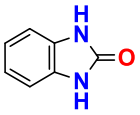
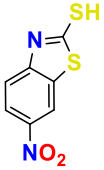
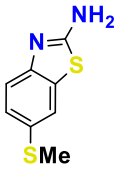
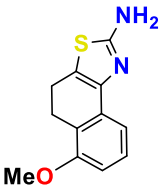
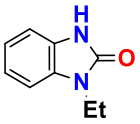
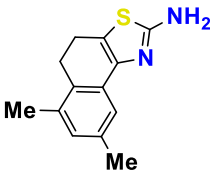
binding cavity is more relaxed and accommodating in reality. Another possible reason could be these putative modulators effect $IK_{Ca}3.1$ by another binding site or they do not bind this target at all. Homology modelling and computational docking cannot disprove empirical data because they are purely theoretical. Thus, docking scores were not used, instead a more traditional medicinal chemistry rational design approach was taken.

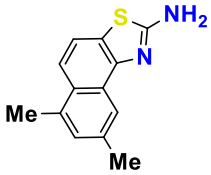
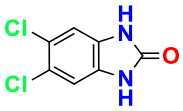
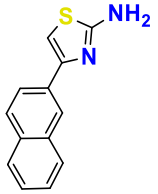
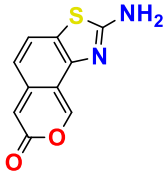
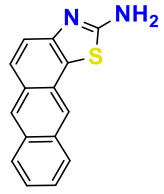
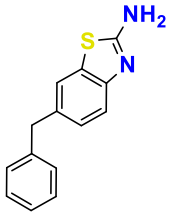
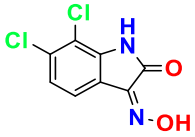
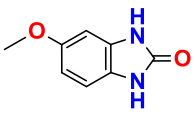
*Table 2.2; List of published naphthothiazole and benzimidazolone modulator analogues in descending order of $IK_{Ca}3.1$ CLC-Drug Discovery calculated docking score. Published $IK_{Ca}3.1$ EC_{50} values given where applicable.[48] Where EC_{50}s remain unpublished, published raw data is given in italics. Published $IK_{Ca}3.1$ ligand (60 μM) relative activities determined by $^{84}Rb^+$ uptake denoted with * and italics. Published $IK_{Ca}3.1$ ligand (100 μM) enhanced slope conductance determined by whole cell patch clamp (-80 mV) denoted by † and italics.*

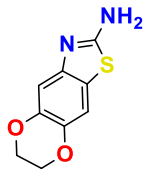
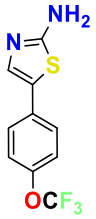
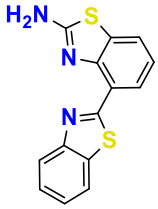
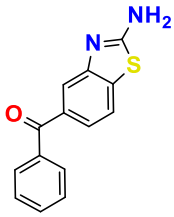
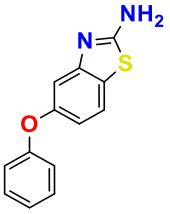
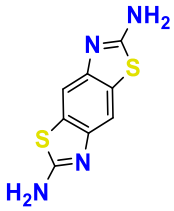
Structure	MW	LogP	EC_{50} (μM)	$SK_{Ca}2.2$ Score	$IK_{Ca}3.1$ Score	Structure	MW	LogP	EC_{50} (μM)	$SK_{Ca}2.2$ Score	$IK_{Ca}3.1$ Score
	218	3.6	*0.61**	-60	-55		176	2.4	*0.00**	-50	-49
	204	3.2	*0.00**	-56	-51		234	3.2	*26†*	-49	-47
	218	3.8	*0.48**	-59	-50		190	2.7	*0.58**	-53	-46
	204	3.1	*0.80**	-60	-49		176	3.0	*0.74**	-50	-46
	190	3.3	*0.52**	-55	-49		218	3.5	*0.19**	-54	-46

Structure	MW	LogP	EC_{50} (μM)	$SK_{Ca}2.2$ Score	$IK_{Ca}3.1$ Score	Structure	MW	LogP	EC_{50} (μM)	$SK_{Ca}2.2$ Score	$IK_{Ca}3.1$ Score
	226	3.5	21.00	-59	-45		197	3.1	*2.04**	-46	-42
	176	2.8	*0.00**	-48	-44		183	3.4	7.80	-50	-42
	199	4.0	7.80	-53	-44		190	3.2	*0.93**	-50	-41
	202	2.6	2.10	-50	-44		208	1.9	1.20	-43	-40
	162	2.4	*0.42**	-44	-44		216	2.9	1.00	-53	-40
	198	2.6	*1.03**	-49	-43		148	2.1	*0.74**	-40	-40
	190	3.0	*0.16**	-48	-43		251	4.0	*23†*	-49	-39
	180	2.5	*1.43**	-48	-43		200	3.3	Ins.	-50	-39
	200	3.3	0.26	-51	-43		231	3.7	0.80	-50	-39
	192	2.6	0.70	-46	-43		226	3.6	1.10	-58	-39
	241	3.1	*1.35**	-46	-42		218	3.4	2.00	-56	-39

Structure	MW	LogP	EC_{50} (μM)	$SK_{Ca}2.2$ Score	$IK_{Ca}3.1$ Score
	218	3.4	4.60	-53	-38
	204	3.4	*36†*	-47	-38
	186	2.2	*14†*	-43	-38
	188	2.3	20	-46	-38
	218	2.9	*32†*	-45	-38
	184	2.7	50.00	-47	-38
	280	5.5	Ins.	-58	-37
	210	3.0	>50	-43	-37
	320	3.8	*1.13**	-49	-37
	234	3.2	*23†*	-46	-37
	206	2.4	15.00	-48	-37
	218	2.9	N.D.	-46	-37
	214	3.6	0.11	-56	-37
	150	2.0	*35†*	-37	-36
	168	2.1	*39†*	-40	-36
	201	2.3	*5†*	-45	-36
	207	2.5	*35†*	-41	-36
	251	3.5	*19†*	-48	-36
	190	2.9	*32†*	-45	-36
	234	3.2	*34†*	-46	-35

Structure	MW	LogP	EC_{50} (μM)	$SK_{Ca}2.2$ Score	$IK_{Ca}3.1$ Score	Structure	MW	LogP	EC_{50} (μM)	$SK_{Ca}2.2$ Score	$IK_{Ca}3.1$ Score
	279	4.0	Ins.	-56	-35		225	3.0	1.20	-52	-34
	235	3.9	2.00	-56	-35		136	2.5		-34	-33
	234	3.2	10.00	-48	-35		148	2.6	*0.00**	-37	-33
	178	2.8	*35†*	-42	-37		162	2.9	*0.10**	-41	-32
	230	3.3	0.90	-50	-35		169	2.8	*0.29**	-37	-32
	185	2.7	*41†*	-39	-35		184	2.7	>50	-46	-32
	152	2.3	*0.00**	-37	-34		217	2.3	*34†*	-43	-32
	134	2.2	*0.00**	-35	-34		212	2.7	*15†*	-41	-32
	196	2.5	*29†*	-41	-34		232	2.6	3.80	-53	-32
	170	2.4	30.00	-41	-34		230	3.3	2.00	-52	-31

Structure	MW	LogP	EC_{50} (μM)	$SK_{Ca}2.2$ Score	$IK_{Ca}3.1$ Score
	228	4.0	2.40	-56	-31
	203	3.4	*0.21**	-41	-31
	226	3.5	>50	-56	-30
	218	3.3	N.D.	-44	-30
	250	4.5	Ins.	-60	-30
	240	3.9	*14†*	-53	-29
	231	5.1	0.02	-40	-28
	164	2.2	0.10	-35	-28

Structure	MW	LogP	EC_{50} (μM)	$SK_{Ca}2.2$ Score	$IK_{Ca}3.1$ Score
	208	1.7	N.E.	-41	-28
	260	4.3	*1†*	-53	-27
	283	4.1	Ins.	-57	-26
	254	3.4	Ins.	-49	-26
	242	3.6	N.E.	-51	-26
	222	2.1	N.E.	-42	-24

2.2.2 Binding cavity Assessment & Novel IKCa3.1 Selective Ligand Design

The residues: Ala477, Leu480 and Ala487, from CaMBD-2a contributing to the $SK_{Ca}2.2$ binding cavity are different in the $IK_{Ca}3.1$ CaMBD-4: Val363, Met366 and Ser487, Figure 2.8. The last residue contributing to the binding domain remains the same between $SK_{Ca}2.2$ and $IK_{Ca}3.1$: Val484 in the former and Val367 in the latter.

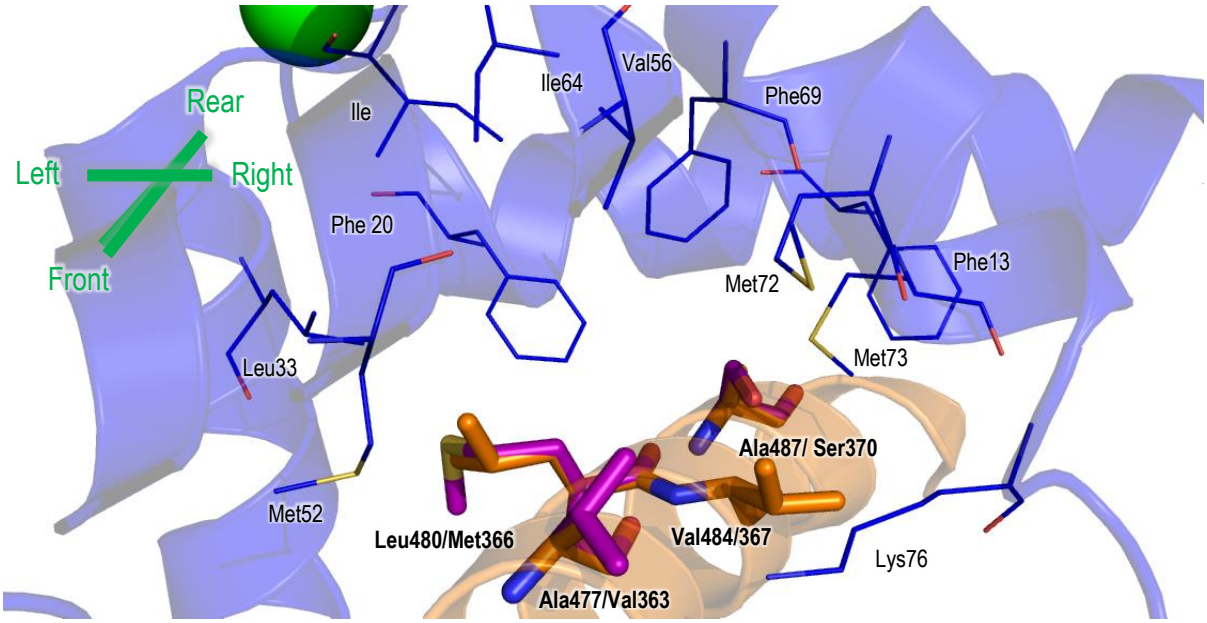


Figure 2.8; Residue differences between $SK_{Ca}2.2$ and $IK_{Ca}3.1$ model 1 modulator binding cavities. CaM presented in blue helices, CaMBD-2a presented in orange helices (PDB: 4G28), CaM modulator binding cavity residues shown in blue lines, CaMBD-2a residues shown as orange sticks and corresponding CaMBD-4 residues shown as purple sticks.[16]

The modulator-binding cavity shape of $IK_{Ca}3.1$ model 1 was predicted to be subtly different from the $SK_{Ca}2.2$ cavity. As seen in Figure 2.8, the change in shape is caused by the important residue differences between the channels.

The first and most prominent residue difference is a change from the $SK_{Ca}2.2$ CaMBD-2 Ala477 to Val363 in the $IK_{Ca}3.1$ CaMBD-4. Valine is a larger residue compared to alanine and while it does not introduce the sought-after polar groups for ligand interaction, it does appear to close the $IK_{Ca}3.1$ modulator binding cavity. A closed

binding cavity means ligands of $IK_{Ca}3.1$ are restricted to a potential maximum size before residue clashing disfavours binding.

The Leu480 to Met366 change in the target $IK_{Ca}3.1$ binding cavity, does not introduce new polar groups. However, this mutation does alter the modulator binding cavity spatially. SWISSMODEL approximated the spatial arrangement of Met366, suggesting the binding cavity of $IK_{Ca}3.1$ may be larger towards the left side than the $SK_{Ca}2.2$ cavity. This observation could account for some of the $IK_{Ca}3.1$ selectivity of the published naphthalene based modulator series.[4,48]

The final and significant change of Ala487 at the back of the $SK_{Ca}2.2$ binding cavity to Ser370 in the $IK_{Ca}3.1$ cavity gave the opportunity to gain a target specific ligand H-bond. This observation lead to the hypothesis: designing ligands with polar groups orientated towards Ser370 would generate $IK_{Ca}3.1$ selectivity over $SK_{Ca}2.2$.

The published positive modulator with the greatest selectivity for the target channel $IK_{Ca}3.1$ is SKA111 with an EC_{50} value of 0.1 µM, and an EC_{50} value of 7.7 µM for $SK_{Ca}2.2$. [48] Therefore**,** SKA111 was chosen as the starting point hit for optimisation, because docking screening had not been corroborated, and no method of biophysical screening was yet developed to identify any alternatives.

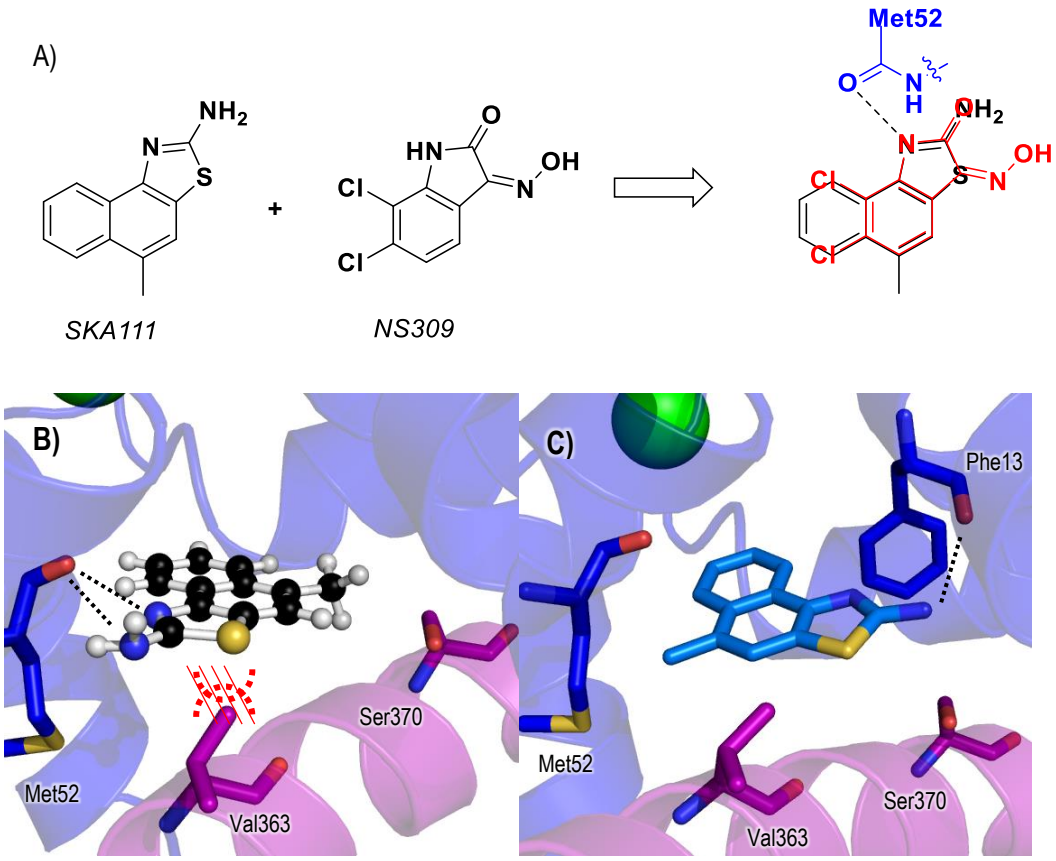


Figure 2.9; SKA111 putative binding orientation vs CLC-Drug Discovery docking prediction, using $IK_{Ca}3.1$ model 1. CaM represented in dark blue helices, CaMBD-4 presented as purple helices, hydrogen bonds shown as dashed lines. A) Structural similarities of SKA111 and NS309 suggesting similar binding modes, , clashing interaction with Val363 indicated with red hashed semi-circles. B) Putative SKA111 binding orientation, SKA111 presented as black ball and sticks, CaM Met52 presented as grey sticks. C) Docked SKA111 pose shown as blue sticks.[10,48]

The binding orientation of SKA111 has been proposed to closely mimic that of NS309, and form a similar H-bond interaction to the backbone carbonyl of CaM Met52, Figure 2.4 and Figure 2.9 B.[10,20] CLC-Drug Discovery predicted a very different SKA111 binding pose with a score of −37, involving no Met52 H-bond interaction. This predicted pose is possibly due to the previously noted clashes with CaMBD-4 Val363, Figure 2.9 C. While CLC-Drug Discovery calculates docking poses using the PLANTS algorithm, allowing for residue side chain flexibility, protein flexibility is not as well modelled. Therefore, it cannot be ruled out that SKA111 binds as NS309 does to SKCa2.2. The SKA111

predicted binding pose may not be correctly orientated, as NS309 wasn't in the IKCa3.1 model 1 positive control experiment, Figure 2.4.

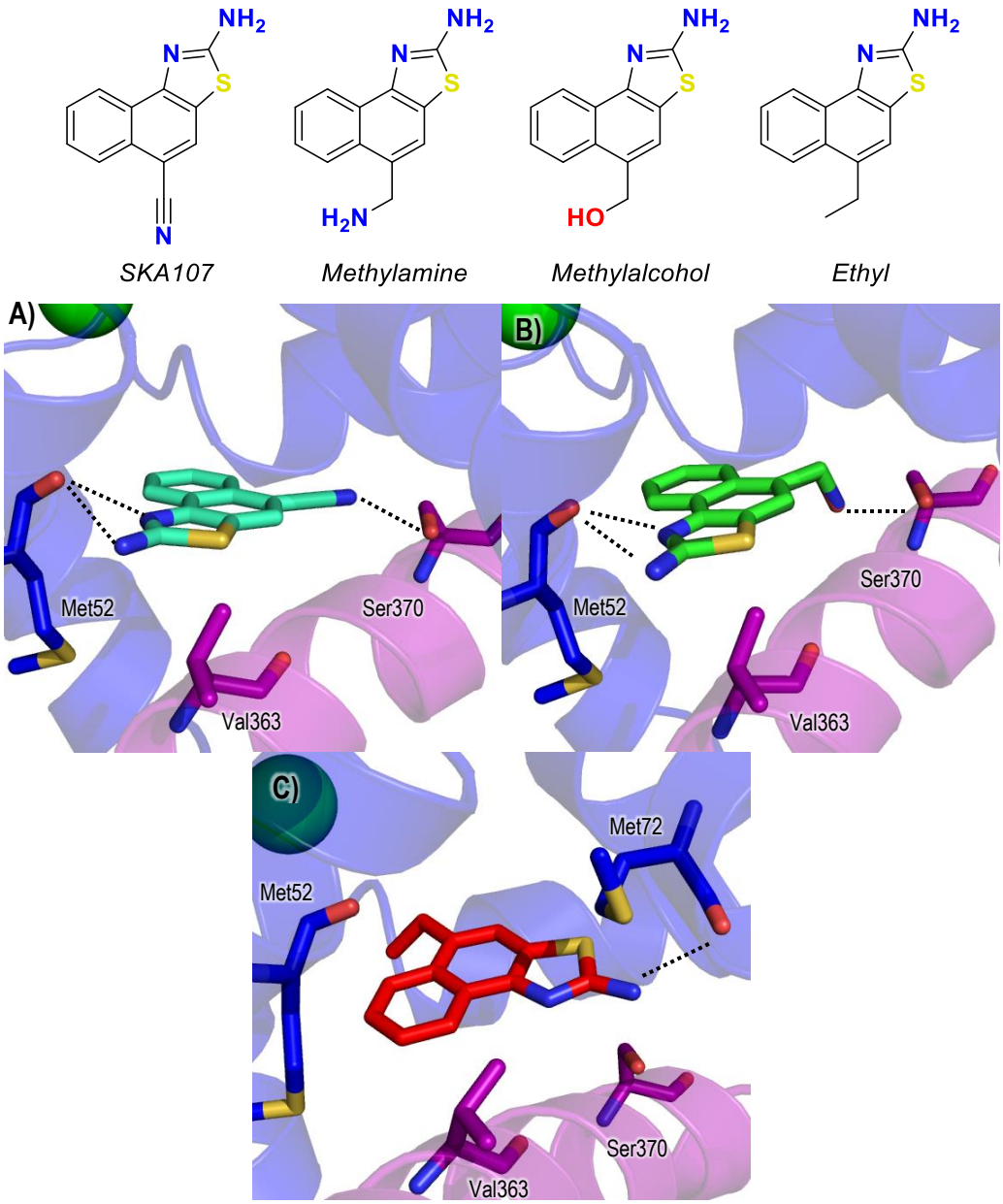


Figure 2.10; Predicted SKA107–Ser370 hydrogen bond and subsequent ligand optimisation, using CLC-Drug Discovery docking and $IK_{Ca}3.1$ model 1. CaM represented as blue helices, $IK_{Ca}3.1$ CaMBD-4 presented as purple helices, CaM Met72, anchor residue Met52 and CaMBD-4 Ser370 residue of interest presented in sticks, hydrogen bonds shown as dashed lines. A) Docked SKA107 modulator presented as cyan sticks. B) Docked novel methylamine analogue presented in light green sticks and methylalcohol analogue in dark green sticks. C) Docked novel ethyl analogue presented in red sticks.

The first docked ligand, predicted by CLC-Drug Discovery to H-bond Ser370 of CaMBD-4, was SKA107 with a binding score of −34, a published naphthothiazole modulator.[48] SKA107 was predicted to form a H-bonded bridge between the CaM residue, Met52, and CaMBD-4 residue, Ser370, Figure 2.10 A. It was subsequently hypothesized: by linking the two macromolecules that form the $IK_{Ca}3.1$ modulator binding cavity with a H-bonded ligand bridge, their protein-protein interaction may be stabilised.

H-bond acceptor lone pairshave direction around their parent atom, defined by its molecular hybrid sp^2 orbitals. Orbital direction requires that H-bonds involving lone pairs have good orbital overlap with the H-bond donor, requiring a linear geometry between bonded groups.[49] While the atoms involved in the predicted polar interactions between SKA107 and binding cavity residues were within possible H-bond distances, their H-bond geometries were poor. SKA107 is a long, flat, rigid molecule and, to satisfy the predicted H-bonds, the ligand may forcibly distort the associated residues and shape of the binding cavity, formed between CaM and CaMBD-4. Distortion of the binding cavity could weaken the protein-protein interaction, instead of strengthening it. If true, this distorting effect may explain SKA107's lower binding score compared to SKA111, which cannot H-bond Ser370.[48]

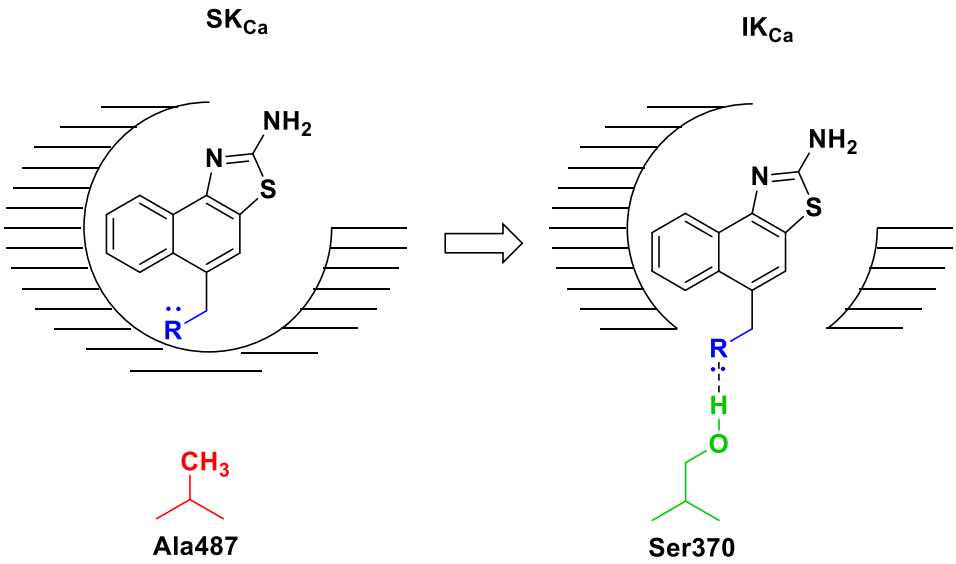
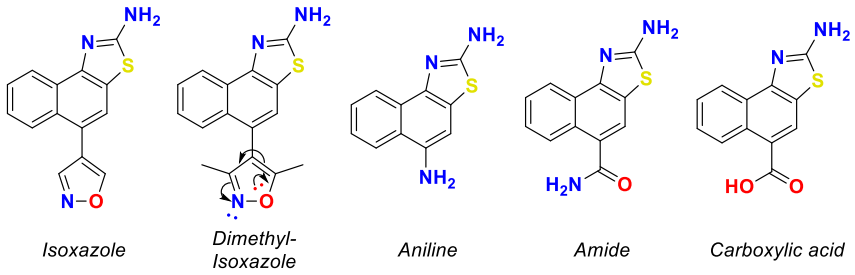


Figure 2.11; Naphthothiazole analogue design hypothesis: Hydrogen bond capable analogues will gain new interaction with IK_{Ca}3.1 Ser487 which is absent in SK_{Ca}2.2 binding cavity and so selectively bind the former. R H-bond acceptor or donor groups.

Designing ideal ligands to form a H-bonded bridge between Met52(CaM) and Ser370(CaMBD-4), led to the structural optimisation SKA107 to the methylamine and methylalcohol analogues, Figure 2.10 B and Figure 2.11.The non-flat geometries of the amine and alcohol analogues enabled predicted poses with better H-bonded angles than SKA107, displayed by their −37 docking scores. The positions of the H-bonded ligand atoms had better angles and closer interatomic distances to Ser370. It was additionally hypothesised: naphthothiazole analogues with polar groups would be prevented from binding the SK_{Ca}2.2 binding

The ethyl naphthothiazole analogue, was designed as a negative control, unable to H-bond Ser370. The ethyl analogue was orientated in the same non-clashing position as the previous docking result for SKA111, with a binding score of −40, Figure 2.10 C. The apparent improvement of the ethyl analogue's binding score over SKA111 may be due to better cavity filling. Based on the similarity between the ethyl analogue and SKA111 docking results, their activities may also be similar.



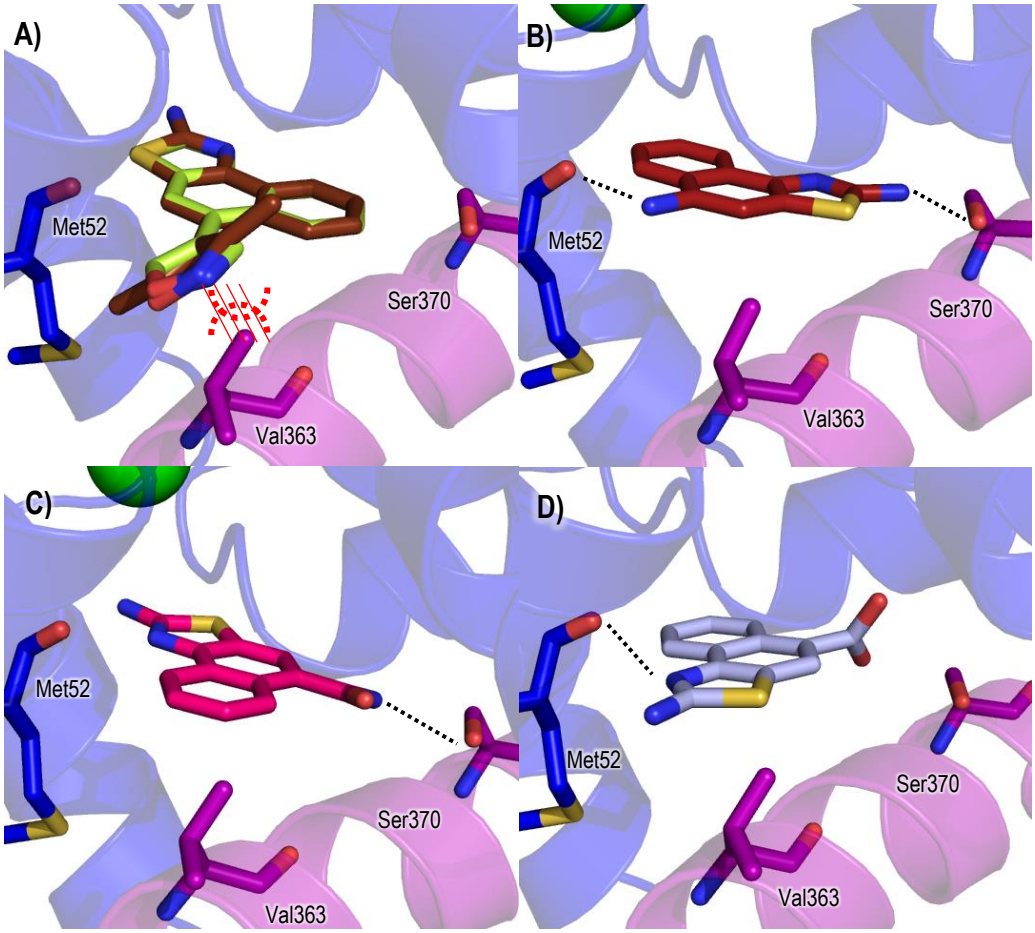


Figure 2.12; Exploration of Met52(CaM)-Ser370(CaMBD-4) hydrogen bond bridging naphthothiazole analogues. CaM represented as blue helices, $IK_{Ca}3.1$ CaMBD-4 presented as purple helices, CaM Phe13, CaM anchor residue Met52 and CaMBD-4 Ser370 and Val363 residues of interest presented as sticks, hydrogen bonds shown as dashed lines. A) Docked isoxazole analogue presented as lemon sticks and dimethyl isoxazole presented as brown sticks, clashing interaction with Val363 indicated with red hashed

semi-circles. B) Docked aniline analogue presented as maroon sticks. C) Docked amide analogue presented as pink sticks. D) Docked carboxylic acid analogue presented as light blue sticks.

Isoxazole is a heteroaromatic cycle due to the donation and delocalisation of an oxygen lone pair around the ring's π system. The resonance state representing this lone pair donation places a negative charge on nitrogen, suggesting it has greater electron density than in other nitrogen containing aromatic systems like pyridine. The greater electron density of nitrogen in isoxazole enables it to better accept hydrogen bonding for donors. Thus, an isoxazole analogue was designed to H-bond Ser370. Isoxazoles, 68 g/mol, are much larger than the designed methylamino, 30 g/mol, and methylalcohol, 31 g/mol, groups. However, if the target binding cavity is much more flexible than docking predicts isoxazoles may be accommodated. 3,5-Dimethyl substituted isoxazoles are larger still, 96 g/mol, yet they are more stable and synthetically tractable than unprotected isoxazoles and so were also designed. Unsurprisingly docking the isoxazole and dimethyl isoxazole analogues clashed heavily with Val363 and did not fit within the binding cavity of model 1 giving relative low binding scores −22 and −10, respectively, Figure 2.12 A.

The docked amide analogue was predicted to bind CaMBD-4 Ser370, achieving a score of -30. The amide was predicted to bind in a similar pose to the SKA111 docking result, avoiding Val363 and making more use of the potentially larger left side target cavity, Figure 2.12 C. The carboxylic acid analogue was predicted to bind to CaM Met52, with a binding score of −27. However, the acid was predicted to bind to another CaM residue, Phe13, instead of CaMBD-4 Ser370. This interaction could have unusual target effects, such as negative channel modulation, Figure 2.12 D. The aniline analogue, shorter than the nitrile, methylamine or alcohol was predicted to bridge both Met52 and Ser370. The aniline conformed most with the previously stated hypothesis, explaining the binding score, −41, Figure 2.12 B. Despite its shorter length and retained rigidity, the

aniline analogue may have increased its score because its smaller size clashed less with CaMBD-4 Val363.

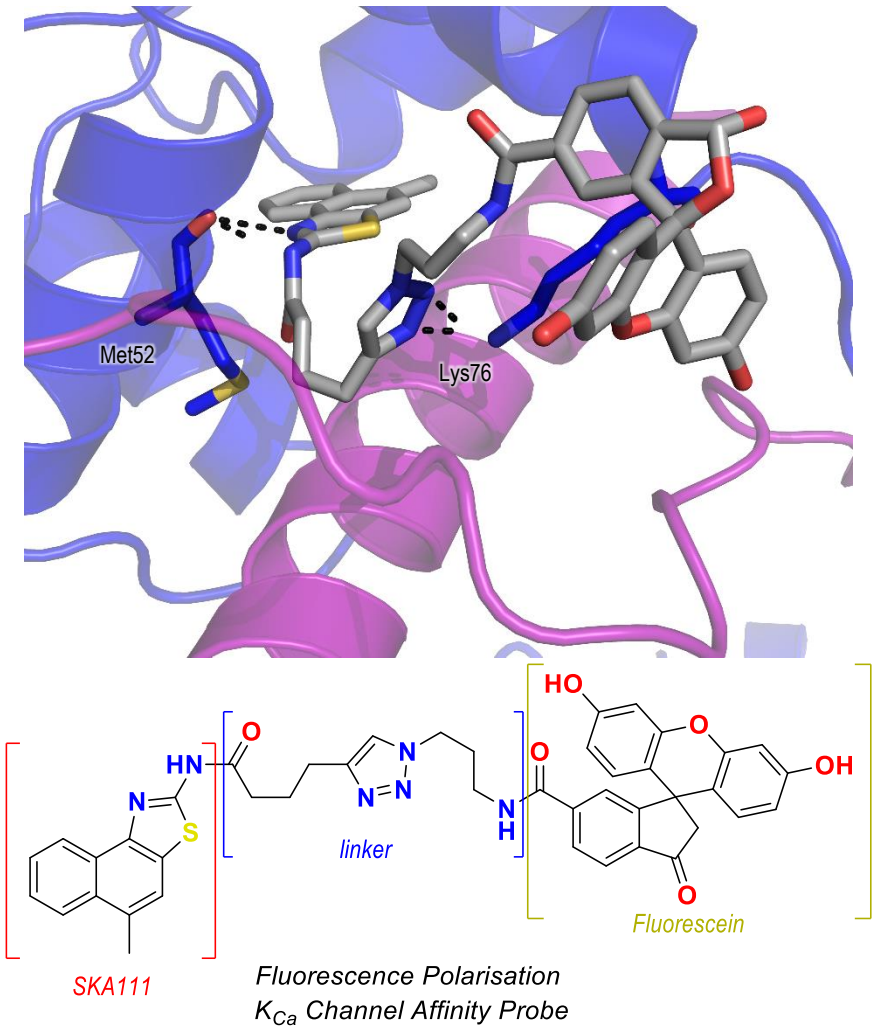
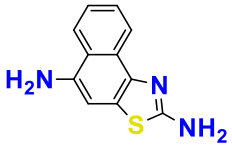
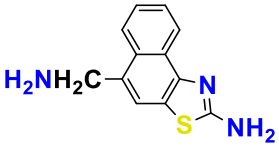
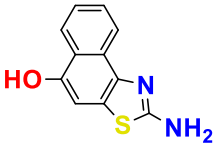
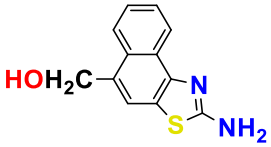
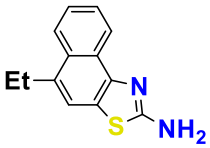
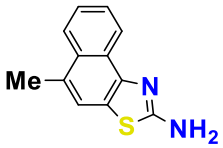
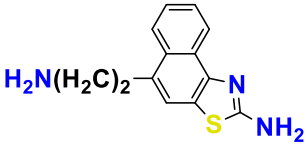
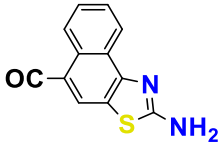


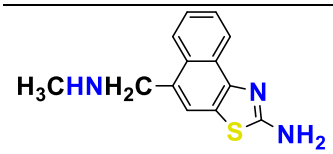
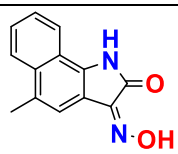
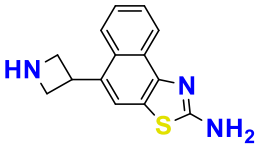
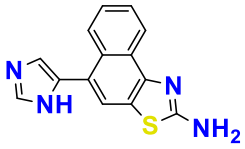
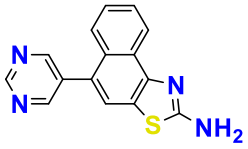
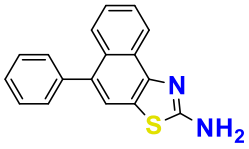
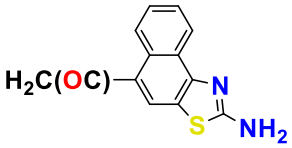
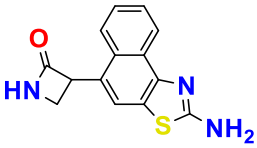
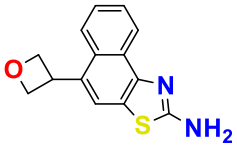
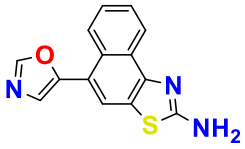
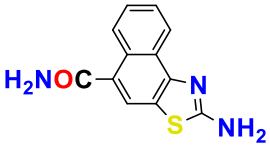
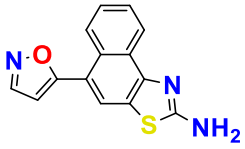
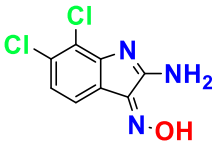
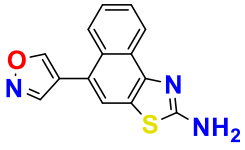
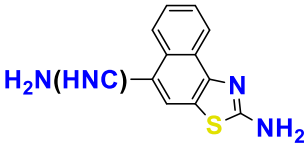
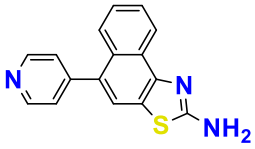
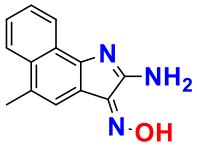
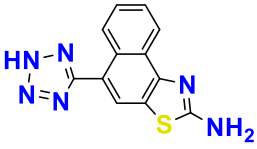
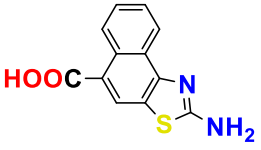
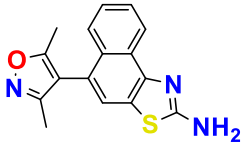
Figure 2.13; Skeletal structure SKA111-fluorescein analogue as fluorescent K_{Ca} channel affinity probe, docked with $IK_{Ca}3.1$ model 1. CaM represented as blue helices, $IK_{Ca}3.1$ CaMBD-4 presented as purple helices, CaM Lys76 and anchor residue Met52 presented as sticks, hydrogen bonds shown as dashed lines (all <3 Å), affinity probe presented in grey sticks.

Homology model 1 of the predicted $IK_{Ca}3.1$ modulator binding site was used to design a bespoke affinity probe, for later use in biophysical assay development. Based on the SKA111 docking orientation, an analogue was designed to allow for the addition of the fluorescent tag, fluorescein, while potentially retaining the original ligand's binding

affinity, Figure 2.13. The 2-amino group of SKA111 enabled an amide linkage to fluorescein *via* a flexible linker section. Ligand optimisation of the published SKA111 binding pose showed the fluorescein-linkage was tolerated, with a predicted binding score of -55 for this pose. The linker section of the probe was positioned to exit the traditional K_{Ca} binding cavity, despite potential Val363 clashes. Interestingly, the linker triazole was predicted to interact with Lys76, shown to be important for NS309 potency, Figure 2.13 and Figure 2.4.[20] Fluorescein is left solvent exposed, however, it is positioned in close proximity to the CaMBD loop region. Stabilisation of this loop region has been suggested to be associated with channel activation.[21,22] Thus, SKA111 analogues might be designed to similarly exit the binding cavity and gain channel specific interactions with this loop, an avenue for selectivity enhancement.

Table 2.3; List of novel naphthothiazole analogues, designed to test the Ser370 H-bonding hypothesis.

Structure	Weight	LogP	$IK_{Ca}3.1$ Score	Structure	Weight	LogP	$IK_{Ca}3.1$ Score
	215	2.6	-41		229	2.1	-37
	216	2.9	-41		230	2.4	-37
	228	4.1	-39		214	3.6	-37
	243	2.6	-38		214	3.6	-37

Structure	Weight	LogP	$IK_{Ca}3.1$ Score	Structure	Weight	LogP	$IK_{Ca}3.1$ Score
	228	2.7	-36		225	5.3	-26
	243	2.6	-35		266	3.1	-26
	255	2.7	-33		276	4.9	-26
	278	3.2	-33		270	3.3	-25
	258	3.6	-31		267	3.4	-23
	243	2.5	-29		267	3.4	-23
	230	4.6	-29		267	3.4	-22
	242	2.6	-28		277	3.8	-21
	225	4.9	-27		268	2.5	-16
	244	3.0	-27		295	4.2	-10

The novel naphthothiazole ligands designed and docked, Table 2.3, all contained either a polar functional group at position-5, capable of forming hydrogen bonds, or similarly

sized non-polar aliphatic groups which could not. Comparison of the results for the two types of novel naphthothiazole ligands, polar and non-polar substituted, would therefore indicate if H-bonding is important in any later observations of ligand potency and selectivity gains. Simple functional groups at position-5 including aniline, phenol, methylalcohol or methylamine, versus more elaborate cyclic groups would demonstrate the potential space within the binding cavity surrounding Ser370.

Several novel ligands were also designed to attempt to bring together the most potent and selective published ligands, SKA111 and NS309. The hybridised novel ligands may produce more potent ligands with the selectivity and pharmacodynamic properties of SKA111 and potency of NS309.

Having rationally designed a set of naphthothiazole analogues to test the hypothesis of Ser370 H-bonding, and including the desired affinity probe, synthesis of these molecules was conducted.

2.3 Synthetic Work

Synthesis was conducted to achieve two aims; to generate novel molecules in the search of specific $IK_{Ca}3.1$ modulator, and to produce modulators of known biological activity, which could be used as positive controls in biological assays. Lacking a computational or biophysical method to screen molecule libraries, and to accelerate the design of novel $IK_{Ca}3.1$ modulators, the existing naphthothiazole and benzimidazolone modulator series were taken as hit molecules for further development.

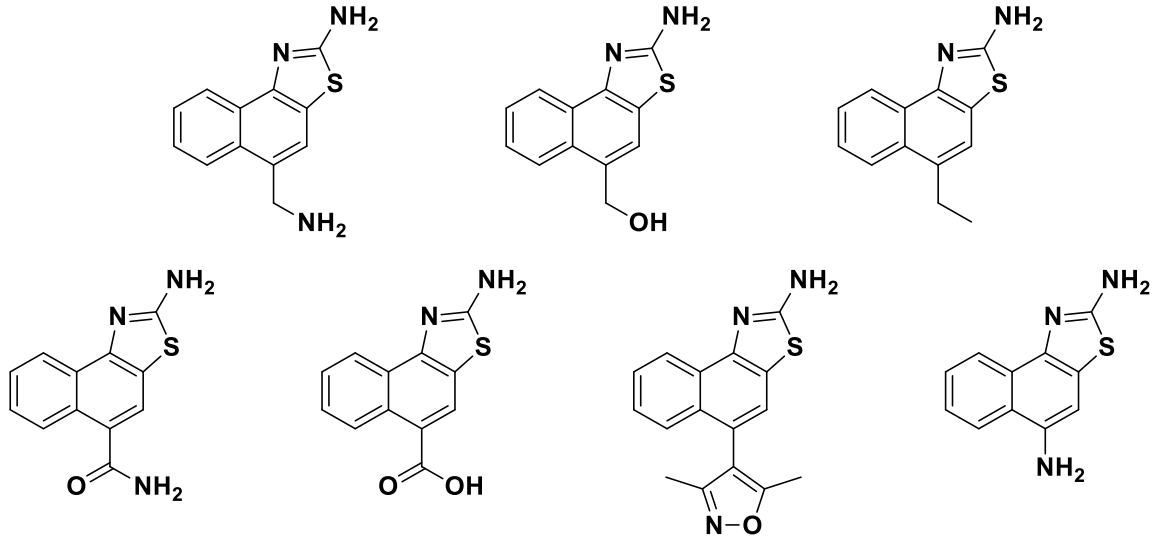
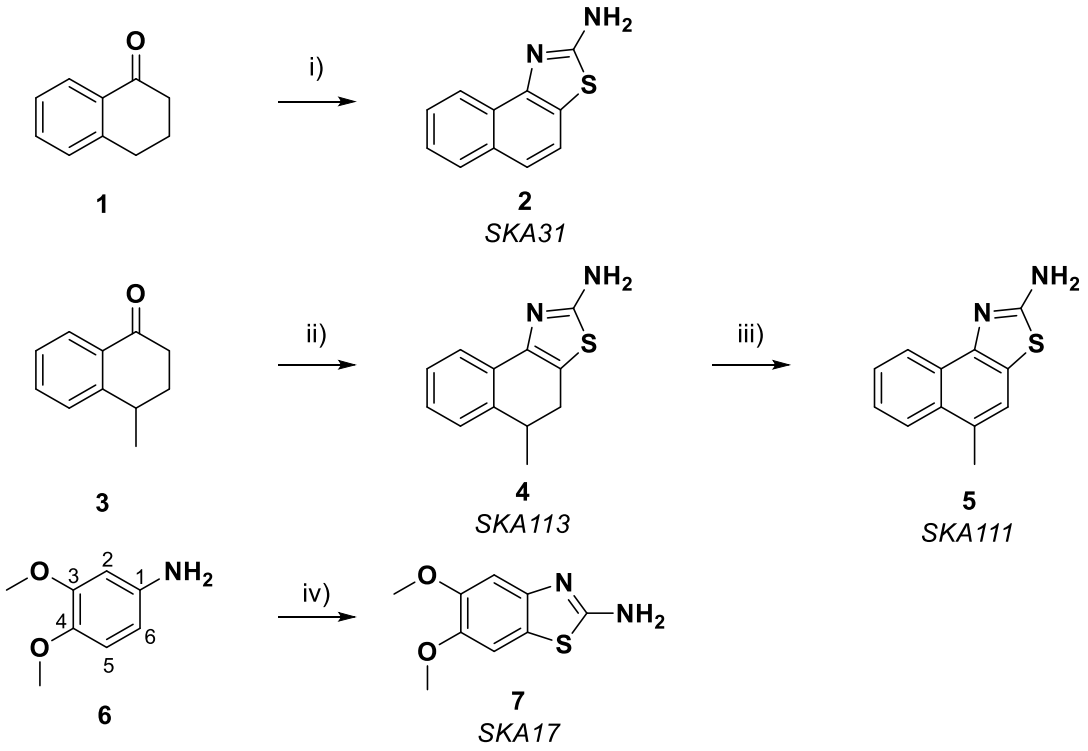


Figure 2.14; Naphthothiazole synthetic targets based on rational design hypothesis.

Published cellular patch clamp assay evidence indicates a series of 2-amino-naphthothiazoles, in particular the molecule SKA111, behave as modulators of the $IK_{Ca}3.1$ channel.[4,48] The naphthothiazole series of modulators was selected as the primary scaffold based on their published 100-fold selectivity for the target $IK_{Ca}3.1$ channel over other K_{Ca} channels. In lieu of naphthothiazole biophysical characterisation, it has been proposed these molecules effect $IK_{Ca}3.1$ *via* the same mechanism as EBIO and NS309 $SK_{Ca}2.2$ modulation. This proposal has been strengthened by mutational analysis of the $IK_{Ca}3.1$ binding cavity residues, and their effects on SKA111 channel modulation.[10] SKA111 was synthesised to further test this proposal and subsequently to be used as a biophysical and pharmacological positive control modulator. The related 2-amino-benzothiazole SKA17 was synthesised as a potential negative control because it was published as not having any effect on K_{Ca} channels.[4,48] Several novel naphthothiazole analogues, designed using the $IK_{Ca}3.1$ homology model 1, discussed in subsection 2.1.2, were synthesized to test the hypothesis involving Ser370 H-bonding, Figure 2.14.

As discussed throughout section 2.1, the $SK_{Ca}2.2$ co-crystals directly show the modulators EBIO and NS309 interact with a target channel homologue. These well characterised, known binding modulators were synthesised as positive assay controls, and reserve scaffolds.

2.3.1 Synthesis of Published IKCa3.1 Naphthothiazole Modulators



Scheme 2.1; Synthetic routes to SKA31 ***2****, SKA111* ***5*** *and SKA17* ***7****. i) Thiourea, iodine, p-toluene-4-sulfonic acid, dimethyl sulfoxide, oxygen, 75 °C, 1 d, 38%. ii) Thiourea, iodine, ethanol, reflux, 20 h, 71%. iii) Activated manganese dioxide, dichloromethane, reflux, 18 h, 72%. iv) Bromine, ammonium thiocyanate, acetic acid, RT, 0.5, 77%.*

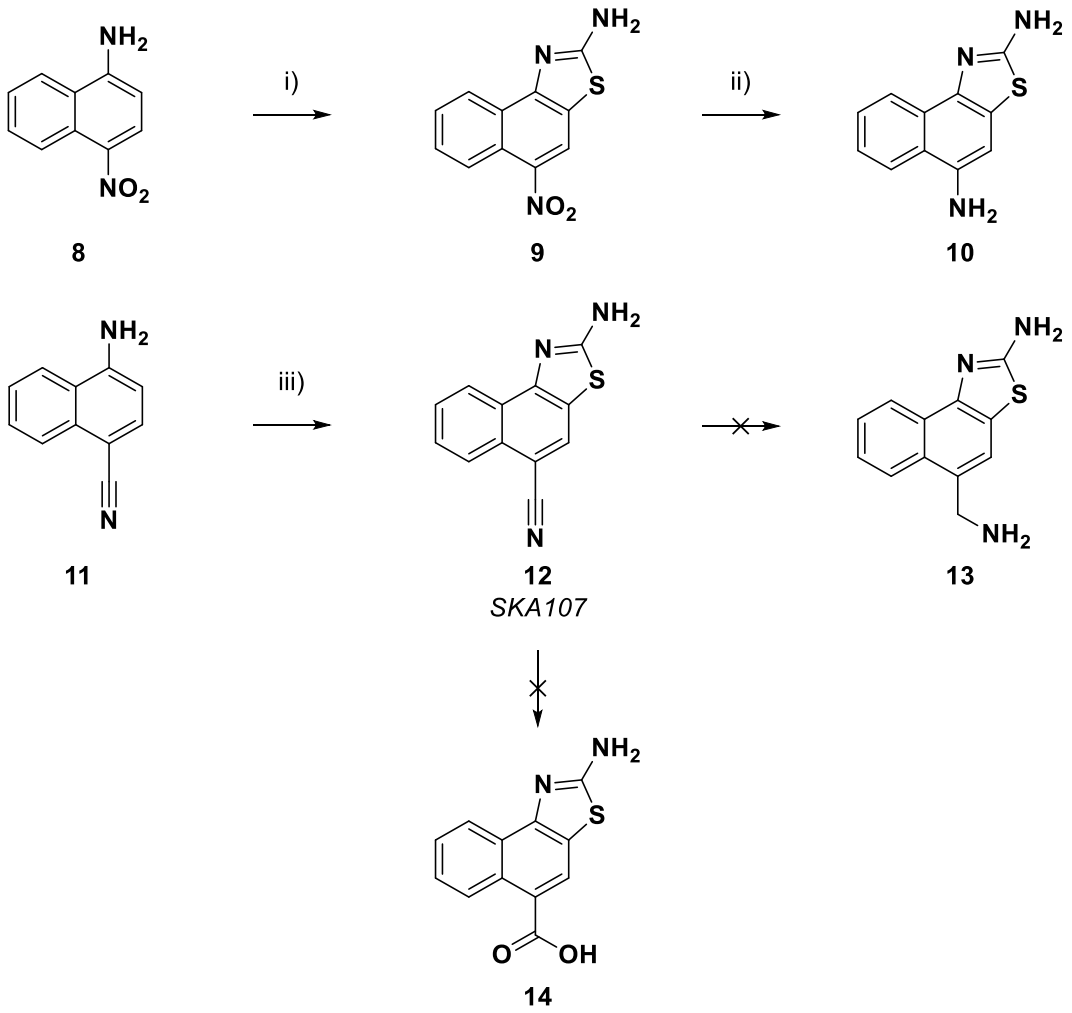
Several alternative synthetic methods for forming the pharmacophore 2-aminothiazole ring were used in the synthesis of several desired control molecules: SKA31 **2**, SKA111 **5** and SKA17 **7**. The first method involved the direct conversion of α-tetralone **1** to **2**, Scheme 2.1 i.[50] Reaction of **1** with thiourea and iodine in dimethyl sulfoxide, under an oxygen atmosphere, gave **2** in 38% yield.

The route to **5** proceeded *via* the unoxidised intermediate, and known $IK_{Ca}3.1$ modulator, SKA113 **4**, Scheme 2.1 ii and iii.[48] Reaction of 4-methyl tetralone with thiourea and iodine in ethanol, formed the 2-aminothiazole ring to give **4.** Oxidation of **4** to **5** was first achieved with 2,3-dichloro-5,6-dicyano-1,4-benzoquinone, DDQ, in 53% yield, instead of the published IBX, which did not convert any starting material.[48] The radical mechanism of DDQ oxidation appeared to attack the 2-aminothiazole ring of **4**, giving a complex mixture of products of lower molecular weights than the starting material, and no NMR NH_2 chemical shifts. The yield of **5** was increased from 50% to 72% by oxidation with activated manganese dioxide in place of DDQ.

The last method formed SKA17 **7** in a single step transformation from 3,4-dimethoxy aniline **6**, Scheme 2.1 iv.[4,51] Reaction with ammonium thiocyanate, and bromine, in acetic acid gave **7** in 72% yield. Due to the wider commercial availability of aniline starting materials compared to tetralones, this third method was selected as a general entry to later naphthothiazole analogues.

2.3.2 Synthesis of Novel Naphthothiazole Analogues

The third method of 2-aminothiazole formation, previously applied to benzothiazole formation of **7**, was adapted to provide the desired naphthothiazole core. This reaction proved to be quite versatile, enabling the synthesis of multiple naphthothiazole analogues bearing different substitutions, from strongly electron withdrawing to donating, and partially tolerating basic functional groups. Compared to the original reaction to **7**, the regioochemistry of 2-aminothiazole formation was restricted to the desired product removing the need for separation of isomers.



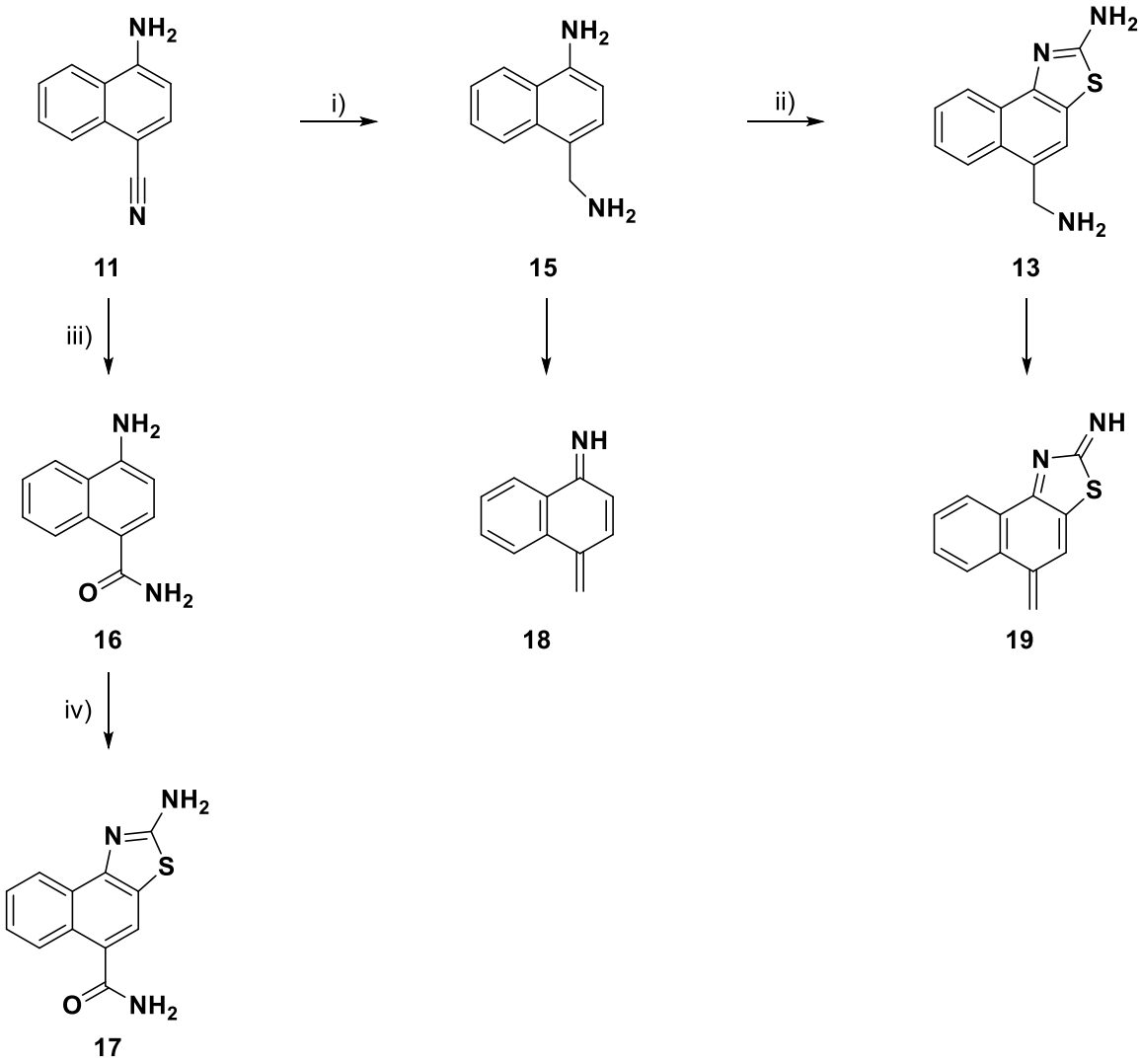
Scheme 2.2; Post naphthothiazole ring formation functional group interconversion to target analogues. i) Bromine, ammonium thiocyanate, acetic acid, RT, 20 h, 22%. ii) Activated zinc powder, ammonium chloride, methanol, RT, 20 h, 81%. iii) Bromine, ammonium thiocyanate, acetic acid, 100 °C, 24 h, 68%.

Initially, three commercial amino-naphthalene starting materials, substituted with adaptable functional groups, were converted to the corresponding naphthothiazoles. The substituted naphthothiazoles were converted to the target naphthothiazole analogues previously designed based on the $IK_{Ca}3.1$ binding cavity homology models, Figure 2.14.

The aniline analogue **10** was synthesised over two steps from 4-nitronaphthalen-1-amine, Scheme 2.2 i and ii. The nitro group of 4-Nitronaphthalen-1-amine **8** had the strongest electron withdrawing effect of the amino-naphthalene substituted starting materials. As such, **8** was not a reactive starting material, requiring heating to 100 °C

before product formation was observed. Even with heating, the nitro group greatly reduced the progression of the 2-aminothiazole-forming reaction compared to the equivalent reactions forming **7**, chloride **21**, and nitrile **12**. Increasing reaction time or adding bromine directly to the reaction mixture, instead of preforming cyanic hypobromous thioanhydride, did not improve upon initial yields of 22%. Reduction of the nitro group to **10** was more difficult than anticipated, despite the strongly donating effect of the 2-aminothiazole group. Nitro reduction was eventually achieved with zinc powder in high yield, 81%, where palladium and iron failed to convert any starting material.

The nitrile-substituted naphthalene **11** was chosen for its strategic downstream synthetic versatility, Scheme 2.2. The 2-aminothiazole forming reaction of **11** furnished the $IK_{Ca}3.1$ modulator, SKA107 **12**, in 68% yield. Conversion of **12** to target analogues proved very difficult: both reduction with lithium aluminium hydride to give the methylamine **13**, or hydrolysis to the acid **14**, failed to convert any starting material. Donation of electron density from the 2-amino group to positions 5, 6 and 8 around naphthothiazole core appeared to further decrease electrophilicity of the nitrile, Figure 2.6.

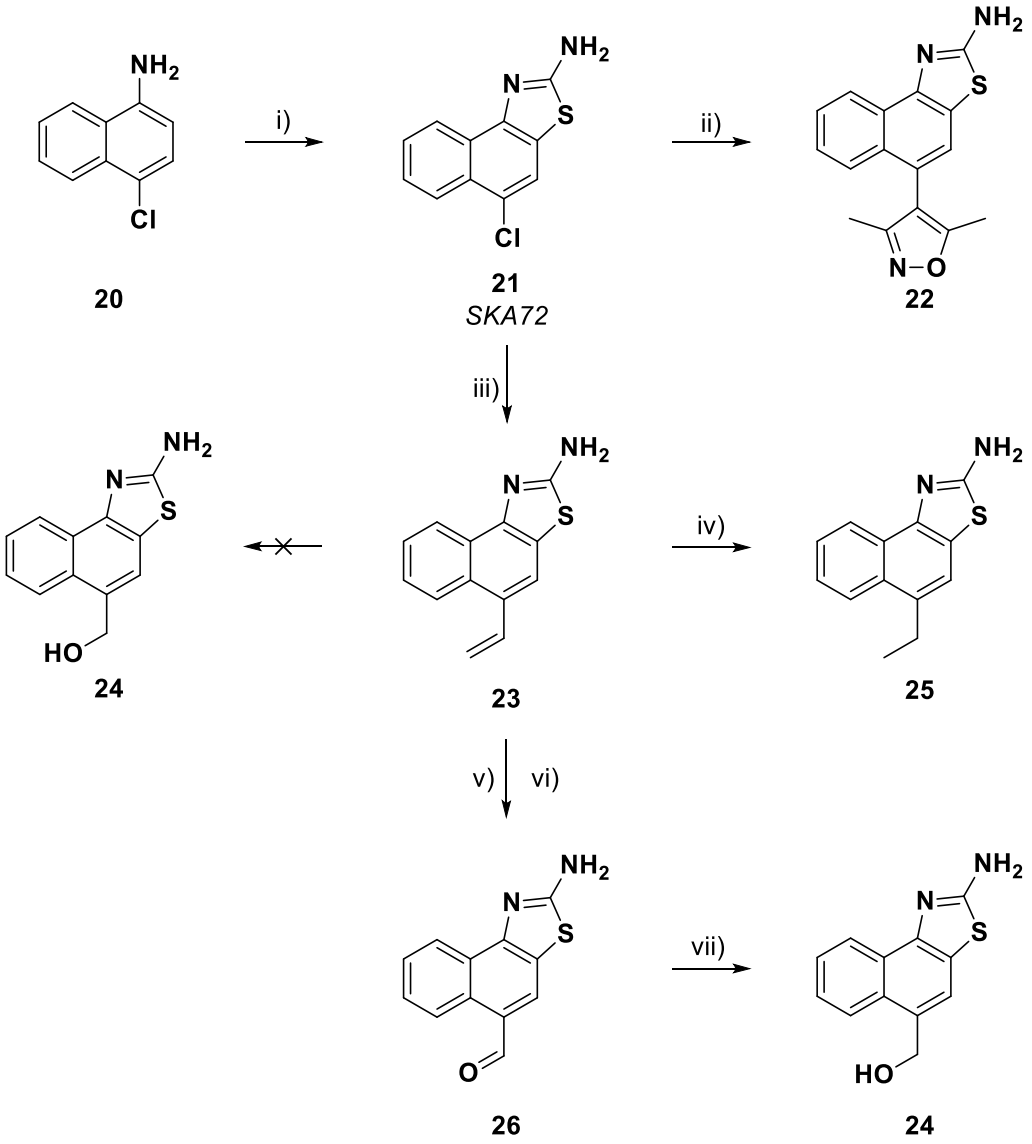


*Scheme 2.3; Synthetic routes to methylamino **13** and amide **17** target analogues. i) Lithium aluminium hydride, tetrahydrofuran, reflux, 20 h, 67%. ii) Bromine, ammonium thiocyanate, acetic acid, RT, 24 h, 8%. iii) potassium carbonate, water, microwave, 150 °C, 23%. iv) Bromine, ammonium thiocyanate, acetic acid, 100 °C, 20 h, 30%.*

The lack of reactivity of **12** led to derivatisation of the starting material **11** instead. Reaction of **11** with lithium aluminium hydride under reflux gave the desired methylamine product **15** and subsequent conversion to the target analogue **13** was successful, Scheme 2.3 i and ii. The intermediate amine **15** readily degraded *via* an ammonia elimination reaction to give the imine product **18** and was used directly in the next reaction. Although **13** also underwent a similar ammonia elimination to give the

imine product **19**, it was more stable than the intermediate **15**, due to the inductive electron withdrawing effects of sulfur and nitrogen of the thiazole ring, reducing the donated electron density from the 2-amino group compared to the aniline.

Reaction of **11** with hydrogen peroxide, potassium carbonate and dimethyl sulfoxide in methanol gave the amide **16**, in 13% yield. Using a published method of hydrating aromatic nitriles to amides *via* strong microwave heating with aqueous sodium hydrogen carbonate provided **16** in an improved 23% yield, Scheme 2.3 iii.[52] Thiazole ring formation of the target amide **17** proceeded in 30% yield.



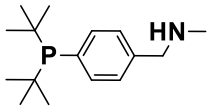
Scheme 2.4; Synthetic routes to target naphthothiazole analogues; 2,5-dimethyl isoxazole ***22****, ethyl* ***25*** *and alcohol* ***24****. i) Bromine, ammonium thiocyanate, acetic acid, 100 °C, 24 h, 68%, ii) Palladium(II) diacetate, RuPhos, potassium 3,5-dimethyl-1,2-oxazol-4-yl-trifluoroborate, sodium carbonate, ethanol, 85 °C, 20 h, 48%. iii) Palladium(II) diacetate, SPhos, potassium vinyl trifluoroborate, sodium carbonate, ethanol, 85 °C, 20 h, 44%. iv) Palladium black, ethyl acetate, hydrogen pressure, RT, 2.5 h, 99%.; v) potassium osmate(IV) dihydrate, N-methylmorpholine, tetrahydrofuran, tert-butanol, water, RT, 2 h, vi) sodium periodate, tetrahydrofuran, water, RT, 20 h, 24%. vii) Sodium borohydride, tetrahydrofuran, methanol, 4 °C, 87%.*

Like **11**, chloronaphthalene **20** was chosen as a starting material due to the available cross-coupling chemistry and its potential versatility. The amine **20** was reacted to give SKA72 **21**, another published $IK_{Ca}3.1$ modulator.[48]

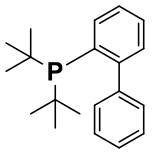
Suzuki couplings taking trifluoroborate substrates with **21** produced the target isoxazole **22** and vinyl **23** compounds, Scheme 2.4 ii and iii.[53,54] Electron-rich commercial catalyst ligands, including SPhos and AmPhos, were required to promote palladium insertion into the strong C-Cl bond of the substrate for the reaction to occur. The sulfur of the aminothiazole predictably appeared to poison the palladium-based catalysts employed, giving yield of around 50%. Catalyst poisoning was surmountable when the catalyst was used in stoichiometric amounts. Conversion of vinyl **23** to the desired ethyl analogue **25** with palladium black occurred in 87% yield, Scheme 2.4 iv. Over reduction of **25** was observed, giving a complex mixture of aliphatic products, if the reaction was left for longer periods of time with palladium on carbon.

Table:2.4; Effect of ligand and catalyst loading on vinyl trifluoroborate and **21** Suzuki cross-coupling.

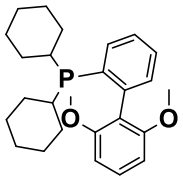
Catalyst (eq.)	Ligand	Conversion	n
0.02	dppf	No reaction	1
0.044	(S)BINAP	No reaction	1
0.044	XantPhos	No reaction	1
0.06	XPhos	No reaction	1
0.06	JohnPhos	11%	1
0.06	RuPhos	57-66%	2
0.06	SPhos	75%	1
0.12	SPhos	67%	1
0.20	SPhos	53-100%	3
0.20	AmPhos	47-91%	4
1.00	AmPhos	100%	1



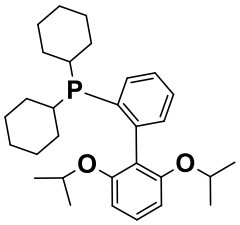
AmPhos
di-*tert*-butyl-
(4-dimethylaminophenyl)-
phosphine



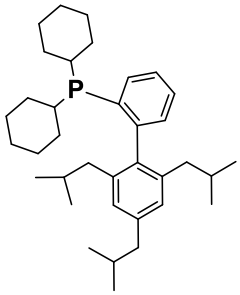
JohnPhos
(2-biphenyl)di-*tert*-
butylphosphine



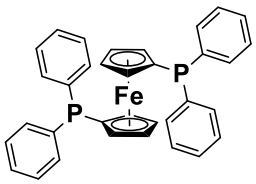
SPhos
2-dicyclohexylphosphino-
2',6'-dimethyoxybiphenyl



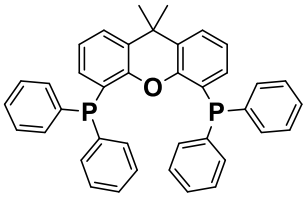
RuPhos
2-dicyclohexylphosphino-
2',6'-diisopropoxybiphenyl



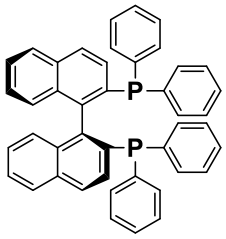
XPhos
2-dicyclohexylphosphino-
2',4',6'-trisopropylbiphenyl



dppf
1,1'-ferrocenediyl-
bis(diphenylphosphine)



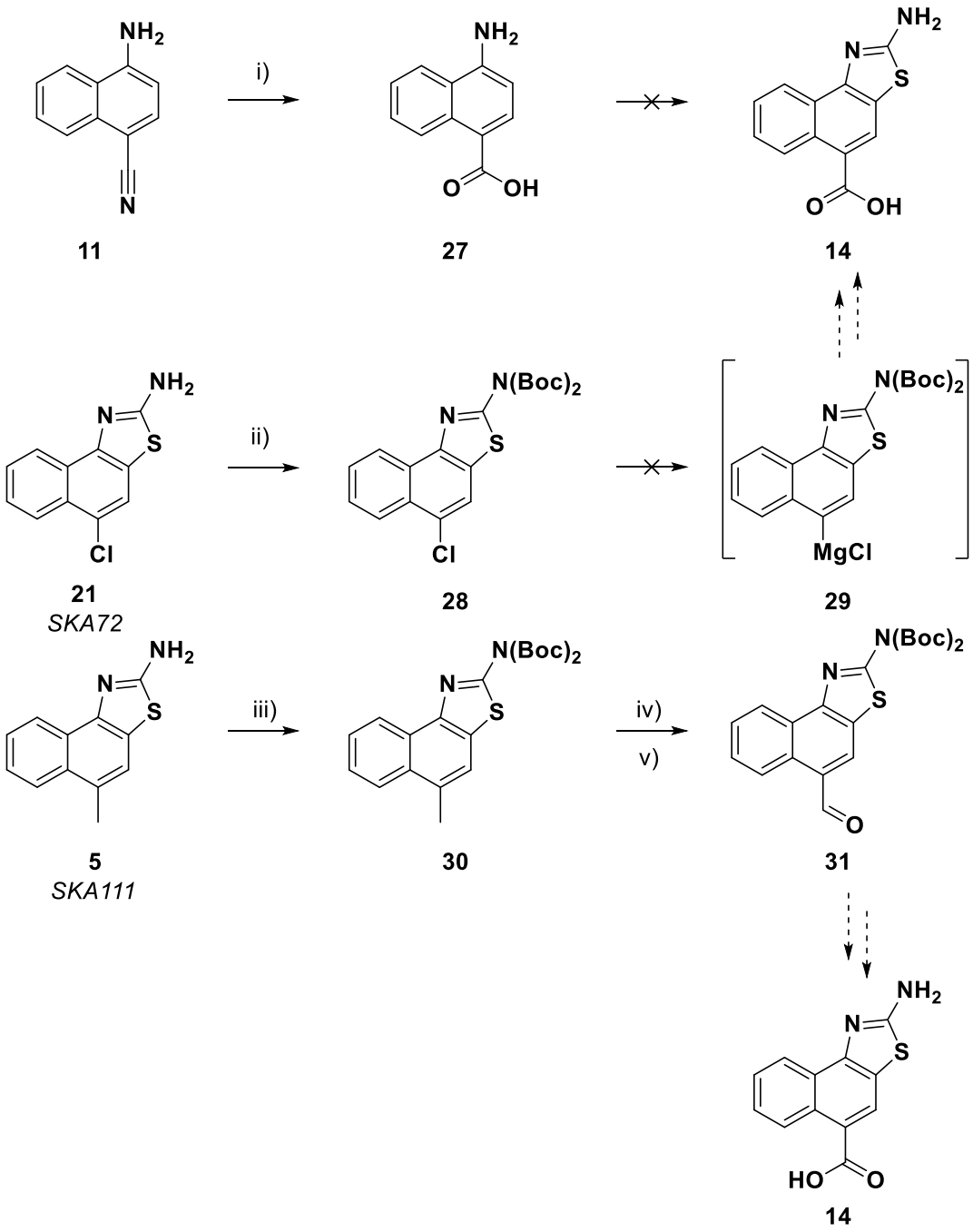
XantPhos
4,5-bis(diphenylphosphino)-
9,9-dimethylxanthen



(S)-BINAP
(S)-(-)-
4,5-binaphthalene-2,2'-diyl)-
bis(diphenylphosphine)

Figure 2.15; Skeletal structures of the commercial phosphine ligands used in Suzuki coupling reaction of **21**.[54–56]

The coupling of vinyl trifluoroborate with **21** to give **23** gave a mixture of starting material, product and dehalogenated product during reaction optimisation. This mixture was inseparable by forward, reverse and silver nitrate TLC or column chromatographies. However, an attempt to scavenge the valuable vinyl product for use in later steps was made, and the vinyl component of the mixture was converted to the separable aldehyde **26**. Ozonolysis of the mixture with a reductive workup to directly furnish the target alcohol analogue **24** was unsuccessful, instead producing a black tar, Scheme 2.4 v. The 2-aminothiazole rings of both **21** and **23** in the mixture were observed to decompose during the reaction with ozone giving a complex mixture of products. Instead, the vinyl mixture was subjected to dihydroxylation with potassium osmate followed by oxidative cleavage with sodium periodate to give benzaldehyde **26** which was separable. Reduction of **26** to the desired alcohol **24** was achieved in 87% yield, Scheme 2.4 vi–viii.



Scheme 2.5; Towards a synthetic route to the target carboxylic acid naphthothiazole analogue ***14****. i) Sodium hydroxide, ethanol, 100 °C, 1 w, 36%. ii) 4-Dimethylaminopyridine, triethylamine, di*tert*-butyl dicarbonate, tetrahydrofuran, RT, 2 h, 31%. iii) 4-Dimethylaminopyridine, di*tert*-butyl decarbonate, tetrahydrofuran, RT, 33.5 h, 58%. iv) 2,2'-Azobis(2-methylpropionitrile), N-bromosuccinamide, carbontetrachloride, reflux, 2 h, v) silver nitrate, acetone, water, reflux, 0.5 h, 22%.*

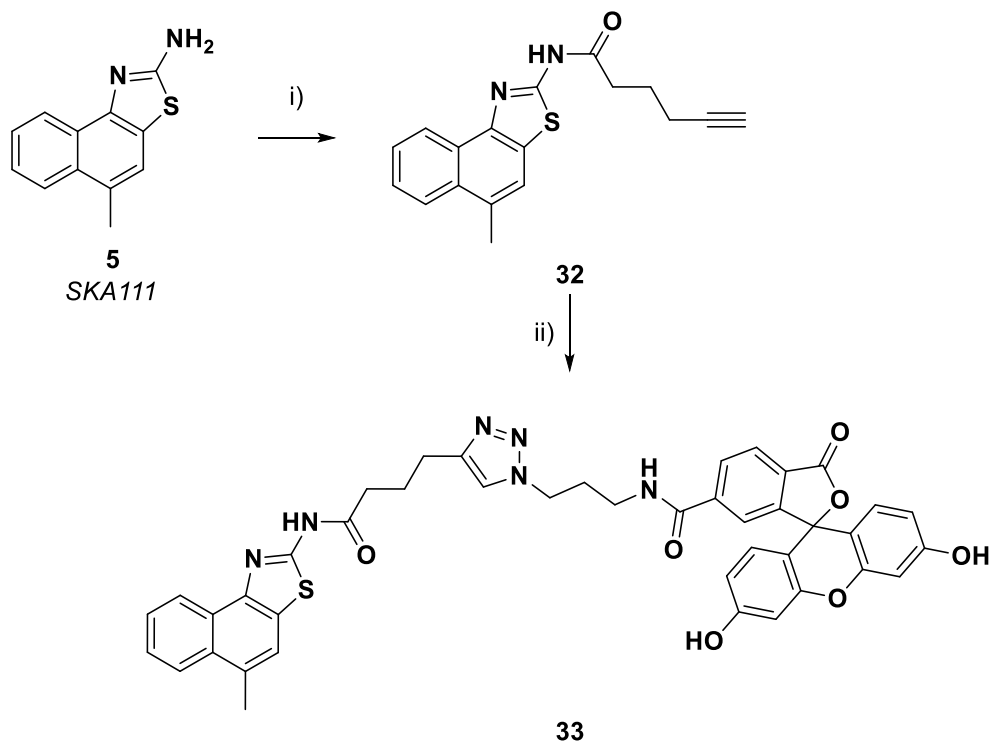
When subjected to aqueous sodium hydroxide at high temperature over a week, **11** was hydrolysed to carboxylic acid **27**, yet still in 35% yield, Scheme 2.5 i. Unfortunately,

conversion of **27** to the desired analogue **14** was problematic and gave a complex mixture of inseparable products. It is possible the amino acid **14** underwent a condensation reaction to form unwanted amide side products .

Despite 2-amino group protection of **21** to give **28**, heating of **28** under reflux with magnesium turnings followed by addition of diethylcarbonate, did not give the expected ethyl ester, Scheme 2.5 ii. The 5-chloride **28** did not react to give the desired Grignard **29**, instead **28** was deprotected by thermolysis of the Boc groups to the unprotected or monoprotected forms. While examples can be found, chlorides are not ideal substrates for Grignard formation due to the stronger C-Cl bond resisting magnesium insertion compared to other halogens.[57] The higher electron density at the 5-position of the naphthothiazole core further strengthens the C-Cl bond adding to the difficulty of Grignard formation.

Synthesis of the desired carboxylic acid **14** was attempted *via* the functionalisation of **5**. After protection of **5** to give **30**, a radical bromination reaction was conducted to give the corresponding gem dibromo intermediate, Scheme 2.5 iii and vi. The dibromo product was unstable to moisture and underwent slow hydrolysis to the aldehyde **31**. To ensure full conversion the dibromide was hydrolysed with silver nitrate in 22% yield, Scheme 2.5 v.

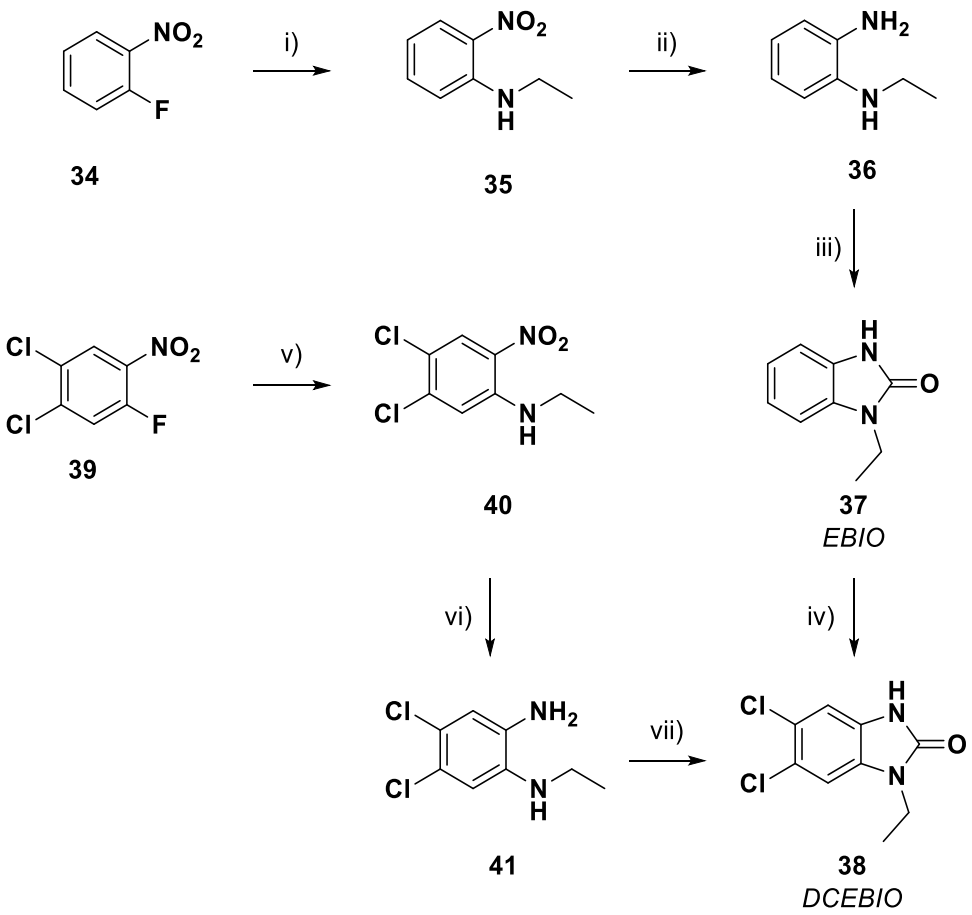
.



*Scheme 2.6; Synthetic route to SKA111-fluorescein coupled fluorescence polarisation probe **33**. i) Hex-5-ynoyl chloride, 4-dimethylaminopyridine, triethylamine, dichloromethane, tetrahydrofuran, 4 °C–RT, 2 h, 47%. ii) Sodium L-ascorbate, 4-((3-azidopropyl)carbamoyl)-2-(3,6-dihydroxy-9H-xanthen-9-yl)benzoic acid, tris[(1-benzyl-1H-1,2,3-triazol-4-yl)methyl]amine, copper sulfate, tert-butanol, water, dimethylformamide, RT, 20 h, 66%.*

The K_{Ca} channel affinity probe **33**, discussed in subsection 2.2.2, was synthesised by taking **5** with hex-5-ynoyl chloride to form amide **32** in 47% yield, followed by a copper-catalysed alkyl-azide cycloaddition with 6-FAM azide to furnish the desired compound, **33**, in 66% yield, Scheme 2.6.

2.3.3 Synthesis of Published K_{Ca} Channel Modulators: EBIO, DCEBIO and NS309

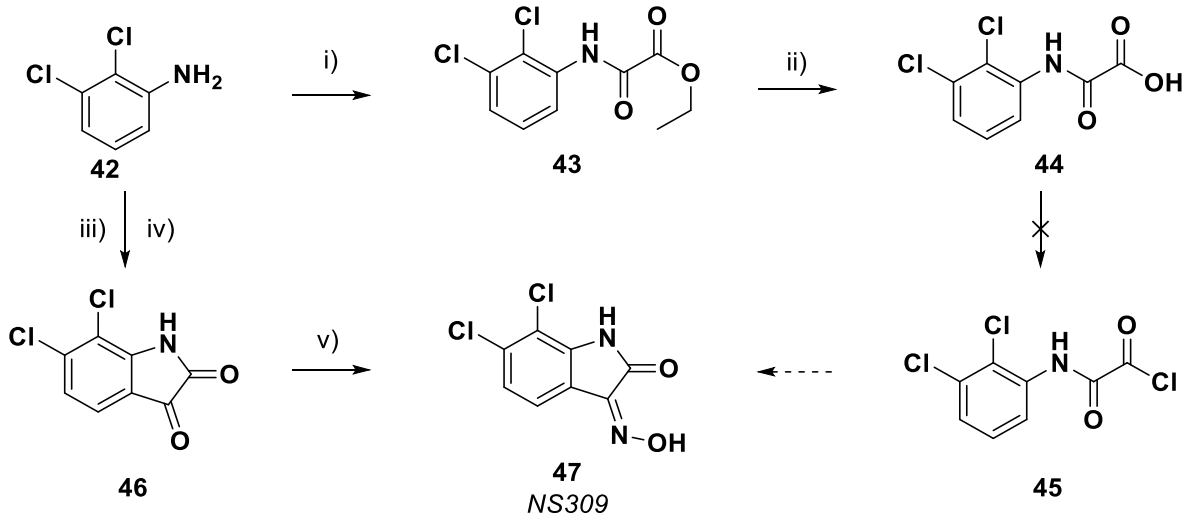


Scheme 2.7; Synthetic routes to, EBIO **37**, and, DCEBIO **38**. i) Ethylamine, dimethylformamide, RT, 22h, 99%. ii) Methanol, sodium borohydride, 5% palladium on carbon, tetrahydrofuran, RT, 1.5 h, 81%. iii) Carbonyldiimidazole, tetrahydrofuran, RT, 26.5 h, 81%. iv) *N*-chlorosuccinamide, dimethylformamide, RT, 23.5 h, 44%; v) ethylamine, dimethylformamide, RT, 3 d, 86%. vi) Activated iron powder, acetic acid, 100 °C, 1 h, 47%. vii) Carbonyldiimidazole, tetrahydrofuran, RT, 46 h, 70%.

Synthesis of EBIO **37** was achieved in 65% overall yield from nitrofluorobenzene **34** using the published route shown in Scheme 2.7 i–iii.[58] To begin with, the nitrofluorobenzene starting material **34** was aminated *via* S_NAr with ethylamine to give **35** in 99% yield, then reduced using palladium to the diamine **36** in 81% yield. Carbonylation of **36** with carbonyl diimidazole produced the target EBIO **37** in 81% yield and 99% purity by analytical HPLC.

Synthesis of the more potent 5,6-dichloro EBIO analogue, DCEBIO **38**, was achieved using two alternative strategies. Direct chlorination of 37 to 38 with *N*-chlorosuccinamide proceeded in 44% yield, Scheme 2.7 iv. Unfortunately mono-chlorinated product impurities were not separable by forward or reverse chromatography and are known to be bioactive.[58] As such, an alternative route to **38** was needed that did not introduce any uncertainty in the sample's biological properties. Instead, **38** was synthesised using a method analogous to that used for **37**, beginning with the commercial starting material dichloro starting material **39**, Scheme 2.7 v-vii.

As before, the nitroamine **40** was given in 86% yield *via* S_NAr of the nitrofluorobenzene starting material **39** with ethylamine. Reduction of **40** to the diamine **41** was achieved using activated iron in acetic acid to avoid possible palladium proto-dechlorination Scheme 2.7 v. It was observed that **41** was much less stable to atmospheric oxygen than **36**. It was therefore necessary to convert **41** to **38** with carbonyldiimidazole without further purification. The second route gave **38** in 99% purity by analytical HPLC with no monochlorinated impurities observed, much higher than the previous route.



Scheme 2.8; Synthetic routes to NS309 ***47****; i) Triethylamine, ethyl oxylyl chloride, dichloromethane, –14 °C – RT, 13.5 h, 64%. ii) Sodium hydroxide, ethanol, RT, 20 h, 64%. iii) Hydrochloric acid, chloral hydrate, sodium sulfate, water, reflux, 1 h, iv) sulfuric acid, 65 °C, 1 h, 29%. v) Hydroxylammonium chloride, water, reflux, 0.5 h, 43%.*

Of the benzimidazolone modulator class, NS309 **47**, is the most potent with a $SK_{Ca}2.2$ EC_{50} of 440 nM. Initially, synthesis of **47** began with acylation of **42** to give amide **43**, Scheme 2.8. Hydrolysis of **43** to the oxylacetic acid **44** was followed by reaction with thionyl chloride to give the acid chloride **45**. This step was complicated by product instability and considering the moderate 41% yield over the two first steps, this route was considered inefficient. **47** was instead synthesised from **42** *via* the published route seen in Scheme 2.8 iv-v.[59] Formation of isatin **46** was low yielding as was the following conversion to the target **47**. However, this route did provide the desired compound in high purity, 99% by analytical HPLC.

2.4 Summary

An *in silico* pre-screening filter was desired to reduce the number of molecules for assay screening, and to develop structural rationale for modulator design. Homology models of the target positive modulator binding site, the activated $IK_{Ca}3.1$ gating complex, were generated. The calmodulin binding domain (CaMBD-4) of $IK_{Ca}3.1$ was

identified and modelled simultaneously with calmodulin (CaM) using the $SK_{Ca}2.2$ co-crystals as templates, PDB: 4G28 and 4J9Z. The $IK_{Ca}3.1$ homology models were validated for use in screening by their acceptable peptide backbone geometries and close similarity to their template structures. However, the second $IK_{Ca}3.1$ homology model was quickly identified as too restrictive for screening and was discarded. Published analogues of the positive K_{Ca} channel modulators EBIO **37** and SKA111 **5** were docked against the first $IK_{Ca}3.1$ homology model. The disparity between the known modulator simulated affinities for the channels and their published experimental data indicated the docking was not reliable.

No biophysical or computational method was available to screen libraries of molecules to identify binding, therefore, published K_{Ca} channel modulators were selected as the initial hits for development.

Instead of using the homology models as a filter, observations of the predicted $IK_{Ca}3.1$ modulator binding cavity were made. Some hypotheses were proposed for the relation of $IK_{Ca}3.1$ specific mutations to modulator structure and activity. Analysis of CaMBD-4 identified three unique residues contributing to the $IK_{Ca}3.1$ modulator binding cavity: valine363, methionine366 and Ser370.

Valine363 is potentially the most important mutation because it appeared to close the $IK_{Ca}3.1$ binding cavity. A closed binding cavity suggested a limit to the design of more selective larger modulator structures. The published modulator analogue docking results did support this hypothesis; however, the reliability of those results was not deemed adequate. Ser370, at the back of the $IK_{Ca}3.1$ cavity, was deemed the most useful mutation because it potentially enabled the development of modulators, which specifically bind this $IK_{Ca}3.1$ residue. Published modulator analogues that could

hydrogen bond (H-bond) to Ser370 were hypothesised to gain selectivity for the target channel.

Development of the naphthothiazole core was prioritised because of SKA111 **5**, which has the highest selectivity for the target $IK_{Ca}3.1$ channel. The binding mode of SKA111 **5** was predicted to be similar to that of NS309 **47**, which directed the 5-methyl group towards Ser370. A set of SKA111 analogues with polar groups at position 5 were thus designed with docking guidance.

The known K_{Ca} channel positive modulators were synthesised using the published routes, with some alterations to be used as positive controls in the development of biophysical and pharmacological assays.

The naphthothiazole core was not easily functionalised, complicating the synthesis of the SKA111 analogues. Direct radical dibromination of the di-Boc protected SKA111, **30**, 5-methyl group, followed by immediate hydrolysis to the aldehyde **31**, proceeded in very low yield. This was due to Boc group deprotection or other degradation of the starting material.

Delocalisation of the unprotected 2-amino group lone pair into the ring system of the naphthothiazole core, placed high electron density at the 5-position. This extra electron density made converting the SKA111 nitrile analogue **12** very difficult. Nitrile **12** was so resistant to functional group interconversion, that it was abandoned as a starting material for conversion to the aldehyde **26**, alcohol **24**, amide **17** or amine **13**. Suzuki couplings with the chloride **21** were successful in generating the ethyl **25** and dimethyl isoxazole **22** analogues. However, the sulfur of the thiazole ring, poisoned the palladium catalysed coupling reactions with the chloride analogue **21**. Increasing the catalyst loading to undesirable stoichiometric amounts was required to push the reaction to completion. Instead of direct functionalisation of SKA111 or its nitrile

analogue, the relatively adaptable naphthothiazole ring forming reaction with thiocyanate was used on several substituted amino naphthalenes to give the target 5-position amine **13**, amide **17** and aniline **10** analogues directly.

Chapter 2 References

1. Zhang, Y. Progress and challenges in protein structure prediction. *Curr Opin Struct Biol* **18,** 342–348 (2009).
2. Schumacher, M. a, Rivard, a F., Bächinger, H. P. & Adelman, J. P. Structure of the gating domain of a Ca2+-activated K+ channel complexed with Ca2+/calmodulin. *Nature* **410,** 1120–1124 (2001).
3. Zhang, M., Pascal, J. M., Schumann, M., Armen, R. S. & Zhang, J.-F. Identification of the functional binding pocket for compounds targeting small-conductance Ca2+-activated potassium channels. *Nat. Commun.* **3,** 1021 (2012).
4. Sankaranarayanan, A. *et al.* Naphtho[1,2-d]thiazol-2-ylamine (SKA-31), a new activator of KCa2 and KCa3.1 potassium channels, potentiates the endothelium-derived hyperpolarizing factor response and lowers blood pressure. *Mol. Pharmacol.* **75,** 281–95 (2009).
5. Chin, D. & Means, A. R. Calmodulin: A prototypical calcium sensor. *Trends Cell Biol.* **10,** 322–328 (2000).
6. Saimi, Y. & Kung, C. Calmodulin as an ion channel subunit. *Annu. Rev. Physiol.* **64,** 289–311 (2002).
7. Zhang, M. *et al.* Structural basis for calmodulin as a dynamic calcium sensor. *Structure* **20,** 911–923 (2012).
8. Crouchl, T. H. & Klee, C. B. Positive cooperative binding of calcium to bovine brain calmodulin. *Biochemistry* **19,** 3692–3698 (1980).
9. Westerlund, A. M. & Delemotte, L. Effect of Ca2+ on the promiscuous target-protein binding of calmodulin. *PLOS Comput. Biol.* **14,** e1006072 (2018).
10. Brown, B. M., Shim, H., Zhang, M., Yarov-Yarovoy, V. & Wulff, H. Structural determinants for the selectivity of the positive KCa3.1 gating modulator 5-methylnaphtho[2,1-d]oxazol-2-amine (SKA-121). *Mol Pharmacol* **92,** 469–480 (2017).
11. Schäffer, A. A. *et al.* Improving the accuracy of PSI-BLAST protein database searches with composition-based statistics and other refinements. *Nucleic Acids Res.* **29,** 2994–3005 (2001).
12. Sayle, R. A. & Milner-White, E. J. RASMOL: biomolecular graphics for all. *Trends Biochem. Sci.* **20,** 374–376 (1995).
13. Chothia, C. & Lesk, A. M. The relation between the divergence of sequence and structure in proteins. *EMBO J.* **5,** 823–6 (1986).
14. Lee, U. S. & Cui, J. BK channel activation : structural and functional insights. *Trends Neurosci.* **33,** 415–423 (2010).
15. Guéguinou, M. *et al.* KCa and Ca2+channels: The complex thought. *Biochim. Biophys. Acta - Mol. Cell Res.* **1843,** 2322–2333 (2014).
16. Cui, M., Qin, G., Yu, K., Bowers, M. S. & Zhang, M. Targeting the small- and intermediate-conductance Ca2+-activated potassium channels: the drug-binding pocket at the channel/calmodulin interface. *Neurosignals* **22,** 65–78 (2014).
17. Arnold, K., Bordoli, L., Kopp, J. & Schwede, T. The SWISS-MODEL workspace: A web-based environment for protein structure homology modelling. *Bioinformatics* **22,** 195–201 (2006).

18. Biasini, M. *et al.* SWISS-MODEL: Modelling protein tertiary and quaternary structure using evolutionary information. *Nucleic Acids Res.* **42,** 1–7 (2014).

19. Klosowski, J. T. *et al.* Deep View : High-Resolution Reality. *IEEE Comput. Graph. Appl.* **22,** 12–15 (2002).

20. Zhang, M., Pascal, J. M. & Zhang, J.-F. Unstructured to structured transition of an intrinsically disordered protein peptide in coupling Ca^{2+}-sensing and SK channel activation. *Proc. Natl. Acad. Sci. U. S. A.* **110,** 4828–33 (2013).

21. Zhang, M. *et al.* Selective phosphorylation modulates the PIP2 sensitivity of the CaM-SK channel complex. *Nat Chem Biol* **10,** 753–759 (2014).

22. Zhang, M., Meng, X.-Y., Zhang, J.-F., Cui, M. & Logothetis, D. E. Molecular overlap in the regulation of SK channels by small molecules and phosphoinositides. *Sci. Adv.* **1,** e1500008 (2015).

23. Wallner, B. & Elofsson, A. All are not equal: A benchmark of different homology modeling programs. *Protein Sci.* **14,** 1315–1327 (2005).

24. Kleywegt, G. J. & Jones, T. A. Phi/Psi-chology: Ramachandran revisited. *Structure* **4,** 1395–1400 (1996).

25. Tanramluk, D., Akavipat, R. & Charoensawan, V. Toward mobile 3D visualization for structural biologists. *Mol. Biosyst.* **9,** 2956–2960 (2013).

26. Maiorov, V. N. & Crippen, G. M. Significance of RMSD in comparing three-dimensional structures of globular proteins. *J. Mol. Biol.* **235,** 625–634 (1994).

27. Damm, K. L. & Carlson, H. A. Gaussian-weighted RMSD superposition of proteins: A structural comparison for flexible proteins and predicted protein structures. *Biophys. J.* **90,** 4558–4573 (2006).

28. Hooft, R. W., Sander, C. & Vriend, G. Objectively judging the quality of a protein structure from a Ramachandran plot. *Comput. Appl. Biosci.* **13,** 425–430 (1997).

29. Ramachandran, G. N., Ramakrishnan, C. & Sasisekharan, V. Stereochemistry of polypeptide chain configurations. *J. Mol. Biol.* **7,** 95–99 (1963).

30. Lovell, S. C. *et al.* Structure validation by C alpha geometry: phi, psi and C beta deviation. *Proteins-Structure Funct. Genet.* **50,** 437–450 (2003).

31. Vainio, M. J. & Johnson, M. S. Generating conformer ensembles using a multiobjective genetic algorithm. *J. Chem. Inf. Model.* **47,** 2462–2474 (2007).

32. Wang, Q. & Pang, Y. P. Preference of small molecules for local minimum conformations when binding to proteins. *PLoS One* **2,** 1–10 (2007).

33. Grosdidier, A., Zoete, V. & Michielin, O. Fast docking using the CHARMM force field with EADOCK DSS. *J. Comput. Chem.* **32,** 2149–2159 (2011).

34. Ou-Yang, S.-S. *et al.* Computational drug discovery. *Acta Pharmacol. Sin.* **33,** 1131–40 (2012).

35. Lipinski, C. & Hopkins, A. Navigating chemical space for biology and medicine. *Nature* **432,** 855–861 (2004).

36. Kitchen, D. B., Decornez, H., Furr, J. R. & Bajorath, J. Docking and scoring in virtual screening for drug discovery: Methods and applications. *Nat. Rev. Drug Discov.* **3,** 935–949 (2004).

37. Huang, S.-Y. & Zou, X. Ensemble docking of multiple protein structures: considering protein structural variations in molecular docking. *Proteins* **66,** 399–421 (2007).

38. Cole, J. C., Murray, C. W., Nissink, J. W. M., Taylor, R. D. & Taylor, R. Comparing protein-ligand docking programs is difficult. *Proteins Struct. Funct. Genet.* **60,** 325–332 (2005).

39. Cross, J. B. *et al.* Comparison of several molecular docking programs: Pose prediction and virtual screening accuracy. *J. Chem. Inf. Model.* **49,** 1455–1474 (2009).

40. Zoete, V., Cuendet, M. A., Grosdidier, A. & Olivier, M. SwissParam: a fast force field generation tool for small organic molecules. *J. Comput. Chem.* **32,** 2359–2368 (2011).

41. Grosdidier, A., Zoete, V. & Michielin, O. SwissDock, a protein-small molecule docking web service based on EADock DSS. *Nucleic Acids Res.* **39,** 270–277 (2011).

42. Hopkins, A. L., Keserü, G. M., Leeson, P. D., Rees, D. C. & Reynolds, C. H. The role of ligand efficiency metrics in drug discovery. *Nat. Rev. Drug Discov.* **13,** 105–21 (2014).

43. Reynolds, C. H. & Holloway, M. K. Thermodynamics of ligand binding and efficiency. *ACS Med. Chem. Lett.* **2,** 433–437 (2011).

44. Bjarne Knudsen & Thomas, K. CLC Drug Discovery Workbench User Manual. 1–367 (2014).

45. Korb, O., Stützle, T. & Exner, T. E. Empirical scoring functions for advanced protein-ligand docking with PLANTS. *J. Chem. Inf. Model.* **49,** 84–96 (2009).

46. Strobaek, D. *et al.* Inhibitory gating modulation of small conductance Ca2+-activated K+ channels by the synthetic compound (R)-N-(benzimidazol-2-yl)-1,2,3,4-tetrahydro-1-naphtylamine (NS8593) reduces afterhyperpolarizing current in hippocampal CA1 neurons. *Mol. Pharmacol.* **70,** 1771–1782 (2006).

47. Congreve, M., Carr, R., Murray, C. & Jhoti, H. A 'Rule of Three' for fragment-based lead discovery? *Drug Discov. Today* **8,** 876–877 (2003).

48. Coleman, N. *et al.* New positive Ca2+ -activated K+ channel gating modulators with selectivity for KCa3.1. *Mol. Pharmacol.* **86,** 342–357 (2014).

49. Nobeli, I., Price, S. L., Lommerse, J. P. M. & Taylor, R. Hydrogen bonding properties of oxygen and nitrogen acceptors in aromatic heterocycles. *J. Comput. Chem.* **18,** 2060–2074 (1997).

50. Zhao, J. *et al.* Metal-free synthesis of 2 - aminobenzothiazoles via aerobic oxidative cyclization/dehydrogenation of cyclohexanones and thioureas. *Org. Lett.* **15,** 2604–2607 (2013).

51. Hirose, W., Sato, K. & Matsuda, A. Selective detection of 5-formyl-2'-deoxyuridine, an oxidative lesion of thymidine, in DNA by a fluorogenic reagent. *Angew. Chemie - Int. Ed.* **49,** 8392–8394 (2010).

52. Tu, T., Wang, Z., Liu, Z., Feng, X. & Wang, Q. Efficient and practical transition metal-free catalytic hydration of

organonitriles to amides. *Green Chem.* **14,** 921 (2012).

53. Molander, G. A. & Bernardi, C. R. Suzuki-Miyaura cross-coupling reactions of potassium alkenyltrifluoroborates. *J. Org. Chem.* **67,** 8424–8429 (2002).

54. Molander, G. A., Canturk, B. & Kennedy, L. E. Scope of the Suzuki - Miyaura cross-coupling reactions of potassium heteroaryltrifluoroborates. *J. Org. Chem.* **74,** 973–980 (2009).

55. Wang, B., Sun, H. X., Sun, Z. H. & Lin, G. Q. Direct B-alkyl Suzuki-Miyaura cross-coupling of trialkyl-boranes with aryl bromides in the presence of unmasked acidic or basic functions and base-labile protections under mild non-aqueous conditions. *Adv. Synth. Catal.* **351,** 415–422 (2009).

56. Martin, R. & Buchwald, S. L. Palladium-catalyzed Suzuki-Miyaura cross-coupling reactions employing dialkylbiaryl phosphine ligands. *Acc. Chem. Res.* **41,** 1461–1473 (2008).

57. Vedejs, E., Kruger, A. W. & Suna, E. Enantioselective enolate protonation: Matching chiral aniline and substrate acidity. *J. Org. Chem.* **64,** 7863–7870 (1999).

58. Singh, S., Syme, C. a, Singh, a K., Devor, D. C. & Bridges, R. J. Benzimidazolone activators of chloride secretion: potential therapeutics for cystic fibrosis and chronic obstructive pulmonary disease. *J.Pharmacol.Exp.Ther.* **296,** 600–611 (2001).

59. Wang, Z. *et al.* A novel strategy to the synthesis of 4-anilinoquinazoline derivatives. *Tetrahedron* **70,** 906–913 (2014).

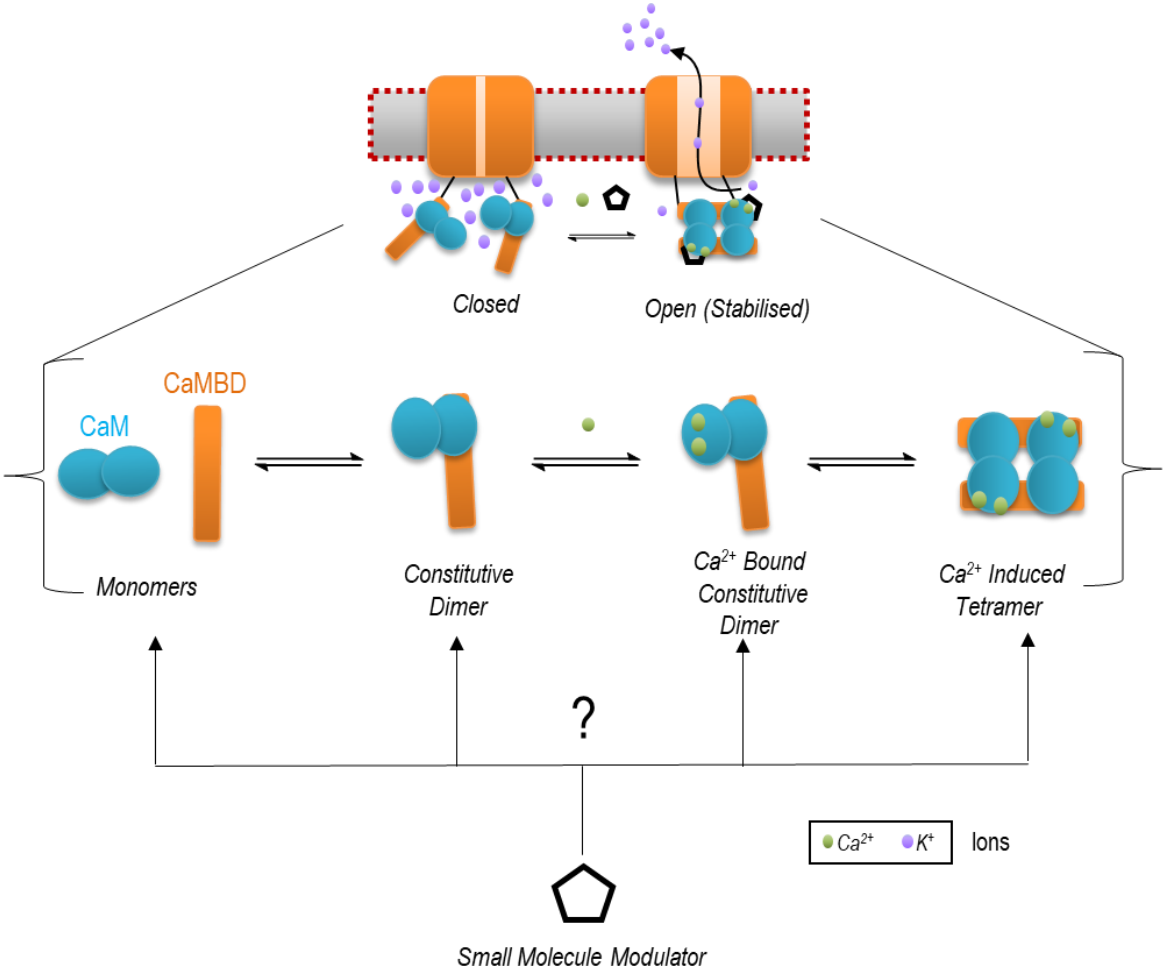


Figure 3.1; The putative activation sequence of CaM gated K_{Ca} channels. Mechanism expanded schematically to demonstrate all the constituent oligomeric stages to which small molecule channel modulators might bind. Whole membrane bound K_{Ca} channel including cytosolic CaMBD shown in orange, cell membrane shown as a grey box with red broken outline and constitutively associated CaM protein shown in blue. Ions shown in key, (bottom right).

No biophysical data exists for any small molecule modulator of calcium activated potassium (K_{Ca}) channels; all evidence of K_{Ca} channel modulation has been provided by cellular and pharmacological techniques.[1–4] Not only are biological techniques comparatively low throughput to biophysical assays, but they do not provide direct evidence of target engagement. Pharmacological effects, observed *in vivo via*

biological assays, can be produced by ligand alteration of any protein involved in associated biochemical pathways, not just the intended target protein.[5] The only modulators demonstrated to directly bind a K_{Ca} channel are NS309 and EBIO, both have been co-crystallised with the $SK_{Ca}2.2$ gating complex, PDB: 4G28 and 4J9Z, respectively.[6–8]

K_{Ca} channels, $IK_{Ca}3.1$ and $SK_{Ca}2.1$-3, are formed of four identical membrane bound subunits. The Ca^{2+} sensing protein calmodulin (CaM) is constitutively bound to each subunit's binding domain (CaMBD).[9,10] Without Ca^{2+}, CaM forms the inactivated K_{Ca} channel gating complex CaM:CaMBD, Figure 3.1. Binding of Ca^{2+} to CaM induces it to make a second protein-protein interaction (PPI) with the channel. Activated CaM binds another adjacent subunit's CaMBD creating an inter-channel subunit CaM bridge. This is mirrored by the CaM associated with the second subunit. The pair of CaM interactions produces a symmetrical tetrameric 2CaM:2CaMBD structure, physically leading to channel pore opening.[9] The published protein crystals of the activated $SK_{Ca}2.2$ gating complex provide snapshots of where positive modulators bind to K_{Ca} channels. The crystals, however, do not tell us the affinity or the process of how these ligands bind, which may occur at several possible oligomerisation stages of the channel gating complex, Figure 3.1.

Only a biophysical binding assay can dissect the mechanism of small molecule binding to the gating complex of K_{Ca} channels, helping to understand how ligand structure influences affinity and selectivity. In this chapter, work towards development of a biophysical binding assay to enable the identification and characterisation of K_{Ca} potential modulators, was conducted.

3.1 Production and Characterisation of K_{Ca} Channel Gating Proteins

Small molecule modulators of the $SK_{Ca}2.2$ channel bind its activated 2CaM:2CaMBD-(2) gating complex; therefore, it is assumed that putative modulators of the target $IK_{Ca}3.1$ channel bind its equivalent gating complex, 2CaM:2CaMBD-(4).[2,6,7] Hence, to develop a biophysical binding assay involving the target $IK_{Ca}3.1$ channel, the proteins of its gating complex were required. Using the primary sequences of CaM and the $IK_{Ca}3.1$ CaMBD-4, identified in Chapter 2, the target $IK_{Ca}3.1$ gating complex proteins were produced. Protein production was achieved using an adapted method from the published production procedure of the $SK_{Ca}2.2$ complex.[7,9]

3.1.1 Molecular Cloning

The structure of CaM is made of two globular terminal lobes joined by a linker section.[11] *In vivo*, it is the C-terminal lobe of CaM that is constitutively bound to the K_{Ca} channel CaMBD, leaving the N-terminal lobe free.[9,10] The constitutive CaM:CaMBD dimer can be replicated *in vitro* with a truncated CaMBD protein. The published method for obtaining the *in vitro* $SK_{Ca}2.2$ gating complex consists of expressing and purifying the constituent proteins individually. These gating proteins are carefully combined, in a 1:1 ratio, forming the CaM:CaMBD-2 dimer, which is re-purified.[8,9] This known production strategy was repeated to provide the individual $SK_{Ca}2.2$ gating proteins and adapted to give the $IK_{Ca}3.1$ CaMBD-4. Co-transcription, co-expression and co-purification of the respective constitutional CaM:CaMBD dimers was attempted. This method avoided protein degradation during the long combining processes and dimer re-purification.

Several plasmids, containing the genes for the $SK_{Ca}2.2$ and $IK_{Ca}3.1$ gating complex proteins, were required for expression in a bacterial host. Reverse translation of the target protein sequences gave the genes *cam*, *cambd-2* and *cambd-4*. The genes were

optimised for expression in *E. coli* and synthesised as DNA fragments commercially. The vector pNIC28-Bsa4, Figure 3.2, was subsequently recombined with these synthetic gene fragments *via* Gibson assembly to give the desired plasmids. Gibson assembly uses additional endonucleases, unlike traditional restriction enzyme recombination. Endonucleases remove the original restriction site and sticky end overhang, producing instead, a new much larger new overhang. Deletion of the initial restriction site sticky ends removes the possibility of their re-annealing to re-create the original DNA strands. The greater number of complementary uncoupled DNA bases in the new sticky end overhangs produced by the endonucleases, dramatically increases the success rate of intended DNA annealing.[12]

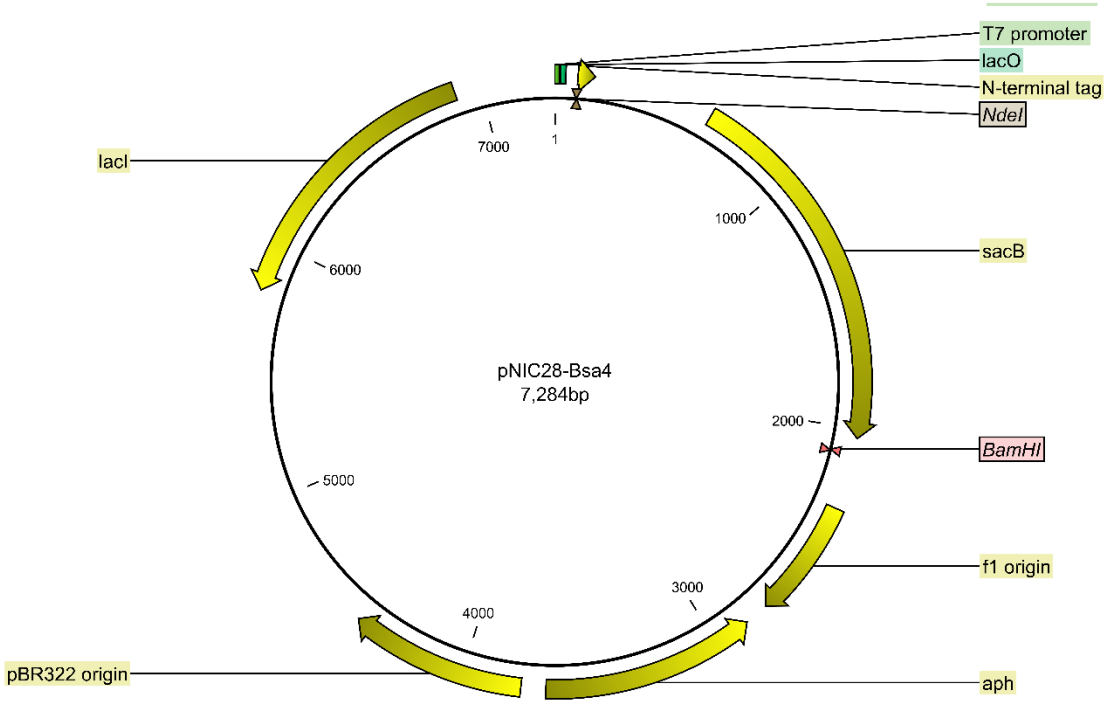


Figure 3.2; Vector plasmid diagram. Gene coding regions and their direction of expression shown as yellow arrows, restriction sites shown as hourglass symbols, protein binding regions shown as green blocks, and recombination displaced region bracketed in red.[13]

pNIC-Bsa4 was selected as a plasmid vector to transform *E. coli* due to its pBR322 origin and inducible gene expression *via* the regulatory T7*Lac* operon.[14–16] Each

synthetic gene; *cam*, *cambd-2* and *cambd-4,* was recombined with the vector to give one plasmid construct containing each. Recombination of the vector with synthetic DNA fragments of linked *cam-cambd* genes, gave co-transcriptional plasmid constructs for co-expression of *cam* with either *cambd-2* or *cambd-4*.

The conferred kanamycin resistance gene, *aph,* was used for positive selection of bacterial transformants.[17,18] The gene *sacB,* removed during vector restriction with BamHI and NdeI, was not utilised for negative selection, Figure 3.2.[19] The large linearised product of the vector restriction reaction was purified by electrophoresis, before its recombination with the synthetic genes. This purification step ensured no original vector remained during *E. coli* transformation and therefore no negative selection was required. A more intensive preparative two-stage process, linearising and assembling the desired plasmid constructs, was preferred to the difficulty of troubleshooting one pot recombination reaction failures.

The plasmid constructs were amplified in the NEB-5α *E. coli* host. The purified plasmid DNA was digested, and the restriction products were separated using electrophoresis, confirming the identity of their gene inserts by expected migration. Plasmid genes were also commercially sequenced, ensuring the correct expression of target protein primary sequences.

3.1.2 Protein Expression and Purification

Using the complement of gene constructs, induction of protein expression with isopropyl β-D-1-thiogalactopyranoside (IPTG) was achieved in the BL21(DE3) *E. coli* host, resulting in protein yields between 5 mg/L − 10 mg/L of cell culture. These yields provided each set of expressed proteins for use in later biophysical experiments.

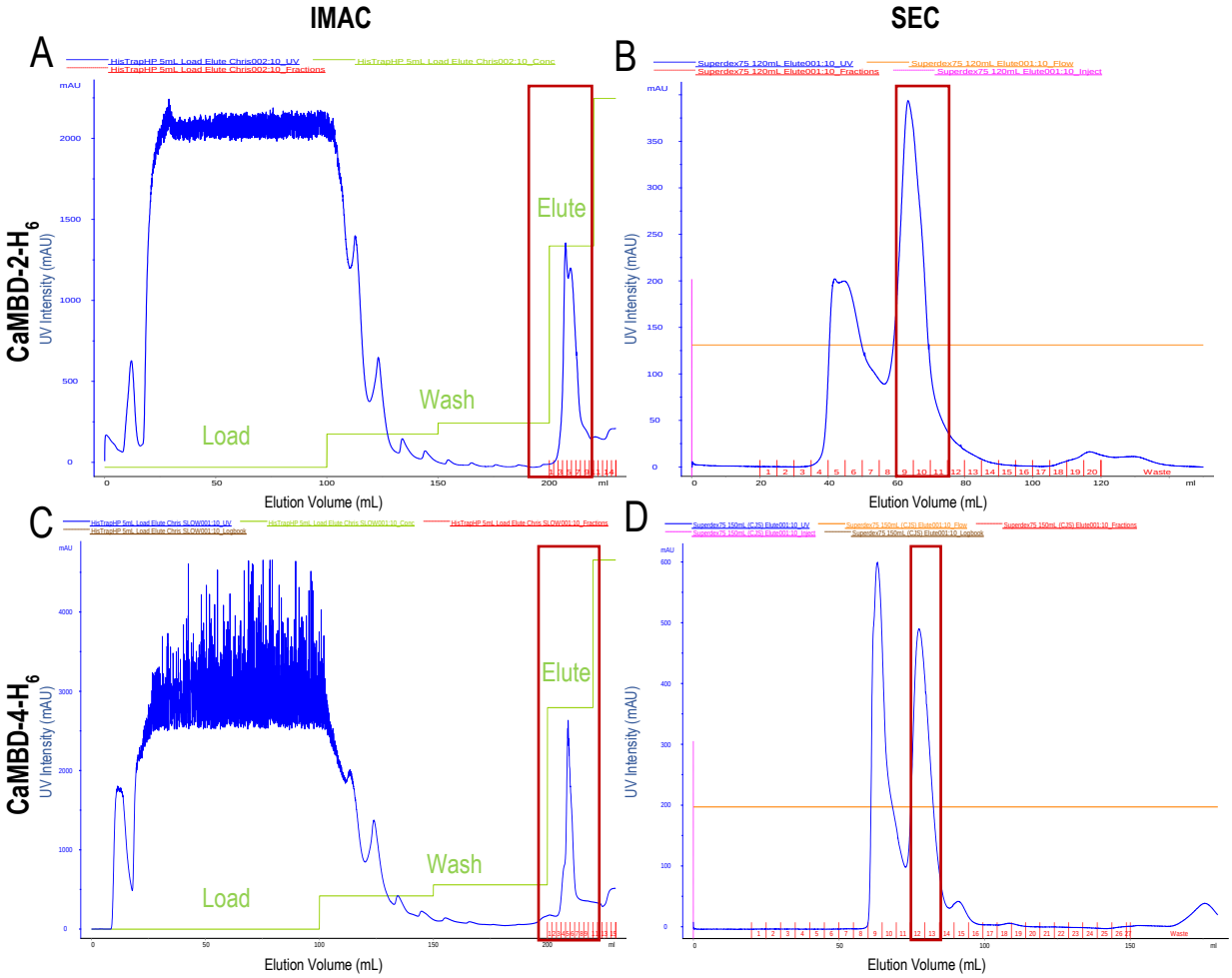


Figure 3.3; Purification of CaMBD-2-(H_6) and CaMBD-4-(H_6) by IMAC and SEC. U.V. absorbance shown in blue, %B IMAC eluent (500 mM imidazole) in green, flow rate in orange, fractions in red and selected fractions containing desired protein peaks highlighted in red boxes. A) and C) IMAC profiles; B) and D) SEC profiles.

Following published methods, immobilised metal affinity chromatography (IMAC) was used to purify the C-terminal hexa-histidine (H_6) tagged CaMBD-2-H_6 and CaMBD-4-H_6, Figure 3.3.[6] The proteins were further purified by size exclusion chromatography (SEC), concentrated and flash frozen.

The detergent sodium lauroyl sarcosinate (sarkosyl) was essential, at 0.2% concentration, for the stability of the CaMBD-H_6s, at all stages of their purification. The high ratio of 2:3 hydrophobic to hydrophilic residues, typical of CaM binding partners,

caused the CaMBD-H$_6$s to be unstable in solution.[11,20] The solution instability of the CaMBD-H$_6$s was also apparent from their tendency to precipitate at higher concentrations, despite the presence of sarkosyl detergent. Attempts to purify CaMBD-2-H$_6$ in the absence of detergent were unsuccessful, leading to no pure protein recovered, or only aggregate observed by SEC. The yield of the CaMBD-H$_6$s in the presence of detergent was 5-6 mg/L of cell culture.

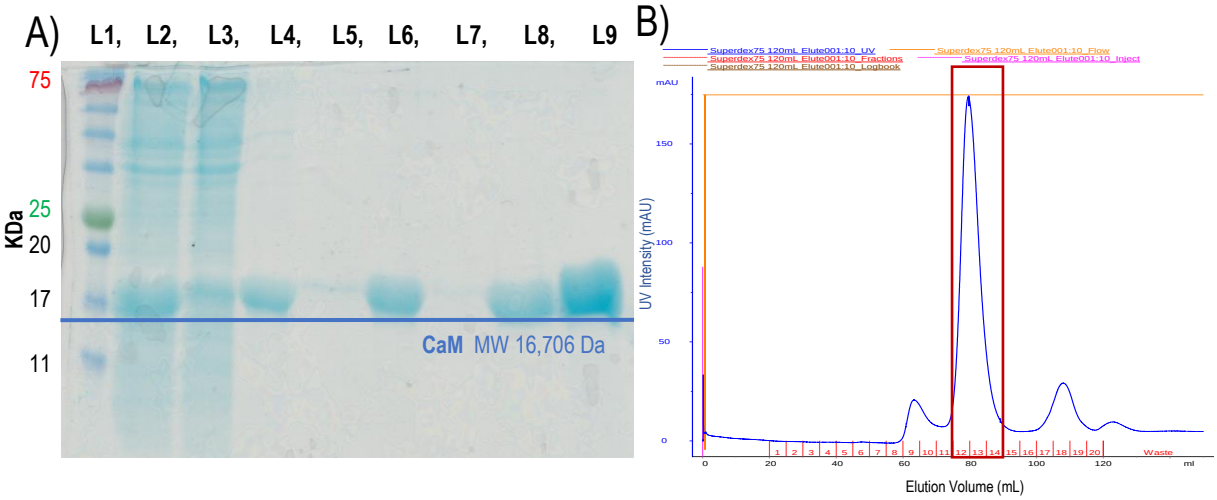


Figure 3.4; Room temperature HIC purification of CaM, followed by cold room SEC purification. A) SDS-PAGE of CaM HIC purification fractions, L1 = colour pre-stained protein standard broad range (11–245 KDa) (New England Biolabs Inc.), L2 = Cell lysate, L3 = Cell lysate HIC flow through, L4 = HIC Buffer I flow through, L5 = HIC Buffer II flow through, L6 = CaM standard, L7 = HIC Buffer III frac 1, L8 = HIC Buffer III frac 2, L9 = HIC Buffer III frac 3. B) CaM SEC profile, U.V. absorbance shown in blue, flow rate in orange, fractions in red and selected fractions containing desired protein peaks highlighted in red boxes.

CaM is a well-studied protein and was produced following a published protocol.[21,22] The two terminal lobes of CaM have EF hand moieties which bind Ca^{2+}.[11,23] CaM was expressed without an affinity tag due to the possible effect on the function of these terminal lobes or their EF hands. Once bound, Ca^{2+} causes the hydrophobic interiors of CaM's lobes to become exposed.[11,24] CaM was therefore purified using hydrophobic interaction chromatography (HIC), by inducing the exposure of its hydrophobic lobe interiors with Ca^{2+}.[21] Traditional HIC purification promotes the binding of hydrophobic

proteins with high buffer salt concentrations. HIC column bound hydrophobic proteins elute based on their overall polarity, as buffer salt concentration decreases over a gradient.[25,26] Instead of high salt, CaM was selectively bound to the hydrophobic column by induction with Ca^{2+}, allowing other hydrophobic proteins to elute from the column. Ca^{2+} was stripped from the bound CaM by EGTA, causing the CaM hydrophobic lobe interiors to re-internalise, allowing the selective elution of the desired protein.[21]

The purification of proteins is commonly conducted at 4 °C (cold room conditions) to reduce protein degradation during the process. HIC purification of CaM did not work under cold room conditions and was therefore performed on the bench at room temperature. The room temperature HIC purification of CaM was monitored by SDS-PAGE, due to the lack of a connected UV detector, Figure 3.4. It was thought that the initial cold room CaM purification failed because the hydrophobic effect is entropically driven, Equation 3.1.[26,27]

$$\Delta G = \Delta H - T\Delta S \qquad \textit{Equation 3.1}$$

Where ΔG is free energy, ΔH is enthalpy, T is temperature and ΔS is entropy.

In a polar solvent, hydrophobic molecules cause the ordering of a shell of surrounding polar solvent molecules, decreasing system entropy and generating a positive ΔG of solvation. To mitigate the increase in ΔG, hydrophobic molecules congregate to create a more efficient single solvent shell, requiring fewer ordered solvent molecules. However, the magnitude of lowering the $T\Delta S$ term of Equation 3.1 on ΔG is greatly reduced at lower temperatures.[27]

Subsequent SEC purification of CaM gave a protein yield 7 mg/L of cell culture, Figure 3.4.

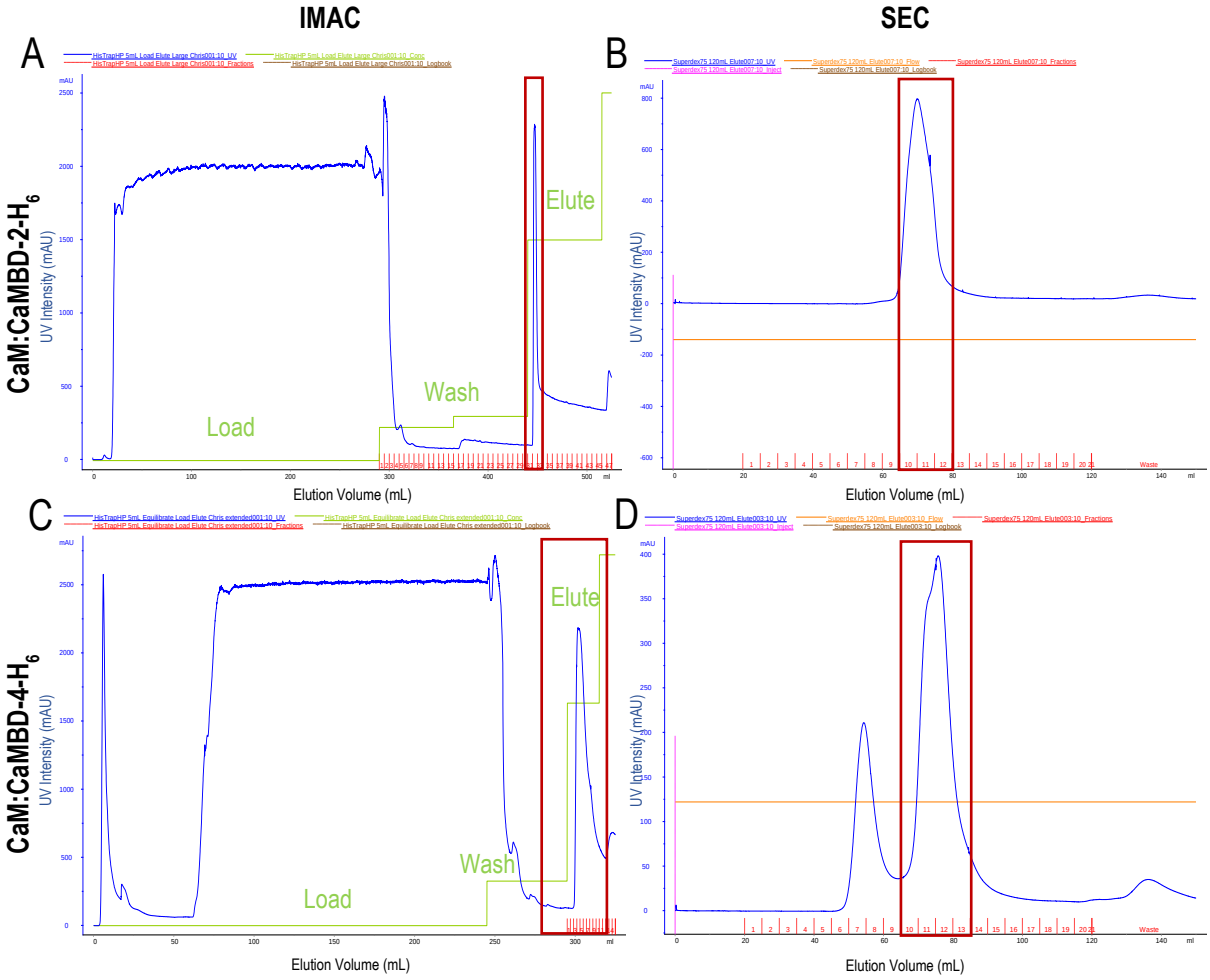


Figure 3.5; Co-purification of Cam and CaMBDs via their CaM:CaMBD-2-H_6 and CaM:CaMBD-4-H_6 constitutive dimers. U.V. absorbance shown in blue, %B IMAC eluent (500 mM imidazole) in green, flow rate in orange, fractions in red and selected fractions containing desired protein peaks highlighted in red boxes. A) and C) respective IMAC profiles; B) and D) respective SEC profiles.

Co-expressions of CaM with CaMBD-2-H_6 or CaMBD-4-H_6 was successful in providing each CaM:CaMBD-H_6 dimer, Figure 3.5. The CaMBD-H_6 hexa-histidine tag, enabled IMAC co-purification of both proteins together, exploiting the constitutive CaM association to the CaMBD-H_6s.

The association of CaM appeared to stabilise the CaMBD-H_6s in solution, not requiring sarkosyl detergent. The CaMBD-H_6s possess hydrophobic patches, enabling their association with the hydrophobic interiors of the CaM lobes.[9,28] These large CaMBD-H_6 hydrophobic patches possibly caused their solution instability. However,

when constitutively associated with CaM, one of these hydrophobic binding patches is sequestered within the soluble CaM C-terminal lobe. This stabilising effect meant there was no need to remove sarkosyl detergent, which may interfere with CaM:CaMBD-H_6 dimer assembly and affect subsequent biological assays.

The co-purification procedure provided a quick and efficient method to obtain the CaM:CaMBD-2-H_6 dimer in 10 mg/L of cell culture. This yield was double the maximum theoretical yield of the published combination procedure. The higher hydrophobicity of CaMBD-4-H_6, was thought to mean CaM stabilisation was less effective than for CaMBD-2-H_6, providing the dimer in 5 mg/L cell culture yield. This yield was the same as the maximum combination procedure yield; however, the procedure was more efficient on time and manpower. Quick production of both CaM:CaMBD-2-H_6 dimers was important for generating enough protein for use in assay development and potential crystallography experiments.

With a working procedure for the production of the $IK_{Ca}3.1$ and $SK_{Ca}2.2$ gating complex proteins and a collection of known small molecule modulators as positive and negative ligand controls, work on developing a biophysical binding assay began. However, the gating complex proteins were first assessed to confirm their expected behaviours in solution, before assumptions on their oligomeric states during assay conditions could be made.

3.1.3 Protein Characterisation

The identities and abilities of the purified proteins to form the expected 2CaM:2CaMBD-H_6 tetramers were investigated, to avoid false negative results in later biophysical assays. The expected masses of CaM, CaMBD-2-H_6 and CaMBD-4-H_6, were confirmed before assay development, to ensure no detectable modifications had been made, affecting their expected behaviours. The purified proteins abilities to form

their respective tetramers were characterised because the 2CaM:2CaMBD-2-H_6 tetramer is the only oligomeric state known to bind K_{Ca} channel modulators. Thus, observation of the tetrameric states of each set of proteins enabled the assumption that the same state would be present under assay conditions. This assumption discounted the potential false negative: the test molecule did not bind due to the lack of the required 2CaM:2CaMBD-H_6 tetramer state.

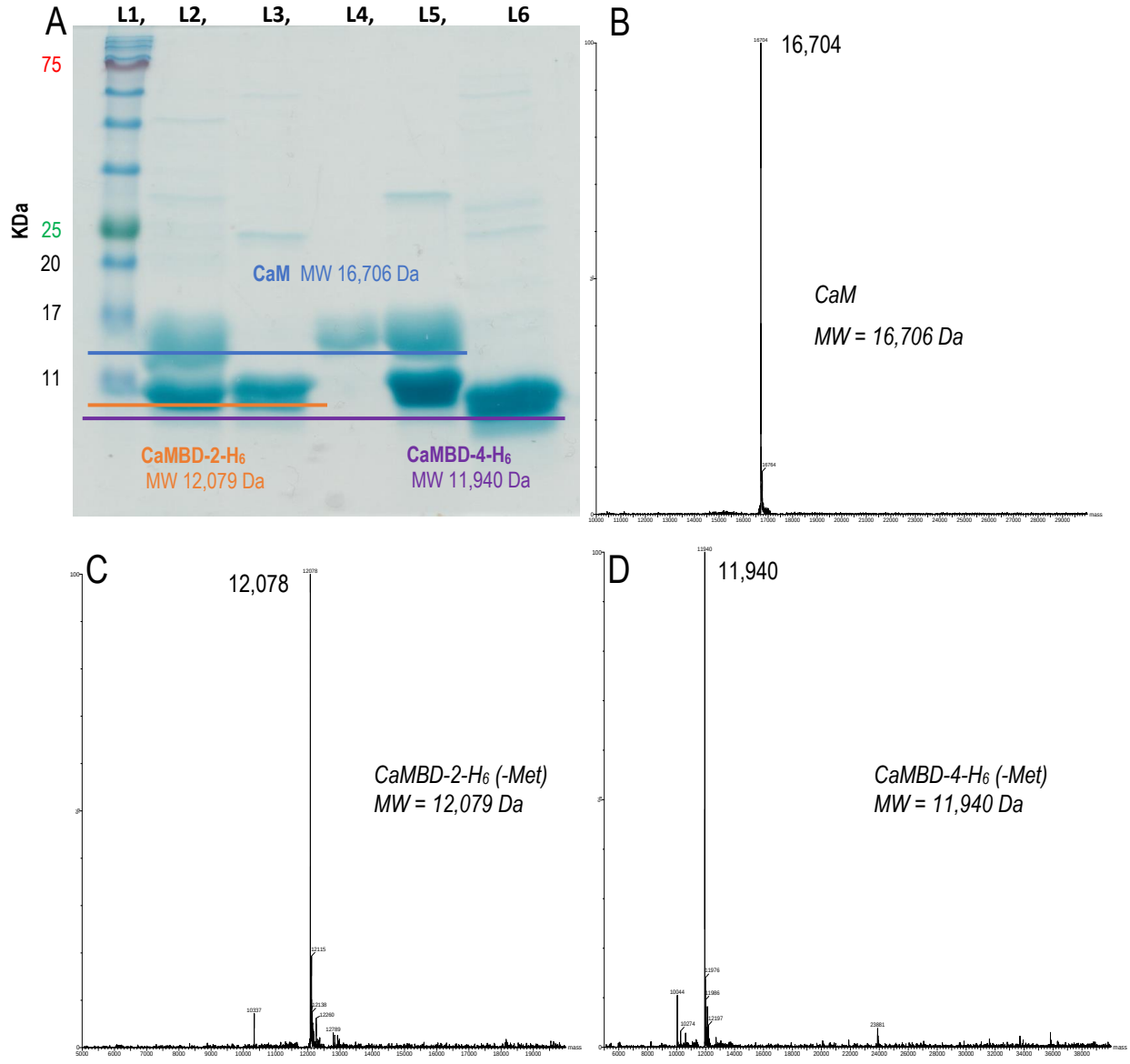


Figure 3.6; Identification of CaM, SKCa2.2 CaMBD-2-H_6, IKCa3.1 CaMBD-4-H_6 and the co-purified CaM:CaMBD-2-H_6 and CaM:CaMBD-4-H_6 dimers; A) SDS-PAGE of purified proteins, L1 = Colour pre-stained protein standard broad range (11–245 KDa) (New England Biolabs Inc.), L2 = CaM:CaMBD-2-H_6, L3 = CaMD-2, L4 = CaM, L5 = CaM:CaMBD-4-H_6, L6 = CaMBD-4-H_6; B) mass spectrum of purified CaM; C) mass spectrum of purified CaMBD-2-H_6; D) mass spectrum of purified CaMBD-4-H_6.

The CaM, CaMBD-H_6 and CaM:CaMBD-H_6 dimer purities were demonstrated by polyacrylamide gel electrophoresis migration, under sodium dodecyl sulfate conditions (SDS-PAGE), Figure 3.6 A, in conjunction with each purification SEC profile, Figure 3.3, Figure 3.4 and Figure 3.5. The relative ratio of CaM to CaMBD-H_6, in each CaM:CaMBD-H_6

dimer purification, appeared not to be 1:1, based on the SDS-PAGE protein bands' colour densities. This discrepancy can be explained by the dye-protein complexation mechanism of the protein visualisation stain Coomassie Brilliant Blue. The anionic sulfate groups of this stain complexes proteins *via* electrostatic attraction to positively charged protein residues, lysine and arginine.[29,30] Both CaMBD-H_6s appear darker because they have 22 conserved positive residues, so bind more dye molecules per protein than CaM, which has only 14 positively charge residues, Figure 3.6 A. The ratio of CaM to CaMBD-H_6 was therefore estimated by other means, discussed below. The SDS-PAGE bands did confirm the identity of the expressed and purified proteins by expected migration.

The initiator methionine, first residue of all protein sequences, is often deleted as a common *E. coli* post-translational modification.[31,32] These methionine deletions were detected in the expressed CaMBD-H_6s, *via* protein mass spectrometry (protein MS). The same initiator methionine deletions were present in the published $SK_{Ca}2.2$ 2CaM:2CaMBD-2-H_6 crystal structures, suggesting these modifications would not affect the proteins oligomerisation activities.[7,9] The confirmation of the expected protein masses by protein MS, suggested the primary sequences of the proteins were unchanged during production. Previous DNA sequencing of the plasmid constructs proved their genes contained the correct codon sequences. It was assumed to be very unlikely the protein sequences could have been altered during production, yet retain their expected masses, though this was not proven by protein sequencing.

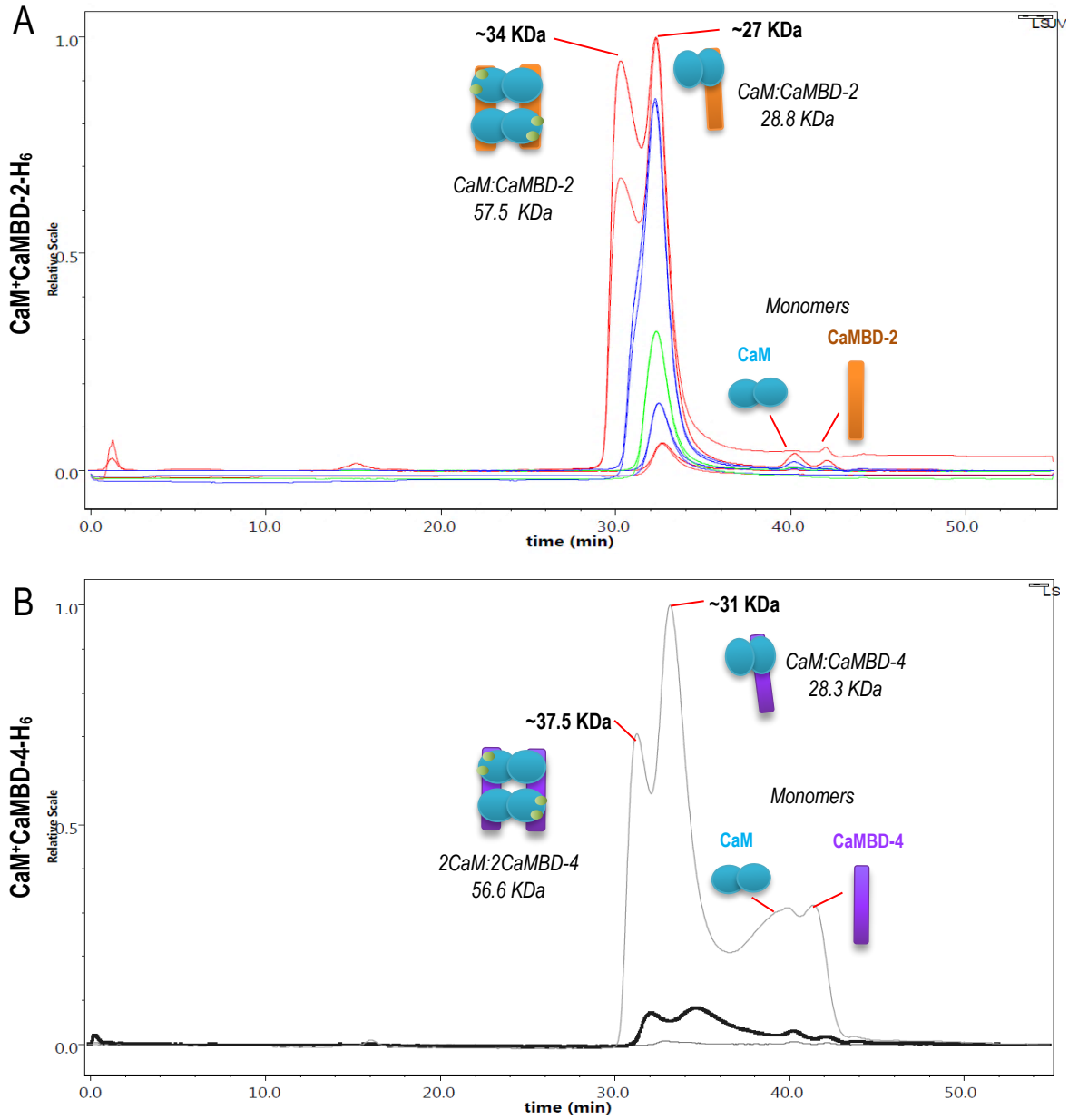


Figure 3.7; Observing complexation of $SK_{Ca}2.2$ and $IK_{Ca}3.1$ CaM:CaMBD-H_6 samples in the presence of Ca^{2+} (2 mM) as the protein concentrations are increased from 0.1−10 mM, using SEC-MALS. The increasingly larger molecular weight oligomeric states of the complexes are observed using MALS as the protein concentration of each CaM:CaMBD-H_6 sample injected onto the SEC column is increased. MALS determined absolute molar masses of the expected dimer and tetramer peaks are given in bold. Theoretical molecular weights (or molar masses) of the CaM:CaMBD-H_6 dimers and 2CaM:2CaMBD-H_6 tetramers given in italic below diagrams of each. A) Overlaid SEC chromatograms of increasing concentrations of CaM:CaMBD-2-H_6; 0.1 mM (lower red line), 0.3 mM (lower blue line), 1 mM (green line), 3 mM (higher blue line) and 10 mM (higher red line). B) Overlaid SEC chromatograms of increasing concentrations of CaM:CaMBD-4-H_6: 1 mM (lower line), 3 mM (middle line) and 10 mM (higher line).

Dynamic light scattering (DLS) is able to determine the hydrodynamic radii, thus, the shape and mass of molecules in solution, such as proteins.[33] DLS is commonly used to determine whether a sample contains only one size of molecule, mono-disperse, or several, polydisperse; however, the DLS resolution between molecular sizes is limited.[34] Published experimental DLS assessments of the $SK_{Ca}2.2$ gating complex in solution suggested that 10 mM $CaCl_2$ induced the formation of the 2CaM:2CaMBD-2-H_6 tetramer in a monodisperse state.[9] This experiment was reproduced using SEC with a multi angle light scattering detector (MALS), which has greater resolution than DLS, Figure 3.7. Enhanced resolution in SEC-MALS is achieved by separating protein complexes by their overall size, before determining their absolute molecular weight (molar masses) in solution.[35]

The affinities of complexed proteins for each other can also be determined by repeating SEC-MALS analysis of a protein complex sample, in increasing concentrations. As concentration increases, proteins assemble into complexes based on their PPI affinities. Protein complexes with high constituent protein affinities form rapidly. This means the lower order oligomeric state, such as monomers, assemble into higher order oligomeric states over a narrow window of relatively lower protein concentrations. Weaker inter-protein affinities cause complexes to form slowly, allowing for both lower and higher order oligomeric states to be present over a broader range of higher protein concentrations.[36] Repeated SEC-MALS experiments with increasing concentrations of the gating complex proteins of $SK_{Ca}2.2$, CaM+CaMBD-2-H_6, and $IK_{Ca}3.1$, CaM+CaMBD-4-H_6, in the presence of 10 mM $CaCl_2$ are shown in Figure 3.7.

Repeating SEC-MALS experiments, with increasing concentrations of the CaM:CaMBD-2-H_6 and CaM:CaMBD-4-H_6 samples, allowed for the observation of dimer and tetramer formations, based on their constituent PPI affinities. The

concentrations of CaM:CaMBD-2-H_6 and CaM:CaMBD-4-H_6 were assessed by SEC-MALS between 0.01 mg/mL and 1.00 mg/mL. The constitutive CaM:CaMBD-2-H_6 dimer was observed at all concentrations, demonstrating its stability in solution. The constitutive association affinities between the CaM and CaMBD-2 monomers must be very high, explaining why they remain associated even at low concentrations, Figure 3.7 A. The dimer of CaM and CaMBD-4-H_6 was less stable; the monomers could be seen even at higher concentrations of 1 mg/mL. It follows that the constitutive association affinities, between the CaM and CaMBD-4-H_6 monomers, must be much lower because they remained partially disassociated, even at higher concentrations, Figure 3.7 B. This comparatively lower exhibited affinity may be attributed to greater instability of the CaMBD-4-H_6 protein, compared to CaMBD-2-H_6.

Formation of the tetrameric state of either 2CaM:2CaMBD-2-H_6 or 2CaM:2CaMBD-4-H_6 were not observed by their expected molar masses. Instead, as the protein sample concentrations increased, new peaks of increasingly higher molar masses than the dimers were observed. The greater molar mass peaks of the highest protein concentration tested in with each complex, 1 mg/mL, gave the absolute molar masses, 34 and 37 KDa. These masses were smaller than the expected tetramer masses, 57.5 and 56.6 KDa, for 2CaM:2CaMBD-2-H_6 and 2CaM:2CaMBD-4-H_6, respectively. The molar masses of the larger tetrameric peaks increased with sample concentration. This increase suggested both 2CaM:2CaMBD-H_6 tetramers were in fast equilibrium with their CaM:CaMBD-H_6 dimeric states, tending towards the tetramers. The published DLS experiments were conducted at 10 mg/mL; however, the SEC column diluted injected samples by around 10-fold, meaning that 10 mg/mL samples produced only 1 mg/mL, observed by MALS. Injecting more concentrated samples might produce larger observed tetramer peaks, with absolute molar masses closer to

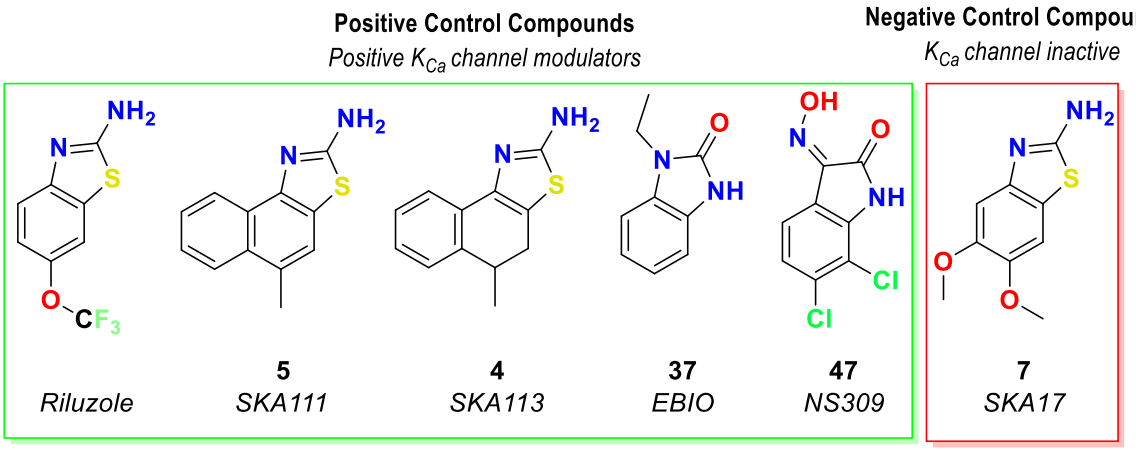
the expected masses of the tetramers. Unfortunately, this was not possible when observing the CaM:CaMBD-4-H_6 complex, which began to precipitate at concentrations above 10 mg/mL.

The intensity of the 2CaM:2CaMBD-2-H_6 tetramer peak was observed in equal proportion with the CaM:CaMBD-2-H_6 dimer; whereas, 2CaM:2CaMBD-4-H_6 was present as a smaller proportion with CaM:CaMBD-4-H_6. This observation suggested that the Ca^{2+} induced PPI between CaM and CaMBD-4-H_6 was weaker than with CaMBD-2-H_6. It is possible the CaM:CaMBD-4-H_6 complexes suffer from the lower stability of CaMBD-4-H_6, compared to CaMBD-2-H_6.

In summary, the gating complex proteins were successfully expressed. It was demonstrated that their function was correct, with both sets appearing to produce the expected tetrameric states. Therefore, these proteins were used to attempt binding studies.

3.2 Developing a KCa Gating Complex Binding Biophysical Screening Platform

The aim of developing a biophysical assay, capable of detecting ligand binding to the target 2CaM:2CaMBD-4-H_6 $IK_{Ca}3.1$ gating complex, was complicated by the equilibria between the monomeric, dimeric and tetrameric states. The $SK_{Ca}2.2$ 2CaM:2CaMBD-2-H_6 tetramer is the only known modulator binding oligomeric state; hence, several assay formats were assessed for their ability to detect expected binding of ligands to this state.



EC_{50} (μM)						
$SK_{Ca}2.1$	X	8.1	X	X	X	X
$SK_{Ca}2.2$	**10-20**	**13.7**	X	X	X	**N.E.**
$SK_{Ca}2.3$	10-20	7.7	7.2	395	0.4	X
$IK_{Ca}3.1$	X	**0.1**	**1.0**	**290**	**0.01**	**N.E.**

Figure 3.8; Chemical structures of published K_{Ca} positive modulators used as positive control molecules in assay development. Positive control molecules with published positive modulation activities in green rectangle. Negative control compound published as inactive against K_{Ca} channels in red box. Individual K_{Ca} channel EC_{50} concentrations of each molecule directly below it in μM, values relevant to subsequent biophysical experiments in bold. N.E. = no effect.[1,37,38]

Promotion of a PPI is an unusual mode of target modulation and not well studied in the literature compared to inhibition of PPIs.[39] There are few assay protocols developed to detect the binding of PPI-promoting modulators to as complicated a target as the K_{Ca} gating complex. Additionally, it is unknown to which oligomeric state of the dynamic K_{Ca} gating complex modulator binding occurs. There are several potentially detectable ligand interactions between each of the K_{Ca} complex states, Figure 3.1. Dissection of the mechanism of K_{Ca} channel modulator binding was required to understand which potential ligand interaction would be detected in a biophysical assay. Previously

synthesised published modulators were used as positive and negative controls to aid in interpretation of assay results, Figure 3.8.

3.2.1 Differential Scanning Fluorimetry as a Biophysical Binding Assay

With the gating proteins of $SK_{Ca}2.2$ and the target $IK_{Ca}3.1$ available, experiments were conducted to assess whether differential scanning fluorimetry (DSF), or thermal shift analysis, would be a suitable binding assay. DSF is often employed to identify reagents and conditions that stabilise proteins of interest, enhancing their ability to crystallise for structure determination.[40,41] This technique is also able to identify the binding of any ligand *via* its stabilising effect on a subject protein and has been subsequently adapted as a high throughput assay.[42]

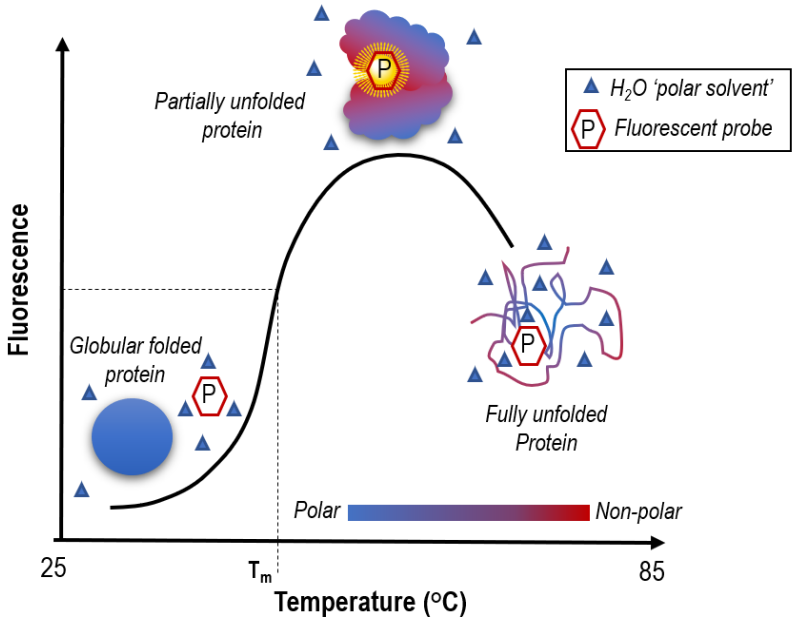


Figure 3.9; Model DSF curve of a soluble globular protein. Sigmoidal protein unfolding curve shown in solid black. Folded soluble globular protein with polar surface residues shown as a sphere, partially unfolded protein shown as an irregular solid shape with exposed hydrophobic interior, fully unfolded protein shown as a disordered solvent accessible peptide chain. SYPRO orange probe shown as solvent quenched hexagon P, and fluorescent when sequestered from polar solvent. Polarity of residues, solvent and probe indicated by blue to red colour scheme. Mid-point of sigmoidal protein unfolding curve shown as melting temperature (T_m) by dashed lines.

DSF utilises a probe, usually SYPRO orange, which is fluorescent in hydrophobic environments and not in polar environments. Experiments are performed over a temperature gradient where the subject protein is unfolded, or 'melted', Figure 3.9. As the protein melts, it exposes its hydrophobic interiors, allowing the probe to bind. The sequestered probe fluoresces. Once the protein is fully unfolded, including its hydrophobic environments, the probe is no longer excluded from the solvent and its fluorescence is again quenched. Ligands that thermodynamically affect the proteins stability upon binding 'shift' its melting temperature (ΔT_m).[42]

While DSF is typically applied to a single soluble globular protein, it has also been applied to measure small molecule stabilisation of protein complexes. Plasmodium's 'glideosome', responsible for the parasites movement across the host cell's surface, is formed from an actin-myosin associated macromolecular complex. DSF was used to observe the stabilisation of critical components in this protein complex in the presence of small molecule ligands.[43]

Rotamer is a protein complex responsible for trafficking protein cargo away from endosomes. This complex was stabilised by computationally identified small molecules, observed by DSF complex $\Delta T_{m.}$[43]

The Ca^{2+} induced, tetrameric 2CaM:2CaMBD-H_6 complexes, involve one poorly soluble protein, and are more complex than the literature dimer example. The amalgam of interactions involved in K_{Ca} gating proteins' complexation introduced several variables concerning each constituent protein-protein, protein-Ca^{2+} and protein-ligand interaction, Figure 3.1. All these variables presumably affect the overall DSF signal output for the entire desired $4Ca^{2+}$:2CaM:2CaMBD:2Ligand complex. Thus, several control experiments were conducted to try to disassemble the potential effects of these constituent interactions on the overall complex DSF signal.

The objective of the DSF experiments was to observe ligand induced stabilisation of the 2CaM:2CaMBD-H_6 tetramer. The tetramer is the only known oligomeric state of the K_{Ca} channel gating complex, known to contain the binding cavity of the positive modulators; however, this information is based on the $SK_{Ca}2.2$ co-crystal structures with EBIO and NS309 ligands. Crystallography is not representative of protein solution state behaviour and does not preclude the possibility that these small molecule modulators bind to the lower oligomeric stages of the gating complex; the monomers or dimer. Therefore, control experiments were required to identify which stage of the complex, if any, was stabilised by the known K_{Ca} channel positive modulators. All the composite interactions of the target K_{Ca} channel gating complex 2CaM:2CaMBD-H_6 tetramer can be seen in Figure 3.1.

A control experiment was performed on each of the stages of 2CaM:2CaMBD-H_6 complexation to understand how each stage of oligomerisation, monomers, dimer and tetramer effected the DSF signal. Any effect on the DSF signal of each known K_{Ca} channel positive modulator in Figure 3.8 at each oligomeric state was also observed. . Unfortunately, it was not possible to observe the effect of Ca^{2+} binding to the dimer as this would cause tetramerization. Instead, the effect of Ca^{2+} on CaM alone was observed. Finally, DSF experiments observing the effect of the control compounds on each oligomeric state and protein were performed to understand the mechanism of modulator binding, Figure 3.8.

The $SK_{Ca}2.2$ gating complex has been well-studied; its stability and solution behaviour was greater than that of the target $IK_{Ca}3.1$. Thus, $SK_{Ca}2.2$ was used as a model complex before $IK_{Ca}3.1$ proteins were studied.

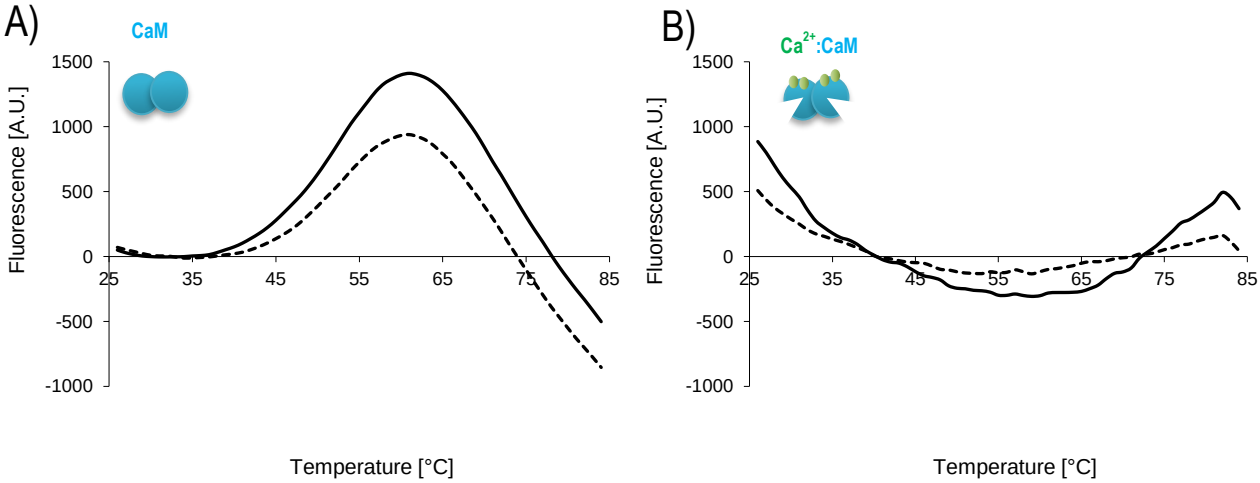


Figure 3.10; CaM DSF Experiments. A) CaM experiments in the absence of Ca^{2+}. B) CaM experiments in the presence of Ca^{2+}. CaM without ligands shown as solid lines. CaM with SKA113 ***4*** *shown as broken lines.*

The Ca^{2+} sensing regulator protein CaM is a globular soluble protein, giving a typical DSF profile, Figure 3.10 A; however, upon addition of Ca^{2+}, the CaM profile was completely altered, Figure 3.10 B. When Ca^{2+} bound, CaM's two terminal lobe hydrophobic interiors become exposed, enabling CaM to bind hydrophobic protein partners.[11,24] In theory, exposure of CaM's lobe interiors may allow SYPRO orange to bind, giving the initial high fluorescent signal in Figure 3.10 B. As temperature increased, Ca^{2+} may have dissociated from CaM, causing its lobes to reclose, excluding the probe and reducing the signal. Lastly, as the temperature continued to increase, CaM itself may have melted, re-exposing its hydrophobic interior, bringing up the signal once more, Figure 3.10 B. If true, the higher melting temperature of Ca^{2+} bound CaM would represent a ΔT_m of 21 °C. This is a very large, yet reasonable thermal shift, because CaM binds four Ca^{2+} ions tightly in its role as a Ca^{2+} sensor.[10,24]

The addition of known $SK_{Ca}2.2$ gating complex ligands NS309 **47**, and EBIO **37** or the putative $IK_{Ca}3.1$ modulators SKA111 **5**, or SKA113 **4**, to the CaM DSF experiment, caused a lowering of the fluorescence under both conditions, Figure 3.10. Neither of

these modulator-altered CaM results represented a $\Delta T_{m,}$ so they are not positive results. The modulators did cause a change to the DSF profiles, however. It is possible the modulators were able to bind the exposed cavities of CaM *via* non-specific hydrophobic interactions, in the same manner as the probe. The modulators may therefore compete with SYPRO orange, causing the decrease in overall fluorescence.

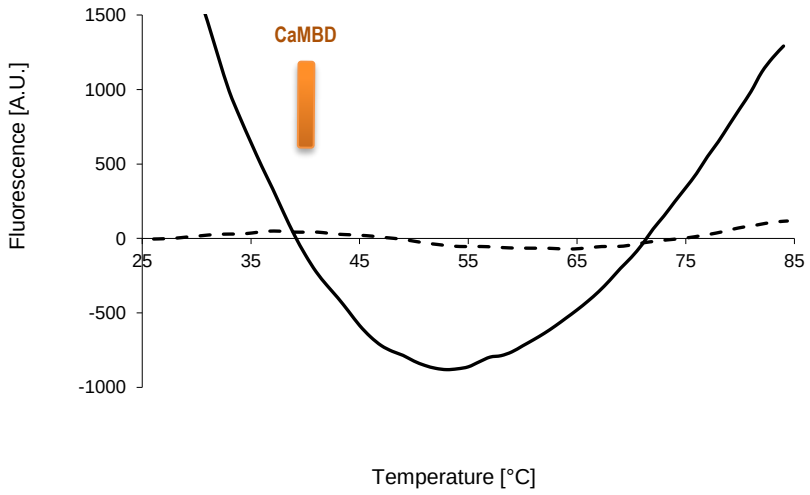


Figure 3.11; CaMBD-H_6 DSF Experiments. Both CaMBD-2-H_6 or CaMBD-4-H_6 results were identical. . CaMBD-H_6s without detergent shown as a broken line. Addition of sarkosyl detergent shown as a solid line (sarkosyl detergent without protein gave an identical signal).

No SYPRO orange fluorescent signal was given at any temperature during the DSF experiment with either CaMBD-2-H_6 or CaMBD-4-H_6 because these are not globular proteins, but α-helical coiled coils, Figure 3.11. While the CaMBD-H_6s have hydrophobic patches, they could not sequester the probe from the polar aqueous solvent; thus, no fluorescent signal was given at any temperature. The addition of detergent sarkosyl to the CaMBD-H_6 DSF experiments did give a signal. Control detergent experiments without protein gave an identical DSF profile, however. The signal observed in experiments containing detergent was given by the detergent itself, rather than making the CaMBD-H_6s more soluble, altering their responses. The initial high detergent signal

is likely due to the formation of detergent micelles which have hydrophobic interiors accessible to the probe. Upon heating, the critical micelle concentration is altered, first lowering the micelle count and then bringing it back up in line with the fluorescent signal.[44]

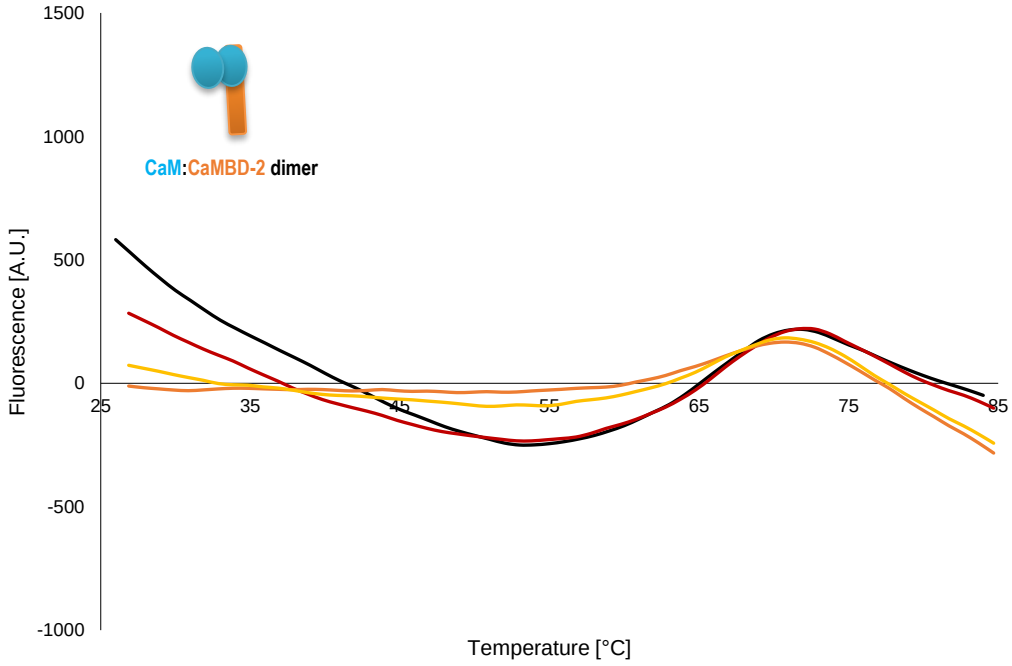


*Figure 3.12; CaM:CaMBD-2-H_6 dimer DSF experiments in the absence of Ca^{2+}. Constitutive dimer alone shown in black. Addition of EBIO (1 mM) in red. Addition of SKA113 **4** (0.5 mM) in orange. Addition of SKA111 **5** in yellow.*

The first PPI assessed by DSF was of the CaM:CaMBD-2-H_6 dimer, a control experiment performed in the absence of Ca^{2+}, Figure 3.12. When compared to the previous CaM control experiments in the presence of Ca^{2+}, this dimer DSF trace appears similar. It is not clear what caused the higher initial fluorescence of the dimer trace because no Ca^{2+} is present to open the CaM terminal domains. The binding of CaMBD-2-H_6 to the C-terminal lobe of CaM, may act allosterically to partially open the N-terminal domain, causing fluorescence in the same way as the Ca^{2+} CaM control, Figure 3.10 B. It follows that the same effect of increased heating would cause

dissociation of the CaMBD-2-H_6, closing the CaM lobes and lowering the fluorescent signal. Melting of CaM at higher temperatures caused the final fluorescent peak. The CaM:CaMBD-2-H_6 dimer DSF experiment could be interpreted as the effect of CaMBD-2-H_6 on the stability of CaM, representing a CaM ΔT_m of 13 °C, Figure 3.12.

Addition of the positive control modulator compounds, in Figure 3.8, to the CaM:CaMBD-2-H_6 dimer DSF experiment, decreased the fluorescent signal but did not change the shape of the DSF trace. Similar to the Ca^{2+} CaM control DSF experiment, Figure 3.10 B, the signal lowering effect suggested small molecule competition with the SYPRO orange probe for the CaM lobe hydrophobic environments yet did not indicate specific binding to the protein.

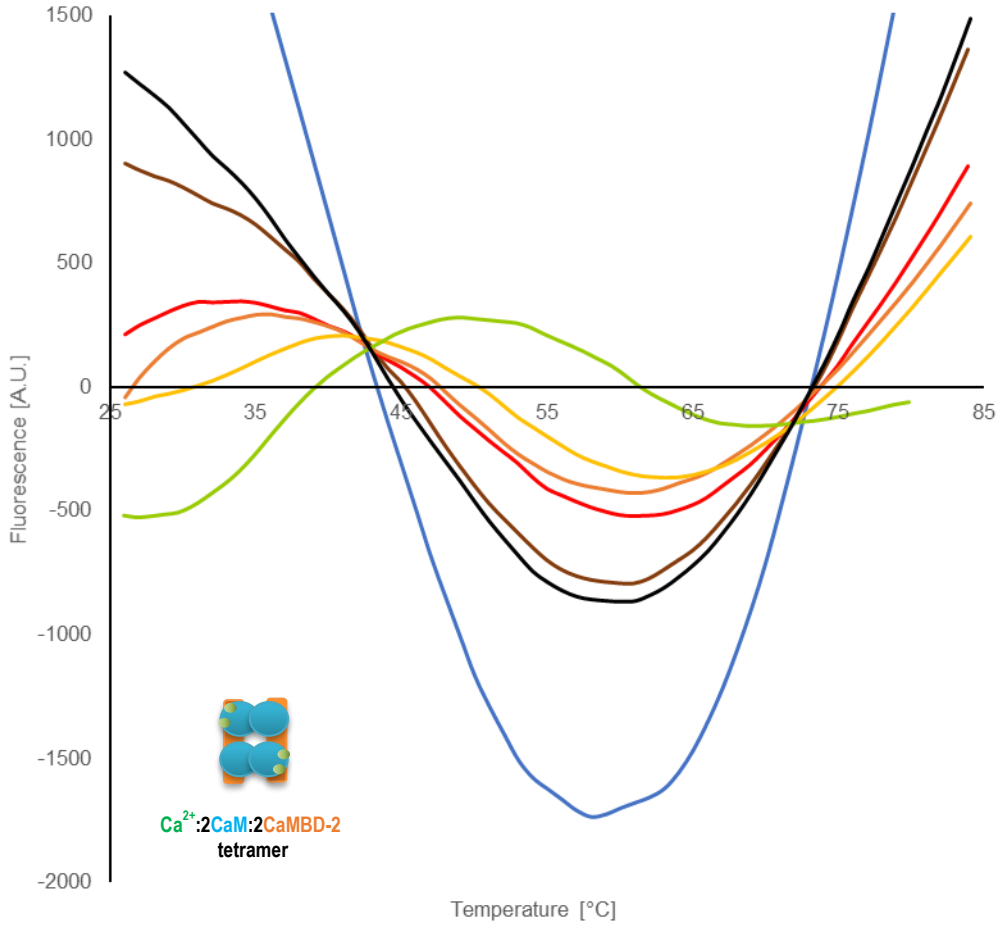


*Figure 3.13; 2CaM:2CaMBD-2-H$_6$ DSF experiments in the presence of Ca^{2+}. 2CaM:2CaMBD-2-H$_6$ with Ca^{2+} alone shown in black. Addition of modulator EBIO **37** (1 mM, EC$_{50}$ 0.4 mM) in brown. Addition of SKA113 **4** (0.5 mM) in red. Addition of putative modulator SKA111 **5** (0.05 mM, EC$_{50}$ 0.008 mM) in orange. Addition of modulator NS309 **47** (0.05 mM, EC$_{50}$ 0.0004 mM) in yellow. Addition of modulator drug riluzole (1 mM, EC$_{50}$ 0.03 mM) in green. Addition of negative control ligand SKA17 **7** (1 mM, no EC$_{50}$) in blue.*[1,2,38]

The final DSF experiment aimed to investigate the Ca^{2+} induced PPI of the SK$_{Ca}$2.2 2CaM:2CaMBD-2-H$_6$ tetramer, known to contain the K$_{Ca}$ channel modulator binding site, Figure 3.13. This tetramer is present at concentrations of 10 mM $CaCl_2$, shown by SEC-MALS analysis, subsection 3.1.3. This was assumed to still be true in the DSF experiment including $CaCl_2$.

The trace of the $CaCl_2$ containing 2CaM:2CaMBD-2-H$_6$ DSF experiment appears as the complete inversion of the ideal globular protein melting trace, Figure 3.9.

CaMBD-2-H_6 has previously been ruled out as a likely source of probe fluorescence by analysis of the control experiments, Figure 3.11. By comparing the 2CaM:2CaMBD-2-H_6 tetramer containing DSF experiment, Figure 3.13, with the previous CaM containing DSF control experiments, Figure 3.10 and Figure 3.12, the tetramer trace could be explained by CaM. It follows, the initial low temperature descending fluorescence signal slope, in the 2CaM:2CaMBD-2-H_6 tetramer containing DSF experiment, Figure 3.13, could correspond to the exposure of Ca^{2+} bound CaM hydrophobic interiors. As in the hypothetical explanation of Figure 3.10 B, the descending fluorescent signal slope possibly represented the increasing dissociation of Ca^{2+} from CaM. The higher temperature ascending signal slope in Figure 3.13, may therefore have been CaM melting, re-exposing its hydrophobic interiors to SYPRO orange and increasing its fluorescence. Beyond this analysis, the original tetramer trace in Figure 3.13 is difficult to interpret because the apex of both slopes is not observed, so no T_ms could be extracted.

Addition of K_{Ca} channel negative modulator, SKA17 **7**, and positive modulators; EBIO **37**, SKA113 **4**, SKA111 **5**, NS309 **47**, to the 2CaM:2CaMBD-2-H_6 tetramer experiment, Figure 3.13, produced significant fluorescent signal trace alterations. A trend in Figure 3.13 showed the addition positive modulators produced a new low temperature signal peak. This modulator induced peak shifted to higher temperatures as modulator potency increased. The low temperature, modulator induced, fluorescent signal peaks were not observed in previous DSF control experiments, Figure 3.10 and Figure 3.12, suggesting that this peak must relate to the tetrameric state, 2CaM:2CaMBD-2-H_6.

Both 2CaM:2CaMBD-H_6 tetrameric states were observed to be in rapid equilibrium with their CaM:CaMBD-H_6 dimeric states at room temperature *via* SEC-MALS, Figure 3.7. It follows that the tetrameric complexes would have low T_m, potentially lower

than room temperature. DSF experiments begin at 25 °C, so the origin of the low temperature fluorescent signal peak of Figure 3.13, was not observed in the absence of positive modulators, only its downward slope. Theoretically, the DSF traces could continue below 25 °C, where the ascending slopes of these low temperature peaks may be seen. Without this low temperature data, a true set of modulator-induced presumed tetramer ΔT_ms could not be generated.

The amyotrophic lateral sclerosis drug riluzole, which interacts with many proteins, was the first known K_{Ca} channel modulator. All subsequent modulators were modelled on riluzole.[2,38,45] Despite having an $SK_{Ca}2.2$ EC_{50} of 20-30 µM, riluzole shifted the presumed tetramer peak, Figure 3.13, to resemble an ideal globular protein trace, Figure 3.9. The most potent $SK_{Ca}2.2$ modulator, NS309, which has an $SK_{Ca}2.2$ EC_{50} of 440 nM, did not produce as large an effect, Figure 3.13. Riluzole was tested at 1 mM, and NS309 at 50 µM due to their relative limiting solubilities. It is possible that the greater excess of riluzole enabled protein saturation. Better saturation of riluzole might be the cause of the greater thermal shift of the presumed, 2CaM:2CaMBD-2-H_6 tetramer peak, rather than its potency. Lower concentrations of riluzole were not assessed in the 2CaM:2CaMBD-2-H_6 tetramer DSF experiment to test this hypothesis.

The negative control molecule SKA17 **7** has no reported effect on whole K_{Ca} channels, Figure 3.8.[1] Addition of SKA17 **7** to the 2CaM:2CaMBD-2-H_6 containing DSF experiment, Figure 3.13, did alter the tetramer DSF trace. SKA17 **7** caused the descending slope of presumed tetramer peak, and the ascending slope of CaM melting to both become steeper than without any small molecule addition. Thus, SKA17 **7** may destabilise the presumed 2CaM:2CaMBD-2-H_6 tetrameric peak and lower the CaM T_m. This would mean SKA17 **7** acts as a negative modulator, disrupting gating complex formation. This

effect may not have been highlighted in the published patch clamp experiments, which looked specifically for channel activation, and so positive modulation only.

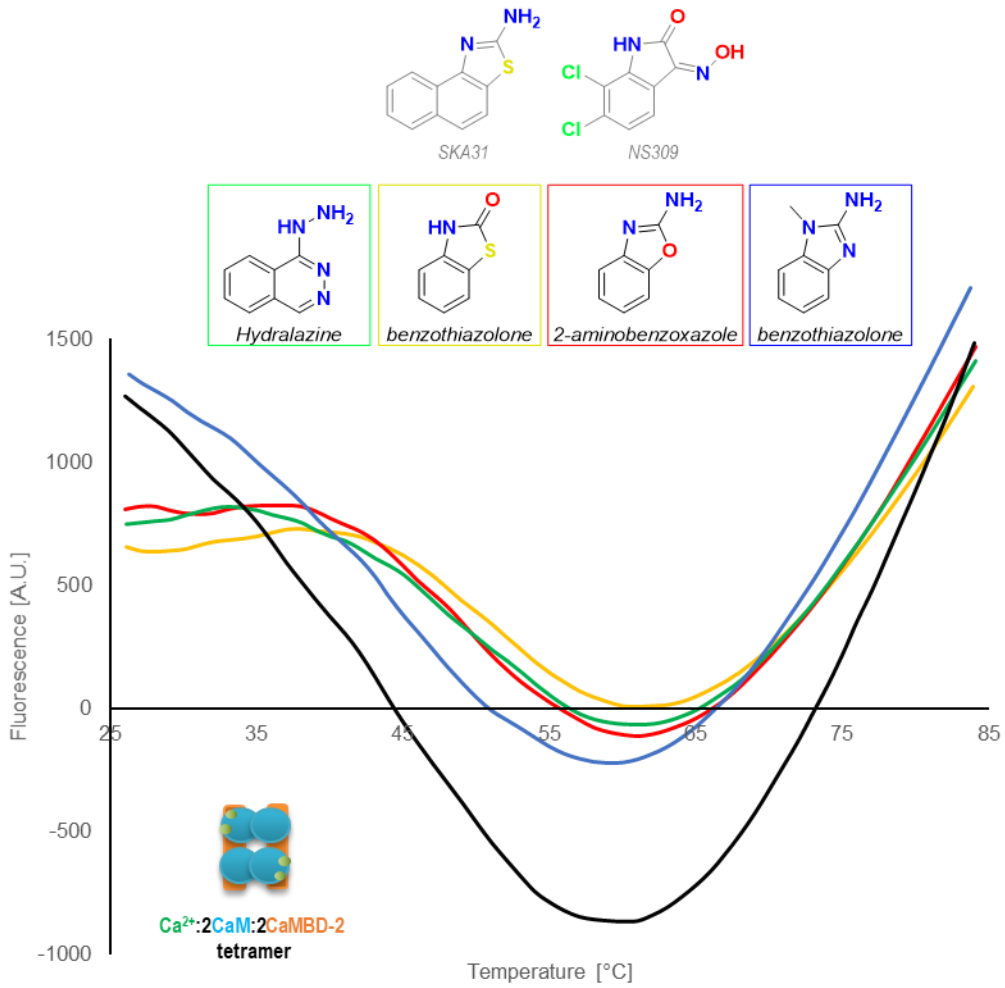


Figure 3.14; Applying DSF assay format to screen for unknown potential ligands. Experiments conducted using CaM:CaMBD-2-H_6 (10 µM) in the presence of Ca^{2+} (2 mM). Reference control without ligand shown in black. The structures of each test molecule (1 mM) shown in boxes corresponding to the DSF signal given. The structures of the known modulators SKA111 ***5*** *and NS309* ***47*** *also shown for comparison to test molecules only.*

DSF experiments in the presence of 2 mM Ca^{2+} as a biophysical screening technique. CaM:CaMBD-2-H_6 in the presence of Ca^{2+} in black, additions of ligands shown in broken lines. A) Effect of 2-aminoisoxazole. B) Effect of benzothiazolone. C) Effect of hydralazine. D) Modulators SKA111 ***5*** *and NS309* ***47****.*

The K_{Ca} channel, positive modulator induced, presumed tetramer peak in Figure 3.13, suggested the 2CaM:2CaMBD-H_6 DSF experiment with $CaCl_2$, could be used to identify

unknown binders of the modulator binding site. This theory was tested with four simple commercial fragments, similar in structure to the published K_{Ca} channel modulators SKA111 **5** and NS309 **47**, Figure 3.14. Included in the small set of screened compounds, was the blood pressure drug hydralazine; a fragment sized vasodilator drug, with an unknown mechanism thought to include the function of potassium ion channels.[46,47] Hydralazine also bares some structural similarity to the naphthothiazole core. It was hypothesized to potentially act on K_{Ca} channels *via* the positive modulation mechanism under investigation. These simple small molecule fragments were screened *via* the tetramer containing DSF technique, Figure 3.14.

Of the five heterocycle fragments screened, benzothiazolone and 2-aminobenzoxazole were identified as potential binders in the DSF screening format, producing the same presumed tetramer peak as the known positive modulators, Figure 3.14. Hydralazine was shown to potentially bind to the $SK_{Ca}2.2$ gating complex tetramer, giving credence to the hypothesis that K_{Ca} modulation is at least one of its possible mechanisms of action, Figure 3.14.

Having shown DSF could be used to detect $SK_{Ca}2.2$ gating complex binders, the same method was applied to the target $IK_{Ca}3.1$ complex, Figure 3.15.

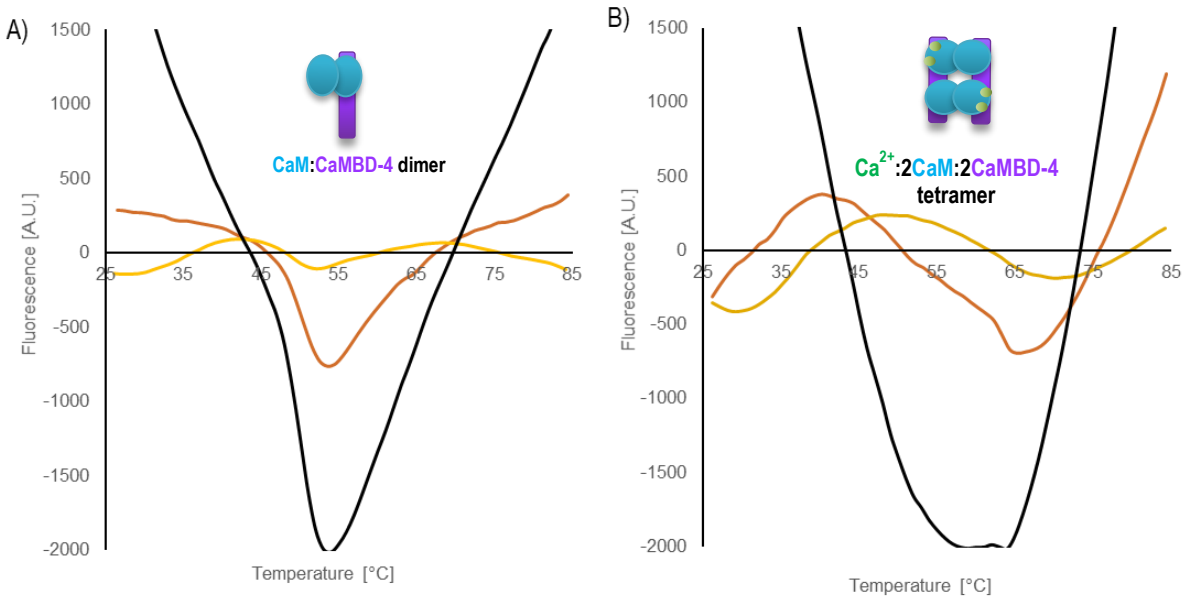


Figure 3.15; CaM:CaMBD-4 DSF experiments. A) CaM:CaMBD-4 constitutive dimer experiments in the absence of Ca^{2+}. B) 2CaM:2CaMBD-4 tetramer experiments in the presence of Ca^{2+}(2 mM). Experiments without ligands are shown as black lines. Additions of the $IK_{Ca}3.1$ modulator SKA111 ***5*** *(0.05 mM) are shown as orange lines. Additions of riluzole are shown as yellow lines.*

The CaM:CaMBD-4-H_6 dimer control experiment, in the absence of Ca^{2+}, produced a different DSF trace to that of the CaM:CaMBD-2-H_6 dimer, Figure 3.15 A. This dimer signal appeared similar to the final 2CaM:2CaMBD-2-H_6 tetramer experiment, in the presence of Ca^{2+}, Figure 3.13. SEC-MALS experiments demonstrated both the dimer and tetramer states, of the CaM:CaMBD-4-H_6 gating proteins, were less stable than the CaM:CaMBD-2-H_6 oligomers, Figure 3.7. It was, therefore, unlike the CaM:CaMBD-4-H_6 dimer experiment, Figure 3.15 A, meant that the 2CaM:2CaMBD-4-H_6 tetramer was present in the absence of Ca^{2+}. Potentially, the less stable CaM:CaMBD-4-H_6 dimer could have produced a greater allosteric N-terminal opening of CaM, giving more access to the SYPRO orange probe.

The 2CaM:2CaMBD-4-H_6 tetramer DSF experiment, Figure 3.15 B, gave a very similar trace the corresponding 2CaM:2CaMBD-2-H_6 experiment, Figure 3.13. Addition of SKA111 **5** to the 2CaM:2CaMBD-4-H_6 experiment, Figure 3.15 B, induced the expected

low temperature peak associated with the 2CaM:2CaMBD-4-H_6 tetrameric state, similar to the 2CaM:2CaMBD-2-H_6 DSF experiments, Figure 3.13. This low temperature peak effect was not observed in the CaM:CaMBD-4-H_6 dimer experiment, suggesting the two sets of gating complex proteins were behaving in the same fashion. Again, riluzole shifted the 2CaM:2CaMBD-4-H_6 presumed tetramer peak the most.

In light of these experiments, it has been demonstrated DSF could be applied to the stabilising effect of small molecules, on such a complicated protein complex. However, these results needed to be verified by corroborating results from a second, orthogonal biophysical assay, before larger scale screenings were undertaken.

3.2.2 Fluorescence Polarisation as a Biophysical Binding Assay

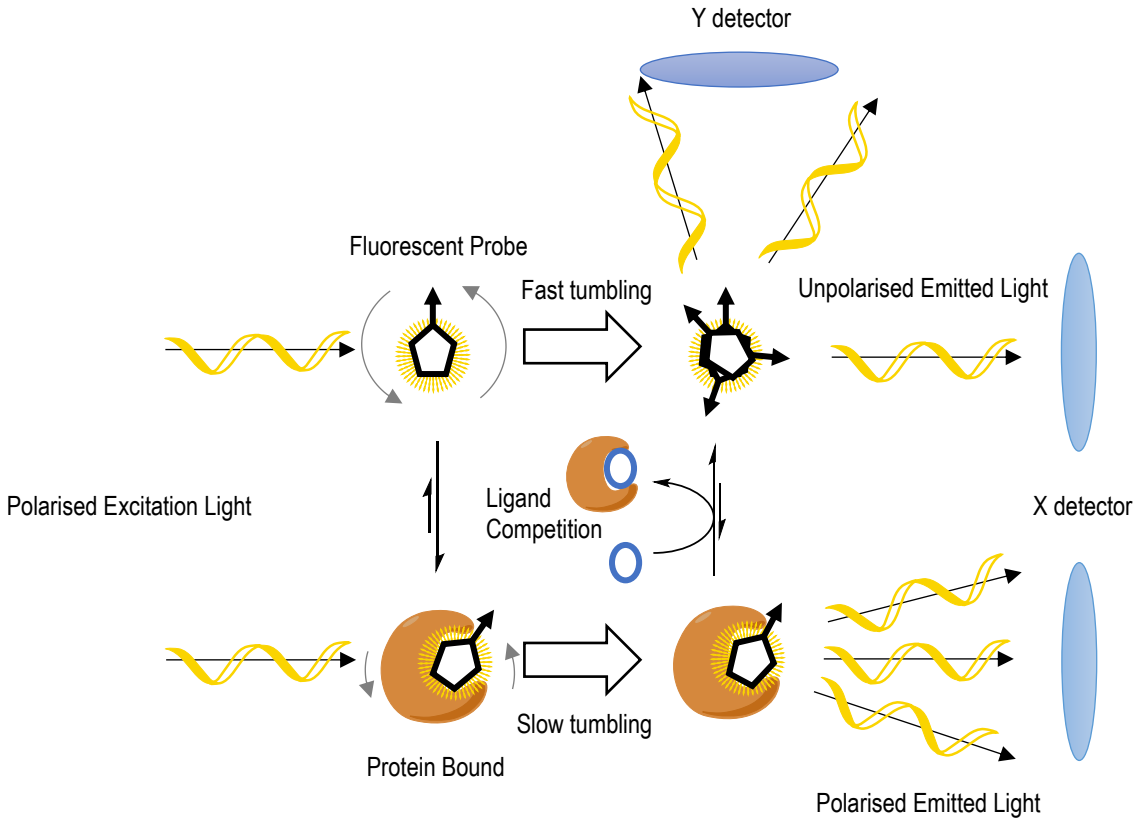


Figure 3.16; Schematic depiction of the principles of a fluorescence polarisation assay.

Fluorescence polarisation (FP) was investigated as an orthogonal secondary assay platform to DSF. FP assays function on the principle that the rate of molecular tumbling is inversely proportional to molecular weight, Figure 3.16. This means small molecular fluorophores excited by plane polarised light, such as fluorescein, tumble quickly enough, during their excited state, to depolarise their subsequent emitted light. However, if the same fluorophore is bound to a macromolecule such as a protein or complex, its rate of tumbling is reduced, and its emitted light remains largely polarised. Finally, if a ligand can competitively displace the affinity fluorophore, then its emitted light is once again depolarised.[48,49] Therefore, unlike DSF probes, FP assays employ fluorescently-labelled probes with high affinity for the subject protein or complex. FP assays are competition-based and prove ligands bind to the target protein specifically whilst also determining their dissociation values (K_D). An additional advantage of using

an affinity probe, was its stabilisation of the tetrameric form of the $SK_{Ca}2.2$ and $IK_{Ca}3.1$ gating complexes, shifting the observed equilibrium towards this state of interest.

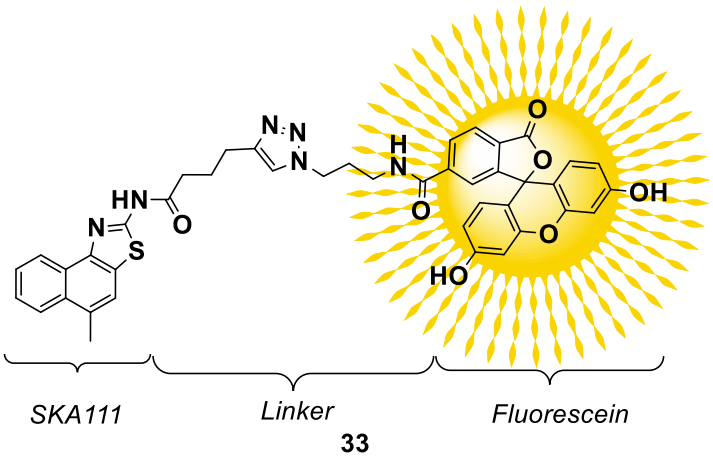


*Figure 3.17; Structure of the synthesised novel K_{Ca} FP probe **33**.*

An FP probe, with affinity for the target $IK_{Ca}3.1$ channel gating complex CaM:CaMBD-4-H_6, was designed by covalently linking fluorescein to a known positive modulator. The most potent putative $IK_{Ca}3.1$ modulator is SKA111 **5**, with an EC_{50} of 111 nM.[1] SKA111 **5** was easily synthetically linked to fluorescein *via* amide bond formation to its 2-amino group, Chapter 2.3.2, Figure 3.17. Published data on the SKA pharmacophore does indicate that substitution on the amino group could abolish the resulting probe's K_{Ca} activity.[1] This $IK_{Ca}3.1$ modulation activity loss may be due to clashing interactions with the predicted 2CaM:2CaMBD-4-H_6 modulator binding cavity gating residue valine363, discussed in Chapter 2. Docking of the proposed SKA111 probe molecule **33** was well tolerated, despite observed clashing with valine363. The literature evidence for effective activity loss is not necessarily linked to affinity and so the probe was synthesised for experimentation.

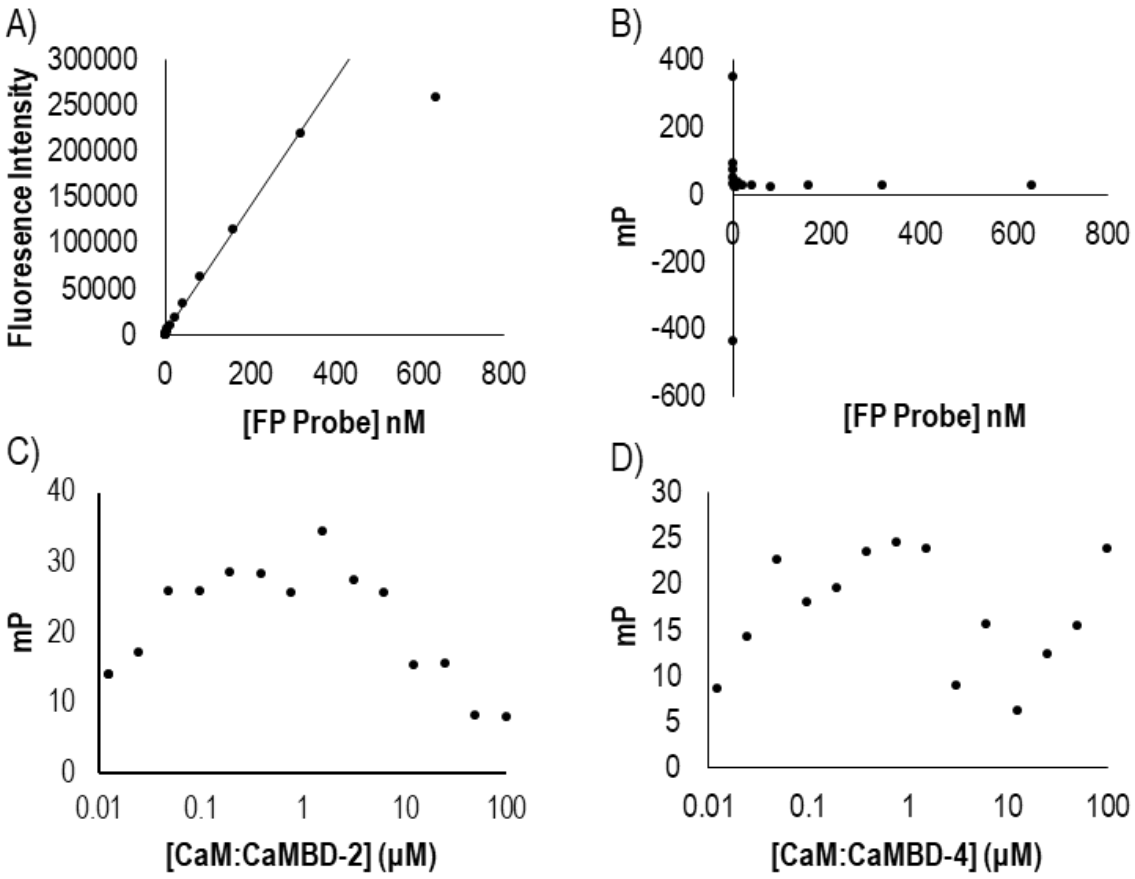


Figure 3.18; Testing the bespoke synthesized K_{Ca} FP probe. A) Total fluorescence of the probe under test conditions with 313 nM probe reference. B) Probe fluorescence polarization stability. C) $SK_{Ca}2.2$ gating complex probe binding experiment. D) $IK_{Ca}3.1$ gating complex probe binding experiment.

After synthesising the FP probe, a serial dilution in buffer was made covering 20 pM to 640 nM. Plotting the fluorescence polarisation intensities of the serial dilutions against probe concentration demonstrated good linearity, using a detector probe reference of 320 nM. The fluorescence intensity of the probe as low as 10 nM was significantly greater than that of the buffer control. A plot of the dilution series calculated fluorescent polarity (mP) against probe concentration, indicated a stable signal of around 27 mP at concentrations exceeding 1.25 nM, Figure 3.18 A and B. These results confirmed the probe did not quench the fluorescence of the fluorescein and was stable in solution.

Based on the probe experiments, 40 nM was chosen as the working assay FP probe concentration, Figure 3.18. This concentration was selected to be advantageous because the EC_{50} of SKA111 for $SK_{Ca}2.2$ and $IK_{Ca}3.1$ is 7.7 μM and 0.1 μM, respectively. Thus, if the ligand's affinity was retained, the FP probe should easily saturate both IK_{Ca} and SK_{Ca} gating complexes, giving a high polarised fluorescence signal. Subsequent probe binding experiments showed the synthesised FP probe did not bind to either gating complex, Figure 3.18 C and D. No fluorescence polarisation increase was observed across a gradient of either complex protein up to 100 μM. It is likely the docking of the probe was incorrect and the probe didn't bind, perhaps because of the aforementioned Val363 steric interaction, Section 2.2.2. Thus, this FP assay format, using the naphthotriazole derived probe, was not suitable for screening compounds against K_{Ca} gating complexes.

3.2.3 Towards Isothermal Titration Calorimetry as a Biophysical Binding Assay

Isothermal titration calorimetry (ITC) was investigated next as a DSF orthogonal K_{Ca} channel binding assay. This technique improved on the previous probe dependant assays because it does not require a reporter probe but directly detects molecular interactions *via* their effect on the overall system temperature, Equation 3.1. If two molecules form favourable enthalpic interactions, they form a lower energy complex, releasing heat. By titrating one molecule against a binding partner, the saturation of the molecular interaction can be achieved, providing stoichiometry values and ΔH.[50–52] From these parameters, all other thermodynamic parameters can be calculated. The disadvantage of ITC was that it is a medium to low throughput assay technique, requiring far more time and protein to perform than DSF or FP. However, ITC would only be applied as a secondary assay after potential ligands are pre-identified by DSF screening.

Before it could be used as an assay, ITC would be used to examine each constituent PPI of the $SK_{Ca}2.2$ channel gating complex, dissecting the mechanism of K_{Ca} channel gating complex formation. Additionally, the effect of the control molecules, Figure 3.8, on any of these oligomeric states would be assessed by ITC, to help understand at which stage K_{Ca} channel modulators bind to the CaM, CaMBD-H_6 monomers, CaM:CaMBD-H_6 dimers or 2CaM:2CaMBD-H_6 tetramer, Figure 3.1.

ITC results might be misleading if a ligand were able to bind lower oligomeric states of the K_{Ca} channel gating complex, affecting the interactions of the higher oligomeric states. The aim of this work was to study by ITC each interaction of the K_{Ca} channel gating complex, using $SK_{Ca}2.2$ as a previously studied model. Once full saturation of the 2CaM:2CaMBD-2-H_6 tetramer was observed, the binding of the positive modulator molecules could be investigated.

The tetramerisation of the $SK_{Ca}2.2$ gating complex has been studied before in literature using ITC.[11] In the literature experiment, CaM was titrated against CaMBD-2-H_6 in the presence of Ca^{2+}, observing CaM:CaMBD-2-H_6 dimerisation and 2CaM:2CaMBD-2-H_6 tetramerisation PPIs, simultaneously. The end of this published ITC experiment saw the saturation of CaMBD-2-H_6 with CaM as the 2CaM:2CaMBD-2-H_6 tetramer. Tetramer saturation would enable an assay based on ITC to reliably detect small molecule binding to this state alone.

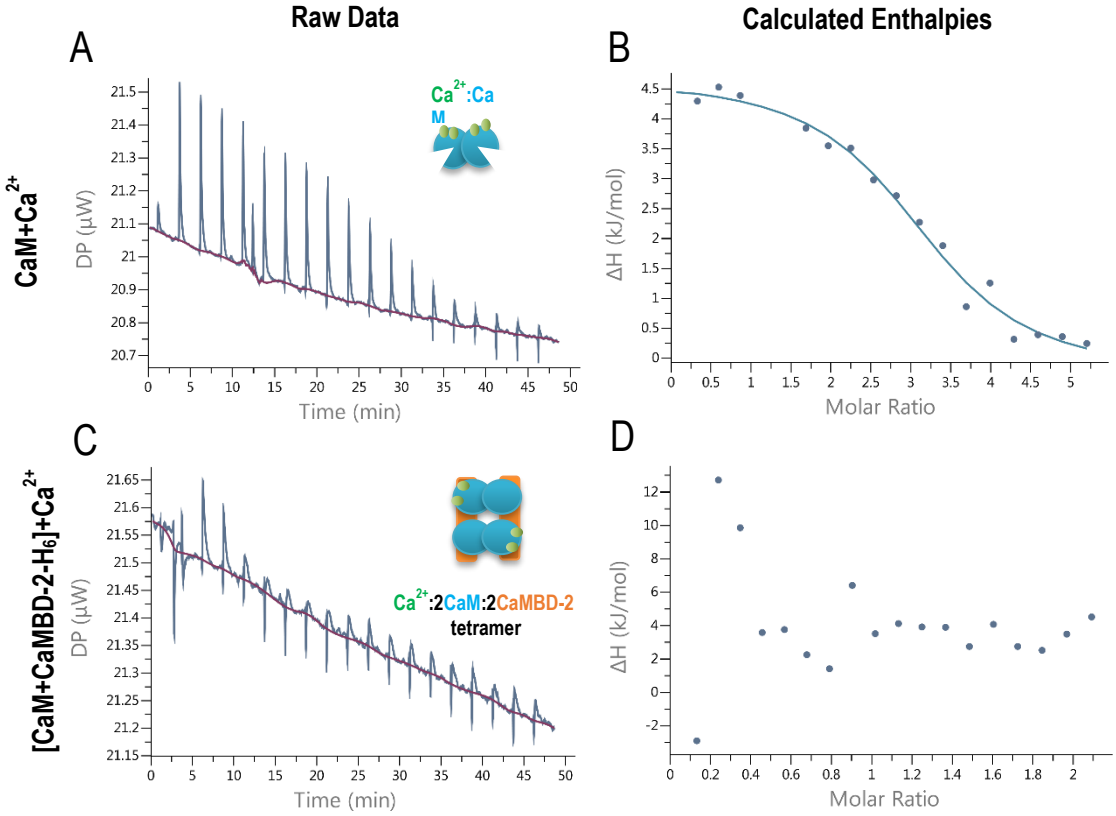


Figure 3.19; CaM and CaM:CaMBD-2-H$_6$ ITC experiments. A) (raw data) and B) (calculated enthalpies) Addition of CaM to CaMBD-2 in the presence of Ca^{2+} (2 mM). C) (raw data) and D) (calculated enthalpies) Addition of Ca^{2+} to CaM as a control, one set of binding sites model line fitted to enthalpy points.

The first ITC experiment aimed to reproduce the published ITC experiment, saturating the SK$_{Ca}$2.2 gating proteins' tetrameric state, Figure 3.19, A and C. No binding was observed in this experiment of either the CaM:CaMDB-2-H$_6$ constitutive dimer or 2CaM:2CaMDB-2-H$_6$ tetramer. This was an unexpected result because the dimer had enabled the co-purification of CaM *via* IMAC, without a hexa-histidine tag; both the dimer and tetramer had also been observed by SEC-MALS. The tetramerization ITC experiment, Figure 3.19 A, required the use of individually produced and isolated CaM and CaMBD-2-H$_6$ monomer proteins, instead of the more stable CaM:CaMDB-2-H$_6$ dimer. This was unlike the DSF and SEC-MALS techniques that used the co-purified CaM:CaMBD-H$_6$ dimers, and in which the tetramer and dimer states were observed. It is possible that one of the monomer proteins in the ITC experiment, Figure 3.19 A, was

not folded correctly or did not have the required activity for dimerisation or tetramerisation. Experiments to determine the correct activities of the constituent gating complex proteins were conducted.

The Ca^{2+} binding activity of CaM is vital for the formation of the tetramer, and while its activity was demonstrated in its Ca^{2+} induced HIC purification, it may have degraded since then. The next ITC experiment was performed to check the Ca^{2+} binding ability of CaM, Figure 3.19 B and D. This experiment proved the activity of CaM remained correct with 4 Ca^{2+} binding per CaM observed. The addition of Ca^{2+} to CaM was an endothermic and not exothermic process, producing the opposite sigmoidal curve to typical exothermic ITC experiments. This effect was caused by the opening of the CaM lobes and exposure of their hydrophobic interiors, a disfavourable process. However, this process is spontaneous due to the overall driving entropic gain, caused by the chelation of four Ca^{2+} ions by one molecule, thereby releasing many ordered waters.[50,53] These ITC results corroborated the observed Ca^{2+} binding activity of CaM, observed in the control DSF experiments. Thus, CaM inactivity was not the fault of the CaM:CaMBD-2-H_6 tetramerisation experiment failure. Logically, CaMBD-2-H_6 must be the fault.

To perform the published ITC experiment, both CaM and CaMBD-2-H_6 were first exchanged into the same buffer, containing Ca^{2+} and without sarkosyl detergent. Removing the detergent from CaMBD-2-H_6 predictably caused aggregation yet left enough protein in solution for use in the experiments. There remains a possibility that the insoluble CaMBD-2-H_6 continued to aggregate before it could be used in the ITC experiment. This potential fault presented a problem because the was no other control experiment to assess the function of CaMBD-2-H_6 alone. The aqueous stability of the target CaMBD-4-H_6 was shown to be even worse than CaMBD-2-H_6; CaMBD-4-H_6

would be less likely to behave well under ITC conditions and procedures. Thus, the individually produced isolated proteins were not used for later assay experiments

3.2.4 Towards Native Protein Mass Spectrometry as a Biophysical Binding Assay

Native mass spectrometry (native MS) is a relatively new and emerging field and could be used as a biophysical assay format.[54,55] 'Native' MS refers to the electrospray ionisation of biomolecules from non-denaturing solvents. This means that the proteins remain under simulated native *in vitro* environments prior to transfer into the gas phase. Debate remains about whether proteins retain their structure in the gas phase, however, evidence suggests this is possible. Proteins that unfold prior to electron spray ionisation have larger surface area than when folded, allowing for higher charge states to be achieved as sprayed protein droplets evaporate. Proteins that remain in their native states sequester ionisable interior residues, producing lower charge states. By assessing the charge envelope of a protein, in combination with its ion mobility, its structure or complexation can therefore be determined. Consequently, Native MS is able to observe protein conformation, interaction partners, binding stoichiometry, disassembly and topology.[56–58]

Native MS requires low amounts of protein and ligand and is a medium throughput assay technique. Most importantly, native MS is able to decipher the K_Ds of multiple associations simultaneously from one sample. This would be ideal for use with the K_{Ca} gating complex proteins and their modulator molecules. The co-purified dimer proteins could be used instead of individual isolated proteins, which proved unstable and unsuitable under ITC conditions. This work was performed in collaboration with Shane Chandler of the Justin Benesch group of the University of Oxford.

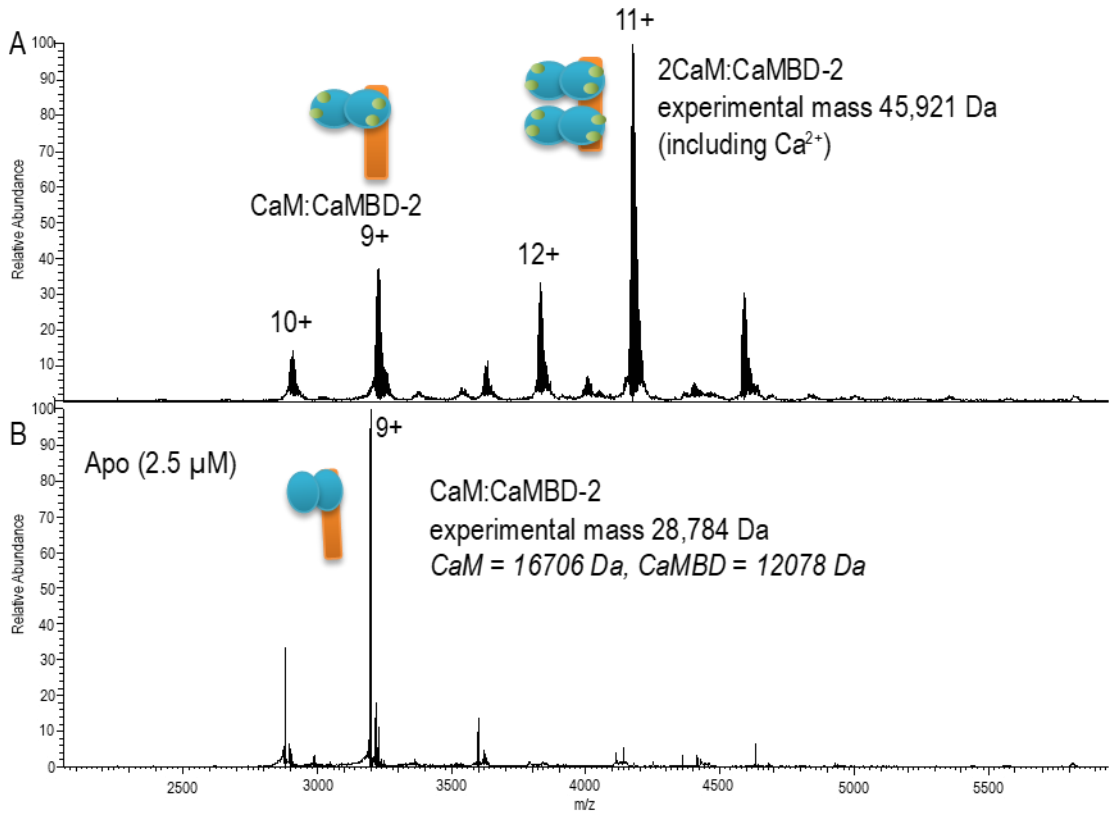


Figure 3.20; Native mass spectra results of CaM:CaMBD-2 with and without $CaCl_2$. A) CaM:CaMBD-2 in the presence of $CaCl_2$, peaks split into multiples based on additional surface Ca^{2+} binding. B) CaM:CaMBD-2 in the absence of $CaCl_2$. Charge number (z) indicated above each peak, peak molecular size (m) calculated by m/z × z.

Work was performed by Chandler to observe the CaM:CaMBD-2-H_6 dimer and 2CaM:2CaMBD-2-H_6 tetramer of the $SK_{Ca}2.2$ gating complex proteins *via* an increasing concentration of Ca^{2+}. Initial experimentation was partially successful at observing desired complexation. The CaM:CaMBD-2-H_6 dimer, previously seen to be stable, was observed in the absence of Ca^{2+} and identified by total expected mass, Figure 3.20 B. Upon addition, Ca^{2+} was observed to bind to the CaM:CaMBD-2-H_6 sample multiple times. This led to the production and observation of a Ca^{2+} bound 2CaM:CaMBD-2-H_6 trimer molecular weight, not the intended tetramer, Figure 3.20 A. This is a partial success, because even the trimer should contain at least one modulator binding site, found in the 2CaM:2CaMBD-2-H_6 tetramer. A trimer could still be used to observe

ligand binding. This experiment was performed only once, and so it is difficult to assert whether this observed 2CaM:CaMBD-2-H_6 trimer is an intermediate oligomeric state in tetramerization or not. Unfortunately, the collaboration did not progress further than this. Further experiments aimed at observing the intended 2CaM:2CaMBD-2-H_6 tetramer, may also determine if formation of the trimer species is an intermediate oligomerisation step. Unfortunately, observation of the addition of positive control molecules, Figure 3.8, was limited by the lack of observation of the tetramer and so screening of novel molecules was not conducted.

3.2.5 Protein Crystallography

There are no empirically determined structures of the target $IK_{Ca}3.1$ gating complex. A structure of a drug target binding site is important for the rational design of strong binding ligands, especially designing ligand specificity.[59–62] The $IK_{Ca}3.1$ homology models based on the $SK_{Ca}2.2$ gating complex modulator co-crystals, discussed in Chapter 2, were useful for designing $IK_{Ca}3.1$ ligands. Models, however, only provide theoretical predictions of ligand molecular interactions and ensuing residue side chain positioning. Unfortunately, models do not include static waters, which are potentially important in understanding protein stability through hydrogen bonding networks. Static waters held within protein binding sites also provide strategic opportunities for ligand replacement, aiding entropic favourability in ligand binging.[63] Other than robust molecular dynamics, only protein crystals, cryo-electron microscopy or intensive protein NMR investigations, can provide such detailed data on target structures. This is because these techniques include how ligands alter and potentially stabilise a protein *via* its binding site. An empirical $IK_{Ca}3.1$ gating complex structure would be the first of its kind and may help to understand ligand specificity between SK_{Ca} and IK_{Ca} channel

ligands. Hence, a broad screen of conditions was made to try to crystallise the $IK_{Ca}3.1$ gating complex proteins.

Crystallography was not intended as a screening technique. While crystallography proves target interaction and mode of binding, it does not give ligand affinity; the major benefit of a biophysical binding assay. Aided by automation, the throughput of crystallography can be high, yet it requires large ammounts of protein and ligand.[59,64–66] Crystals are grown at incredibly high protein and ligand concentrations, not necessarily reflecting native protein behaviour or conditions *in vivo*. Consequently, weak ligands identified at saturating concentrations by crystallography, may not represent tight binding ligands which bind *in vivo*.[67]

The co-purified CaM:CaMBD-4-H_6 dimer was purified in the presence of 500 mM NaCl, stabilising the proteins in solution. Crystallography requires very low salt concentrations to avoid salt crystal false positives.[68] The dimer was therefore prepared for crystallisation by exchange into a low salt buffer. Several commercial crystallography condition screens were made and the screening plates were incubated at both room temperature and 4 °C. Typically, crystallography of proteins is attempted at very high concentrations to reach near solution saturation, where nucleation begins.[69] Concentration of the 2CaM:2CaMBD-4-H_6 tetramer was challenging due to its solution instability. Protein precipitation was observed over concentrations of 6 mg/mL. However, CaM:CaMBD-4-H_6 was used without concentration in the crystallographic experiments, because its low solubility suggested it was already near its saturation point. This was supported by the protein precipitation, present in nearly 50% of the condition wells for each screening plate. Despite this, the experiment produced no crystals. Ligands stabilise proteins upon binding, thus small molecules were added as

potential ligands to increase the stability of the 2CaM:2CaMBD-4-H_6 complex, in further experiments.

Molecular crystallography requires crystals with highly ordered repeating unit cells of molecules, orientated identically throughout. This is because increasing regularity produces more mathematically precise X-ray diffraction patterns.[70] Thus, the more regular and ordered the molecules in a crystal, the better the resolution of the diffracted X-ray patterns. The quality of the diffraction pattern from a crystallographic experiment determines the resolution of the solved protein structure. Correctly determining molecular interaction requires high resolution to provide certainty in molecular positioning. This means in ligand-protein co-crystals, every ligand binding site must be filled with identically orientated ligands, providing discernible and usable diffraction patterns.[68,71] The concentration of ligand added for crystallisation must therefore be at least in a 1:1 ratio with the protein subject, ensuring binding site saturation.[68,71] The most potent putative $IK_{Ca}3.1$ modulators, such as SKA111 **5**, were not soluble enough to reach the required 1:1 ratio. The synthesised methylamine and aniline naphthothiazole analogues, **13** and **10**, were the only potential ligands soluble enough to reach this ratio limit. Subsequent ligand-complex incubations lead to crystals; however, these were salt crystals.

Without further progress on a second binding assay to confirm the interpretation of the DSF results and due to time constraints, the synthesised naphthothiazole analogues were assessed using pharmacological techniques to identify any potential biological activities.

3.3 Summary

A robust biophysical assay was required to efficiently screen either libraries of molecules. Screening studies would be used to find a novel $IK_{Ca}3.1$ hit with

advantageous properties or characterise sets of analogues during modulator development. Therefore, the known positive modulator binding site and gating complex proteins for $SK_{Ca}2.2$, CaM and CaMBD-2-H_6, were reproduced using published molecular- and micro- biology methods. These methods were also adapted to provide the additional target $IK_{Ca}3.1$ proteins, CaMBD-4-H_6. The calcium sensing regulator protein CaM was purified *via* the published Ca^{2+} induced hydrophobic interaction chromatography procedure, simultaneously confirming its correct solution behaviour. The hexahistadine (H_6) tag fused CaMBDs were each purified by immobilised metal affinity chromatography (IMAC). Finally, the CaM:CaMBD-H_6 dimers of both channels were also co-purified by IMAC, utilising the constitutive association of CaM with each CaMBD-H_6.

The solution stabilities of CaMBD-2-H_6 and CaMBD-4-H_6 were shown to be poor during their individual purifications, and this remained a continuing problem throughout assay development. The solution instability of $IK_{Ca}3.1$ and $SK_{Ca}2.2$ CaMBD-H_6s was caused by the high proportion of hydrophobic residues. The detergent sodium lauroyl sarcosinate was vital to prevent the individual CaMBD-H_6s from aggregating. Fortunately, the CaMBD-H_6s were stabilised by their respective constitutive dimers with CaM. However, the CaM:CaMBD-4-H_6 dimer and 2CaM:2CaMBD-4-H_6 tetramer continued to precipitate at higher concentrations, CaMBD-4-H_6 being less soluble than CaMBD-2-H_6. Attempts to crystallise the $IK_{Ca}3.1$ CaM:CaMBD-4-H_6 tetramer with and without the most soluble naphthothiazole analogues were prevented by this solubility limiting factor.

Characterisation of the solution behaviour of combined CaM with the CaMBD-H_6s by SEC-MALS, revealed an equilibrium between the CaM:CaMBD-H_6 dimeric and expected Ca^{2+} induced 2CaM:2CaMBD-H_6 tetrameric forms. The 2CaM:2CaMBD-4-H_6

tetramer was less stable than the 2CaM:2CaMBD-2-H_6 tetramer; further demonstrating the impact of the greater instability of CaMBD-4-H_6. The dimer and tetramer equilibria inferred that the binding cavity in a biophysical assay would be transient, complicating assay design.

The suitability of several biophysical techniques for characterising and understanding K_{Ca} gating complex oligomerisation during ligand binding were assessed. Published ITC experiments observed the tetramerisation of the individual CaM and CaMBD-2-H_6 proteins in the presence of Ca^{2+}, until saturation. Unfortunately, this experiment was not reproducible due to the lack of solubility of the CaMBD-2-H_6 during buffer exchange, in preparation for ITC experimentation.

Assay development was refocused on utilising the more stable co-purified constitutive CaM:CaMBD-H_6 dimers. A bespoke modulator-based affinity probe **33** was hypothesised to push the gating complex oligomerisation equilibrium toward the desired 2CaM:2CaMBD-H_6 tetrameric state. Fluorescence polarisation (FP) was therefore attempted after an FP affinity probe was designed and synthesised as an analogue of the most potent IK_{Ca}3.1 modulator, SKA111 **5**. The FP probe **33** did not appear to bind the target IK_{Ca}.3.1 gating complex tetramer, possibly caused by the amide bond linkage to the fluorescein moiety. Substitution on the SKA111 2-amino group, as well as similar functionalisation of EBIO **37** and NS309 **47** has been shown to cause loss of function.

Initial assay success was first observed in differential scanning fluorimetry, where individual proteins and their complexed structural stabilities are observed directly, over a temperature gradient. A low temperature melting peak, missing in the absence of published K_{Ca} channel modulators, was presumed to be the ligand stabilised 2CaM:2CaMBD-H_6 tetrameric peak. If correct, the appearance of this peak could be

used as an indicator of modulator binding and stabilisation. Published modulators near their saturating concentrations, appeared to shift this peak to higher temperatures in relation to their potencies. This effect suggested modulator binding and stabilisation of the 2CaM:2CaMBD-H_6 tetramer. Of the published K_{Ca} channel modulators, riluzole produced the greatest presumed tetramer peak shift, despite not being the most potent modulator. It was proposed that this discrepancy could be due to the much greater solubility of riluzole, compared to the other modulators assayed. Based on this information the addition of the known binder riluzole might produce $IK_{Ca}3.1$ gating complex co-crystals and could be attempted in future crystallisation attempts.

Finally, initial native protein mass spectrometry indicated the homogeneity of the CaM:CaMBD-2-H_6 dimeric species, as well as oligomerisation upon addition of Ca^{2+}. Only a trimeric state of 2CaM:1CaMBD-2-H_6 was observed instead of the tetramer. Further experimental repeats and refinement may well provide the first direct observation of tetramerisation of the K_{Ca} channel gating complex

Chapter 3 References

1. Coleman, N. *et al.* New positive Ca2+ -activated K+ channel gating modulators with selectivity for KCa3.1. *Mol. Pharmacol.* **86,** 342–357 (2014).

2. Sankaranarayanan, A. *et al.* Naphtho[1,2-d]thiazol-2-ylamine (SKA-31), a new activator of KCa2 and KCa3.1 potassium channels, potentiates the endothelium-derived hyperpolarizing factor response and lowers blood pressure. *Mol. Pharmacol.* **75,** 281–95 (2009).

3. Christophersen, P. & Wulff, H. Pharmacological gating modulation of small-and intermediate-conductance Ca2+-activated K+ channels (KCa2.x and KCa3.1). *Channels* **9,** 336–343 (2015).

4. Damkjaer, M. *et al.* Pharmacological activation of KCa3.1/KCa2.3 channels produces endothelial hyperpolarization and lowers blood pressure in conscious dogs. *Br. J. Pharmacol.* **165,** 223–234 (2012).

5. Cronk, D. High-Throughput Screening. in *Drug Discovery and Development: Technology in Transition* (eds. Hill, R. & Rang, H.) 95–118 (Churchill Livingstone, 2012).

6. Zhang, M., Pascal, J. M., Schumann, M., Armen, R. S. & Zhang, J.-F. Identification of the functional binding pocket for compounds targeting small-conductance Ca2+-activated potassium channels. *Nat. Commun.* **3,** 1021 (2012).

7. Cui, M., Qin, G., Yu, K., Bowers, M. S. & Zhang, M. Targeting the small- and intermediate-conductance Ca2+-activated potassium channels: the drug-binding pocket at the channel/calmodulin interface. *Neurosignals* **22,** 65–78 (2014).

8. Zhang, M., Pascal, J. M. & Zhang, J.-F. Unstructured to structured transition of an intrinsically disordered protein peptide in coupling Ca^{2+}-sensing and SK channel activation. *Proc. Natl. Acad. Sci. U. S. A.* **110,** 4828–33 (2013).

9. Schumacher, M. a, Rivard, a F., Bächinger, H. P. & Adelman, J. P. Structure of the gating domain of a Ca2+-activated K+ channel complexed with Ca2+/calmodulin. *Nature* **410,** 1120–1124 (2001).

10. Saimi, Y. & Kung, C. Calmodulin as an ion channel subunit. *Annu. Rev. Physiol.* **64,** 289–311 (2002).

11. Zhang, M. *et al.* Structural basis for calmodulin as a dynamic calcium sensor. *Structure* **20,** 911–923 (2012).

12. Gibson, D. G. *et al.* Enzymatic assembly of DNA molecules up to several hundred kilobases. *Nat. Methods* **6,** 343–5 (2009).

13. Keates, T. *et al.* Expressing the human proteome for affinity proteomics: Optimising expression of soluble protein domains and in vivo biotinylation. *N. Biotechnol.* **29,** 515–525 (2012).

14. Hippel, P. H. V., Revzin, A., Gross, C. A. & Wang, A. C. Non-specific DNA binding of genome regulating proteins as a biological control mechanism: 1. The lac operon: equilibrium aspects. *Proc. Natl. Acad. Sci.* **71,** 4808–4812 (1974).

15. Marbach, A. & Bettenbrock, K. Lac operon induction in Escherichia coli: Systematic comparison of IPTG and TMG induction and influence of the transacetylase LacA. *J. Biotechnol.* **157,** 82–88 (2012).

16. Hayashi, N., Matsubara, M., Takasaki, A., Titani, K. & Taniguchi, H. An expression system of rat calmodulin using T7

phage promoter in Escherichia coli. *Protein Expr. Purif.* **12,** 25–28 (1998).

17. Gray, G. S. & Fitch, W. A. Evolution of antibiotic resistance genes: the DNA sequence of a kanamycin resistance gene from Staphylococcus aureus. *Mol. Biol. Evol.* (1984). doi:10.1093/oxfordjournals.molbev.a040298

18. Kotra, L. P., Haddad, J. & Mobashery, S. Aminoglycosides: Perspectives on mechanisms of action and resistance and strategies to counter resistance. *Antimicrob. Agents Chemother.* **44,** 3249–3256 (2000).

19. Pelicic, V., Reyrat, J. M. & Gicquel, B. Expression of the Bacillus subtilis sacB gene confers sucrose sensitivity on mycobacteria. *J. Bacteriol.* **178,** 1197–1199 (1996).

20. Westerlund, A. M. & Delemotte, L. Effect of Ca2+ on the promiscuous target-protein binding of calmodulin. *PLOS Comput. Biol.* **14,** e1006072 (2018).

21. Gopalakrishna, R. & Anderson, W. B. Ca2+-induced hydrophobic site on calmodulin: Application for purification of calmodulin by phenyl-Sepharose affinity chromatography. *Biochem. Biophys. Res. Commun.* **104,** 830–836 (1982).

22. Bader, M. F., Hikita, T. & Trifaro, J. M. Calcium-dependent calmodulin binding to chromaffin granule membranes: presence of a 65-kilodalton calmodulin-binding protein. *J. Neurochem.* **44,** 526–539 (1985).

23. Gifford, J. L., Walsh, M. P. & Vogel, H. J. Structures and metal-ion-binding properties of the Ca^{2+} -binding helix–loop–helix EF-hand motifs. *Biochem. J.* **405,** 199–221 (2007).

24. Chin, D. & Means, A. R. Calmodulin: A prototypical calcium sensor. *Trends Cell Biol.* **10,** 322–328 (2000).

25. McCue, J. T. Theory and Use of Hydrophobic Interaction Chromatography in Protein Purification Applications. in *Methods in Enzymology: Guide to Protein Purification* (eds. Burgess, R. R. & Deutscher, M. P.) **463,** 405–414 (Elsevier Inc., 2009).

26. Queiroz, J. A., Tomaz, C. T. & Cabral, J. M. S. Hydrophobic interaction chromatography of proteins. *J. Biotechnol.* **87,** 143–159 (2001).

27. Chandler, D. Interfaces and the driving force of hydrophobic assembly. *Nature* **437,** 640–647 (2005).

28. Brokx, R. D., Lopez, M. M., Vogel, H. J. & Makhatadze, G. I. Energetics of target peptide binding by calmodulin reveals different modes of binding. *J. Biol. Chem.* **276,** 14083–14091 (2001).

29. Chial, H. J., Thompson, H. B. & Splittgerber, A. G. A spectral study of the charge forms of Coomassie blue G. *Analytical Biochemistry* **209,** 258–266 (1993).

30. Meyer, T. S. & Lamberts, B. L. Use of coomassie brilliant blue R250 for the electrophoresis of microgram quantities of parotid saliva proteins on acrylamide-gel strips. *Biochim. Biophys. Acta* **107,** 144–145 (1965).

31. Hirel, P. H., Schmitter, M. J., Dessen, P., Fayat, G. & Blanquet, S. Extent of N-terminal methionine excision from Escherichia coli proteins is governed by the side-chain length of the penultimate amino acid. *Proc. Natl. Acad. Sci. U. S. A.* **86,** 8247–51 (1989).

32. Liao, Y.-D., Jeng, J.-C., Wang, C.-F., Wang, S.-C. & Chang, S.-T. Removal of N-terminal methionine from recombinant proteins by engineered *E. coli* methionine aminopeptidase. *Protein Sci.* **13,** 1802–1810 (2004).

33. Michael Schurr, J. & Bloomfield, V. Dynamic light scattering of biopolymers and biocolloid. *Crit. Rev. Biochem. Mol. Biol.* **4,** 371–431 (1977).

34. Dynamic Light Scattering. *Wyatt Technology* Available at: https://www.wyatt.com/solutions/techniques/dynamic-light-scattering-nanoparticle-size.html. (Accessed: 19th December 2018)

35. Folta-Stogniew, E. Oligomeric states of proteins determined by size-exclusion chromatography coupled with light scattering, absorbance, and refractive index detectors. in *Methods in Molecular Biology: New and Emerging Proteomic Techniques* (eds. Nedelkov, D. & Nelson, R. W.) 71–96 (Humana Press, 2006).

36. Some, D. Light-scattering-based analysis of biomolecular interactions. *Biophys. Rev.* **5,** 147–158 (2013).

37. Strøbæk, D. *et al.* Activation of human IK and SK Ca2+-activated K+ channels by NS309 (6,7-dichloro-1H-indole-2,3-dione 3-oxime). *Biochim. Biophys. Acta* **1665,** 1–5 (2004).

38. Singh, S., Syme, C. a, Singh, a K., Devor, D. C. & Bridges, R. J. Benzimidazolone activators of chloride secretion: potential therapeutics for cystic fibrosis and chronic obstructive pulmonary disease. *J.Pharmacol.Exp.Ther.* **296,** 600–611 (2001).

39. Thiel, P., Kaiser, M. & Ottmann, C. Small-molecule stabilization of protein-protein interactions: An underestimated concept in drug discovery? *Angew. Chemie - Int. Ed.* **51,** 2012–2018 (2012).

40. Ericsson, U. B., Hallberg, B. M., DeTitta, G. T., Dekker, N. & Nordlund, P. Thermofluor-based high-throughput stability optimization of proteins for structural studies. *Anal. Biochem.* **357,** 289–298 (2006).

41. Semisotnov, G. V. *et al.* Study of the “molten globule” intermediate state in protein folding by a hydrophobic fluorescent probe. *Biopolymers* **31,** 119–128 (1991).

42. Pantolliano, M. W. *et al.* High-density miniaturized thermal shift assays as a general strategy for drug discovery. *J. Biomol. Screen.* **6,** 429–440 (2001).

43. Nemetski, S. M. *et al.* Inhibition by stabilization: targeting the Plasmodium falciparum aldolase-TRAP complex. *Malar. J.* **14,** 324 (2015).

44. Khoshnood, A., Lukanov, B. & Firoozabadi, A. Temperature Effect on Micelle Formation: Molecular Thermodynamic Model Revisited. *Langmuir* **32,** 2175–2183 (2016).

45. Cao, Y. J., Dreixler, J. C., Couey, J. J. & Houamed, K. M. Modulation of recombinant and native neuronal SK channels by the neuroprotective drug riluzole. *Eur. J. Pharmacol.* **449,** 47–54 (2002).

46. Kandler, M., Mah, G., Tejani, A., Stabler, S. & Salzwedel, D. Hydralazine for essential hypertension (Review). *Cochrane Database Syst Rev* 1–16 (2011). doi:10.1002/14651858.CD004934.pub4.www.cochranelibrary.com

47. Cohn, J. N., McInnes, G. T. & Shepherd, A. M. Direct-acting vasodilators. *J. Clin. Hypertens.* **13,** 690–692 (2011).

48. Lea, W. A. & Simeonov, A. Fluorescence polarization assay in small molecule screening. *Expert Opin Drug Discov.* **6,** 17–32 (2011).

49. Nielsen, K., Lin, M., Gall, D. & Jolley, M. Fluorescence polarization immunoassay: Detection of antibody to Brucella

abortus. *Methods* **22,** 71–76 (2000).

50. Frelre, E., Mayorgal, O. L. & Straume, M. Isothermal Titration. *Anal. Chem.* **62,** 950–959 (1990).

51. Pierce, M. M., Raman, C. S. & Nall, B. T. Isothermal titration calorimetry of protein–protein interactions. *Methods* **19,** 213–221 (1999).

52. Leavitt, S. & Freire, E. Direct measurement of protein binding energetics by isothermal titration calorimetry. *Curr. Opin. Struct. Biol.* **11,** 560–566 (2001).

53. Brath, U., Lau, K., Van Petegem, F. & Erdélyi, M. Mapping the sevoflurane-binding sites of calmodulin. *Pharmacol. Res. Perspect.* **2,** 1–12 (2014).

54. Katta, V. & Chait, B. T. Observation of the heme—globin complex in native myoglobin by electrospray-ionization mass spectrometry. *J. Am. Chem. Soc.* **113,** 8534–8535 (1991).

55. Coelho, E. D., Arrais, J. P. & Oliveira, J. L. From protein-protein interactions to rational drug design: are computational methods up to the challenge? *Curr. Top. Med. Chem.* **13,** 602–18 (2013).

56. Leney, A. C. & Heck, A. J. R. Native mass spectrometry: what is in the name? *J. Am. Soc. Mass Spectrom.* **28,** 5–13 (2017).

57. Clark, S. M. & Konermann, L. Determination of ligand-protein dissociation constants by electrospray mass spectrometry-based diffusion measurements. *Anal. Chem.* **76,** 7077–7083 (2005).

58. Lössl, P., van de Waterbeemd, M. & Heck, A. J. The diverse and expanding role of mass spectrometry in structural and molecular biology. *EMBO J.* **35,** 2634–2657 (2016).

59. Keseru, G. M. & Makara, G. M. Hit discovery and hit-to-lead approaches. *Drug Discov. Today* **11,** 741–748 (2006).

60. Mandal, S., Moudgil, M. & Mandal, S. K. Rational drug design. *Eur. J. Pharmacol.* **625,** 90–100 (2009).

61. Blundell, T. L. *et al.* Structural biology and bioinformatics in drug design: opportunities and challenges for target identification and lead discovery. *Philos. Trans. R. Soc. Lond. B. Biol. Sci.* **361,** 413–23 (2006).

62. Whittle, P. & Blundell, T. Protein Structure- Based Drug Design. *Annu. Rev. Biophys. Biomol. Struct.* **23,** 349–375 (1994).

63. Spyrakis, F. *et al.* The roles of water in the protein matrix: a largely untapped resource for drug discovery. *J. Med. Chem.* **60,** 6781–6828 (2017).

64. Bleicher, K. H., Böhm, H.-J., Müller, K. & Alanine, A. I. Hit and lead generation: beyond high-throughput screening. *Nat. Rev. Drug Discov.* **2,** 369–378 (2003).

65. Hughes, J. P., Rees, S., Kalindjian, S. B. & Philpott, K. L. Principles of early drug discovery. *Br. J. Pharmacol.* **162,** 1239–49 (2011).

66. Savitsky, P. *et al.* High-throughput production of human proteins for crystallization: The SGC experience. *J. Struct. Biol.* **172,** 3–13 (2010).

67. Davis, A. M., St-Gallay, S. A. & Kleywegt, G. J. Limitations and lessons in the use of X-ray structural information in drug design. *Drug Discov. Today* **13,** 831–841 (2008).

68. Müller, I. Guidelines for the successful generation of protein-ligand complex crystals. *Acta Crystallogr. Sect. D Struct. Biol.* **73,** 79–92 (2017).

69. Blow, D. M. *et al.* Control of nucleation of protein crystals. *Protein Sci.* **3,** 1638–1643 (1994).

70. Bragg, W. H. The reflection of X-rays by crystals. *Nature* **91,** 428–438 (1913).

71. Mcnae, I. W. *et al.* Studying protein-ligand interactions using protein crystallography. *Crystallogr. Rev.* **11,** 61–71 (2005).

CHAPTER 4 PHARMACOLOGY

In this chapter, wire myography was performed on rat mesenteric resistance arteries to probe the reported activities of published K_{Ca} modulators. These experiments aimed to determine the activity of the novel naphthothiazole analogues, Figure 4.1.

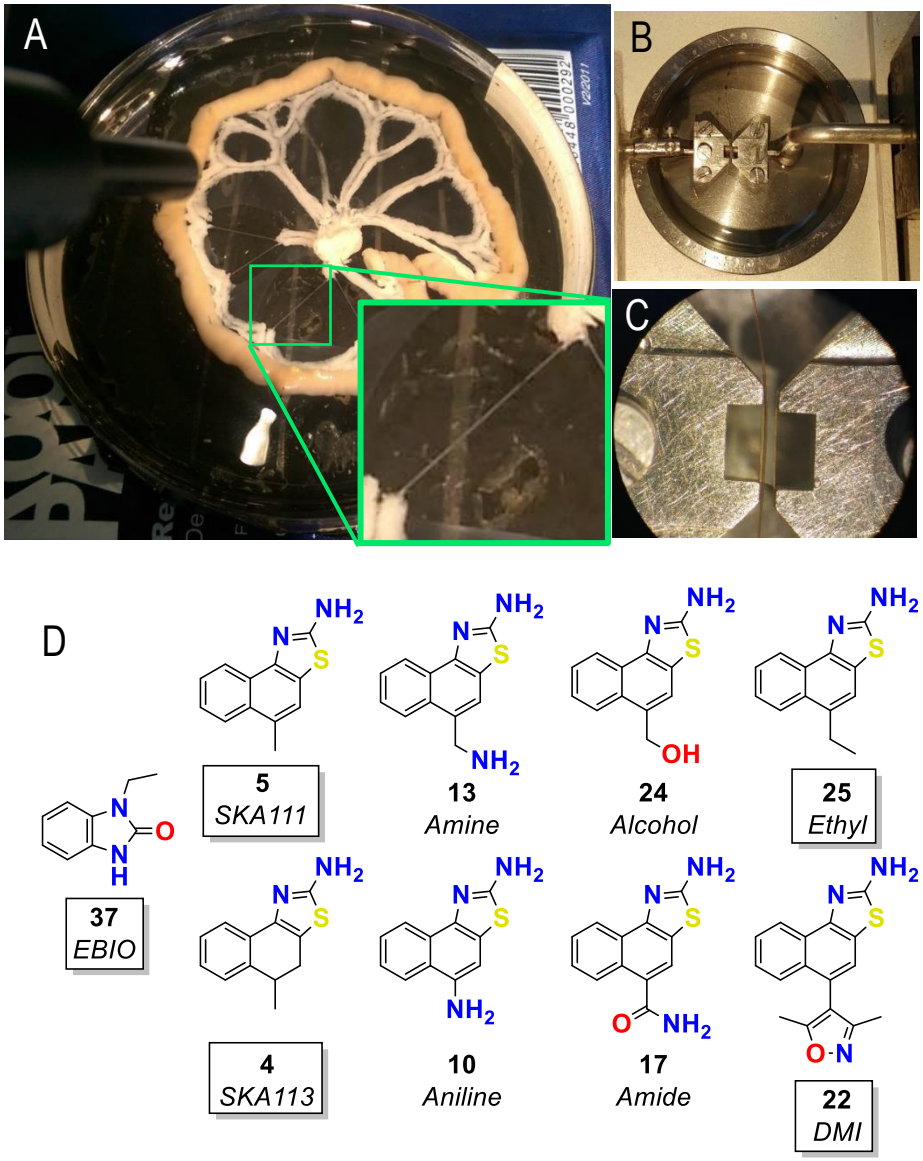


*Figure 4.1; Arterial dissection, wire myography preparation and tested molecule structures. A) Dissection of micro resistance arteries from male wistar rat mesentery, expansion of an exposed artery in green. B) Wire myograph stage, force transducer head (left) and micrometre head (right). C) Mounted artery preparation during endothelium denudation with human hair. D) Structures of EBIO **37**, SKA113 **4**, SKA111 **5** and its novel naphthothiazole analogues: **10**, **13**, **17**, **22**, **24** and **25**. Active compounds highlighted with label boxes.*

4.1 Modulation of Endothelium Derived Hyperpolarisation

The biophysical assay format based on differential scanning fluorimetry, discussed in Chapter 3.2.1, presented a potential screening technique for the fast identification of Ca^{2+} activated potassium (K_{Ca}) channel ligands. Biophysical screening, however, cannot determine an identified ligand's strength or mode of effect on ion channel function.[1] A biologically relevant *in vivo* assay was required to establish effective concentrations (EC_{50}) of each ligands' ability to vasodilate resistance arteries, as a model for hypertensive treatment.

Automated inside-out and whole cell patch clamp assays can be used to screen potential ion channel ligands.[2–4] In patch clamp experiments, the EC_{50}s of screened ligands are based on their ability to alter the function of subject ion channels: observed *via* channel electrochemical currents. The reported EC_{50} for the published benzimidazolone and naphthothiazole K_{Ca} channel modulators, such as SKA111 **5**, were determined using this technique.[5–10]

In living tissues, the function of K_{Ca} channels is to manipulate voltage across cell membranes. However, membrane channel ion conductance only lasts if a chemical concentration gradient of the conducted ion, or a strong electrical voltage, exists across the cell membrane.[11,12] Thus, efflux of K^+ through membrane channels is negligible if the motive electrical voltage, and or chemical gradient, across the cell membrane is removed. Often, in room temperature and isolated cell patch clamp experiments, the gradient of a conducted ion, or a strong electrical potential across the cell membrane, is artificially maintained at constant voltage.[2] Artificially constant electrochemical gradients, applied across a cell membrane, may alter the function of membrane channels under observation, producing data that is not strictly biologically relevant. Wire myography on isolated arteries was chosen as a more biologically relevant

technique, instead of patch clamp experiments. K_{Ca} channel modulation, and ultimately the vasorelaxant capacity of the test ligands, was identified using wire myography, better reflecting the potential use against hypertension.

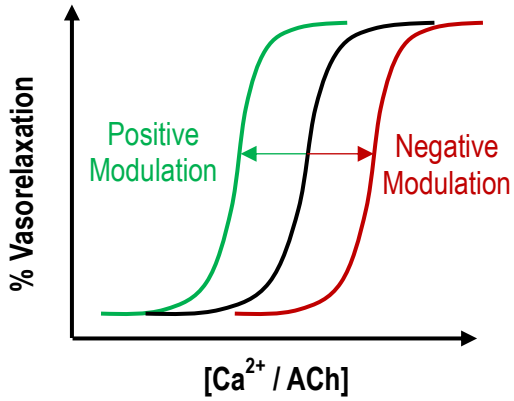


Figure 4.2; Diagram representing EDH modulation in resistance arteries and the effect on dose response curves of vasorelaxant stimulants ACh or intracellular Ca^{2+}. Positive EDH modulation increases artery sensitivity to vasorelaxants, causing vasorelaxation at lower concentrations of relaxant shown in green (leftward dose response shift). Negative EDH modulation decreases artery sensitivity to vasorelaxants, causing vasorelaxation to higher concentrations of relaxant shown in red (rightward dose response shift).[13]

Arteries maintain a level of tone by the balancing vasoconstrictor and vasorelaxant stimuli. As discussed in Chapter 1.2.2, resistance arteries have two endothelium produced vasorelaxatory pathways: the nitric oxide (NO) pathway and endothelium derived hyperpolarisation (EDH).[14–17] Following stimulation by the vasorelaxant acetylcholine (ACh), Ca^{2+} is released from stores within the endothelium activating $SK_{Ca}2.3$ and $IK_{Ca}3.1$ channels, giving rise to EDH *via* endothelial cell K^+ efflux.[18,19] Small molecule modulation of K_{Ca} channels theoretically increases their Ca^{2+} sensitivity and subsequently lowers their Ca^{2+} activation threshold.[5,7,8,10] When observed in resistance arteries, K_{Ca} channel modulation results in vasorelaxation to lower concentrations of ACh, Figure 4.2. Published wire myography experiments demonstrate the EC_{50} shift of ACh vasorelaxation in the presence of small molecule modulators.[8] This experimental

format was reproduced here, to confirm the activities of the positive control molecules SKA111 **5** and EBIO **37**, using isolated rat mesenteric arteries, Figure 4.3.

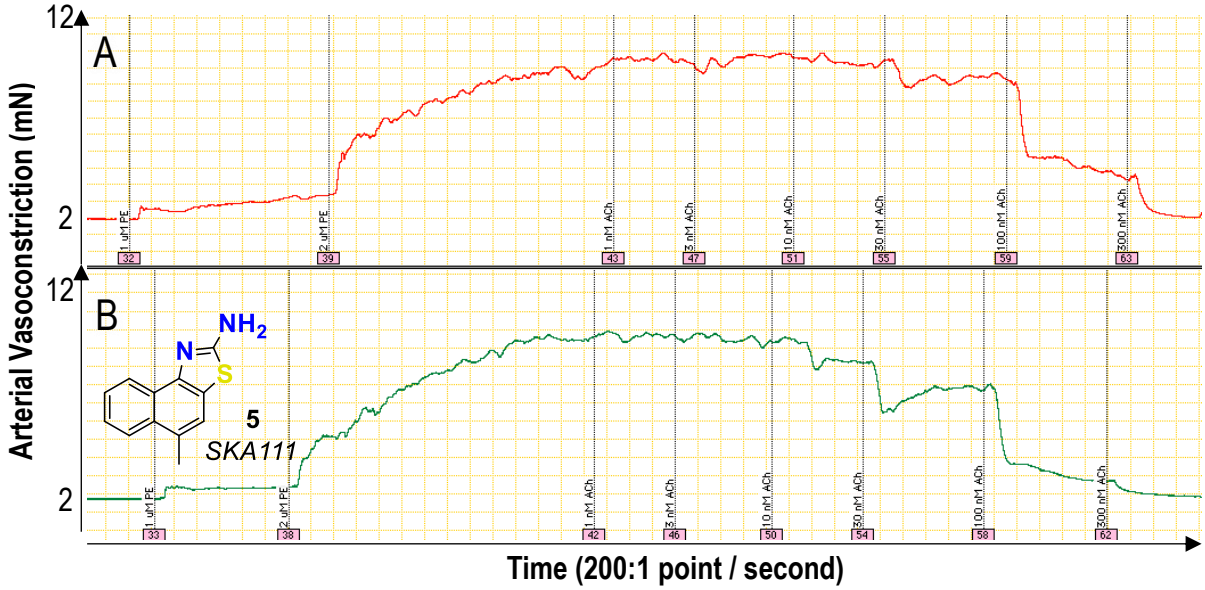


Figure 4.3; Example wire myograph trace of ACh dose response assay in MOPS buffer containing L-NAME (100 μM). A) Force plot of arterial vasoconstriction in red, untreated artery control conditions in the absence of modulators. B) Force plot of arterial vasoconstriction in green, artery preincubated (treated) with the published K_{Ca} channel modulator SKA111 ***5*** *(1 μM).*

K_{Ca} channel modulation was observed using the literature conditions to repeat and confirm the published myography experiments. These conditions were: MOPS buffer containing the endothelium NO synthase inhibitor L-NAME, inhibiting endothelial NO synthase and leaving only EDH vasorelaxation.[8] Phenylephrine (PE) pre-constricted arteries were relaxed with a series of ACh concentrations 1 nM – 1 μM, producing a vasorelaxatory ACh dose response curve. Incubating the arteries with the positive control modulators, EBIO **37**, SKA111 **5** and SKA113 **4**, before performing ACh vasorelaxations, produced treatment ACh dose response curves, Figure 4.4. Each modulator was incubated at 10-fold higher concentrations than their respective reported EC_{50}, to ensure channel saturation and maximise any ACh dose response shift effect.

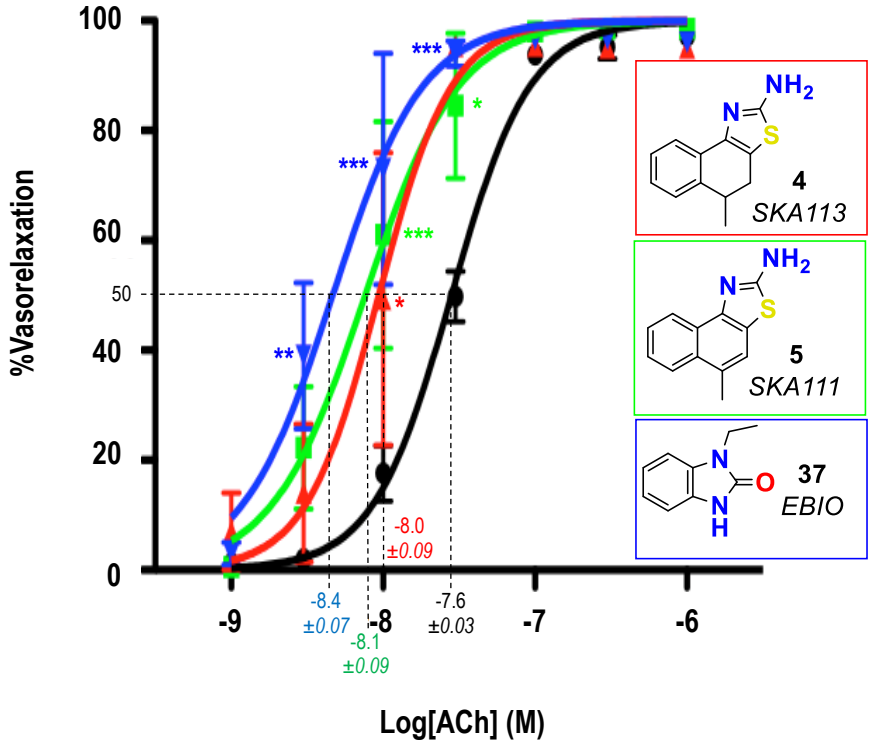


*Figure 4.4; Plot of untreated resistance artery control and K_{Ca} channel modulated ACh dose response curves in MOPS buffer containing L-NAME (100 µM). Untreated control curve in black (n = 4), EBIO **37** (300 µM) modulated curve in blue (n = 4) SKA111 **5** (1 µM) modulated curve in green (n = 4), SKA113 **4** (10 µM) modulated curve in red (n = 3), where n is the number of animals and the error bars represent error around the mean. The data points of each treatment curve that were shown to have statistically significant difference to the respective untreated points denoted with *. Statistical significance determined using ANOVA analysis of treatment to untreatment data points. P values as follows; * = <0.05, ** = 0.01 and *** = <0.001.*

Repeated measures ANOVA statistical tests were used to determine the probabilities that each test molecule treated ACh dose response curve was different from the control by chance. As such, the confidence of the statistical difference of each treatment data point was qualified by the probability of how unlikely the same result might be generated randomly. The statistical confidence, or certainty, was considered significant if the statistically calculated value of the possibility of a chance result (P) was 0.05 or less. The confidence rose as the P value decreased further.

Pre-assay incubation of the arteries with each of the positive control modulators tested caused statistically significant shifts in the ACh dose response curve, Figure 4.4. Specifically, the slope ACh concentration points of the control and treatment curves were statistically different. The points close to total vasocontraction or vasorelaxation were not statistically different. EBIO **37** treatment produced the statistically most confident difference, with P values of <0.001 for 10–30 nM ACh, and <0.01 for 3 nM. SKA111 **5** produced the next statistically most confident difference, with P values of <0.001 for 10 nM ACh and <0.05 for 30 nM. SKA113 **4** gave the least confident difference, with only one P value of <0.05 for 10 nM ACh.

Table 4.1; Calculated ACh EC_{50}s before and after artery treatment with K_{Ca} channel positive modulators, EBIO, SKA111 and SKA113.

	Untreated Control	EBIO Treatment	SKA111 Treatment	SKA113 Treatment
ACh EC_{50} (nM)	24.4	4.4	8.1	9.4
Stnd Err (±)	3.5	1.5	3.0	4.0

The ACh EC_{50}s, calculated *via* non-linear regression of each dose response curve, were statistically different from the control, all had P values of <0.0001, Figure 4.4 and Table 4.1. The ACh dose response data confirmed previous observations and the biological activity of the positive control molecules. All of the modulators gave similar shifts in ACh EC_{50} from 30 nM in the control to 5–10 nM after treatment. No greater effect of one modulator over another was seen, suggesting that there may be a maximum limit to K_{Ca} modulation, regardless of each K_{Ca} channel modulator's potency. Both the naphthothiazole and benzimidiazolone modulator class compounds produced positively modulated results with decreased ACh EC_{50}s. These data validated the use of the published modulators as positive controls in biophysical experiments and for derivatisation.

A potential issue remained with the interpretation of the ACh vasorelaxation assay: does a shift in ACh dose response correspond to direct K_{Ca} channel modulation? It is impossible to definitively confirm whether a molecule is a ligand of a membrane protein, such as a channel, using *in vivo* testing alone.[1] It is an assumption that a small molecule induced ACh dose response shift demonstrates a test molecule's ability to directly modulate K_{Ca} channels as a ligand. It is possible that an ACh dose response shift may be due to the small molecule modulation of other proteins in the EDH pathway that cause the same effect.

The literature interpretation of the ACh vasorelaxation assay is based on the ACh response shift theory: a shift in ACh dose response corresponds to the increased Ca^{2+} sensitivity of modulated K_{Ca} channels. Channels are therefore activated with less intracellular Ca^{2+} release, caused with less ACh stimulation. The ACh response shift theory presumes ACh stimulation and Ca^{2+} release from cellular stores, is a linear relationship. ACh stimulation can therefore be used as an indicator cellular Ca^{2+} concentration. Thus, as ACh increases over a dose response curve, the cellular concentration of Ca^{2+} rises in a similar way. As the concentration of cellular Ca^{2+} increases, it activates the $SK_{Ca}2.2$ and $IK_{Ca}3.1$ channels until their activation is saturated, maximising their K^+ efflux function. K^+ efflux leads to greater membrane hyperpolarisation and increasing vasorelaxation, which is observed. A direct K_{Ca} channel modulator would decrease their Ca^{2+} activation thresholds. Subsequently, the level of ACh stimulation required to cause vasorelaxation, in the presence of a K_{Ca} modulator, would be lowered, shifting the ACh dose response.

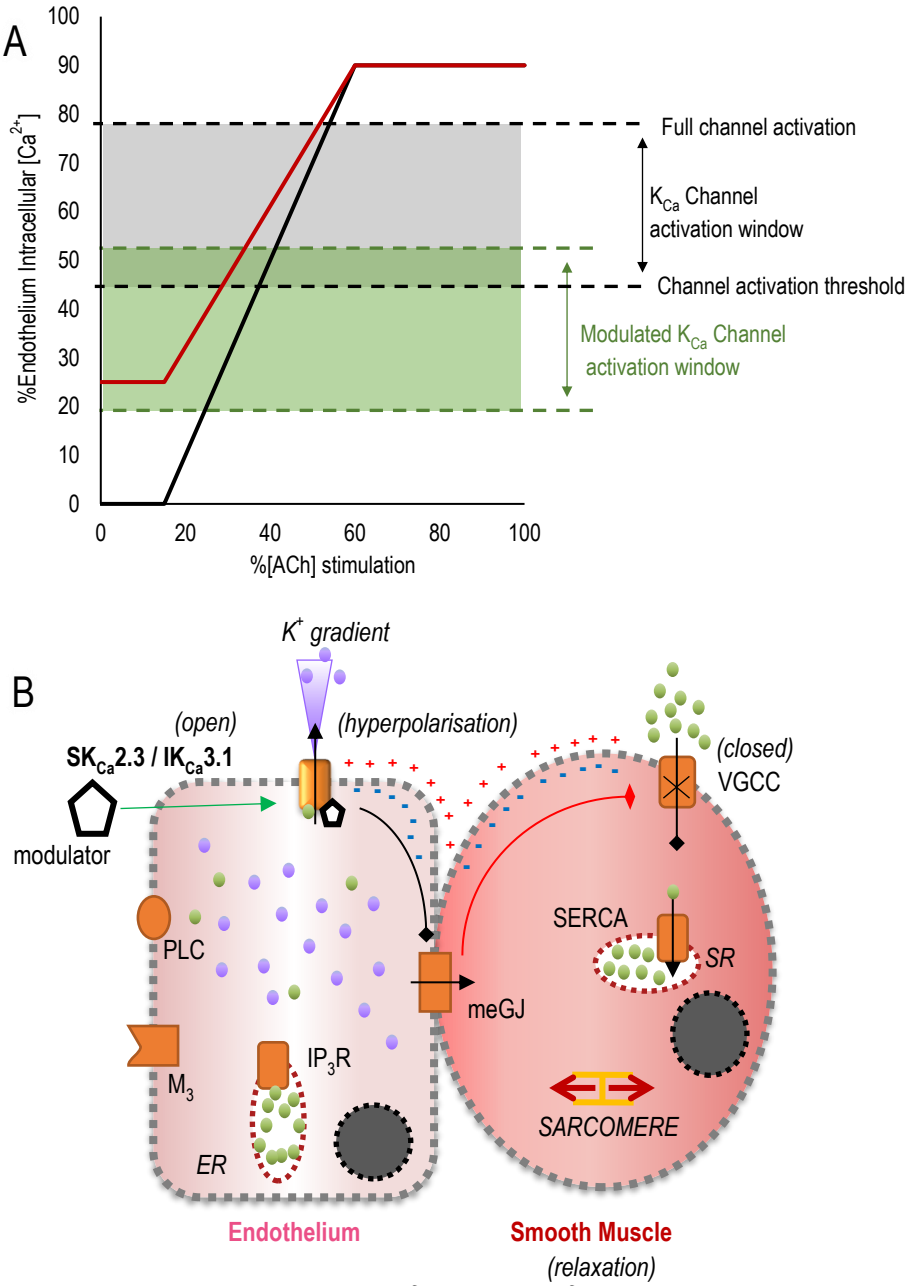


Figure 4.5; Graphical and diagrammatic depiction of the theory of direct K_{Ca} channel activation by small molecule positive modulators. A) A graph demonstrating potential positively modulated K_{Ca} channel activation by the basal concentration of Ca^{2+}. The increased Ca^{2+} sensitivity of modulated K_{Ca} channel shown by the lower green channel activation window compared to unmodulated black window. Channel stimulation during ACh dose response curve, ignoring basal Ca^{2+} concentration, shown as a black line. Potential for direct channel activation to small molecule modulators caused by basal Ca^{2+} shown as a red line. B) Diagram representing direct K_{Ca} channel activation by small molecule modulators. Muscarinic receptor (M_3), phospholipase C (PLC), ryanodine receptor (IP_3R), myoendothelial gap junction (meGJ), voltage gated Ca^{2+} channels (VGCC) and sarcoplasmic endoreticulum Ca^{2+} ATPase (SERCA) rendered in 2D, K_{Ca} channels rendered in 3D, Ca^{2+} ions shown in green and K^+ shown in purple.

A proposed alternative direct modulator response theory of the impact of K_{Ca} channel modulators on the observed ACh dose response, is plausible and contrary to the ACh response shift theory, Figure 4.5. The endothelium cellular concentration of Ca^{2+} is not zero before ACh stimulation but is maintained at a basal level, lower than the Ca^{2+} activation threshold of unmodulated K_{Ca} channels. However, a direct small molecule modulator of K_{Ca} channels would decrease their activation threshold below the cellular basal concentration of Ca^{2+}. Consequently, a direct K_{Ca} channel modulator would cause their immediate activation and artery vasorelaxation, without requiring ACh stimulation. Expanding on this theory would suggest: if a small molecule were a K_{Ca} channel modulator and led to their immediate activation, additional ACh stimulation would not produce further vasorelaxation. This is because the channels are already activated and open at the current concentration of intra cellular Ca^{2+}.

4.2 Investigating Direct K_{Ca} Channel Modulator Induced Vasorelaxation

The SK_{Ca} modulator NS309 does cause direct artery vasorelaxation, which demonstrates that the basal concentration of Ca^{2+} in endothelial cells, is enough to enable direct K_{Ca} channel modulator activation.[10,20] The precise structural mechanism of NS309 K_{Ca} channel activation is known, discussed in detail in Chapter 2. The ability of NS309 to stabilise a loop region in the K_{Ca} channel gating complex, improves the binding of PIP_2 to the activated gating complex, facilitating channel pore opening.[21,22] This effect is true of NS309 K_{Ca} modulation; however, the putative $IK_{Ca}3.1$ naphthothiazole modulator SKA111 **5** is structurally different from NS309 and may not cause as dramatic a stabilisation effect. Control experiments were thus performed to develop an assay, based on direct modulator induced artery vasorelaxation and used to observe SKA111 **5** activity.

4.2.1 *Vasorelaxation Assay Format Based on Direct Response to K_{Ca} Channel Modulators*

The literature observed constricted artery vasodilation induced by NS309 suggested other K_{Ca} channel modulators would produce the same effect. Thus, to identify K_{Ca} channel modulators, an assay was proposed where constricted arteries would be exposed to potential K_{Ca} channel small molecule modulators, instead of ACh. A clear subsequent vasorelaxation, after test molecule addition, would indicate the ability of the molecule to act as a K_{Ca} channel modulator *via* the theory described above.

The ACh dose response was shifted by the control molecules: SKA111 **5**, SKA113 **4** and EBIO **37**. This confirmed the previous literature results and suggested that presumed K_{Ca} channel modulation was observable under the literature MOPS assay conditions used. The same MOPS assay conditions were initially adapted for use in the proposed direct response modulator induced vasorelaxation assay format. When a dose response of SKA111 **5** across its published $IK_{Ca}3.1$ channel EC_{50} of 100 nM was conducted in MOPS buffer, no vasorelaxation was observed in comparison with the parallel buffer control, Figure 4.6.[8]

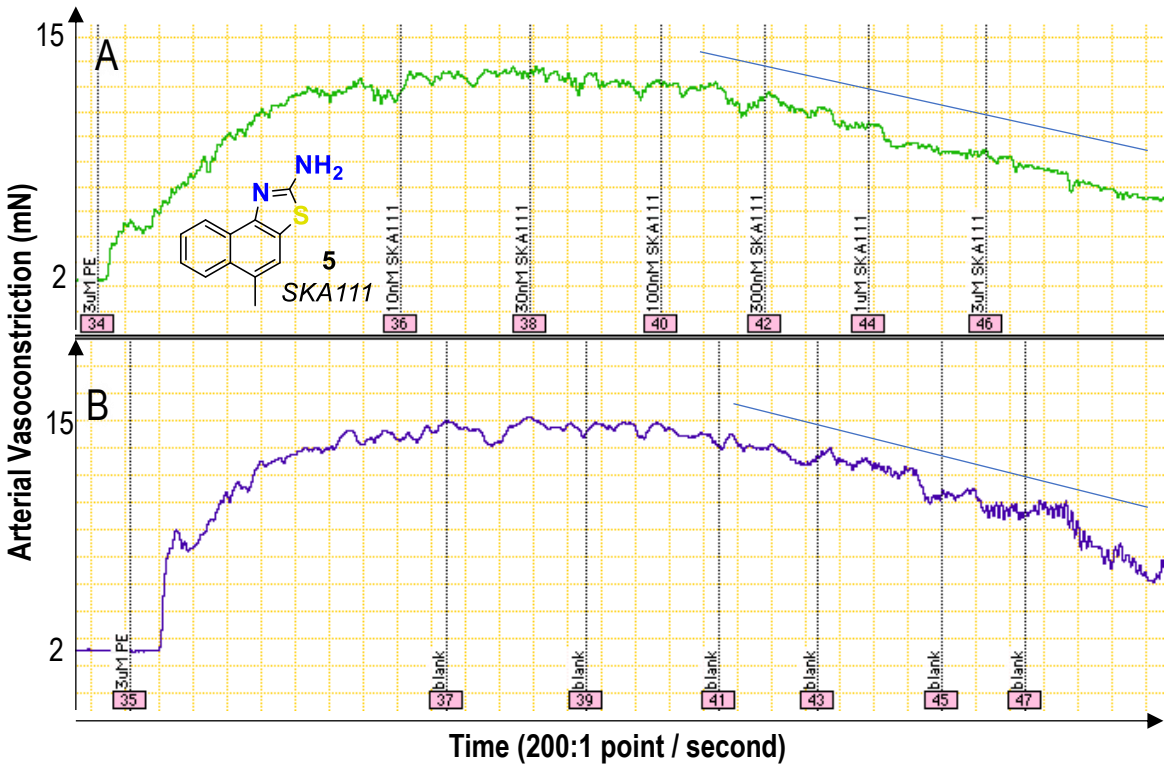


Figure 4.6; Representative wire myograph trace of direct SKA111 ***5*** *vasorelaxation in MOPS. Eventual vasoconstriction fade highlighted in blue for both traces. A) Force plot of arterial vasoconstriction in green, dose response of SKA111* ***5****. B) Force plot of arterial vasoconstriction in purple, time control with dose response of buffer blanks.*

The vasoconstriction in both the SKA111 **5** and buffer control experiments eventually faded; however, this is a typical spontaneous phenomenon, observed after prolonged phenylephrine (PE) induced vasoconstriction, Figure 4.6.[23] No vasorelaxation was seen in a vehicle control dose response up to 0.2% DMSO. Other than fade, there was no direct vasorelaxation response to increasing concentrations of SKA111 **5**, even above its published patch clamp determined $IK_{Ca}3.1$ EC_{50} of 100 nM.[8] The discrepancy between the observed naphthothiazole modulators' patch clamp and wire myography biological activities has been published before, yet not convincingly explained.[7] The published interpretation of this phenomenon suggested the lack of effect was because full modulator channel activation was not achieved under wire myography conditions.[24] Another explanation for the negative SKA111 **5** direct vasorelaxation result in wire

myography could be the stabilisation of the K_{Ca} gating complex is not as prominent as that of NS309. If so, SKA111 **5** may not reduce the K_{Ca} channel activation threshold by as much as NS309.[21,25] The large amount of $IK_{Ca}3.1$ patch clamp experimentation, including the effect of mutational analyses on observed SKA111 **5** modulation, strongly seems to suggest that SKA111 **5** is a modulator. However, as stated, it is impossible to definitively prove small molecule direct target engagement *in vivo* alone, and so SKA111 **5** may yet not be a K_{Ca} modulator as expected.

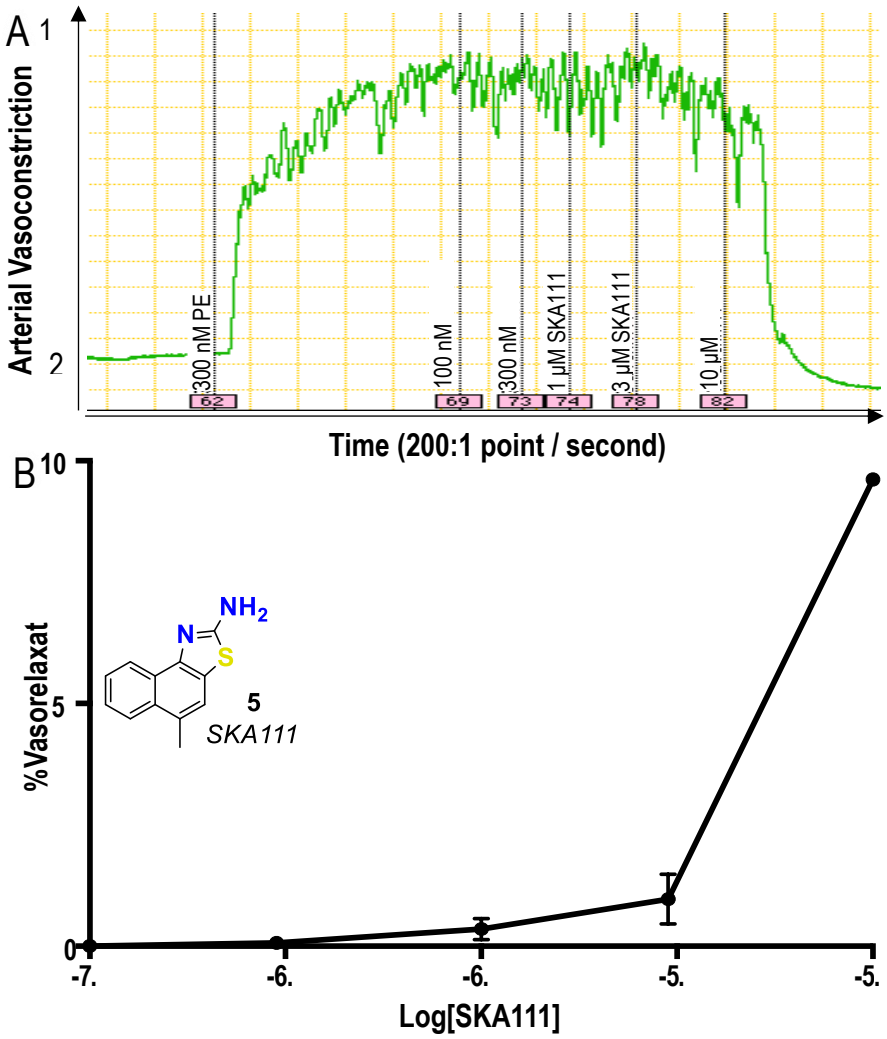


*Figure 4.7; Direct arterial vasorelaxation to the putative $IK_{Ca}3.1$ modulator SKA111 **5** in Krebs solution. A) Representative wire myograph trace of SKA111 **5** dose response, force plot of arterial vasoconstriction in green. B) Arterial dose response curve of SKA111 **5** (n = 5), where n is the number of animals and the error bars represent error around the mean.*

Krebs solution has greater buffering capacity than MOPS, because its pH is constantly corrected by the bubbling of CO_2 through the solution.[26] MOPS is a common biological buffer but its capacity to resist pH change is limited to its original component concentrations.[27] Krebs solution is thus much more commonly used for *ex vivo* tissue preparations.[26] The assay buffer was optimised and swapped to Krebs solution instead of MOPS. Under these conditions a large SKA111 **5** dose response was observed. At a relatively high concentration of 3-10 µM, SKA111 **5** caused complete arterial vasorelaxation, generating a steep dose response curve, Figure 4.7. In addition to this result, attempting to perform the previous SKA111 **5** incubated ACh dose response was not possible. The pre-incubation of SKA111 **5** under Krebs solution conditions caused the complete suppression of arterial contraction to the vasopressor PE. The suppression of contraction added evidence that K_{Ca} channel modulation should not be compatible with ACh dose response curves.

The EC_{50} of SKA111 **5** could not be reliably calculated from its direct dose response curve, due to the lack of recorded concentration points around and above the midpoint, Figure 4.7. The $LogD_{7.4}$ of SKA111 **5** was calculated using ACD I-Lab as 3.16, explaining its limited maximum solubility of 10 µM despite 0.1% dimethylsulfoxide (DMSO) vehicle. Further addition of DMSO in achieving higher concentrations of SKA111 **5** was not attempted, due to the known effects of 0.3% DMSO on artery vasoconstriction and health.[28] An estimation based on the recorded points suggested the EC_{50} of SKA111 **5** was ~ 6 µM, which is much higher than the published 100 nM EC_{50} recorded in patch clamp experiments. It may be possible that EDH type relaxation is only observed once a threshold of K_{Ca} activity is reached, similar to a neuronal action potential. Full activation of all K_{Ca} channels, at higher saturating concentrations of SKA111 **5** modulator, may be required for EDH to be generated. It is not unusual for an EC_{50} to

be ~10 fold higher *in vivo* than *in vitro.* A high EC_{50} was concerning because it increases the probability of off target interactions.[29] Off target interactions complicate the origin identification of the assay observed effect.[1]

SKA111 **5** was seen to directly dilate resistance arteries and so this assay was considered suitable for the identification of other molecules with similar biological activities. Using these buffer conditions, the direct vasorelaxation assay was repeated with several novel naphthothiazole analogues to identify if any retained or improved upon the biological activity of SKA111 **5**, Figure 4.8.

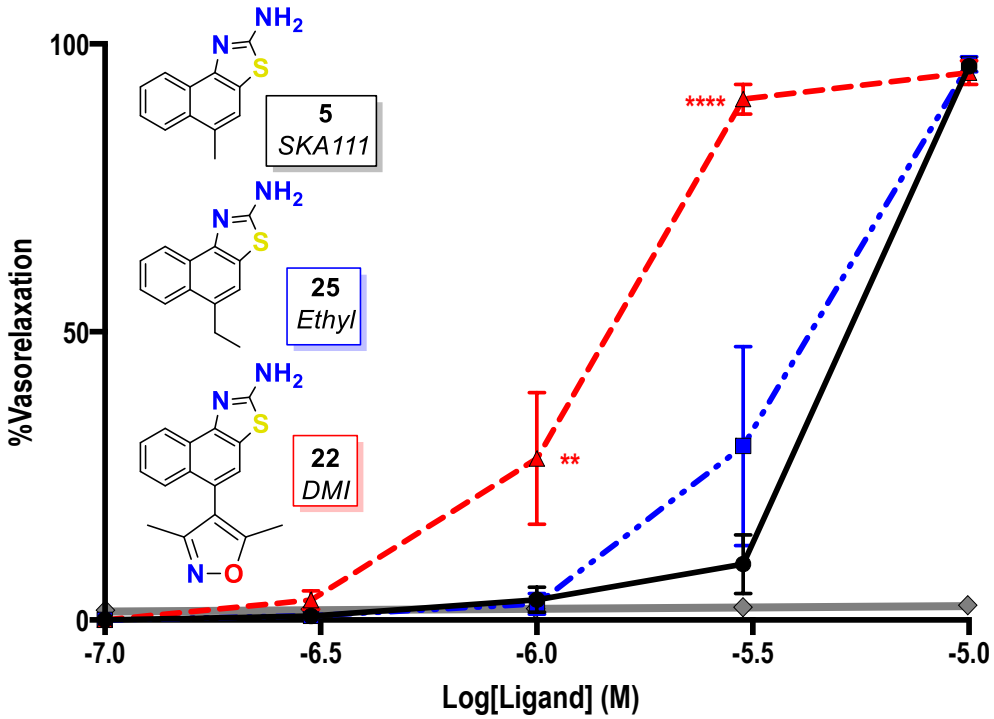


*Figure 4.8; Direct arterial vasorelaxation to the SKA111 **5** novel analogues. Arterial dose response curve of SKA111 **5** in solid black line (n = 5), response of ethyl analogue **25** in blue dot and dashed line (n = 4), response of DMI analogue **22** in red dashed line (n = 5), where n is the number of animals and the error bars represent error around the mean. All other test compounds were inactive (for structures see Figure 4.1), each producing no observable change at any concentration, shown by grey line. The data points of each coloured curve that were shown to have statistically significant difference to the respective black SKA111 points denoted with *. Statistical significance determined using ANOVA analysis of treatment to untreatment data points. P values as follows: ** = 0.01 and **** = <0.0001.*

Many of the naphthothiazole analogues screened did not exhibit any vasorelaxatory activities. This result did not corroborate the K_{Ca} binding rationale developed from the *in silico* structural analysis of the binding region, Chapter 2. Yet, pharmacological assessment alone, could not discount the possibility of the analogues to bind the K_{Ca} channels or even act as modulators *in vitro*. Biological assays are highly complex and the failure of a molecule to elicit a response may be caused by several different issues regarding target engagement and interaction. The methylamine analogue **13** has a calculated $LogD_{7.4}$ of -0.11 because of it's conjugate acid pK_a, 10.64 and subsequent protonated form in solution. Despite the excellent solubility of **13**, modulators would need to cross the membrane to access the K_{Ca} channel gating complex, within the cell interior.[30–32] The charged form of **13** may therefore not have crossed the cell membrane to engage the target channel, which is not a condition in a biophysical assay. Additionally, as discussed in Chapter 2, **13** degraded *via* ammonia elimination under protic conditions, likely reducing its probability of binding the target in the assay. This instability under assay conditions prompted the synthesis of the more stable methylalcohol analogue **24**. The effect of the stabilities of **13** and **14** on target binding would be more clearly demonstrable in a biophysical assay, where fewer negative result causes might apply.

The aniline **10,** amide **17**, and methylalcohol **24** all have $LogD_{7.4}$ values of less than 2.3 and conjugate acid pK_a's of under 4, predicting improved solubility without being protonated in solution. Based on these physical properties, each of the analogues should be able to pass the cell membrane to engage the target K_{Ca} channels, unlike **13**. None of these molecules exhibited vasorelaxant activity in the direct vasorelaxation assay, removing them as potential therapeutics but not as potential IK_{Ca} binders. Even if **10**, **17** or **24** were to bind the target channels, they may not act as positive modulators.

These analogues may instead act as negative modulators; however, this activity would not be identified in a direct vasorelaxation response assay. Only a biophysical assay can specifically determine whether these molecules directly interact with the target, at the expected binding region.

The simple addition of a methylene group to SKA111 **5,** giving the ethyl analogue **25**, did not change the activity of the molecule dramatically and was seen to produce a similar dose response curve to SKA111 **5**, Figure 4.8. **25** was intended to demonstrate the difference in the activities with the polar hydrogen bond (H-bond) capable analogues **13** and **24**. The ethyl analogue's activity suggested the equivalent polar compounds, **14** and **24**, would be sterically accommodated in the K_{Ca} channel binding cavity; thus, this was not the cause of the other analogues inactivities. Like SKA111 **5**, **25** retained the $LogD_{7.4}$ of 3.16 and solubility: its EC_{50} was not calculable due to the same lack of recorded points above the midpoint. The estimated EC_{50} of **25**, ~4 µM, was lower than the estimated EC_{50} for SKA111 **5**. The points of the two dose response curves were not statistically different according to ANOVA analysis, however, meaning the EC_{50} values were not different, and remained the same.

The 3,5-dimethyl isoxazole (DMI) naphthothiazole analogue **22** was also observed to have vasorelaxation activity. This result suggested a much larger group, like an aromatic ring, was still accommodated by the K_{Ca} channel binding cavity, despite the poor docking results and analysis, Chapter 2. The *in silico* analysis, based on the snap shot $SK_{Ca}2.2$ crystal structures, may be too static. The cavity formed by a protein-protein interaction (PPI) is possibly far more flexible than a more traditional enzyme biding pocket.

The calculated EC_{50} of **22**, 1.4 µM, was lower than the estimated EC_{50} of SKA111. The dose response curve of **22**, was statistically different from that of SKA111 at 1 and

3 µM, with P values of 0.005 for the former and 0.0001 for the later. It is difficult to know if the increase in potency of **22** is related to its potential to H-bond to Ser370 of the $IK_{Ca}3.1$ binding region. Thus, a number of control experiments were performed to help identify the origin of the observed vasorelaxatory effects of each of the positive result compounds.

4.2.2 *Proving the Mechanism of Naphthothiazole K_{Ca} Modulator Action*

Although the published wire myography assay format was able to identify small molecules capable of modulating the EDH pathway, it was difficult to prove that this modulation was caused by direct modulation of K_{Ca} channels. It has been assumed, because naphthothiazole EDH positive modulation mimicked the known K_{Ca} binder EBIO **37** modulation, that these molecules interact with the same target in the same manner.[7,8] To help establish which K_{Ca} channels were involved with the action of the naphthothiazole modulators, $SK_{Ca}2.3$ and $IK_{Ca}3.1$ were selectively blocked before the direct vasorelaxation assays were repeated. Initially, each channel was blocked separately using either the $SK_{Ca}2.3$ blocker, and bee venom component, apamin, or the small molecule $IK_{Ca}3.1$ blocker TRAM34, Figure 4.9. The experiments were designed to help rule out the direct or component source of the naphthothiazole modulator action.

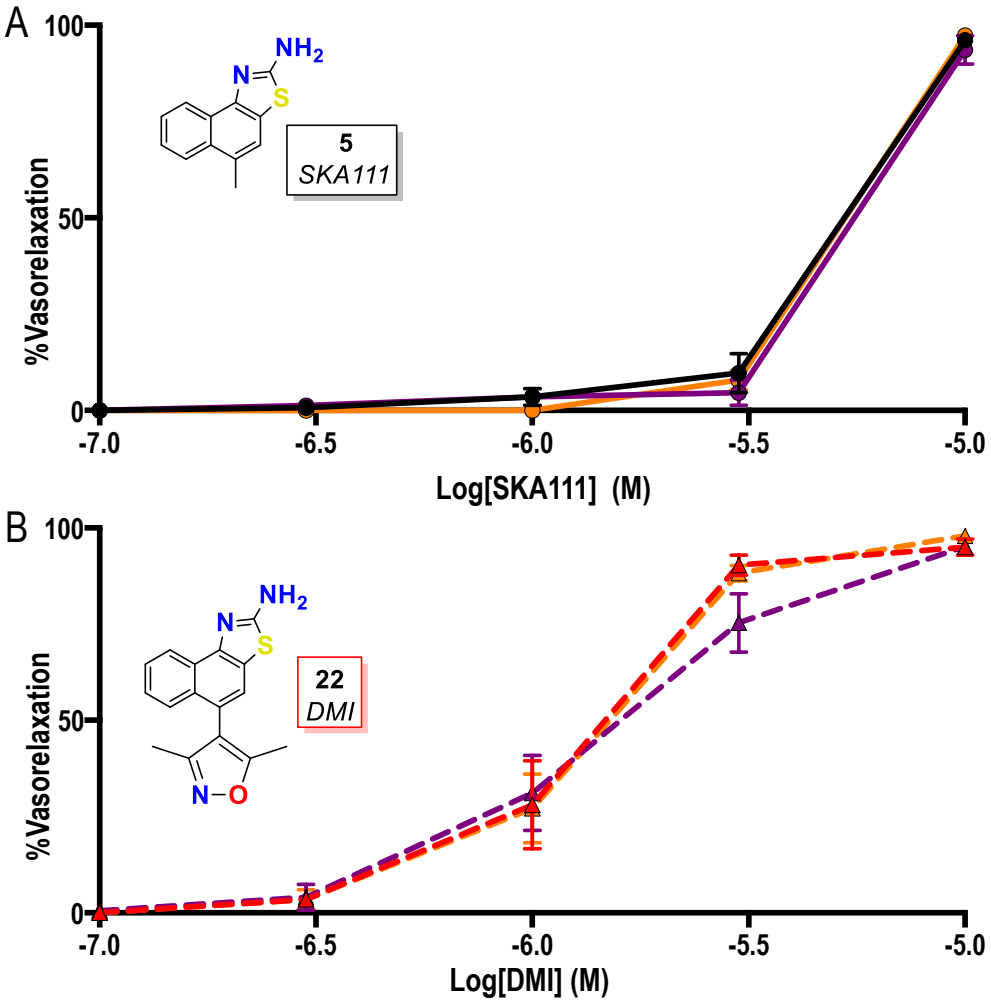


Figure 4.9; Direct resistance artery vasorelaxation to dose response curves of SKA111 ***5*** *and the DMI analogue* ***22,*** *with and without $SK_{Ca}2.3$ or $IK_{Ca}3.1$ channel blockade. Dose response experiments in the presence of $SK_{Ca}2.3$ apamin (100 nM) blockade shown as orange lines. Dose response experiments in the presence of $IK_{Ca}3.1$ TRAM34 (1 μM) blockade shown as purple lines. A) SKA111 dose response experiments shown in solid lines. No K_{Ca} channel blockade experiments shown as a black line (n = 5), $SK_{Ca}2.3$ blockade experiments (n = 4), $IK_{Ca}3.1$ blockade experiments (n = 6). B) DMI analogue* ***22*** *dose response experiments shown in dashed lines. No K_{Ca} channel blockade experiments shown as a red line (n = 5), $SK_{Ca}2.3$ blockade experiments (n = 4), $IK_{Ca}3.1$ blockade experiments (n = 5). Where n is the number of animals and the error bars represent error around the mean.*

The direct vasorelaxation assays of SKA111 **5** and the DMI analogue **22** conducted under $IK_{Ca}3.1$ or $SK_{Ca}2.3$ channel blockade conditions, were statistically no different

from the control without any blockade. This result disagreed with the published 100-fold selectivity of SKA111 **5** for the $IK_{Ca}3.1$ channel over $SK_{Ca}2.3$, EC_{50} ~13 μM.[8] Possibly, under blockade of each K_{Ca} channel, the opposite was able to continue to give EDH mediated vasorelaxation.[33] Alternatively, the observed vasorelaxation to either naphthothiazole may not be as a result of K_{Ca} modulation but another unknown target. The lack of blockade effect on **22** dose responses suggested its target(s) remained the same as SKA111 **5**.

The next control experiments demonstrated the effect of removing EDH type relaxation, by K_{Ca} channel modulation, on the direct artery vasorelaxation responses of SKA111 **5** and **22**. The endothelium K_{Ca} channels were simultaneously blocked *via* artery pre-incubation with combined apamin and TRAM34, before performing the direct vasorelaxation assays. Separately, the endothelium itself was denuded before direct vasorelaxation assays to remove any possible endothelium derived signalling, and any endothelium based target, Figure 4.10.

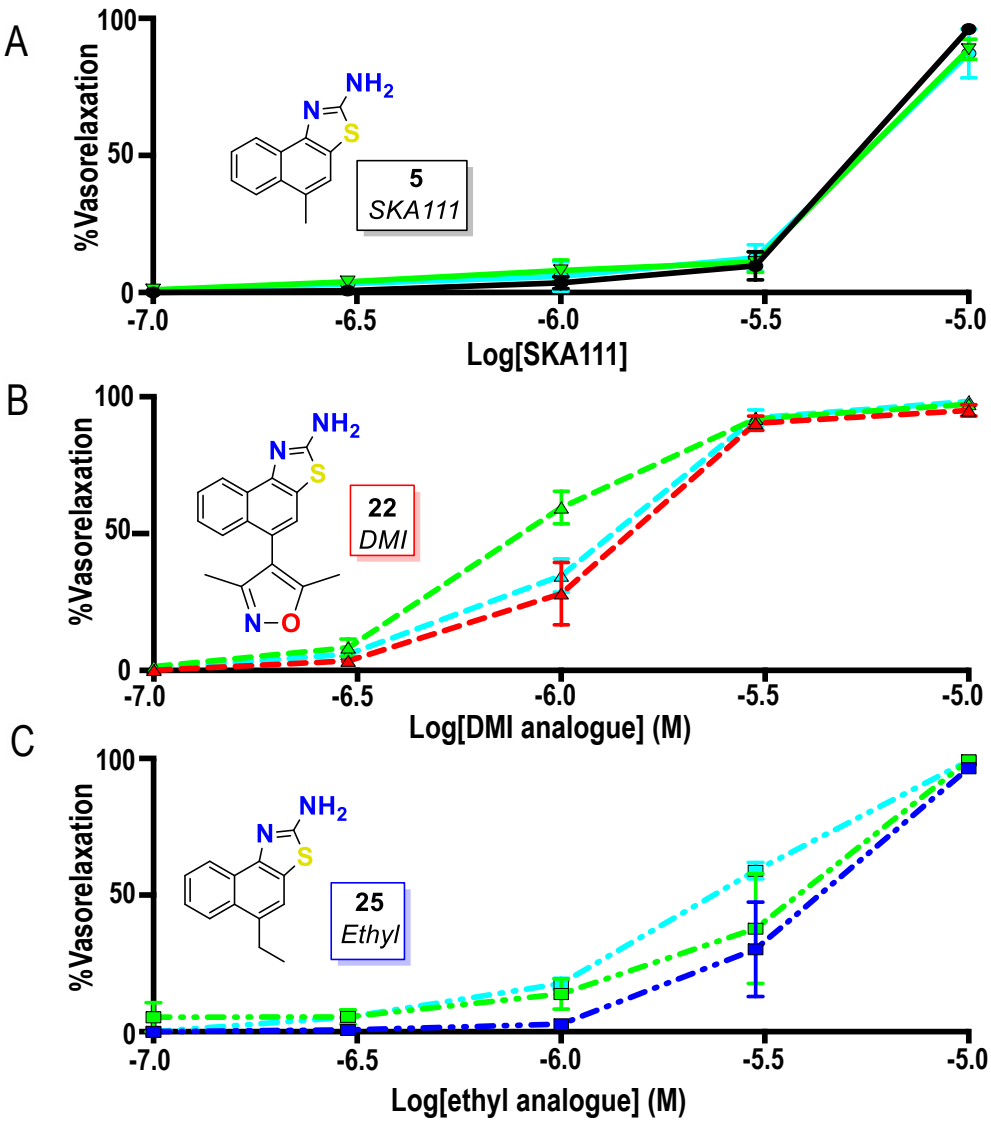


Figure 4.10; Direct resistance artery vasorelaxation to dose response curves of SKA111 ***5****, the DMI analogue* ***22*** *and the ethyl analogue* ***25****, with and without double $SK_{Ca}2.3$ and $IK_{Ca}3.1$ channel blockade or removal of artery endothelium (denudation). Dose response experiments in the presence of double $SK_{Ca}2.3$ apamin (100 nM) and $IK_{Ca}3.1$ TRAM34 (1 μM) blockades shown as green lines. Dose response experiments with endothelium denuded arteries shown as light blue lines. A) SKA111* ***5*** *dose response experiments. No blockade or denudation experiments shown as black line (n = 5), double $SK_{Ca}2.3$ and $IK_{Ca}3.1$ blockade experiments (n = 5), denuded artery experiments (n = 3). B) DMI analogue* ***22*** *dose response experiments. No blockade or denudation experiments shown as red line (n = 5), double $SK_{Ca}2.3$ and $IK_{Ca}3.1$ blockade experiments (n = 5), denuded artery experiments (n = 4). C) Ethyl analogue* ***25*** *dose response experiments. No blockade or denudation experiments shown as dark blue line(n = 4), double $SK_{Ca}2.3$ and $IK_{Ca}3.1$ blockade experiments (n = 3), denuded artery experiments (n = 2). Where n is the number of animals and the error bars represent error around the mean.*

No EDH type mechansm of vasorelaxation should be possible under double blockade conditions; removing the activities of both $SK_{Ca}2.3$ and $IK_{Ca}3.1$, Figure 4.5. Even without EDH, the naphthothiazole analogues **22**, **25** and SKA111 **5** all retained their activities, each statistically no different from their respective controls, Figure 4.10. Only the 1 µM concentration point of **22**, during double channel blockade, was statistically different from the control, with a P value of 0.0001. The effect of denudation on the response of **22** was not statistically different, disproving the possible involvement of K_{Ca} channel modulation. The entire set of control experiments proved the naphthothiazole vasorelaxatory mechanism, observed under these conditions, was not derived from K_{Ca} channels and was the product of an unrelated target. Removal of the endothelium before the direct vasorelaxation assay did not deminish the observed vasorelaxatory effect of any of the naphthothiazoles. This result proved the target of the naphthothiazoles was not within the endothelium, but in the smooth muscle itself.

It was difficult to determine the actual target of the observed naphthothiazole vasorelaxatory effect. One K_{Ca} channel remains in the smooth muscle which is $BK_{Ca}3.1$. This channel, unlike the other K_{Ca} channels, does not have a calmodulin (CaM) based gating mechanism and was not considered a potential target. A last set of control experiments were conducted on the positive control SKA111 **5** to determine if this last K_{Ca} channel was the target of the naphthothiazoles. All K_{Ca} channels were simultaneously blocked, as before, but including the small molecule $BK_{Ca}3.1$ blocker paxilline. Blockade of the $BK_{Ca}3.1$ channel, in arteries with the endothelium denuded, was conducted before direct vasorelaxation assays to further prove no endothelium target was present, leaving only $BK_{Ca}3.1$, Figure 4.11.

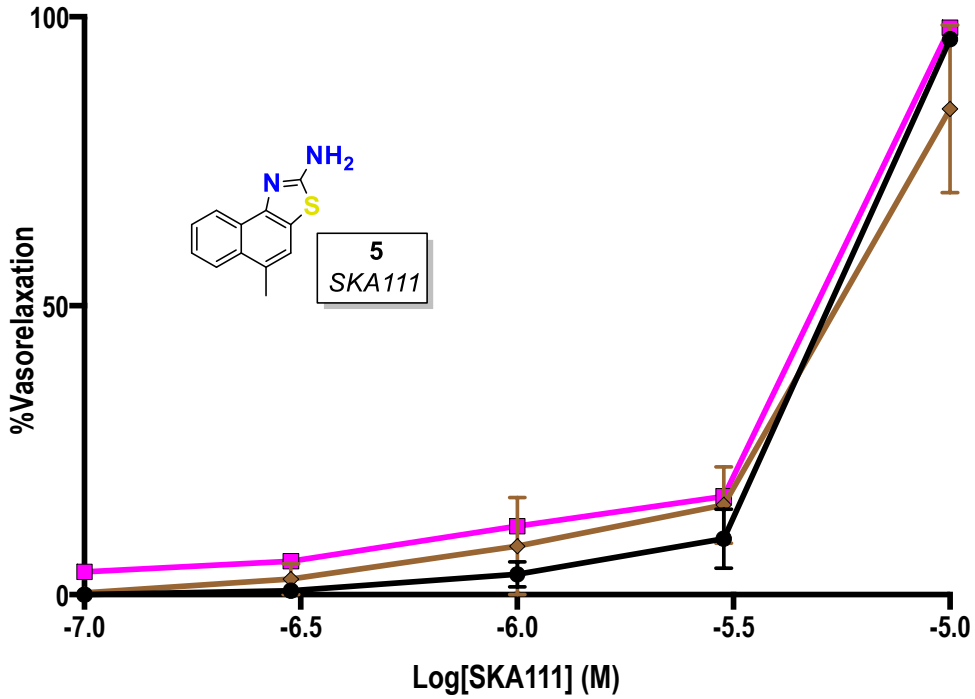


Figure 4.11; *Direct resistance artery vasorelaxation to dose response curves of SKA111* ***5,*** *with and without triple* $SK_{Ca}2.3$, $IK_{Ca}3.1$ *and* $BK_{Ca}1.1$ *channel blockade or removal of artery endothelium (denudation) with* $BK_{Ca}1.1$ *blockade. Dose response curves of SKA111* ***5*** *without blockade or denudation shown as a black line (n = 5). Apamin (100 nM), TRAM34 (1 μM) and paxilline (100 nM)* $SK_{Ca}2.3$, $IK_{Ca}3.1$ *and* $BK_{Ca}1.1$ *triple blockade experiments (n = 2). Endothelium denuded arteries with paxilline (100 nM)* $BK_{Ca}1.1$ *blockade experiment (n = 1). Where n is the number of animals and the error bars represent error around the mean.*

Blockade of $BK_{Ca}3.1$, with and without endothelium denudation, had little to no effect on the vasorelaxatory action of SKA111 **5**. This result ruled out the action of any K_{Ca} channel modulation by the naphthothiazoles and meant another smooth muscle target must be the origin instead. The identification of this off target interaction was not within the remit of this thesis and no further experiments were conducted in order to determine one. There are, however, several possible targets within the smooth muscle, which could be the source of the observed naphthothiazole based vasorelaxation effect.

Ca^{2+} channels are present throughout the cardio vasculature. As seen in Figure 4.5 B, voltage gated Ca^{2+} channels (VGCCs) allow the influx of Ca^{2+} ions stimulating smooth muscle contraction. Ca^{2+} channel blockers are a known class of vasorelaxants which

block the action of VGCCs as a hypertensive treatment, discussed in Chapter 1.[34] Ca^{2+} channels may be one possible target of the naphthothiazoles, although they are structurally dissimilar to the typical dihydropyridine pharmacophore of this class of drugs.[35] Some activity on the action of L-type Ca^{2+} channels was observed and reported as ~50% current inhibition at 25 µM SKA111, which could give evidence to this hypothesis.[8] One side effect of Ca^{2+} channel blockers is reduction in heart rate, an observed effect of SKA111 in rat models, giving more credence to this hypothetical new target.[8]

Another potential target of the naphthothiazoles might be calmodulin itself. Calmodulin is involved in multiple functions within the endothelium and smooth muscle. The action of calmodulin at the sarcomere is directly responsible for smooth muscle contraction.[36,37] If the naphthothiazoles directly inhibited the PPI between calmodulin and the other proteins of the sarcomere this would be a novel mechanism of smooth muscle relaxant.

Unfortunately, it was not possible to observe naphthothiazole K_{Ca} channel modulation *via* direct activation using the published modulator SKA111 **5** or analogues of it. A new and potentially important unknown vasorelaxant effect of SKA111 **5** and analogues has been discovered, prompting more investigation into this effect and its implications for unintended *in vivo* side effects. The negative K_{Ca} modulation results in the direct vasorelaxation assay do not disprove the patch clamp evidence of naphthothiazole K_{Ca} channel modulation. The negative results of the naphthothiazole analogues generated in the direct vasorelaxation assay, therefore, do not disprove them as potential K_{Ca} modulators. The published ACh dose response shift assay was repeated to show apparent EDH modulation by SKA111 **5**, SKA113 **4** as the same as the known K_{Ca} channel modulator EBIO **37**. It may be possible that similar modulation may have been

observed for the naphthothiazole analogues yet due to time restrictions these experiments were not conducted.

4.3 Summary

Published positive modulator wire myography experiments, utilising *ex vivo* resistance arteries, were reproduced to confirm reported bioactivates of known K_{Ca} channel positive modulators and assay format. Potential ambiguity concerning the indirect mechanism of K_{Ca} channel modulation, proposed in the published mechanism of vasorelaxation, prompted a shift to Krebs solution over MOPS buffered test conditions. Under these conditions, the amine **13**, aniline **10**, amide **17** and alcohol **24** naphthothiazoles were not observed to have any vasorelaxant activity.

The 5-ethyl SKA111 analogue **25** was designed to compare the difference between polar and non-polar analogues, as a control for the effect of the proposed H-bond. The DMI analogue **22** was designed to test the size limit of H-bond forming naphthothiazole analogues. Like SKA111 **5**, **22** and **25** produced a clear vasorelaxation. All of these vasorelaxant responses were not related to K_{Ca} channel modulation; continuing in the presence of multiple K_{Ca} channel blockers and even in the absence of the endothelium itself. This observation was true for SKA111 **5** as well as the novel analogues, which suggested that the naphthothiazoles interacted not through the K_{Ca} channels, but with unknown protein partners.

Chapter 4 References

1. Cronk, D. High-Throughput Screening. in *Drug Discovery and Development: Technology in Transition* (eds. Hill, R. & Rang, H.) 95–118 (Churchill Livingstone, 2012).

2. Sakmann, B. & Neher, E. Patch clamp techniques for studying ionic channels in excitable membranes. *Annu. Rev. Physiol.* **46,** 455–472 (1984).

3. Vasilyev, D. V., Merrill, T. L. & Bowlby, M. R. Development of a novel automated ion channel recording method using 'inside-out' whole-cell membranes. *J. Biomol. Screen.* **10,** 806–813 (2005).

4. Sigworth, F. J. & Neher, E. Single Na^+ channel currents observed in cultured rat muscle cells. *Nature* **287,** 447–448 (1980).

5. Singh, S., Syme, C. A., Singh, A. K., Devor, D. C. & Bridges, R. J. Benzimidazolone activators of chloride secretion: potential therapeutics for cystic fibrosis and chronic obstructive pulmonary disease. *J.Pharmacol.Exp.Ther.* **296,** 600–611 (2001).

6. Devor, D. C., Singh, A. K., Frizzell, R. a & Bridges, R. J. Modulation of Cl^- secretion by benzimidazolones. I. Direct activation of a Ca^{2+}-dependent K^+ channel. *Am. J. Physiol.* **271,** L775-84 (1996).

7. Sankaranarayanan, A. *et al.* Naphtho[1,2-*d*]thiazol-2-ylamine (SKA-31), a new activator of $K_{Ca}2$ and $K_{Ca}3.1$ potassium channels, potentiates the endothelium-derived hyperpolarizing factor response and lowers blood pressure. *Mol. Pharmacol.* **75,** 281–95 (2009).

8. Coleman, N. *et al.* New positive Ca^{2+}-activated K^+ channel gating modulators with selectivity for $K_{Ca}3.1$. *Mol. Pharmacol.* **86,** 342–357 (2014).

9. Brown, B. M., Shim, H., Zhang, M., Yarov-Yarovoy, V. & Wulff, H. Structural determinants for the selectivity of the positive $K_{Ca}3.1$ gating modulator 5-methylnaphtho[2,1-*d*]oxazol-2-amine (SKA-121). *Mol Pharmacol* **92,** 469–480 (2017).

10. Strøbæk, D. *et al.* Activation of human IK and SK Ca^{2+}-activated K^+ channels by NS309 (6,7-dichloro-1H-indole-2,3-dione 3-oxime). *Biochim. Biophys. Acta* **1665,** 1–5 (2004).

11. Berg, J. M., Tymoczko, J. L. & Stryer, L. Membrane Channels and Pumps. in *Biochemistry* 572–575 (W.H.Freeman and Company, 2002).

12. Bezanilla, F. Ion Channels: From Conductance to Structure. *Neuron* **60,** 456–468 (2008).

13. Christophersen, P. & Wulff, H. Pharmacological gating modulation of small-and intermediate-conductance Ca^{2+}-activated K^+ channels ($K_{Ca}2.x$ and $K_{Ca}3.1$). *Channels* **9,** 336–343 (2015).

14. Garland, C. J., Hiley, C. R. & Dora, K. A. EDHF: Spreading the influence of the endothelium. *Br. J. Pharmacol.* **164,** 839–852 (2011).

15. Garland, C. J., Plane, F., Kemp, B. K. & Cocks, T. M. Endothelium-dependent hyperpolarization: A role in the control of vascular tone. *Trends Pharmacol. Sci.* **16,** 23–30 (1995).

16. Félétou, M. & Vanhoutte, P. M. Endothelium-Derived Hyperpolarizing Factor. *Clin. Exp. Pharmacol. Physiol.* **23,** 1082–1090 (1996).

17. Van Hove, C. E., Van Der Donckt, C., Herman, A. G., Bult, H. & Fransen, P. Vasodilator efficacy of nitric oxide depends on mechanisms of intracellular calcium mobilization in mouse aortic smooth muscle cells. *Br. J. Pharmacol.* **158,** 920–930 (2009).

18. Garland, C. J. Compromised vascular endothelial cell SK_{Ca} activity: a fundamental aspect of hypertension? *Br. J. Pharmacol.* **160,** 833–5 (2010).

19. Rasmussen, K. M. B., Braunstein, T. H., Salomonsson, M., Brasen, J. C. & Sorensen, C. M. Contribution of K^+ channels to endothelium-derived hypolarization-induced renal vasodilation in rats in vivo and in vitro. *Pflugers Arch. Eur. J. Physiol.* **468,** 1139–1149 (2016).

20. Feng, J. *et al.* Calcium-activated potassium channels contribute to human coronary microvascular dysfunction after cardioplegic arrest. *Circulation* **118,** S46–S51 (2008).

21. Zhang, M., Pascal, J. M. & Zhang, J.-F. Unstructured to structured transition of an intrinsically disordered protein peptide in coupling Ca^{2+}-sensing and SK channel activation. *Proc. Natl. Acad. Sci. U. S. A.* **110,** 4828–33 (2013).

22. Zhang, M., Meng, X.-Y., Zhang, J.-F., Cui, M. & Logothetis, D. E. Molecular overlap in the regulation of SK channels by small molecules and phosphoinositides. *Sci. Adv.* **1,** e1500008 (2015).

23. Seager, J. M., Clark, A. H. & Garland, C. J. Endothelium-dependent contractile responses to 5-hydroxytryptamine in the rabbit basilar artery. *Br. J. Pharmacol.* **105,** 424–428 (1992).

24. Damkjaer, M. *et al.* Pharmacological activation of $K_{Ca}3.1$/$K_{Ca}2.3$ channels produces endothelial hyperpolarization and lowers blood pressure in conscious dogs. *Br. J. Pharmacol.* **165,** 223–234 (2012).

25. Cui, M., Qin, G., Yu, K., Bowers, M. S. & Zhang, M. Targeting the small- and intermediate-conductance Ca^{2+}-activated potassium channels: the drug-binding pocket at the channel/calmodulin interface. *Neurosignals* **22,** 65–78 (2014).

26. Bailey, L. E. & Ong, S. D. Krebs-Henseleit solution as a physiological buffer in perfused and superfused preparations. *J. Pharmacol. Methods* **1,** 171–175 (1978).

27. Houghi, C. Buffer combinations for mammalian cell culture. *Science* **174,** 500–503 (1971).

28. Kaneda, T., Sasaki, N., Urakawa, N. & Shimizu, K. Endothelium-dependent and -independent vasodilator effects of dimethyl sulfoxide in rat aorta. *Pharmacology* **97,** 171–176 (2016).

29. Hann, M. M. Molecular obesity, potency and other addictions in drug discovery. *Multifaceted Roles Crystallogr. Mod. Drug Discov.* **2,** 183–196 (2015).

30. Schumacher, M. A., Rivard, a F., Bächinger, H. P. & Adelman, J. P. Structure of the gating domain of a Ca^{2+}-activated K^+ channel complexed with Ca^{2+}/calmodulin. *Nature* **410,** 1120–1124 (2001).

31. Christophersen, P. & Wulff, H. Pharmacological gating modulation of small- and intermediate-conductance Ca^{2+}-activated K^+ channels ($K_{Ca}2.x$ and $K_{Ca}3.1$). *Channels* **6950,** 00–00 (2015).

32. Wulff, H. & Köhler, R. Endothelial small- and intermediate-conductance K_{Ca} channels: an update on their pharmacology and usefulness as cardiovascular targets. *J. Cardiovasc Pharmacol.* **61,** 102–112 (2013).

33. Coleman, H. A., Tare, M. & Parkington, H. C. Nonlinear effects of potassium channel blockers on endothelium-dependent hyperpolarization. *Acta Physiol.* **219,** 324–334 (2017).

34. Fleckenstein, A., Frey, M. & Fleckenstein-grun, G. Antihypertensive and arterial anticalcinotic effects of calcium antagonists. *Am J Cardiol* **57,** 1D–10D (1986).

35. Chen, N. *et al.* Calcium channel blockers versus other classes of drugs for hypertension. *Cochrane Database Syst Rev* 1–68 (2010). doi:10.1002/14651858.CD003654.pub4

36. Conti, M. A. & Adelstein, R. S. The relationship between calmodulin binding and phosphorylation of smooth muscle myosin kinase by the catalytic subunit of 3':5' cAMP-dependent protein kinase. *J. Biol. Chem.* **256,** 3178–3181 (1981).

37. Tansey, M. G., Luby-Phelps, K., Kamm, K. E. & Stull, J. T. Ca^{2+}-dependent phosphorylation of myosin light chain kinase decreases the Ca^{2+} sensitivity of light chain phosphorylation within smooth muscle cells. *J. Biol. Chem.* **269,** 9912–9920 (1994).

CHAPTER 5 FINAL CONCLUSIONS & FUTURE WORK

The task of identifying and developing novel protein-protein interaction enhancers and K_{Ca} channel binding hits *de novo* was very large for one individual. Ultimately, progress was made in several approaches towards the project aim to identify a novel $IK_{Ca}3.1$ selective positive modulator.

5.1 Rational Design and Evaluation of Existing and Novel K_{Ca} Channel Modulators

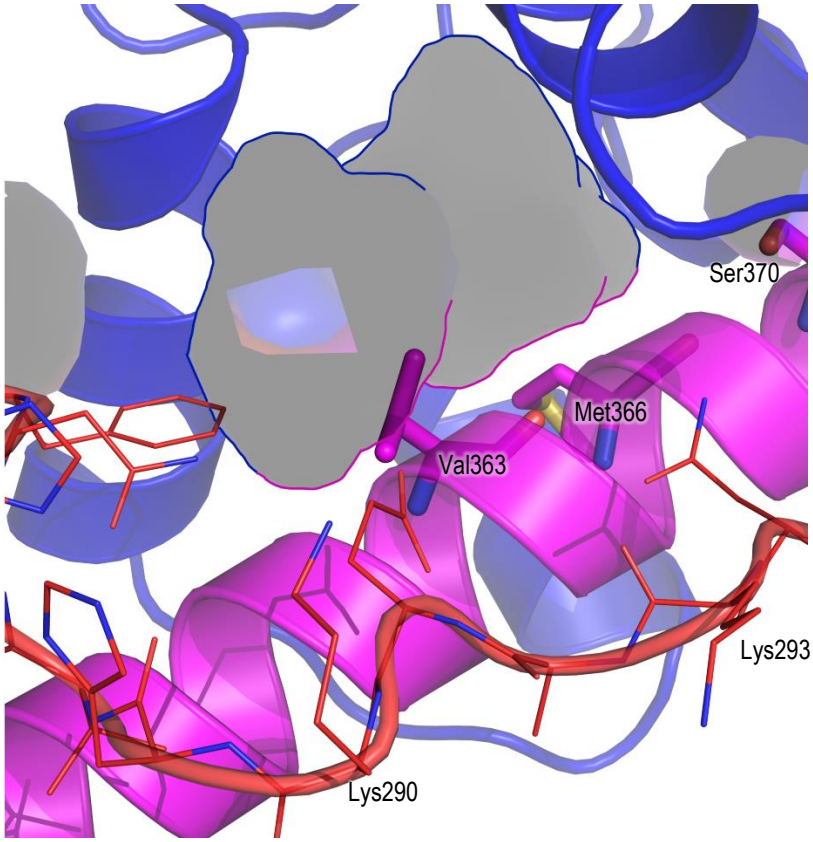


Figure 5.1; Internal surface of the $IK_{Ca}3.1$ homology model 2 modulator binding cavity, predicted from the NS309 $SK_{Ca}2.2$ co-crystal structure, PDB; 4J9Z. Structure of CaM presented in blue helices, and CaMBD-4 in pink helices. The binding cavity is shown in transparent grey and edge highlighted in pink and blue, highlighting the contribution of each constituent protein to the cavity. Important $IK_{Ca}3.1$ residues labelled and shown with sticks, coloured by element. The CaMBD loop region, provided by the NS309 $SK_{Ca}2.2$ co-crystal template, is shown in red with residues shown in lines and coloured by element.

The dynamic behaviour of a binding cavity, which can be split into two dissociable macromolecules, is not demonstrated in static crystallographic or model structures, Figure 5.1. The difference in the size and shape of the $IK_{Ca}3.1$ binding cavity between the two generated homology models or $SK_{Ca}2.2$ templates, demonstrated how variable ligand accommodation is. Without correctly modelling the dynamic movement of the protein backbones, which make up the K_{Ca} channel modulator binding cavity, it is difficult to predict what ligand sizes and shapes may or may not be accommodated or advantageous. The models were therefore hypothesised to be too static to accurately predict the affinity for, or effect of, small molecules docked with the K_{Ca} channel gating complex.

Protein crystals of the 2CaM:2CaMBD-4-H_6 tetramer remain desirable for selective modulator design, because homology model predictions do not include rigid water molecules. Waters are important in rational ligand design because they provide information about the ligand effect on any extended H-bonding network, related to the global protein structure. The H-bond network effect can be seen in the $SK_{Ca}2.2$ co-crystal structure with NS309 and has helped to explain the modulators mechanism of channel modulation, PDB: 4J9Z.[1] Ligand selectivity and potency can be gained by displacing target protein specific static waters *via* selective entropic gain.[2]

Lysine405 and lysine402 in the loop region, visible only in the NS309 stabilised $SK_{Ca}2.2$ co-crystal structure, have been proposed as a PIP_2 binding site, and associated with channel activation. In the second homology model, generated from the NS309 $SK_{Ca}2.2$ co-crystal structure, the residues, lysine290 and lysine293 represent the corresponding $IK_{Ca}3.1$ PIP_2 binding site, Figure 5.2.[3,4] Therefore, the second model represented an important predicted conformation of the target gating complex, not included in docking studies. The variability of the binding cavity could be

better modelled by combining the multiple $IK_{Ca}3.1$ models into an ensemble and docking potential ligands against this.[5] However, the few available crystal structures of the $SK_{Ca}2.2$ gating complex may not be enough to appreciate the full range of possible conformations. Instead, molecular dynamics may be the best way to understand how positive modulators effect gating complex association and quaternary structure. As determined at the beginning of this thesis, an in depth *in silico* investigation of this kind would require the focus of a dedicated research project.

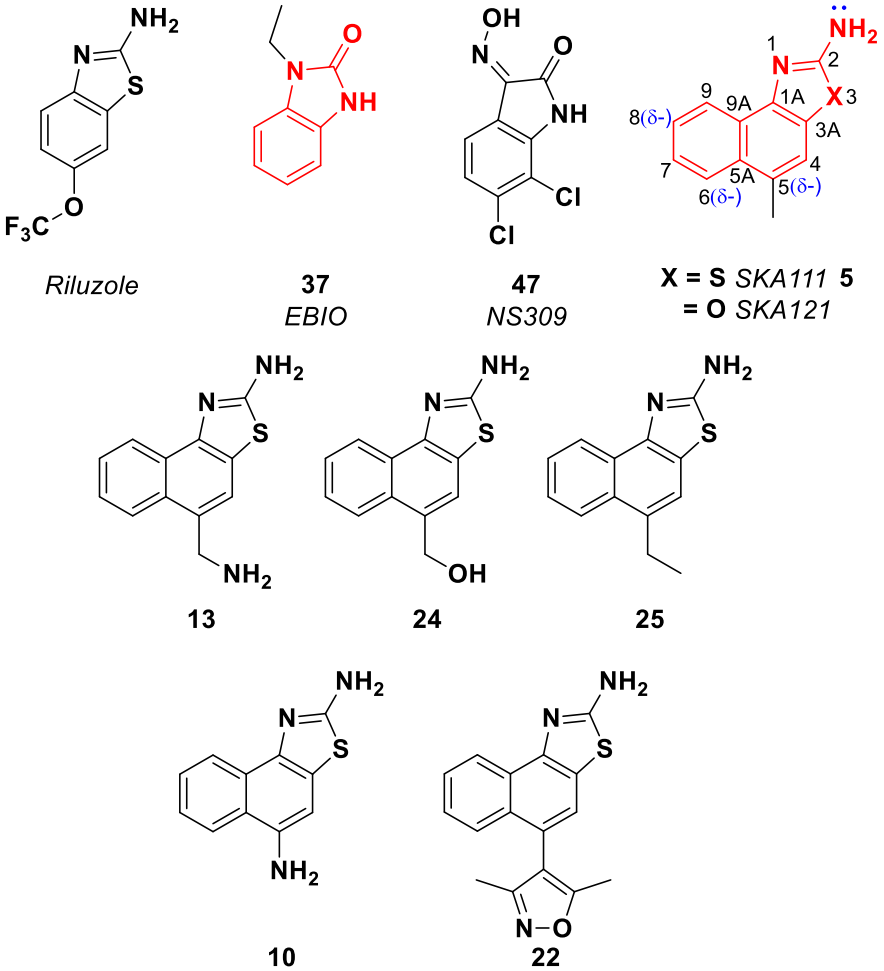


*Figure 5.2; Skeletal structures of the published K_{Ca} channel positive modulators and naphthothiazole analogues **10**, **13**, **22**, **24** and **25**. Red highlight indicates the benzimidazolone core (EBIO **37**) and naphthothiazole core (SKA111 **5**). Delta negative symbols indicate the increased electron density of the naphthothiazole ring positions, caused by 2-amino group lone pair delocalisation.*

The published investigations into riluzole's structure have already established SKA111 **5**, and the isoxazole isostere SKA121, as the most potent and $IK_{Ca}3.1$ selective core.[6,7] Both K_{Ca} channel modulator scaffolds, the benzimidazolones and the naphthothiazoles, are fragment-like heterocycles, Figure 5.2.[8] Simple molecular 'fragments' commonly interact with lots of proteins because they are small enough to fit into most protein cavities.[8–11] The published modulators' fragment qualities suggested that they would not be very selective for the K_{Ca} channel targets against unrelated cellular proteins. Thus, the current modulator failings, represent opportunities for rational improvement of K_{Ca} channel selectivity, by increasing the modulator size and specific target protein polar interactions.

SKA111 **5** was observed to easily cross the blood brain barrier (BBB) to concentrate in the central nervous system, where it may effect important neuronal functions of the SK_{Ca} channels.[12] The design of more polar SKA111 analogues which might interact with the $IK_{Ca}3.1$ modulator binding cavity residue, Ser370, would also prevent BBB passage and protect for neuronal side effects. Unfortunately, the electronic properties of the naphthothiazole core produced less solution stable polar analogues, Figure 5.2. The stability of both amine **13** and aniline **10** analogues in protic solvents, such as water, was poor. The instability was due to the lone pair donation of the 2-amino thiazole ring, which enabled the elimination or oxidation of susceptible basic 5-position substituted groups. It is likely that these degradation mechanisms would occur under assay conditions, giving false negative results, confusing the development of a modulator structure activity relationship. The less basic alcohol **24** was designed as a more stable H-bond capable alternative. Despite its greater solution stability, the lack of vasorelaxant effect of the alcohol **24** in isometric wire myography experiments went against the H-bonding hypothesis. However, it could not be determined if this result

was due to a lack of target engagement *via* non-binding or another unknown reason, such as poor cell permeability.

It is unlikely further derivatisation of the naphthothiazole core itself will generate more selectivity for the $IK_{Ca}3.1$ channel. Beyond Ser370, inspection of the $IK_{Ca}3.1$ binding cavity reveals no other polar residues for new specific interactions. There is also no more space to be filled as the shape complementarity of SKA111 **5** and the K_{Ca} modulator binding cavity is good, purportedly the reason for its current level of selectivity.[13]

Synthetically, the naphthalene and benzothiazole constituents of the naphthothiazole core both hinder or complicate many chemistries that might be used to obtain substituted core analogues, such as palladium catalysed reactions. Thus, generating a large number of further direct naphthothiazole analogues is challenging, which is not conducive to further exhaustive structure activity relationship studies. There exist no published reactions that directly substitute the aryl rings of the naphthothiazole core, all relying instead on the nucleophilicity of the nitrogen lone pair.

A potential direction of modulator expansion may instead be directed out of the binding pocket. Substitutions on the 2-amino group of SKA111 **5** have shown a lack of activity, potentially due to the loss of interaction with the anchor residue Met52.[12] However, expanding out of the small K_{Ca} channel modulator binding pocket would allow for new specific polar interactions with the hydrophilic residues of the loop region. Additionally, while there are no static water molecules within the K_{Ca} modulator binding cavity, there are outside of it, often associated with the loop region. The stabilisation of this loop region may help with channel activation, suggested by NS309 stabilised co-crystals. Specific interactions with $IK_{Ca}3.1$ residue mutations in the loop or associated stabilised waters may gain target selectivity. Synthetically, amide couplings

or reductive aminations with the thiazole 2-amino group are more tractable than ring substitutions and would enable the quick generation of a potentially large library of novel analogues.

Until a high throughput biophysical assay format is developed, any modulator analogue library would have to rely on the current cellular path clamp, or pharmacological wire myography assays. The naphthothiazole analogues were thus assessed by wire myography, all of which did not appear to effect endothelial K_{Ca} channels under Krebs solution conditions.

The wire myography observation of a K_{Ca} channel unrelated and novel vasorelaxant activity of **22**, **25** and **5** itself, may represent a new avenue of investigation for blood pressure reduction. As asserted above, it was predicted such small fragment-like molecules would display affinity for unintended protein partners.

The *in vivo* proteome interaction profile of a fragment molecule can be determined using a functionalised probe analogue containing both photoreactive and clickable chemical groups. Incubation of the fragment-probe molecule with cells followed by U.V. irradiation allows for the capture of all proteins that form reversible interactions with the fragment warhead. Linking the probe captured proteins to a fluorescent reporter molecule via 'click' reaction, followed by cells lysis and SDS-PAGE, demonstrates the fragment warhead's interaction profile.[9] Taking the same probe captured proteins and click linking them instead to a biotin tag allows for captured protein enrichment from cell lysates using streptavidin affinity chromatography. Digestion and MS/MS analysis of the enriched probe captured proteins can identify each protein which the fragment warhead interacts with.[14]

A control experiment using a blank probe containing a methyl group instead of the fragment under investigation, can be used to ensure fragment-probe capture of

proteins via U.V. irradiated linkage reflects the specific protein interaction of the fragment warhead. Incubating the blank probe with 'heavy' cells, grown on media containing C^{13} stable isotopically labelled amino acids (SILAC), in a paired control experiment enables later comparison of the blank-probe and fragment-probe protein interaction profiles. Combining the cell lysates of the control and test probe experiments allows simultaneous analysis of the proteins enriched by both probes. Finally, MS/MS analysis can distinguish between the 'heavy' and 'light' proteins corresponding to capture by the blank-probe and fragment-probe respectively. SILAC ratios of higher than 5:1 light:heavy enriched proteins confirms the fragment warhead dependant protein capture. This SILAC technique can positively identify all the proteins which the fragment of interest reversibly interacts with *in vivo*.[9,15] In the future, the protein(s) responsible for the novel naphthothiazole vasorelaxant effects could be determined using stable isotope labelling of amino acids in cell culture (SILAC) experiments.

The original MOPS buffered wire myography assay observed K_{Ca} channel modulation *via* acetylcholine (ACh) EC_{50} shift of resistance arteries, after incubation with modulator molecules. Under these published MOPS conditions, the published modulators, **5**, **7** and **4** were observed to modulate K_{Ca} channels *via* expected ACh EC_{50} shift. Concerns about observing K_{Ca} channel modulation by ACh EC_{50} shift lead to the use of an assay format observing a more direct activation of K_{Ca} channels to modulators and analogues, in Krebs solution. However, the apparent K_{Ca} channel modulating abilities of the published modulators assessed in the MOPS buffered assay, could be further validated with K_{Ca} channel blockade conditions. MOPS buffered control and modulated ACh EC_{50}s under $IK_{Ca}3.1$ and or $SK_{Ca}2.3$ blockade conditions could be compared. K_{Ca} channel modulation could be indicated if the

modulators abilities to shift ACh EC_{50}s under K_{Ca} channel blockade conditions are abolished. If ACh EC_{50} shifts to observe K_{Ca} channel modulation are validated, the naphthothiazole analogues could be assayed using the original format. These results would better compare the analogues to the published and observed activities of the known K_{Ca} positive modulators.

The naphthothiazole analogues could still be assayed using the conventional patch clamp assays to examine their K_{Ca} channel modulation potential in a simpler system. This was not done in part due to a lack of expertise and equipment, which would enable general screening of candidate K_{Ca} channel modulators. However, the few naphthothiazole analogues synthesised could be screened commercially.

5.2 Investigating the Biophysics of the K_{Ca} Channel Gating Complex

Whole cell assays ensure that drug molecules pass through cell membranes and survive the internal environment long to effect target proteins in the context of living systems. However, this complex set of conditions means that negative results may be caused by numerous non-target related issues, this was seen in the wire myograph results. Biophysical assays are simpler, involving only the protein(s) of interest in buffer, and only assessing ligand-target affinity. Thus, biophysical assays are easier to set up and run, and more suited to larger volume high throughput screening.[16]

The most promising biophysical assay technique developed for the analysis of K_{Ca} channel ligands was differential scanning fluorimetry, in which modulator molecules created a new peak, potentially indicating the stabilisation of the desired 2CaM:2CaMBD-4-H_6 tetramer. Future experiments observing how concentration gradients of the K_{Ca} channel modulators effects the presumed tetramer peak, could be used to confirm their specific binding. If the magnitude of the peak shift correlates to the concentrations of the proteins, their affinities (K_D) for the tetramers could also be

determined. Due to the composite signal of the proteins and their oligomeric states, a second unrelated biophysical technique is still required to confirm the analyses of the DSF data.

Redesigning the fluorescein labelled SKA111 probe with different linkage sites at other positions on the naphthothiazole core may provide probes retaining SKA111's 2CaM:2CaMBD tetramer complex affinity. A fluorescence polarisation assay would enable competition experiments displacing the probe with binding ligands. This assay format would strongly suggest the site-specific interaction of the identified binders.

If all SKA111 probe analogues containing linkages to a reporter tag such as fluorescein lose their affinity for the 2CaM:2CaMBD-H_6 tetramer complex, a radiolabelled analogue of SKA111 could be generated. Tritium (H^3) is an unstable isotope of hydrogen which emits observable radiation as it decays. Substituting one or more of SKA111's H^1 hydrogens for H^3 would eliminate the steric difference between labelled and unlabelled compound, retaining its target affinity. Immobilising the protein target allows for incubation with radiolabelled ligand followed by washing with unlabelled ligand. Observing a drop in radioactivity of nickel immobilised 2CaM:2CaMBD-H_6 incubated with the radiolabelled SKA111, corresponding to displacement of the radiolabelled SKA111 by a ligand in a competition assay, would also indicate site specific binding of the identified binder.

The closest second biophysical assay technique for observing 2CaM:2CaMBD-4-H_6 tetramerisation was native protein mass spectrometry. One experiment saw the increasing oligomerisation of the intended tetramer up to a 2CaM:CaMBD-2-H_6 trimeric state. Future focus on repeating this experiment and including the addition of the known K_{Ca} modulators like **5** or **47** may enable the first direct solution observed

stabilisation of the K_{Ca} gating complex by small molecules. This technique would thus confirm and validate the DSF assay results.

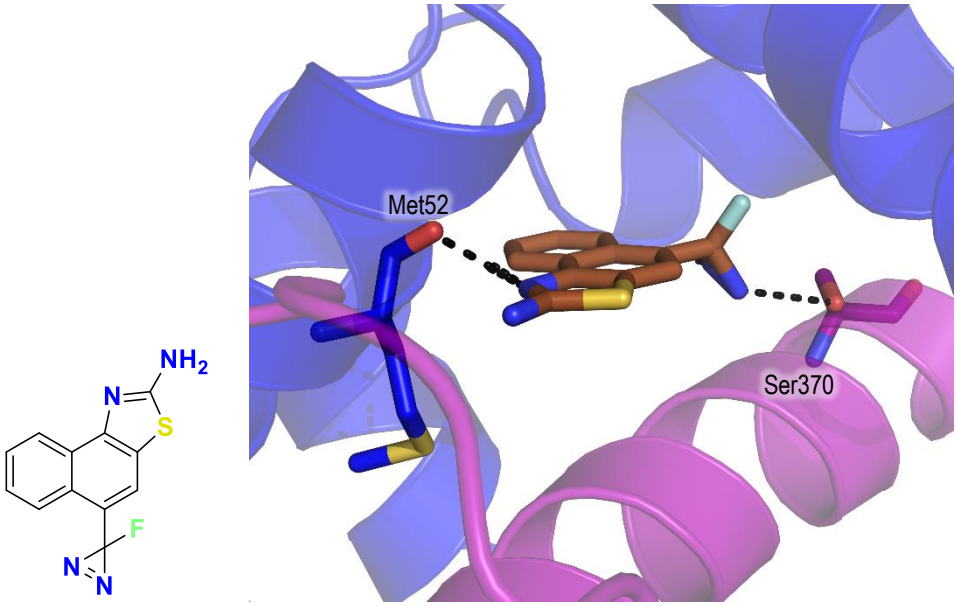


Figure 5.3; Docking of diazirine naphthothiazole analogue into IKCa3.1 homology model 1. Structure of CaM presented in blue helices, and CaMBD-4 in pink helices. Important IK_{Ca}3.1 residues labelled and shown with sticks, coloured by element. Docked diazirine pose shown in brown sticks with heteroatoms in elemental colours, polar contacts shown with black dashed lines, skeletal structure given.

No direct evidence has been generated which definitively proves naphthothiazole binding to the K_{Ca} gating complex. With the gating complex proteins for IK_{Ca}3.1 and SK_{Ca}2.2 available, a photo-crosslinking experiment could be designed. Diazirine may be a small enough functional group to be tolerated in the IK_{Ca}3.1 modulator binding cavity. A 5-position diazirine substituted naphthothiazole was docked to show that the photo-crosslinking group may potentially hydrogen bond to Ser370, giving a score of -32. Incubation of a diazirine containing naphthothiazole analogue with the IK_{Ca}3.1 gating complex, followed by irradiation with ultra-violet light could cause ligand-Ser370 cross linking. Analysis with protein mass spectrometry would confirm the covalent linkage to the expected residue and so prove the theoretical docking pose.[9,17]

A major limiting factor in all the biophysical work was the poor solubility of the CaMBD-H_6s. N-Terminal fusion with the common solubilising tags glutathione-S-transferase or maltose binding protein may improve the unsatisfactory solubility of the K_{Ca} CaMBD-H_6s.[18] All the biophysical techniques discussed above would be assisted by solubility enhanced CaMBD-H_6-fusions, including crystallisation and the ITC measurement of the tetramer PPIs and ligand interactions.

Although close, the major limiting experiment of this work remained in the development of a biophysical assay. With such an assay, the project could be driven forward with precise understanding of the effects of modulator structural changes on their affinity for the K_{Ca} gating complex. Results from a biophysical assay, assessed in conjunction with the aid of homology models, or potentially $IK_{Ca}3.1$ crystal structure, could reveal how these small molecules enable channel activation, leading to new designs for more effective ligands. Alternatively, the compiled affinity results of a library of naphthothiazole analogues could be used to create a quantitative structure activity model, with which more novel and improved analogues could be iteratively generated, without structural rational design necessary.[19,20]

Finally, a significant effort to develop a positive modulator of the $IK_{Ca}3.1$ channel has been made at several different research groups around the world.[1,6,21,22] A main aim of this compiled work has been to investigate $IK_{Ca}3.1$ as an antihypertensive pharmaceutical target, due to its significant role in vascular smooth muscle relaxation in resistance arteries. However, its presence in cardiac tissue has been largely ignored, yet its role in pacemaker tissue and cardiac rhythm makes this fact an important concern.[23] In animal experiments the published $IK_{Ca}3.1$ modulator SKA111 **5** produced an unexpected and strong effect, reducing heart rate (bradycardia), until loss of consciousness was observed.[12] The explanation of this side effect by the

authors was to highlight the high concentration of the modulator in the central nervous system, where $IK_{Ca}3.1$ is important in neuronal function in the brain. Dysfunction of neurones controlling heart rate may be the cause of SKA111's bradycardic effect, however, its altered function in pacemaker tissue may also be the cause. As well as this, the discovery of the K_{Ca} channel unrelated vasorelaxant mechanism of the naphthothiazole analogues and published modulator SKA111 **5** made in this project may also explain these side effects. Positive modulation of the $IK_{Ca}3.1$ channel may not be a useful mechanism of vasorelaxation, yet more research must be performed to confirm this caution.

Chapter 5 References

1. Zhang, M., Pascal, J. M. & Zhang, J.-F. Unstructured to structured transition of an intrinsically disordered protein peptide in coupling Ca^{2+}-sensing and SK channel activation. *Proc. Natl. Acad. Sci. U. S. A.* **110,** 4828–33 (2013).
2. Spyrakis, F. *et al.* The roles of water in the protein matrix: a largely untapped resource for drug discovery. *J. Med. Chem.* **60,** 6781–6828 (2017).
3. Zhang, M. *et al.* Selective phosphorylation modulates the PIP2 sensitivity of the CaM-SK channel complex. *Nat Chem Biol* **10,** 753–759 (2014).
4. Zhang, M., Meng, X.-Y., Zhang, J.-F., Cui, M. & Logothetis, D. E. Molecular overlap in the regulation of SK channels by small molecules and phosphoinositides. *Sci. Adv.* **1,** e1500008 (2015).
5. Huang, S.-Y. & Zou, X. Ensemble docking of multiple protein structures: considering protein structural variations in molecular docking. *Proteins* **66,** 399–421 (2007).
6. Sankaranarayanan, A. *et al.* Naphtho[1,2-d]thiazol-2-ylamine (SKA-31), a new activator of KCa2 and KCa3.1 potassium channels, potentiates the endothelium-derived hyperpolarizing factor response and lowers blood pressure. *Mol. Pharmacol.* **75,** 281–95 (2009).
7. Coleman, H. A., Tare, M. & Parkington, H. C. Nonlinear effects of potassium channel blockers on endothelium-dependent hyperpolarization. *Acta Physiol.* **219,** 324–334 (2017).
8. Congreve, M., Carr, R., Murray, C. & Jhoti, H. A 'Rule of Three' for fragment-based lead discovery? *Drug Discov. Today* **8,** 876–877 (2003).
9. Parker, C. G. *et al.* Ligand and target discovery by fragment-based screening in human cells. *Cell* **168,** 1–15 (2017).
10. Brough, P. a. *et al.* Combining hit identification strategies: Fragment-based and in silico approaches to orally active 2-aminothieno[2,3-d]pyrimidine inhibitors of the Hsp90 molecular chaperone. *J. Med. Chem.* **52,** 4794–4809 (2009).
11. Taylor, A. M. *et al.* Fragment-based discovery of a selective and cell-active benzodiazepinone CBP/EP300 bromodomain inhibitor (CPI-637). *ACS Med. Chem. Lett.* **7,** 531–536 (2016).
12. Coleman, N. *et al.* New positive Ca2+ -activated K+ channel gating modulators with selectivity for KCa3.1. *Mol. Pharmacol.* **86,** 342–357 (2014).
13. Brown, B. M., Shim, H., Yarov-Yarovoy, V. & Wulff, H. Structural determinants for selectivity of the positive KCa channel gating modulator, SKA-121. *Biophys. J.* **110,** 114a (2016).
14. Hulce, J. J., Cognetta, A. B., Niphakis, M. J., Tully, S. E. & Cravatt, B. F. Proteome-wide mapping of cholesterol-interacting proteins in mammalian cells. *Nat. Methods* **10,** 259–264 (2013).
15. Niphakis, M. J. *et al.* A Global Map of Lipid-Binding Proteins and Their Ligandability in Cells. *Cell* **161,** 1668–1680 (2015).
16. Cronk, D. High-Throughput Screening. in *Drug Discovery and Development: Technology in Transition* (eds. Hill, R. & Rang, H.) 95–118 (Churchill Livingstone, 2012).
17. Sinz, A. Chemical cross-linking and mass spectrometry to map three-dimensional protein structures and protein-protein interactions. *Mass Spectrom. Rev.* **25,** 663–682 (2006).
18. Hammarström, M., Woestenenk, E. A., Hellgren, N., Härd, T. & Berglund, H. Effect of N-terminal solubility enhancing fusion proteins on yield of purified target protein. *J. Struct. Funct. Genomics* **7,** 1–14 (2006).
19. Karelson, M., Lobanov, V. S. & Katritzky, A. R. Quantum-chemical descriptors in QSAR/QSPR studies. *Chem. Rev.* **96,** 1027–1044 (1996).

20. Tropsha, A. Best practices for QSAR model development, validation, and exploitation. *Mol. Inform.* **29,** 476–488 (2010).
21. Singh, S., Syme, C. a, Singh, a K., Devor, D. C. & Bridges, R. J. Benzimidazolone activators of chloride secretion: potential therapeutics for cystic fibrosis and chronic obstructive pulmonary disease. *J.Pharmacol.Exp.Ther.* **296,** 600–611 (2001).
22. Brown, B. M., Shim, H., Zhang, M., Yarov-Yarovoy, V. & Wulff, H. Structural determinants for the selectivity of the positive KCa3.1 gating modulator 5-methylnaphtho[2,1-d]oxazol-2-amine (SKA-121). *Mol Pharmacol* **92,** 469–480 (2017).
23. Weisbrod, D. *et al.* SK4 Ca2+ activated K+ channel is a critical player in cardiac pacemaker derived from human embryonic stem cells. *Proc. Natl. Acad. Sci.* **110,** E1685–E1694 (2013).

Chapter 6 Experimental Section

6.1 Computational Modelling and Docking Details

6.1.1 Molecular Homology Modelling

The Co-crystal structures of the $SK_{Ca}2.2$ gating complex (PDB: 4G28 and 4J9Z) are the closest possible known homologous structures to the $IK_{Ca}3.1$ gating complex target. These crystal structures were used as the templates for producing the target homology models without further template searches being conducted.[1]

The DELTA-BLAST of $SK_{Ca}2.2$ and $IK_{Ca}3.1$ CaMBDs showed 52% sequence identity, which was taken to be close enough as a template to produce plausible homology models.[2,3] The $SK_{Ca}2.2$ co-crystal structures of 2CaM:2CaMBD-2, complexed with EBIO (PDB ID: 4G28) and NS309 (PDB ID: 4J9Z), were prepared as templates by removing all molecules other than the chains of 1 CaM and 1 CaMBD-2.

The target primary sequences of $IK_{Ca}3.1$ CaMBD-4, *Homo sapiens,* and CaM, *Homo sapiens*, were simultaneously fitted, *via* sequence threading, to each of the prepared $SK_{Ca}2.2$ crystal structures, using the freeware DeepView v4.1 (ExPASy, Swiss Institute of Bioinformatics). The resulting aligned fits were generated to agree with the DELTA-BLAST results obtained previously. The DeepView $IK_{Ca}3.1$ fits were submitted to the online modelling server SWISS-MODEL (ExPASy, Swiss Institute of Bioinformatics) (http://swissmodel.expasy.org/), rewarding the $IK_{Ca}3.1$ homology models, each based on one modulator $SK_{Ca}2.2$ co-crystal.

As a means of model validation, the architectural similarity of the homology models to their known real template structures was assessed by root mean square deviation (RSMD). The RMSD of all the homology model protein chain backbones, in PyMOL v1.7.6.3 (Schrödinger LLC.), were found to be closely fitted to the originating $SK_{Ca}2.2$

crystal structures: PHU = 0.071, EBIO = 0.124 and NS309 = 0.072. Secondly, the dihedral φ (phi) and ψ (psi) protein backbone angles of the proposed target homology models was assessed by Ramachandran plots. The Ramachandran plots of each $IK_{Ca}3.1$ homology model was generated by the freeware UCSF Chimera 1.11rc (UCSF RBVI), see Chapter 2.1.2.

6.1.2 Docking Assessment

The following protocol was adopted for docking to the $IK_{Ca}3.1$ homology models and validation by docking to $SK_{Ca}2.2$ template co-crystal structures.

The target $IK_{Ca}3.1$ homology models and $SK_{Ca}2.2$ template co-crystal structures were prepared for docking using the DockPrep tool in UCSF Chimera. Incomplete sidechains were replaced using the Dunbrack rotamer library. Protons were added to sidechains based on physiological conditions. Charges were assigned to sidechains using AMBER ff14SB force field. Ligand structures were generated in ChemBioOffice Ultra v15.1**.** [4–7]

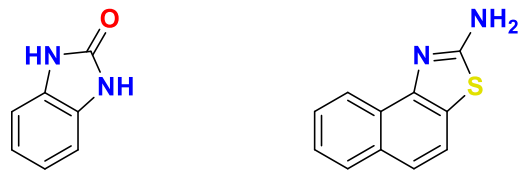
The homology models, co-crystals and ligands, were docked twice in a side by side comparison using two docking software programs: the online docking server SWISS-DOCK (ExPASy, Swiss Institute of Bioinformatics) and the commercial docking software CLC-DrugDiscovery Workbench 3 (Qiagen).

The prepared structures were submitted to SWISS-DOCK. The original crystal ligands, PHU, EBIO and NS309, were docked to each template $SK_{Ca}2.2$ crystal structure and each target $IK_{Ca}3.1$ homology model. For the validation of the SWISS-DOCK docking, the closest iteration to the original ligand crystal positions of each returned result was assessed in PyMOL by RMSD.

The prepared structures were imported into the commercial software CLC-DrugDiscovery Workbench 3 (Qiagen). The binding region was identified as a 13 Å sphere around the corresponding known $SK_{Ca}2.2$ co-crystal ligand positions: this

encompassed both CaM and CaMBD-2/4 chains at the PPI interface, see Chapter 2.1.2. Each ligand was docked into each protein structure binding region, the results of were compared to the original ligand crystal positions in PyMOL by RMSD.

6.1.3 Dock Screening



Benzimidazolone core *Naphthothiazole core*

Figure 6.1; Known K_{Ca} channel modulator small molecule cores.

Published analogues of the benzimidazolone and naphthothiazole modulator cores were screened, *via* docking against the $IK_{Ca}3.1$ homology models with CLC-Drug Discovery, using the default settings with 500 iterations per molecule, Figure 6.1.[8] The ligands were converted to give an initial 3D structure in CLC-Drug Discovery, using the Balloon algorithm add-on (http://users.abo.fi/mivainio/balloon/news.htm).[9]

6.1.4 Rational Ligand Design

The binding region of the $IK_{Ca}3.1$ homology model, overlaid with the corresponding $SK_{Ca}2.2$ EBIO co-crystal structure, was visually inspected in CLC-Drug Discovery. The differences identified the substitution of Ala487Ser in the target $IK_{Ca}3.1$ model. Using the CLC-Drug Discovery Ligand Optimisation tool, analogues of the benzimidazolone and naphthothiazole cores were rationally designed to introduce new potential hydrogen bonding interactions to Ser487, see Chapter 2.2.2. Designed novel ligand analogues were re-docked, and compared with published benzimidazolone and naphthothiazole analogues, *via* their binding ranking based on their predicted

CLC-Drug Discovery docking scores. The docking results of the novel ligands informed subsequent synthetic targets.

6.2 Experimental Biochemistry Details

Glycerol and NaCl were bought from Thermo Fisher Scientific Inc. All other chemicals were purchased from Sigma-Aldrich Co. unless otherwise specified. All the buffers, used in the purification procedures and biophysical assays, were pre-filtered through 0.2 μm pore size filter papers (Sartorius UK Ltd.) under vacuum, to remove insoluble precipitates.

6.2.1 Molecular Cloning

The protein primary sequence of the literature reported $SK_{Ca}2.2$ calmodulin binding domain (CaMBD-2) was reverse translated in CLC-Main Workbench 7 (Qiagen), giving the predicted DNA sequence of the gene, *cambd-2*. The *cambd-2* gene fused to that of calmodulin (*cam*) *via* a spacer sequence, including cap sequences, was designed (*cam/cambd*-2). The cap sequences were designed with complementarity to the vector plasmid pNIC28-Bsa4 (Opher Gileadi), enabling Gibson assembly of novel plasmid constructs.

The protein primary sequence of the $IK_{Ca}3.1$ CaMBD-4, *Homo sapiens,* was identified by alignment of the known $SK_{Ca}2.2$ CaMBD-2, *Rattus norvegicus*, primary sequence against the National Centre for Biotechnology Information (NCBI) database of non-redundant protein sequences. Alignment was conducted using the domain enhanced lookup time accelerated – basic local alignment search tool (DELTA-BLAST) with an initiating word size of 3, the BLOSUM62 Matrix and composition-based statistics adjustments (http://blast.ncbi.nlm.nih.gov/Blast.cgi?PAGE=Proteins).

The predicted *cambd-4* genetic sequence was also reverse translated from the identified CaMBD-4 protein sequence. The *cambd-4* gene was designed with cap sequences identical to the *cambd-2* cap and spacer sequences. Both *camb-2* and *cambd-4* genes included terminal codon sequences corresponding to 5′ fused poly histidine tagged protein products, with 3′ methionine start codons. The synthetic gene fragments and primers for sequencing and cloning thereof were optimised for expression in *E. coli.* The genes for *cambd-4*, *cam/cambd-2* were synthesised commercially by GeneArt® Gene Synthesis (Thermo Fisher Scientific Inc).

The synthetic gene fragments were amplified by PCR, applying Q5® High-Fidelity DNA Polymerase (New England Biolabs Inc.) with the primers in Table 6.1, producing the gene fragments *cambd-2*, *cam*, *cam/cambd-2*. A set of mutational PCR reactions was used to create and amplify the hybrid gene fragment *cam/cambd-4,* employing the additional primers in Table 6.2. The first PCR reaction amplified only the *cam* gene of the synthetic *cam/cambd-2* fragment, producing a modified *cam*-tail (489 bp) product, by applying primers *cam_f* and *cambd-4_f2r*. The second PCR reaction amplified the synthetic *cambd-4* fragment, yielding a modified *cambd-4*-tail (343 bp) product, by applying primers *cambd-4_f2* and *cambd_r*. Finally, the third PCR reaction united the two complementary tails of the modified PCR reaction 1 and 2 products, amplifying the target fused *cam/cambd-4* (810 bp) product, using the primers *cam_f* and *cambd_r* with both *cam*-tail and *cambd-4*-tail templates.

Table 6.1; PCR Primer Sequences for cam, cambd-2 and cam/cambd-2 Amplification.[1] Regions for initial annealing to DNA templates are underlined.[2] Melting temperatures (Tm) are predicted by NEB Tm Calculator (http://tmcalculator.neb.com) for use with Q5 High-Fidelity DNA Polymerase.[3] Comercial DNA sequencing primers are available at Source BioScience (http://www.sourcebioscience.com).

Sequencing Primer	**Orientation**	**Sequence (5' to 3') [1]**	**Tm (°C) [2]**
T7F [3]	Forward	TAATACGACTCACTATAGGG	55
T7R [3]	Reverse	GCTAGTTATTGCTCAGCGG	61
cam_f	Forward	TTAACTTTAAGAAGGAGATATACATATG	56
cam_r	Reverse	CGGAGCTCGAATTCGGATCCTTATCATTTGGCGGTCATC	57
cambd-2_f	Forward	TTAACTTTAAGAAGGAGATATACATATGGGTCGTAAACTGGA	57
cambd-2_r	Reverse	CGGAGCTCGAATTCG	57

Table 6.2; Additional PCR Primers for cam-4 and cam/cambd-4 Mutagenesis and Amplifiation.[1] Regions for initial annealing to DNA templates are underlined.[2] Melting temperatures (Tm) are predicted by NEB Tm Calculator (http://tmcalculator.neb.com) for use with Q5 High-Fidelity DNA Polymerase.

Sequencing Primer	**Orientation**	**Sequence (5' to 3') [1]**	**Tm (°C) [2]**
cambd-4_f2r	Reverse	GTCTGTTTCCTTTATCATTTGG	59
cambd-4_f2	Forward	CCAAATGATAAAGGAAACAGAC	59

The plasmid vector pNIC28-Bsa4 was linearised *via* restriction with *Bam*H1 and *Nde*1 nucleases, in CutSmart™ buffer (New England Biolabs Inc.), incubated at 37 °C for 2 h

and purified by 1% agarose electrophoresis (100 V, 0.5 h), in TAE Buffer [Tris (30 mM), acetic acid (0.1% *v/v*), (ethylenedinitrilo)tetraacetic acid (EDTA) (1 mM)]. The linear pNIC28-Bsa4 large fragment product (5.3 Kb) was recombined with each of the gene fragments; *cambd-4, cambd-2, cam, cam/cambd-4* or *cam/cambd-2, via* Gibson assembly procedure, using NEBuilder® HiFi DNA Assembly Cloning Kit (New England Biolabs Inc.), creating five new plasmid constructs; pCaMBD-4-H_6, pCaMBD-2-H_6, pCaM, pCaM/CaMBD-4-H_6 and pCaM/CaMBD-2-H_6. The raw Gibson assembly reaction mixtures, for each plasmid construct, were separately transformed *via* heat shock procedure into individual chemically competent samples of the amplification host *E. coli* strain NEB5α.[10] The NEB5α samples were spread on 2× TY media (Oxoid™ Tryptone (Thermo Fisher Scientific Inc.) (16 g/L), Oxoid™ Yeast Extract (Thermo Fisher Scientific Inc.) (10 g/L), NaCl (5 g/L), kanamycin (100 µg/mL)), 1.5% bacto agar plates incubated at 37 °C for 15 h. Transformants were selected for *via* plasmid conferred kanamycin resistance, colonies were picked and incubated at 37 °C in 10 mL 2× TY liquid cultures. The plasmid DNA was extracted from the NEB5α cultures *via* GeneJET Plasmid miniprep kit (Thermo Fisher Scientific Inc.) following the manufacturer's instructions. The plasmid DNA was sequenced by Source BioScience services, employing the commercial primers in Table 6.1 to ensure the correct base sequence and subsequent protein expression. Recombinant plasmid DNA was linearised by restriction with *BamH*1 and *Nde*1 nucleases and assessed by 1% agarose gel electrophoresis. Insert genes; *cambd-4* (343 bp), *cambd-2* (357 bp), *cam* (498 bp) *cam/cambd-4* (810 bp), *cam/cambd-2* (822 bp) and linearised vector plasmid (5,272 bp) bands were identified by expected size migration. The excised insert gene of each construct plasmid was extracted *via* GeneJET gel extraction kits (Thermo Fisher Scientific Inc.).

The prepared pDNA of the construct plasmids was used to transform the expression host *E. coli* strain BL21(DE3) *via* heatshock procedure. Samples of each construct transformed cells were spread on 2× TY, 1.5% bacto agar, 50 µg/L kanamycin plates incubated at 37 °C for 15 h.

6.2.2 Protein Expression

Protein expression was achieved in host BL21(DE3), transformed with one of the previously prepared plasmid constructs; pCaMBD-4-(H_6), pCaMBD-2-(H_6), pCaM, pCaM/CaMBD-4-(H_6) or pCaM/CaMBD-2-(H_6). Resultant kanamycin resistant transformants were aerobically cultured as 1 L batch cultures in 2.5 L Tunair™ shake flasks (Sigma Aldrich Co.) of 2× TY medium at 37 °C with an agitation speed of 180 r.p.m., in the presence of 100 µg/L of kanamycin (Apollo Scientific Ltd.). Induction of gene transcription was achieved with the chemical inducer, isopropyl β-D-1-thiogalactopyranoside (IPTG) (Apollo Scientific Ltd.), (0.1 ngL^{-1}) once bacterial culture optical density reached 0.700 (600 nm) and were further incubated at 16 °C for 20 h. Cells were harvested by centrifugation (Rotor: F10BCI-6x500y, Avanti™ J-25 Centrifuge, Beckman Coulter Inc) at 11,305 × g, 4 °C and stored at –80 °C until purification.

6.2.3 Protein Purification

Prior to protein purification, frozen cell pellets were first thawed and resuspended in Extraction Buffer (1 Sigma*FAST* Protease Inhibitor Cocktail tablet (EDTA Free) in 100 mL of Binding Buffer) (100 mL / 20 g cellpellet). The cells were lysed by sonication (50% amplitude, 5 s pulse interrupted by 5 s pauses for 60 cycles; Ultrasonic Processor, Sonics & Materials, Inc.) at 4 °C to release cytosolic proteins. Digestion and removal of DNA from cell lysates was facilitated by addition of benzonase nuclease (10 U) (Merck

Millipore Corp.). Precipitation of residual DNA was facilitated with addition of polyethylenimine (15% *v/v*), incubated at 4 °C for 0.5 h. Insoluble cell contents were removed by centrifugation (Rotor: JA25.50, Avanti™ J-25 Centrifuge, Beckman Coulter Inc) at 25,000 ×g, 4 °C for 0.25 h. Lysate supernatants were clarified with 0.45 µm pore size syringe filters (Merck Millipore Corp.), further diluted to 100 mL with Extraction Buffer, supplemented with 20 mM imidazole and 10 mM β-mercaptoethanol (Bio-Rad Laboratories, Inc).

Poly histidine tagged proteins and protein complexes were isolated *via* immobilised ion affinity chromatography (IMAC) at a constant flow rate of 1 mL/min. Prepared 100 mL cell lysates of containing either CaMBD-4-H_6, CaMBD-2-H_6, CaM:CaMBD-4-H_6 or CaM:CaMBD-2-H_6, were loaded onto Ni^{2+} charged HisTrap HP 5 mL columns (GE Healthcare), pre-equilibrated with 10 column volumes (CV) of IMAC Binding Buffer (HEPES (50 mM), NaCl (500 mM), glycerol (10%), pH 7.5) and connected to an automated ÄKTA FPLC system (GE Healthcare). Increasing isocratic gradient steps (10 CV) of IMAC Binding Buffer and IMAC Elution Buffer (HEPES (50 mM), NaCl (500 mM), imidazole (500 mM), glycerol (10%), pH 7.5) were applied mixed in different ratios. 12% and 16% IMAC Elution Buffer washing steps removed bound non-target proteins. Pure target polyhistidine-tagged proteins; CaMBD-4-H_6 or CaMBD-2-H_6, with and without associated co-expressed CaM, were eluted with 60% IMAC Elution Buffer.

Untagged CaM was isolated *via* Ca^{2+} induced hydrophobic interaction chromatography (HIC) with a flow of 1 mL/min. Using a syringe pump, prepared 100 mL CaM lysates were loaded onto a HiTrap Phenyl(LS) 5-mL column (GE Healthcare) at room temperature pre-equilibrated with HIC Buffer I (Tris (50 mM), β-ME (10 mM), $CaCl_2$ (0.1 mM), pH 7.6) (10 CV). The column was washed with HIC Buffer I (10 CV) then HIC Buffer II (Tris (50 mM), β-ME (10 mM), $CaCl_2$ (0.1 mM), NaCl (500 mM), pH

7.6) (10 CV). The target CaM protein was eluted with HIC Buffer III (Tris (50 mM), β-ME (10 mM), Ethylene glycol-bis(2-aminoethylether)-*N,N,N′,N′*-tetraacetic acid (EGTA) (1 mM), pH 7.6) (10 CV).

All IMAC or HIC isolated proteins were further purified by size exclusion chromatography (SEC) operated at a constant flow rate of 1 mL/min over 150 mL of a total flow volume. Purified protein target containing fractions from IMAC or HIC procedures were combined into single protein samples, respectively, and concentrated with 5 or 10 mL Vivaspin™ sample concentrators (3,000 and 10,000 MWCO) (GE Healthcare) before they were loaded separately onto gel filtration columns XK 16/70 (GE Healthcare) packed with 120 mL of Superdex 75 resin (GE Healthcare) pre-equilibrated with 150 mL degassed SEC Buffer (HEPES (50 mM), NaCl (500 mM) pH 7.5). The SEC purified protein containing fractions were concentrated by 10 mL Vivaspin sample concentrators and their final concentrations estimated with a NanoDrop 1000 spectrophotometer (Thermo Fisher Scientific Inc.) with the respective ExPASy ProtParam tool calculated 280 nm extinction coefficients (https://web.expasy.org/cgi-bin/protparam/protparam).

During all methods concerning the purification of isolated CaMBD-4-H_6 or CaMBD-2-H_6, all buffers were supplemented with the detergent sarkosyl (0.2%, sodium lauroyl sarcosinate), improving the stability of the peptide and ensuring as little aggregation as possible, during purification.

6.2.4 Protein Characterisation

Identity and purity of the proteins was assessed by sodium dodecyl sulphate polyacrylamide gel electrophoresis (SDS-PAGE). The SDS-PAGE experiments were conducted using self-made 16% acrylamide gels with Tris based buffers. The gels were loaded with 20 µL aliquots of previously prepared protein samples. Protein samples

were prepared with Laemmli buffer and β-ME, the mixtures boiled for 10 min prior to use. Gels were run in SDS-PAGE Buffer (Tris (200 mM), glycine (1.9 M), SDS (35 mM)) for 1 hour at 200 V and visualised with coomassie blue stain. Proteins were identified *via* their expected migration distances in reference to a colour pre-stained protein standard broad range (11 – 245 KDa) (New England Biolabs Inc.); CaMBD-4-H_6 (11,940 Da), CaMBD-2-H_6 (12,079 Da), CaM (16,706 Da). Proteins were additionally characterised by protein mass spectrometry (Waters LCT Premier/XE, ProwSwift™ RP-4H 50×1 mM column Thermo Fisher Scientific Inc.) to ensure their correct precise primary sequences.

The dimerisation and Ca^{2+} induced αβαβ tetramerisation of CaM with either CaMBD-4-H_6 or CaMBD-2-H_6 was characterised *via* a size exclusion chromatography coupled multi angle light scattering detector (SEC-MALS). Co-purified CaM:CaMBD-4-H_6 or CaM:CaMBD-2-H_6 complex samples were submitted in ranges of concentrations 10, 8, 6, 3, 2, 1, 0.5, 0.25, 0.125 mg/mL to the University of Oxford Department of Biochemistry biophysics suite and run on Superdex 200, Superose 6 analytical column with a Shimadzu chromatography system connected to Wyatt Heleos8+ and T-rEX detectors. Samples were diluted with and run in SEC Buffer containing additional $CaCl_2$ (10 μM) when observing tetrameric states. Proteins and complexes were determined *via* their calculated molecular weights from their observed hydroscopic radii. Native protein mass spectrometry was additionally used to observe dimer and tetramer complex formations in collaboration with Shane Chandler of the Benesch group, University of Oxford.

6.2.5 Differential Scanning Fluorimetry (DSF)

General: DSF experiments and analyses were performed following the protocols described by Niesen *et al*.[11] Investigations into the viability of DSF screening as a high

throughput platform for small molecule binding to CaMBD-4-H_6, CaMBD-2-H_6, CaM, and their respective dimeric and tetrameric forms were conducted using a Stratagene M×3005P real time PCR machine (Sybr filter, ex. 465 nm, em. 590 nm) (Agilent), 96-well PCR plates (Axygen) and the commercial fluorescent dye SYPRO® Orange (Invitrogen, CA). Experiments ranged from an initial temperature of 25 °C increasing to 85 °C by 1 °C /30 s^{-1} and fluorescence readings were recorded at each interval. Stock solutions of ligands under examination were prepared in DMSO (200 mM) and diluted with DSF Buffer (SYPRO orange (5×),Tris (50 mM), NaCl (50 mM), (±) $CaCl_2$ (10 mM), pH 7.5) to test concentrations. Test protein samples were diluted to test concentrations with DSF Buffer. Samples of purified individual and co-purified proteins were diluted with DSF buffer to test concentrations. Experiment 96-well plates were prepared with the appropriate protein samples (45 µL) and test ligands (5 µL) then centrifuged for 2 min, 1000 rpm at 25 °C before measurement. Negative controls replaced test ligand with either DMSO or DSF Buffer as control (5 µL).

Assay Optimisation and Control Experiments: Several variables were assessed for optimal intensity and stability of fluorescence employing the CaM:CaMBD-2-H_6 dimer as a protein standard. Buffers (50 mM); Tris, HEPES, Tricine and MOPS, the effect of pH; 7.0 and 7.5, sodium chloride concentration; 50, 100 and 150 mM, protein concentration 5, 10 and 20 µM and dye concentration 1×, 5× and 10× were assessed. Addition of 0.2% sarkosyl in combination with CaMBD-2-H_6 and CaMBD-4-H_6 (10 µM) was investigated. Addition of $CaCl_2$ (10 µM) was used to observe possible tetramerisation of 2CaM:2CaMBD-2-H_6 and 2CaM:2CaMBD-4-H_6.

Towards DSF Assay: Initial binding viability screening was conducted investigating the effects of saturating concentrations of synthesized positive control modulators; EBIO, DCEBIO, NS309, SKA111 and SKA113 on CaMBD-4-H_6, CaMBD-2-H_6, CaM,

individually and in dimeric and tetrameric forms. The known drugs hydralazine and riluzole as well as several small molecule fragments (1 mm) were also screened; benzo[*d*]oxazol-2-amine, benzo[*d*]thiazol-2(3H)-one, 1-methyl-1H-benzo[*d*]imidazol-2-amine, against the dimeric and tetrameric forms of CaM:CaMBD-2-H_6 and CaM:CaMBD-4-(H_6). These experiments were performed in DSF Buffer in the presence and absence of Ca^{2+} (2 mM).

6.2.6 Isothermal Titration Calorimetry (ITC)

General: ITC experiments were conducted using a MicroCal Auto-iTC200 (Malvern) and analysed with the MicroCal PEAQ-ITC Analysis software (Malvern, 1.1.0.1262) applying a single set of binding sites model. Machine settings were as follows; cell volume of 420 µL, syring volume of 150 µL, stir speed was 750 rpm, 19 ×4 µL injections (initial injection 0.4 µL) with durations of 0.8 s and 150 s spacings. The initial data point was excluded from analysis. Test samples were prepared in Nunc™ 96-well PP DeepWell™ plates (Thermo Fisher Scientific Inc.) kept in a storage tray at 4 °C.

Calmodulin Control Experiment: samples of CaM (50 µL) were buffer exchanged into ITC Buffer (HEPES (20 mM), NaCl (100 mM), (±) $CaCl_2$ (10 mM), pH 7.5) without $CaCl_2$ with PD SpinTrap G-25 column (GE Healthcare) following the manufacture's instructions, then diluted to 20 µM with the same buffer. The titration of $CaCl_2$ (550 µM) in ITC Buffer to CaM or ITC Buffer without $CaCl_2$ (250 µL) was then observed at 20 °C.

Tetramerisation Control Experiments: samples (100 µL) of isolated CaMBD-4-(H_6), CaMBD-2-(H_6) and CaM were exchanged into ITC buffer *via* Slide-A-Lyzer® Mini dialysis units (0.5 mL, 2000 MWCO) (Thermo Fisher Scientific Inc.) or PD SpinTrap G-25 column, CaM was diluted to 90 µM, CaMBD-4-(H_6) and CaMBD-2-(H_6) were diluted to 10 µM. The titration of CaM to either CaMBD-4-(H_6), CaMBD-2-(H_6) or ITC buffer (250 µL) was observed at, 15, 20 and 25 °C.

6.2.7 Fluorescence Polarisation (FP)

General: test samples were dispensed onto a black 384-well non-binding microplate (Corning Inc.) and incubated for 0.5 h before fluorescence polarisation (P) being measured by a PheraStar FS microplate reader (BMG Labtech Ltd.). The following machine experiment settings were used; excitation filter – FP 485 nm, emission filters 1 – FP p-pol 520 nm, 2 – FP s-pol 520 nm. Values of P were determined by Equation 6.1.

$$P = \frac{(I_s - G \times I_p)}{(I_s + G \times I_p)} \times 1000\ (mP) \qquad \textit{Equation 6.1}$$

Where the blank corrected fluorescence intensity measured in the s-plane is I_s and I_p in the p-plane. G is the instrument specific grating factor. Recorded P data was analysed with Excell Software (Microsoft Corp.).

Towards Assay Development: The synthesised FP probe **33**, see Chapter 2.2.2, was serially diluted from a DMSO stock (1 mM) into FP Buffer (HEPES (25 mM), NaCl (100 mM), bovine serum albumin (1 mg/mL), $CaCl_2$ (10 mM), 0.05% CHAPS, pH 7.5): 10, 1.25 µM, 640, 320, 160, 80, 40, 20, 10, 5, 2.5, 1.25 nM, 625, 314, 156, 40, 20 pM. The fluorescent intensities of the FP Buffer dilutions (20 µL test volume) were recorded to obtain the most stable concentration. Samples of CaM:CaMBD-2-H_6 and CaM:CaMBD-4-H_6 were exchanged into FP Buffer with 40 nM FP probe **33** with PD SpinTrap G-25 columns (GE Healthcare) following the manufacture's instructions. The protein samples were serially diluted with the same buffer to give final test volumes of 20 µL and concentrations; 100, 50, 25, 12.5, 6.25, 3.125, 1.562 µM, 781, 390, 195, 98, 49, 24, 12, 6, 3, 1.5 nM. The fluorescent intensities of the protein dilutions were then recorded.

6.2.8 Crystallography

Co-purified CaM:CaMBD-2-H_6 and CaM:CaMBD-4-H_6 were screened against commercial protein crystallography condition suites; SaltRX HT (Hampton Research), Crystal Screen HT (Hampton Research), JCSG Plus™ HT-96 suite (Qiagen), PACT premier™ HT-96 suite (Qiagen). High throughput 96 well Intelli-Plates® (Art Robbins Instruments LLC.) were prepared using a Crystal Phoenix automated crystallography dispenser (Art Robbins Instruments LLC.) and sealed with clear StarSeal films (STARLAB Ltd.). Protein samples (50 µL) were dispensed in 100-200 µL aliquots as sitting drops (300 µL total) in sub-well buffer ratios of 1:2, 1:1, and 2:1 (protein : reservoir solution) and left to concentrate *via* vapour diffusion.

Co-purified proteins were buffer exchanged into Crystallography Buffer (Tris (10 mM), NaCl (50 mM), $CaCl_2$ (10 mM), pH 7.5) over night at 4 °C with 0.5 mL Slide-A-Lyzer® Mini dialysis devices and concentrated using 0.5 mL Amicon® Ultra centrifugal filters (Sigma Aldrich Co.) to 1 mM for CaM:CaMBD-2-(H_6) and 230 µM for CaM:CaMBD-4-H_6. Duplicate protein crystallography plates were stored at 4 °C and 25 °C for 6 months.

In co-crystallisation experiments co-purified CaM:CaMBD-4-H_6 was buffer exchanged into Crystallography Buffer with added methylamine and aniline novel SKA111 analogues **13** or **10**, respectively, (500 µM), see Chapter 2.3.2, *via* both spin trap column and dialysis cassette methods. Using PD SpinTrap G-25 columns (GE Healthcare) and procedure prepared protein samples were concentrated with 0.5 mL Amicon® Ultra centrifugal filters to 106 µM with **13** and 85 µM with **10**. Using dialysis 0.5 mL PD MidiTrap™ G-25 decives (3,500 MWCO) (GE Healthcare) protein samples (100 µL) were dialysed into 10 mL Buffer over 3 h at 4°C and then changed and dialysed

overnight. Protein samples were concentrated with 0.5 mL Amicon® Ultra centrifugal filters to 50 µM.

Final protein concentrations were estimated with a NanoDrop 1000 spectrophotometer (Thermo Fisher Scientific Inc.) with the respective ExPASy ProtParam tool calculated 280 nm extinction coefficients (https://web.expasy.org/cgi-bin/protparam/protparam).

6.2.9 Expressed Proteins Primary Sequences

>CaM

ADQLTEEQIAEFKEAFSLFDKDGDGTITTKELGTVMRSLGQNPTEAELQDMINEVDADGNGTIDFPEFL TMMARKMKDTDSEEEIREAFRVFDKDGNGYISAAELRHVMTNLGEKLTDEEVDEMIREADIDGDGQVNY EEFVQMMTAK

>SK_{Ca}2.2 CaMBD-2-H_6

GRKLELTKAEKHVHNFMMDTQLTKRVKNAAANVLRETWLIYKNTKLVKKIDHAKVRKHQRKFLQAIHQL RSVKMEQRKLNDQANTLVDLAKTQLEHHHHHH

>IK_{Ca}3.1 CaMBD-4-H_6

GRKLEFNKAEKHVHNFMMDIHYAKEMKESAARLLQEAWMYYKHTRRKDSRAARRHQRKMLAAIHTF RQVRLKHRKLREQVNSMVDISKHHHHHH

6.3 Chemistry Experimental Details

6.3.1 General Experimental

Commercially available reagents were purchased from Acros Organics, Alfa Aesar, Fischer Scientific or Sigma Aldrich, and used without further purification. Celite® refers to Celite® 545 filter aid, treated with sodium carbonate, flux-calcined (Sigma Aldrich). Brine refers to a saturated aqueous (sat. aq.) solution of sodium chloride. All common organic solvents: acetone, acetonitrile, dichloromethane, diethyl ether, ethanol, ethyl acetate, methanol, pentane, *et cetera*, used were HPLC grade or equivalent supplied by Sigma Aldrich Co. (now Merck & Co. Inc.), Thermo Fisher Scientific and Alfa Aesar.

All reactions were conducted at room temperature (~21 °C) under an argon atmosphere with flame-dried glassware, unless otherwise stated. Anhydrous solvents: tetrahydrofuran and dichloromethane, were obtained from an MB SPS5 solvent purification system (MBRAUN Inc.) and stored under an argon atmosphere over 3 Å molecular sieves.

Analytical thin layer chromatography (TLC): was performed using silica gel 60 F_{254} pre-coated aluminium-supported thin layer chromatography sheets (Merck & Co. Inc.) and visualised under U.V. irradiation (λ_{max} = 254 nm) or with the following appropriate stain solutions: potassium permanganate, ninhydrin, Erlich's reagent, *p*-anisaldehyde, iodine, vanillin, dinitrophenylhydrazine. Standard phase silica gel flash column chromatography was carried out under a positive pressure of nitrogen using Geduran® Si 60 (0.040-0.063 mm) silica gel (Merck & Co. Inc.) following published procedures and guidelines.[12] *In vacuo* refers to use of a rotary evaporator attached to a vacuum pump.

Nuclear Magnetic Resonance (NMR) spectra: were recorded on Bruker Avance III 400 and 500 MHz machines and were assigned with the aid of 2D NMR experiments

including COSY, HSQC, HMBC and NOESY. Deuterated solvents were supplied by Sigma Aldrich Co. Residual protic solvent and deuterated carbon signals were used as internal references for ^{1}H and ^{13}C, spectra respectively: Acetone-D_6 ($(CD_3)CO$) (δ_H = 2.05 ppm, δ_C = 29.8 ppm), Chloroform-D_3 ($CDCl_3$) (δ_H = 7.26 ppm, δ_C = 77.2 ppm), Dimethylsulfoxide-D_6 $(CD_3)SO$ (δ_H = 2.50 ppm, δ_C = 39.5 ppm) and Methanol-D_4 (CD_3OD) (δ_H = 3.31 ppm, δ_C = 49.0 ppm). ^{1}H chemical shifts δ_H are quoted in parts per million (ppm) relative to relevant residual solvent peak to the nearest 0.01 ppm. ^{13}C chemical shifts δ_C are quoted as singlets in parts per million (ppm) relative the relevant deuterated carbon solvent peak to the nearest 0.1 ppm, unless peaks are unresolved, where they are quoted to the nearest 0.01 ppm. ^{1}H NMR spectra are reported as follows: chemical shift (number of protons, multiplicity (s = singlet, d = doublet, t = triplet, q = quartet, p = pentet, m = multiplet, br = broadened), coupling constant *J* (averaged and presented to the nearest 0.1 Hz), assignment). NMR data was processed using Mestrenova 10.0 or Bruker Topspin v3.5 software.

Melting points (m.p.): were performed on a Kofler Hotstage microscope and are uncorrected. All solids were re-crystallised from the stated solvent.

Fourier-transform Infrared (FTIR) spectra: were recorded from evaporated films using a Tensor 27 spectrometer (Bruker) fitted with a Pike Miracle Attenuated Total Reflectance (ATR) sampling accessory. Absorption maxima (ν_{max}) are quoted in in wavenumbers (cm^{-1}) and described as weak (w), medium (m), strong (s) and broad (b).

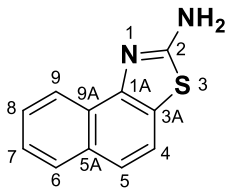
Mass spectra was obtained from samples in acetonitrile or methanol (0.1 mg/mL) using a 6120 Quadrupole spectrometer (Agligent) for low resolution (LRMS) and high for resolution (HRMS) an Exactive orbitrap spectrometer (Thermoscientific). For compounds which did not ionise with ESI, spectra were acquired on a Waters GCT

classic spectrometer using electron impact (EI) or chemical ionisation (CI). *m/z* values are reported in Daltons to the nearest Da in LRMS and the nearest 0.0001 Da in HRMS.

Analytical high-performance liquid chromatography (HPLC): was performed with a PerkinElmer Flexar system with a Binary LC Pump and UV/VIS LC Detector. Standard runs were monitored over 254 nm. Final compounds were monitored over 254 nM and 220 nM. For determination of purity, a Dionex Acclaim® 120 C18 reverse phase column [5 µm, 12 Å, 150 mm × 4.6 mm] was used with a gradient of eluents method (95:5 H_2O:MeCN to 5:95 H_2O:MeCN; 10 min; 5 min hold; 1.5 mL/min). Samples injected were prepared by dissolving in MeCN and filtered through 4 mm 0.22 µm PTFE syringe filters (Gilson Scientific Ltd.). Compounds were run with 0.1% TFA as standard, those which were not at denoted with (*).

6.3.2 Procedures

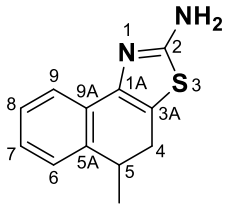
Naphtho[1,2-*d*]thiazol-2-amine (2) (*SKA31*)[13]



A solution of thiourea (31 mg, 0.41 mmol, 1.2 eq.), iodine (52 mg, 0.22 mmol, 0.6 eq.), α-tetralone **1** (45 µL, 0.34 mmol, 1.0 eq.), and *p*-toluenesulfonic acid (323 mg, 1.88 mmol, 5.5 eq.) in dimethyl sulfoxide (2 mL) was heated to 75 °C under an atmosphere of pure oxygen for 1 d. The reaction mixture was cooled to room temperature and basified with sodium bicarbonate (20 mL, sat. aq.). The solution was lyophilised and the residue purified by silica gel flash column chromatography (ethyl acetate / dichloromethane 1:9) to give **2** as an orange solid (26 mg, 38%): R_f 0.20 (diethyl ether / pentane 1:1); m.p. 186–187 °C (from CD_3OD); FTIR: ν_{max} (thin film)/cm^{-1}

3286 (N-H, bw), 3051 (C-H, bw), 1528 (C=C, s), 1503 (C=C, m), 1392 (m); ^{1}H NMR (500 MHz; CD_3OD) δ_H 8.39 (1H, dd, *J* 8.1, 1.3, H-9), 7.82 (1H, dd, *J* 8.1, 1.3, H-6), 7.63 (1H, d, *J* 8.5, H-4), 7.42 (1H, d, *J* 8.5 H-5) 7.39 (1H, ddd, *J* 8.3, 6.8, 1.3, H-8), 7.42 (1H, ddd, *J* 8.3, 6.8, 1.3, H-7); ^{13}C NMR (125 MHz; CD_3OD) δ_C 170.3 (C-2), 148.4 (C-5A), 133.7 (C-1A), 129.1 (C-6), 127.6 (C-9A), 126.8 (C-8), 126.6 (C-3A), 126.2 (C-7), 124.4 (C-9), 123.0 (C-5), 119.7 (C-4); HRMS *m/z* (ESI^+) [Found: 201.0481, $C_{11}H_9N_2{}^{32}S$ requires $[M+H^+]$ 201.0481]; LRMS *m/z* (ESI^+) 201 $[M+H^+]$; HPLC retention time 8.76 m, 90% at 220 nm and 254 nm.

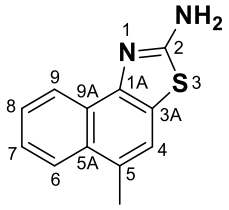
5-Methyl-4,5-dihydronaphtho[2,1-*d*]thiazol-2-amine (4) (*SKA113*)[14]



A solution of 4-methyl-1-tetralone **3** (4.64 mL, 31.3 mmol, 1.0 eq.), iodine (7.95 g, 31.3 mmol, 1.0 eq.) and thiourea (6.65 g, 87.5 mmol, 2.8 eq.) in ethanol (40 mL) was heated under reflux for 20 hours. The reaction mixture was cooled to room temperature and directly concentrated to about 50% volume. The residue stirred with diethyl ether overnight producing colourless precipitate. The precipitate suspension was filtered, the filter cake was washed with dichloromethane and purified by silica gel flash column chromatography (ethyl acetate / dichloromethane 1:9 + 0.1% trimethylamine) to give **4** as a colourless solid (4.83 g, 71%): R_f 0.41 (ethyl acetate / dichloromethane 1:9 + 0.1% trimethylamine); m.p. 114–115 °C (from dichloromethane); FTIR: ν_{max} (thin film)/cm^{-1} 3447 (N-H, w), 3291 (N-H, w), 3092 (C-H, b), 1636 (N-H, m), 1532 (C=C, s), 1351 (s); ^{1}H NMR (500 MHz; $CDCl_3$) δ_H 7.69 (1H, dd, *J* 7.5, 1.3, H-9), 7.28–7.12 (3H, m, H-6, H-7 and H-8), 5.46 (2H, s, NH_2), 3.17 (1H, ddq [apparent sextet], *J* 6.6, H-5), 3.01 (1H, dd, *J* 15.9, 6.6, H-4, CH_AH$_B$), 2.62 (1H, dd, *J* 15.9, 6.6, H-4, CH$_A$$H_B$), 1.32 (3H, d, *J* 6.6,

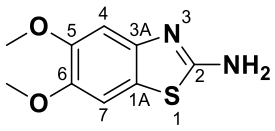
5-C*H*$_3$); ^{13}C NMR (125 MHz; $CDCl_3$) δ_C 165.1 (C-2), 143.5 (C-1A), 138.6 (C-5A), 129.7 (C-9A), 126.0 (C-8), 125.9 (C-7), 125.6 (C-6), 122.0 (C-9), 117.8 (C-3A), 32.7 (C-5), 28.4 (C-4), 19.9 (5-*C*H_3); HRMS *m/z* (ESI$^+$) [Found: 217.080, $C_{12}H_{12}N_2S$ requires [M+H$^+$], 217.079]; LRMS *m/z* (ESI$^+$) 217; HPLC retention time 6.9, 99% at 220 nm and 254 nm.

5-Methylnaphtho[2,1-*d*]thiazol-2-amine (5) (*SKA111*)[14]



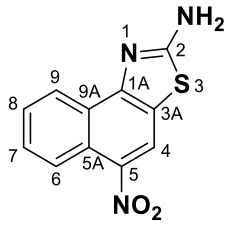
Manganese dioxide (activated with HCl, 1 M, aq.) (8.05 g, 200%) was suspended in a solution of 5-methyl-4,5-dihydronaphtho[2,1-d]thaizol-2-amine **4**, (4.00 g, 18.5 mmol, 1 eq.) in anhydrous dichloromethane (400 mL). The reaction mixture was heated under reflux for 18 h. The reaction mixture was then cooled to room temperature, filtered through a pad of Celite® under vacuum, eluted with ethyl acetate, and concentrated *in vacuo*. The residue was purified by silica gel flash column chromatography (ethyl acetate / dichloromethane 1:9 + 0.1% trimethylamine) to give **5** as a colourless solid (2.86 g, 72%): R_f 0.28 (ethyl acetate / dichloromethane 1:9 + 0.1% trimethylamine); m.p. 218 °C (from ethyl acetate); FTIR: ν_{max} (thin film)/cm^{-1} 2283 (b), 1542 (C=C, m), 757 (s), 668 (s), 647 (s); ^{1}H NMR (500 MHz; $(CD_3)SO$) δ_H 8.38 (1H, dd, *J* 7.0, 2.7, H-9), 7.97 (dd, *J* 7.1, 2.3, H-6), 7.64 (1H, s, H-4), 7.57–7.49 (4H, m, H-7, H-8 and NH_2), 2.63 (3H, s, 5-C*H*$_3$); ^{13}C NMR (125 MHz; $(CD_3)SO$) δ_C 166.7 (C-2), 146.7 (C-1A), 130.6 (C-5A), 126.6 (C-5), 126.0 (C-9A), 125.4 (C-8), 125.0 (C-7), 124.7 (C-3A), 124.5 (C-6), 123.9 (C-9), 119.3 (C-4), 19.1 (5-*C*H_3); HRMS *m/z* (ESI$^+$) [Found: 215.0643, $C_{12}H_{11}N_2S$ requires [M+H$^+$], 215.0638]. LRMS *m/z* (ESI$^+$) 215; HPLC retention time 7.2, 97% at 220 nm and 254 nm.

5,6-Dimethoxybenzo[*d*]thiazol-2-amine (7) (*SKA15*)[13]



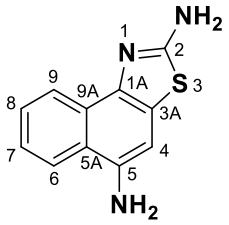
Bromine (81 µL, 1.5 mmol, 1.2 eq.) was added dropwise to a solution of ammonium thiocyanate (178 mg, 2.34 mmol, 1.80 eq.) in acetic acid (6.5 mL) and stirred for 0.5 h. The reaction mixture was filtered to remove precipitate. The filtrate was added to a solution of 3,4-dimethylaniline **6** (200 mg, 1.30 mmol, 1.00 eq.) in acetic acid (6.5 mL) and the mixture was stirred for 24 h. The reaction mixture was assessed by TLC analysis (visualised under U.V. light and stained with ninhydrin). The reaction mixture was concentrated *in vacuo* and the residue resuspended in ethyl acetate (20 mL). The organic component was sequentially washed with sodium bicarbonate (20 mL, sat. aq.) and brine (20 mL), dried over anhydrous magnesium sulfate, filtered, and concentrated *in vacuo.* The residue was purified by silica gel flash column chromatography (ethyl acetate / dichloromethane 3:7) to give **7** as a colourless solid (209 mg, 77%): R_f 0.30 (ethyl acetate / dichloromethane 3:7); m.p. 224–225 °C (from $CDCl_3$); FTIR: ν_{max} (thin film)/cm^{-1} 3300 (N-H, bw), 1543 (C=C, m), 1480 (C-H, s), 1215 (C-O, m), 1167 (N-C, w); ^{1}H NMR (500 MHz; $CDCl_3$) δ_H 7.12 (1H, s, H-4), 7.08 (1H, s, H-7), 5.11 (2H, s, NH_2), 3.91 (1H, s, 5-OC*H*$_3$), 3.89 (s, 1H, 6-OC*H*$_3$). ^{13}C NMR (125 MHz; $CDCl_3$) δ_C 165.1 (C-2), 149.0 (C-5), 146.1 (2C, C-6 and C-3A), 122.5 (C-1A), 103.7 (C-7), 103.0 (C-4), 56.6 (5-O*C*H$_3$), 56.2 (6-O*C*H$_3$); HRMS *m/z* (ESI$^+$) [Found: 211.0536. $C_9H_{11}N_2O_2S$ requires [M+H$^+$] 211.0536]; LRMS *m/z* (ESI$^+$) 211 [M+H$^+$]; HPLC retention time 5.4 min*, 99% at 220 nm and 254 nm.

5-Nitronaphtho[1,2-*d*]thiazol-2-amine (9)



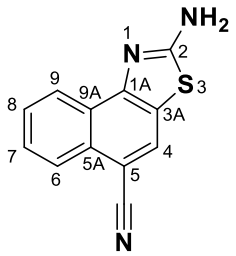
Bromine (165 µL, 3.19 mmol, 1.3 eq.) was added dropwise to a solution of ammonium thiocyanate (365 mg, 4.81 mmol, 1.9 eq.) and 1-nitronathph-4-amine **8** (479 mg, 2.55 mmol, 1.0 eq.) in acetic acid (32.5 mL). The reaction mixture was stirred for 20 h and directly concentrated *in vacuo*. The residue was re-dissolved in potassium carbonate (50 mL, sat. aq.) and extracted with ethyl acetate (3 × 50 mL). The combined organic components were dried over anhydrous magnesium sulfate, filtered, and concentrated *in vacuo*. The residue was purified by silica gel flash column chromatography (diethyl ether / dichloromethane 1:9) to give **9** as an orange solid (140 mg, 22%): R_f 0.30 (1:9 diethyl ether : dichloromethane); m.p. 109–110 °C (decomp) (from dichloromethane): FTIR: ν_{max} (thin film)/cm^{-1} 3387 (N-H, w), 3103 (C-H, wb), 1651 (C=C, m), 1530 (N=O, m), 1256 (C-N, s); ^{1}H NMR (400 MHz; $(CD_3)SO$) δ_H 8.96 (1H, s, H-4), 8.67 (1H, dd, *J* 8.7, 1.6, H-6), 8.54 (1H, dd, *J* 8.2, 1.9, H-9), 8.44 (2H, s, NH_2), 7.77 (1H, ddd, *J* 8.7, 6.9, 1.9, H-7), 7.69 (1H, ddd, *J* 8.2, 6.9, 1.6, H-8); ^{13}C NMR (101 MHz; $(CD_3)SO$) δ_C 172.8 (C-2), 154.7 (C-1A), 138.0 (C-5), 128.8 (C-7), 126.7 (C-8), 124.8 (C-9A), 124.7 (C-9), 124.3 (C-5A), 123.2 (2C, C-6 and C-3A), 121.0 (C-4); HRMS *m/z* (ESI$^+$) [Found: 246.0333, $C_{11}H_8O_2N_3{}^{32}S$ requires [M+H$^+$] 246.0332]; LRMS *m/z* (ESI$^+$) 246; HPLC retention time 8.9 min, 99% at 220 nm and 254 nm.

Naphtho[1,2-*d*]thiazole-2,5-diamine (10)



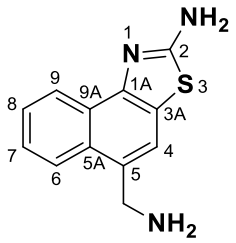
Activated zinc powder (130 mg, 650%) was suspended in a solution of ammonium chloride (108 mg, 2.04 mmol, 25.0 eq.) and 5-nitronaphtho[1,2-*d*]thiazol-2-amine **9** (20 mg, 80 µmol, 1.0 eq.) in methanol (3 mL). The reaction mixture was stirred for 20 h, then directly filtered through a pad of Celite®. The filtrate was concentrated *in vacuo*. The residue was purified by silica flash column chromatography (ethyl acetate / pentane 1:1) to give **10** as a dark red solid (14 mg, 81%): R_f 0.29 (ethyl acetate / pentane 1:1); m.p. >300 °C (from DMSO); FTIR: ν_{max} (thin film)/cm^{-1} 3293 (N-H, bw), 3110 (C-H, bw), 1633 (N-H, m), 1538 (C=C, s), 1397 (m); ^{1}H NMR (400 MHz; $(CD_3)SO$) δ_H 8.25 (1H, dd, *J* 8.4, 1.3, H-6), 8.04 (1H, dd, *J* 8.3, 1.7, H-9), 7.47 (1H, ddd, *J* 8.3, 6.8, 1.3, H-7), 7.37 (1H, ddd, *J* 8.4, 6.8, 1.7, H-8), 7.11 (2H, br s, 2-NH_2), 6.96 (1H, s, H-4), 5.38 (2H, br s, 5-NH_2); ^{13}C NMR (101 MHz; $(CD_3)SO$) δ_C 163.3 (C-2), 139.3 (C-5), 139.5 (C-1A), 126.6 (C-3A), 126.4 (C-9A), 125.5 (C-7), 123.6 (C-6), 123.2 (C-8), 122.9 (C-9), 122.2 (C-5A), 100.2 (C-4); HRMS *m/z* (ESI$^+$) [Found: 216.058,. $C_{11}H_{10}N_3{}^{32}S$ requires [M+H$^+$] 216.0590]; LRMS *m/z* (ESI$^+$) 216; HPLC retention time 4.9 min*, 98% 220 nm and 254 nm.

2-Aminonaphtho[1,2-*d*]thiazole-5-carbonitrile (12) (SKA107)[14]



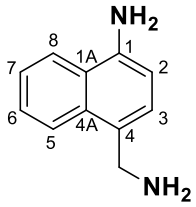
Bromine (186 µL, 3.60 mmol, 1.2 eq.) was added dropwise to a solution of 4−aminonaphthalene-1-carbonitrile **11** (500 mg, 2.97 mmol, 1.0 eq) and ammonium thiocyanate (403 mg, 5.30 mmol, 1.8 eq.) in acetic acid (30 mL). The reaction mixture was heated to 100 °C for 24 h, allowed to cool to room temperature and directly concentrated *in vacuo*. The residue was resuspended in potassium carbonate (10 mL, sat. aq.) and extracted into ethyl acetate (3 × 10 mL). The organic components were dried over anhydrous magnesium sulfate, filtered, and concentrated *in vacuo*. The residue was purified by silica gel flash column chromatography (diethyl ether / dichloromethane 1:9) to give **12** as a yellow solid (459 mg, 68%): R_f 0.30 (diethyl ether / dichloromethane 1:9); m.p. 269–271 °C (from acetone); FTIR: ν_{max} (thin film)/cm^{-1}; 3311 (N-H, wb), 3104 (C-H, wb), 2217 (C≡N, w), 1662 (C=C, m), 754 (s); ^{1}H NMR (700 MHz; (CD$_3$)SO) δ_H 8.51 (1H, s, H-4), 8.46 (1H, dd, *J* 8.2, 1.2, H-9), 8.24 (2H, br s, NH$_2$), 8.07 (1H, dd, *J* 8.3, 1.2, H-6), 7.73 (1H, ddd, *J* 8.3, 6.8, 1.4, H-7), 7.68 (1H, ddd, *J* 8.2, 6.8, 1.2, H-8); ^{13}C NMR (176 MHz; (CD$_3$)SO) δ_C 171.4 (C-2), 152.7 (C-1A), 130.7 (C-5A), 127.9 (C-7), 127.1 (C-4), 127.0 (C-8), 124.9 (C-9A), 124.6 (C-9), 124.4 (C-6), 124.3 (C-3A), 118.5 (C≡N), 99.6 (C-5); HRMS *m/z* (ESI$^+$) [Found: 226.0433, C$_{12}$H$_8$N$_3$^{32}S requires [M+H$^+$] 226.0433]; LRMS *m/z* (ESI$^+$) 226; HPLC retention time 8.3 min, 97% at 220 nm and 254 nm.

5-(Aminomethyl)naphtho[1,2-*d*]thiazol-2-amine (13)



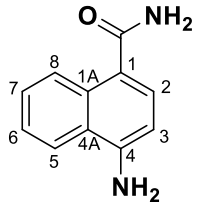
Bromine (70 µL, 1.39 mmol, 1.2 eq.) was added dropwise to a stirring solution of the amine **15** (98 mg, 0.57 mmol, 1.0 eq.) and ammonium thiocyanate (159 mg, 2.09 mmol, 1.8 eq.) in acetic acid (13 mL). The reaction mixture was heated to 100 °C for 24 h, allowed to cool to room temperature and directly concentrated *in vacuo*. The residue was re-dissolved in potassium carbonate (10 mL, sat. aq.) and extracted with ethyl acetate (3 × 10 mL). The combined organic components were dried over anhydrous sodium sulfate, filtered, and concentrated *in vacuo*. The residue was purified by silica gel flash column chromatography (water / isopropylalcohol / ethyl acetate 5:35:60) to give **13** as a colourless solid (33 mg, 25%): R_f 0.48 (water / isopropylalcohol / ethyl acetate 5:35:60); m.p. 164–166 °C (from ethyl acetate); FTIR: ν_{max} (thin film)/cm^{-1} 3127 (C-H, wb), 1705 (m), 1533 (C=C, s), 1364 (C-N, m), 760 (m); ^{1}H NMR (400 MHz; $(CD_3)SO$) δ_H 8.41 (1H, dd, *J* 7.9, 1.8, H-9), 8.09 (1H, dd, *J* 7.6, 1.8, H-6), 7.85 (1H, s, H-4), 7.58 (2H, br s, NH_2), 7.53 (1H, ddd, *J* 7.6, 6.8, 1.8, H-7), 7.50 (1H, ddd, *J* 7.9, 6.8, 1.8, H-8), 4.22 (2H, s, CH_2), $CH_2N\mathit{H_2}$ not observed. ^{13}C NMR (101 MHz; $(CD_3)SO$) δ_C 167.1 (C-2), 147.3 (C-1A), 131.2 (C-9A), 129.5 (C-5A), 126.0 (C-3A), 125.4 (C-8), 125.1 (C-7), 124.6 (C-5), 124.1 (C-6), 124.0 (C-9), 118.1 (C-4), 42.6 (CH_2); HRMS *m/z* (ESI$^+$) [Found: 230.0747, $C_{12}H_{12}N_3{}^{32}S$ requires [M+H$^+$] 230.0746]; LRMS *m/z* (ESI$^+$) 230.

4-(Aminomethyl)naphthalen-1-amine (15)



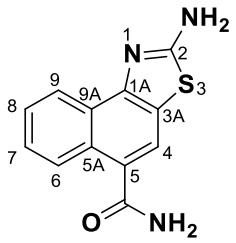
A solution of 4-amino-1-naphthacarbonitrile **11** (200 mg, 1.20 mmol, 1.0 eq.) in anhydrous tetrahydrofuran (3 mL) was added slowly to a suspension of lithium aluminium hydride (162 mg, 4.26 mmol, 4.0 eq.) in anhydrous tetrahydrofuran (2.5 mL) at 4 °C. The mixture was heated under reflux for 20 h, cooled to 4 °C and quenched with water (162 µL), sodium hydroxide (162 µL, 2 M, aq.) then further water (486 µL), added dropwise with 10 min periods between each addition. The mixture was allowed to warm to room temperature for 20 min. The reaction mixture was filtered through a pad of Celite® and the precipitate was washed with methanol (10 mL). The organic components were dried over sodium sulfate, filtered, and concentrated to give **15** (138 mg, 67%). The product was air sensitive and used directly in the next step without further purification: R_f 0.19 (water / isopropylalcohol / ethyl acetate 5:35:60); ν_{max} (thin film)/cm^{-1} 3351 (N-H, w), 2855 (C-H, w), 1624 (N-H, m), 1581 (C=C, m), 1516 (C=C, m); ^{1}H NMR (400 MHz; $(CD_3)SO$) δ_H 8.07 (1H, dd, *J* 8.3, 1.4, H-8), 7.99 (1H, dd, *J* 8.4, 1.6, H-5), 7.44 (1H, ddd, *J* 8.4, 6.7, 1.4, H-6), 7.37 (1H, ddd, *J* 8.3, 6.7, 1.6 H-7), 7.20 (1H, d, *J* 7.6 H-3), 6.62 (1H, d, *J* 7.6 H-2), 5.54 (2H, br s, 1-NH_2), 4.02 (1H, s, C*H*$_2$), *CH_2NH_2 was observed as a very broad signal between the chemical shifts 3.6-1.2; ^{13}C NMR (101 MHz; $(CD_3)SO$) δ_C 144.7 (C-1), 132.8 (C-4A), 127.6 (C-4), 126.8 (C-3), 126.4 (C-6), 124.8 (C-5), 124.3 (C-7), 124.2 (C-1A), 123.8 (C-8), 107.9 (C-2), 44.1 (*C*H_2).

4-Aminonaphthalene-1-carboxamide (16)



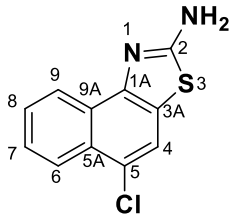
A suspension of amino-1-naphthacarbonitrile **11** (500 mg, 3.00 mmol, 1 eq.) and potassium carbonate (138 mg, 0.60 mmol, 0.2 eq.) in water (10 mL) was heated by microwave irradiation to 150 °C for 4 h. The reaction mixture was cooled and acidified with hydrochloric acid (2 mL, 2 M, aq.), washed with ethyl acetate (3 × 10 mL) and neutralised with potassium carbonate. The aqueous components were lyophilised overnight. The residue was purified by silica gel flash column chromatography (ethyl acetate / dichloromethane 2:3) to give **16** as a colourless solid (130 mg, 23%): R_f 0.38 (ethyl acetate / dichloromethane 2:3); m.p. 176–177 °C (from dichloromethane); FTIR: ν_{max} (thin film)/cm^{-1} 3389 (N-H, w), 3215 (N-H, w), 1563 (C=C, m), 1517 (C=C,m), 1337 (C-N, m); ^{1}H NMR (700 MHz; (CD$_3$)SO) δ_H 8.57 (1H, d, *J* 8.6, H-8), 8.10 (1H, d, *J* 8.4, H-5), 7.58 (1H, bs, CON*H*$_A$H$_B$), 7.52 (1H, d, *J* 7.9, H-2), 7.45 (1H, ddd, *J* 8.6, 6.6, 1.4, H-7), 7.38 (1H, ddd, *J* 8.4, 6.6, 1.4, H-6), 7.04 (1H, bs, CONH$_A$*H$_B$*), 6.61 (1H, d, *J* 7.9, H-3), 6.14 (2H, br s, NH$_2$); ^{13}C NMR (176 MHz; (CD$_3$)SO) δ_C 171.0 (*C*ONH), 147.2 (C-4), 131.9 (C-1A), 128.2 (C-2), 126.2 (C-7), 126.1 (C-8), 123.6 (C-6), 122.3 (C-5), 122.2 (C-4A), 120.1 (C-1), 105.3 (C-3); HRMS *m/z* (ESI$^+$) [Found: 187.0867, C$_{11}$H$_{11}$ON$_2$ requires [M+H$^+$] 187.0866]; LRMS *m/z* (ESI$^+$) 187; HPLC retention time 4.2 min, 99% at 220 nm and 254 nm.

2-Aminonaphtho[1,2-*d*]thiazole-5-carboxamide (17)



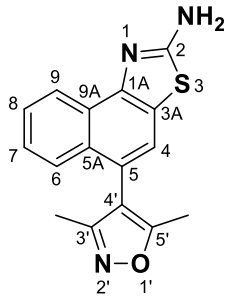
Bromine (5.0 µL, 10 µmol, 1.2 eq.) was added dropwise to a solution of 4-aminonaphthalene-1-carboxamide **16** (15 mg, 8.1 µmol, 1.0 eq.), and ammonium thiocyanate (11 mg, 0.14 mmol, 1.8 eq.) in acetic acid (2 mL). The reaction mixture was heated to 100 °C for 20 h, allowed to cool to room temperature and directly concentrated *in vacuo*. The residue was purified by silica gel flash column chromatography (ethyl acetate / dichloromethane 2:3) to give **17** as a colourless solid (6 mg, 30%): R_f 0.36 (ethyl acetate / dichloromethane, 3:2); m.p. 317-319 °C (from ethyl acetate); FTIR: ν_{max} (thin film)/cm^{-1}; 3296 (N-H, bm), 3179 (N-H, bm), 1643 (C=O, s), 1527 (C=C, s), 1386 C-N, s); ^{1}H NMR (700 MHz; $(CD_3)SO$) δ_H 8.42 (1H, dd, *J* 8.4, 1.6, H-6), 8.40 (1H, dd, *J* 8.2, 1.8, H-9), 8.01 (1H, bs, CONH_AH_B), 7.89 (1H, s, H-4), 7.80 (2H, br s, NH_2), 7.54 (1H, ddd, *J* 8.2, 6.7, 1.6, H-8), 7.51 (1H, ddd, *J* 8.4, 6.7, 1.8, H-7), 7.43 (1H, bs, CONH$_A$$H_B$); ^{13}C NMR (176 MHz; $(CD_3)SO$) δ_C 170.5 (*C*ONH_2), 168.8 (C-2), 149.6 (C-1A), 128.9 (C-5A), 127.0 (C-5), 126.1 (C-6), 125.7 (C-9A), 125.6 (C-7), 125.5 (C-8), 123.7 (C-9), 123.6 (C-3A), 119.5 (C-4); HRMS *m/z* (ESI$^+$) [Found: 244.0540, $C_{12}H_{10}N_3{}^{32}S$ requires [M+H$^+$] 244.0539]; LRMS *m/z* (ESI$^+$) 244; HPLC retention time 5.3 min, 98% at 220 nm and 254 nm.

5-Chloronaphtho[1,2-*d*]thiazol-2-amine (21) (SKA72)[14]



Bromine (337 µL, 6.70 mmol, 1.2 eq.) was added dropwise to a solution of 4-chloronaphth-1-amine **20** (1.00 g, 5.60 mmol, 1 eq.) and ammonium thiocyanate (773 mg, 10.2 mmol, 1.8 eq.) in acetic acid (65 mL). The reaction mixture was heated to 100 °C for 24 h, allowed to cool to room temperature and directly concentrated *in vacuo*. The residue was resuspended in potassium carbonate (10 mL, sat. aq.) and extracted with ethyl acetate (3 × 10 mL). The combined organic components were dried over anhydrous magnesium sulfate, filtered, and concentrated *in vacuo*. The residue was purified by silica gel flash column chromatography (diethyl ether / dichloromethane 1:9) to give **21** as a yellow solid (459 mg, 68%): R_f 0.30 (diethyl ether / dichloromethane 1:9); m.p. 257–259 °C (from acetone); FTIR: ν_{max} (thin film)/cm^{-1} 3456 (N-H, w), 3099 (C-H, wb), 1646 (w), 1541 (C=C, m), 752 (C-Cl, s); ^{1}H NMR (700 MHz; $(CD_3)SO$) δ_H 8.43–8.40 (1H, m, H-6), 8.17–8.12 (1H, m, H-9), 8.07 (1H, s, H-4), 7.77 (2H, br s, NH_2), 7.66–7.59 (2H, m, H-7 and H-8); ^{13}C NMR (176 MHz; $(CD_3)SO$) δ_C 168.2 (C-2), 147.7 (C-1A), 128.2 (C-5A), 126.5 (C-8), 126.4 (C-7), 126.2 (C-9A), 124.9 (C-5), 124.2 (C-6), 124.0 (C-9), 122.1 (C-3A), 119.7 (C-4); HRMS *m/z* (ESI$^+$) [Found: 235.00916, $C_{11}H_8N_2{}^{35}Cl^{32}S$ requires [M+H$^+$] 235.00912]; LRMS *m/z* (ESI$^+$) 235; HPLC retention time 8.6 min, 97% at 220 nm and 254 nm.

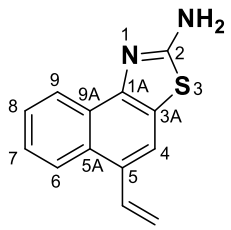
5-(3',5'-Dimethyl-1',2'-oxazol-4'-yl)naphtho[1,2-*d*]thiazol-2-amine (22)



A Schlenk flask was charged with 5-chloronaphtho[1,2-*d*]thiazol-2-amine **21** (100 mg, 430 µmol, 1 eq.), palladium(II) acetate (6 mg, 0.03 mmol, 6 mol%), 2-dicyclohexylphosphino-2′,6′-diisopropoxybiphenyl (RuPhos) (24 mg, 51 µmol, 12 mol%), potassium 3,5-dimethyl-1,2-oxazol-4-yl-trifluoroborate (98 mg, 0.47 mmol, 1.1 eq.) and sodium carbonate (91 mg, 0.86 mmol, 2.0 eq.). The flask was sealed, evacuated and backfilled with argon three times. Degassed ethanol (9 mL), sparged with argon, was added The reaction mixture was heated to 85 °C for 20 h. The reaction mixture was allowed to cool to room temperature, filtered through Celite®, and the filtrate concentrated *in vacuo*. The residue was purified by silica gel flash column chromatography (ethyl acetate / pentane 3:7) to give **22** as a dark brown oil (62 mg, 48%): R_f 0.30 (ethyl acetate / pentane 3:7); m.p. 118–120 °C (from $CDCl_3$); FTIR: ν_{max} (thin film)/cm^{-1} 3295 (N-H, wb), 2123 (C=N, wb), 1646 (w), 1538 (C=C, s), 1398 (C-N, w); ^{1}H NMR (400 MHz; $CDCl_3$) δ_H 8.57 (1H, d, *J* 8.2, H-9), 7.63–7.55 (2H, m, H-8 and H-6), 7.53 (1H, s, H-4), 7.51–7.45 (1H, m, H-7), 6.05 (2H, s, NH_2), 2.28 (3H, s, 5'-C*H*$_3$), 2.11 (3H, s, 3′-C*H*$_3$); ^{13}C NMR (101 MHz; $CDCl_3$) δ_C 167.2 (C-2), 166.7 (C-5'), 160.3 (C-3'), 148.3 (C-1A), 131.2 (C-5A), 127.0 (C-9A), 126.5 (C-8), 126.1 (C-7), 125.9 (C-3A), 125.7 (C-6), 124.4 (C-9), 122.0 (C-5), 121.2 (C-4), 115.1 (C-4'), 11.6 (5'-*C*H_3), 10.8 (3′-*C*H_3); HRMS *m/z* (ESI^+) [Found: 296.0854, $C_{16}H_{14}N_3{}^{32}S$ requires $[M+H^+]$

296.0852]; LRMS *m/z* (ESI$^+$) 296; HPLC retention time 7.6 min, 95% at 220 nm and 254 nm.

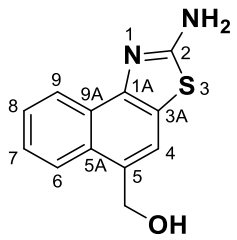
5-Vinylnaphtho[1,2-*d*]thiazol-2-amine (23)



A solution of palladium(II) acetate (10 mg, 44 µmol, 20 mol%) and 2-dicyclohexylphosphino-2′,6′-dimethoxybiphenyl (SPhos) (36 mg, 88 µmol, 40 mol%) in ethanol (2.5 mL), sparged with argon, was stirred for 20 min. The catalyst solution was then added to a vial containing a solution of 5-chloronaphtho[1,2-*d*]thiazol-2-amine 24 (50 mg, 0.22 mmol, 1.0 eq.), sodium carbonate (142 mg, 1.34 mmol, 6.1 eq.) and potassium vinyl trifluoroborate (177 mg, 1.32 mmol, 6.0 eq.) in degassed ethanol (2.5 mL), sparged with argon. The reaction mixture was stirred at 85 °C for 20 h, allowed to cool to room temperature then filtered through a pad of silica and Celite®, eluted with methanol. The filtrate was concentrated *in vacuo* and the residue purified by silica flash column chromatography (ethyl acetate / dichloromethane 1:9) to give **23** as a colourless solid (22 mg, 44%): R_f 0.30 (ethyl acetate / dichloromethane 1:9); m.p. 193–196 °C (from acetone); FTIR: ν_{max} (thin film)/cm^{-1} 3444 (N-H, w), 3085 (C-H, wb), 1638 (w), 1530 (C=C, m), 764 (m); ^{1}H NMR (500 MHz; $(CD_3)_2CO$) δ_H 8.52 (1H, dd, *J* 7.8, 1.8, H-9), 8.16 (1H, dd, *J* 8.1, 1.9, H-6), 7.99 (1H, s, H-4), 7.55 (1H, ddd, *J* 8.1, 6.8, 1.8, H-7) 7.54 (d, *J* = 28, C*H*), 7.52 (1H, ddd, *J* 7.8, 6.8, 1.9, H-8), 7.05 (2H, br s, NH_2), 5.79 (1H, dd, *J* 17.2, 1.5, *trans*-CH_2), 5.39 (1H, dd, *J* 10.9, 1.5, *cis*-CH_2); δ_C 168.4 (C-2), 149.6 (C-1A), 135.1 (*C*H), 130.7 (C-5A), 130.0 (C-5), 127.4 (C-9A), 127.0 (C-3A), 126.3 (C-8), 126.2 (C-7), 125.3 (C-9), 124.6(C-6), 117.28 (C-4), 115.61(*C*H_2); HRMS

m/z (ESI$^+$) [Found: 227.0635, $C_{13}H_{11}N_2{}^{32}S$ requires [M+H$^+$] 227.0638]; LRMS *m/z* (ESI$^+$) 227; HPLC retention time 8 min, 99% at 220 nm and 254 nm.

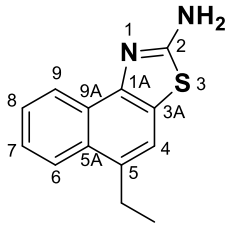
(2-Aminonaphtho[1,2-*d*]thiazol-5-yl)methanol (24)



Sodium borohydride (4 mg, 0.1 mmol, 1.1 eq.) was added to a solution of 2-aminonaphtho[1,2-*d*]thiazole-5-carbaldehyde **26** (20 mg, 90 µmol, 1.0 eq.) in tetrahydrofuran (2 mL) and methanol (8 mL) at 4 °C. The reaction mixture was stirred for 20 min, at which time it was observed complete by TLC (visualised with UV and stained with potassium permanganate). The reaction mixture was quenched with water (2 mL) and allowed to warm to room temperature over 0.5 h. The reaction mixture was diluted with water (10 mL), extracted with ethyl acetate (3 × 10 mL), the organic components dried over anhydrous magnesium sulfate and concentrated *in vacuo* to give **24** as a colourless solid (18 mg, 87%): R_f 0.17 (diethyl ether / dichloromethane, 1:9); m.p. 185–185 °C (from $(CD_3)_2CO$); ν_{max} (thin film)/cm^{-1} 3310 (N-H, wb), 1624 (C-H, w), 1530 (C=C, s), 1398 (C-N, w), 1061 (O-H, w); ^{1}H NMR (400 MHz; $(CD_3)_2CO$) δ_H 8.51 (1H, dd, *J* 6.8, 2.0, H-6), 8.14 (dd, *J* 7.2, 1.9, H-9), 7.83 (1H, d, *J* 0.9, H-4), 7.53 (1H, ddd, *J* 6.8, 6.1, 1.9, H-7), 7.50 (1H, ddd, *J* 7.2, 6.1, 2.0, H-8), 6.92 (2H, s, NH_2), 5.10 (2H, d, *J* 5.6, CH_2), 4.27 (1H, t, *J* 5.6, OH); ^{13}C NMR (101 MHz; $(CD_3)_2CO$) δ_C 168.0 (C-2), 149.0 (C-1A), 132.4 (C-5), 130.9 (C-5A), 127.9 (C-9A), 126.2 (C-3A), 126.2 (C-7), 125.9 (C-8), 125.2 (C-6), 125.1 (C-9), 118.6 (C4), 63.2 (CH_2); HRMS *m/z* (ESI$^+$)

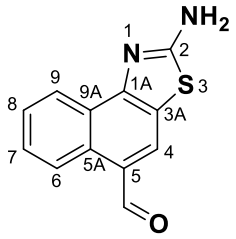
[Found: 231.0588, $C_{12}H_{11}ON_2{}^{32}S$ requires [M+H$^+$] 231.0587]; LRMS *m/z* (ESI$^+$) 231; HPLC retention time 6.7 min, 96% at 220 nm and 254 nm.

5-Ethylnaphtho[1,2-*d*]thiazol-2-amine (25)



Palladium black (4 mg, 36%) was suspended in a degassed solution of 5-vinylnaphtho[1,2-*d*]thiazol-2-amine **23** (11 mg, 49 mmol, 1 eq.) in ethyl acetate (5 mL) under nitrogen. Hydrogen gas was bubbled through the solution for 0.3 h and the mixture stirred for another 2 h under the hydrogen atmosphere. The hydrogen atmosphere was purged with nitrogen for 0.5 h before The reaction mixture was filtered through a pad of silica gel and Celite® and washed with ethyl acetate (3 × 10 mL) under vacuum. The combined organic components were concentrated *in vacuo* to give **25** as a colourless solid (11 mg, 99%): R_f 0.43 (diethyl ether / dichloromethane, 1:9); m.p. 140-142 °C (from $(CD_3)_2CO$); ν_{max} (thin film)/cm^{-1}; 3295 (N-H, wb), 3125 (C-H, wb), 2965 (C-H, m), 1622 (m), 1532 (C=C, s); ^{1}H NMR (400 MHz; $(CD_3)_2CO$) δ_H 8.55–8.48 (1H, m, H-9), 8.11–8.03 (1H, m, H-6), 7.64 (1H, s, H-4), 7.56–7.47 (2H, m, H-7, H-8), 6.83 (2H, br s, NH_2), 3.11 (2H, q, *J* 7.5, C*H*$_2$), 1.36 (3H, t, *J* 7.5, C*H*$_3$); ^{13}C NMR (101 MHz; $CDCl_3$) δ_C. 167.5 (C-2), 148.1 (C-1A), 134.7 (C-5), 131.2 (C-5A), 128.0 (C-9A), 126.7 (C-3A), 126.0 (C-7), 125.8 (C-8), 125.5 9 (C-9), 124.8 (C-6), 118.5 (C-4), 26.5 (*C*H$_2$), 15.6 (*C*H$_3$); HRMS *m/z* (ESI$^+$) [Found: 229.07942, $C_{13}H_{13}N_2{}^{32}S$ requires [M+H$^+$] 229.07940]; LRMS *m/z* (ESI$^+$) 229; HPLC retention time 10.1 min, 98% at 220 nm and 254 nm.

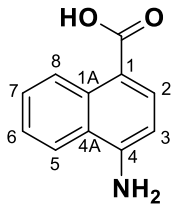
2-Aminonaphtho[1,2-*d*]thiazole-5-carbaldehyde (26)



Potassium osmate(IV) dihydrate (30 mg, 81 µmol, 10 mol%) was added to solution of *N*-methylmorpholine (284 mg, 2.43 mmol, 3.0 eq.) and a 1:1 mixture of 5-chloronaphtho[1,2-*d*]thiazol-2-amine **21** and 5-vinylnaphtho[1,2-*d*]thiazol-2-amine **23** (200 mg, 0.8 mmol, 1 eq.) in tetrahydrofuran (10 mL), *tert* butanol (5 mL) and water (1.5 mL). The mixture was stirred for 2 h. The reaction mixture was quenched with sodium thiosulfate (10 mL, sat. aq.) and stirred for 20 min. The mixture was extracted into ethyl acetate (3 × 20 mL), the organic components were combined, filtered over a pad of Celite® and silica gel, dried over anhydrous magnesium sulfate and concentrated *in vacuo*. The residue was resuspended in tetrahydrofuran (25 mL) and water (10 mL), sodium periodate (693 mg, 3.24 mmol, 4 eq) was added and the mixture stirred for 20 h. The reaction mixture was directly dried over anhydrous magnesium sulfate, filtered, and concentrated *in vacuo*. The residue was purified by silica gel flash column chromatography (diethyl ether / dichloromethane, 1:9) to give **26** (23 mg, 24%): R_f 0.40 (diethyl ether / dichloromethane, 1:9); m.p. 246–248 °C (from acetone); FTIR: ν_{max} (thin film)/cm^{-1} 3300 (N-H, wb), 3111 (C-H, wb), 1660 (C=O, s), 1528 (C=C, m), 1501 (C=C, s); ^{1}H NMR (400 MHz; $(CD_3)SO$) δ_H 10.21 (1H, s, O=C-*H*), 9.25 (1H, dd, *J* 8.6, 1.4, H-6), 8.51 (1H, s, H-4) 8.49 (1H, dd, *J* 7.9, 1.4, H-9), 8.29 (s, 2H, NH_2), 7.69 (1H, ddd, *J* 8.6, 7.9, 1.4, H-7), 7.65 (1H, ddd, *J* 7.7, 6.9, 1.4, H-8); ^{13}C NMR (101 MHz; $(CD_3)SO$)

δ_C 192.0 (C=O), 172.0 (C-2), 154.1 (C-1A), 131.9 (C-4), 129.4 (C-5), 128.0 (C-7), 126.4 (C-8), 125.3 (C-9A), 124.6 (C-6), 124.2 (C-9), 124.1 (C-5A), 119.7 (C-3A); HRMS *m/z* (ESI^+) [Found: 229.0432, $C_{12}H_9ON_2{}^{32}S$ requires $[M+H^+]$ 229.0430]; LRMS *m/z* (ESI^+) 229; HPLC retention time 8.3 min, 86% at 220 nm and 254 nm.

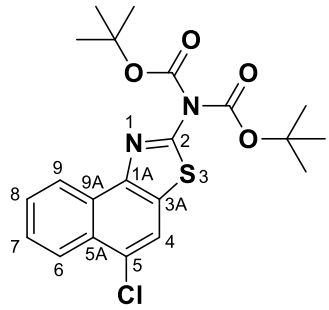
4-Aminonaphthalene-1-carboxylic acid (27)



A solution of sodium hydroxide (952 µL, 50% w/w, aq., 11.9 mmol, 19.8 eq.) was added to a vial containing a solution of 4-amino-1-naphthacarbonitrile **11** (100 mg, 595 µmol, 1.0 eq.) in ethanol (3 mL). The vial was sealed and heated in an oil bath to 100 °C for 1 week. The reaction mixture was directly concentrated *in vacuo*, the residue re-dissolved in hydrochloric acid (10 mL, aq. 2 M) and extracted with ethyl acetate (3 × 10 mL). The combined organic components were dried over anhydrous magnesium sulfate, filtered, and concentrated *in vacuo*. The residue was purified by silica gel flash column chromatography (ethyl acetate / dichloromethane 1:5) to give **27** as a colourless solid (41 mg, 36%): R_f 0.50 (ethyl acetate / dichloromethane 1:5); m.p. 185–189 °C (from acetone); FTIR: ν_{max} (thin film)/cm^{-1} 2918 (w), 1650 (N-H, w), 1572 (C=C, m), 1517 (C=C, m), 1271 (C-N, m); ^{1}H NMR (700 MHz; $(CD_3)SO$) δ_H 12.00 (1H, s, CO_2H), 9.12 (1H, dd, *J* 8.7, 1.3, H-8), 8.15 (1H, dd, *J* 8.4, 1.4, H-5), 8.04 (1H, d, *J* 8.3, H-2), 7.53 (1H, ddd, *J* 8.7, 6.7, 1.4 H-7), 7.40 (1H, ddd, *J* 8.4, 6.7, 1.3, H-6), 6.64 (1H, d, *J* 8.3, H-3), 6.62 (2H, s, NH_2); ^{13}C NMR (176 MHz; $(CD_3)SO$) δ_C 168.5 (CO_2H), 150.2 (C-4), 133.7 (C-2), 133.4 (C-1A), 127.4 (C-7), 125.9 (C-8), 123.6 (C-6), 122.6 (C-5), 121.8 (C-4A), 111.8 (C-1), 105.5 (C-3); HRMS *m/z* (ESI^-) [Found: 186.0559,

$C_{11}H_{10}N_3{}^{32}S$ requires M^- 186.0561]; LRMS *m/z* (ESI^-) 186; HPLC retention time 6.5 min, 99% at 220 nm and 254 nm.

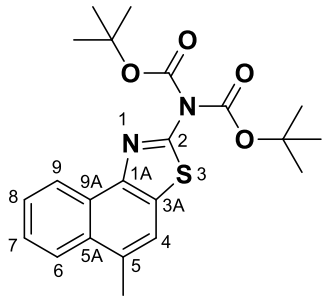
Di-*tert*-butyl (5-chloronaphtho[1,2-*d*]thiazol-2-yl)carbamate (28)



4-Dimethylaminopyridine (156 mg, 1.28 mmol, 1.0 eq.) was added to a solution of 5-chloronaphtho[1,2-d]thiazol-2-amine **21** (300 mg, 1.28 mmol, 1.0 eq.), triethylamine (534 µL, 3.84 mmol, 3.0 eq.) and di-*tert*-butyl dicarbonate (1.18 mL, 5.13 mmol, 40.0 eq.) in tetrahydrofuran (5 mL). The resulting yellow solution was stirred for 2 h. The reaction mixture was quenched by adding hydrochloric acid (20 mL, 1 M, aq.) and stirred for 1 h. The mixture was extracted with ethyl acetate (3 × 20 mL), the combined organic components were dried over anhydrous magnesium sulfate and then concentrated *in vacuo*. The residue was purified by silica gel flash column chromatography (diethyl ether / pentane 1:49) to give **28** as colourless crystalline solid (174 mg, 31%): R_f 0.48 (diethyl ether / pentane 1:49); m.p. 110–112 °C (from acetone); FTIR: ν_{max} (thin film)/cm^{-1} 2985 (C-H, wb), 1767 (m), 1718 (C=O, m), 1510 (C=C, m), 1333 (C-N, s); ^{1}H NMR (700 MHz; $CDCl_3$) δ_H 8.64–8.57 (1H, m, H-9), 8.35–8.25 (1H, m, H-6), 7.94 (1H, s, H-4), 7.71–7.62 (2H, m, H-7 and H-8), 1.63 (18H, s, C(C*H*$_3$)$_3$); ^{13}C NMR (176 MHz; $CDCl_3$) δ_C 157.8 (C-2), 149.5 (C=O), 144.9 (C-1A), 129.4 (C-5A), 128.7 (C-3A), 128.6 (C-9A), 128.2 (C-5), 127.4 (C-8), 126.9 (C-7), 125.0 (C-6), 124.3 (C-9), 118.8 (C-4), 85.5 (2C, 2 × *C*(CH$_3$)$_3$)), 27.9 (6C, 6 × C(*C*H$_3$)$_3$)); HRMS *m/z* (ESI^+) [Found:

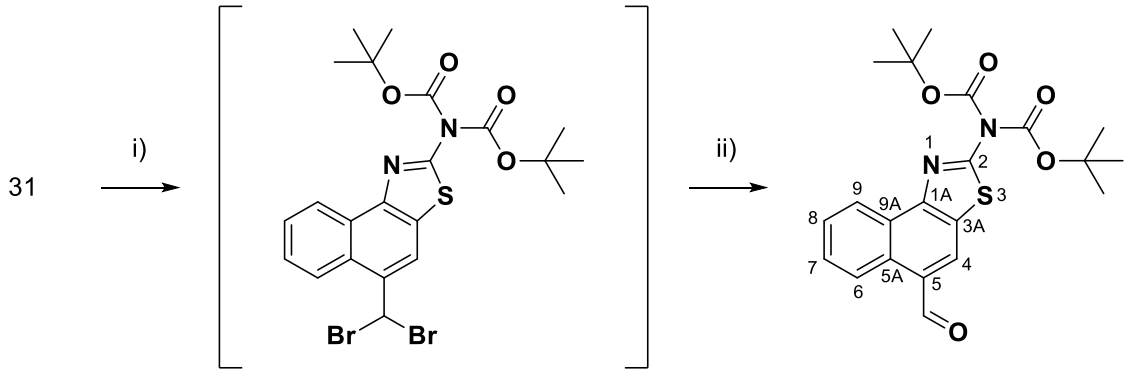
457.0958, $C_{21}H_{23}N_2O_4{}^{35}Cl^{23}Na^{32}S$ requires [M+Na$^+$] 457.0959]; LRMS *m/z* (ESI$^+$) 457; HPLC retention time 8.6 min, >99% at 220 nm and 254 nm.

Di-*tert*-butyl (5-methylnaphtho[1,2-*d*]thiazol-2-yl)iminodicarboxylate (30)



4-Dimethylaminopyridine (18.0 mg, 0.150 mmol, 19.0 mol%) was added to a solution of 5-methylnaphtho[1,2-*d*]thiazol-2-amine **5** (175 mg, 0.80 mmol, 1.00 eq.) and di*tert*butyl dicarbonate (404 µL, 1.76 mmol, 2.20 eq.) in tetrahydrofuran (5 mL). The resulting yellow solution was stirred for 33.5 h. The reaction mixture was quenched by addition of methanol (0.5 mL) and directly concentrated *in vacuo*. The residue was purified by silica gel flash column chromatography (diethyl ether / pentane 1:4) to give **30** as colourless crystalline solid (194 mg, 58%): R_f 0.35 (diethyl ether / pentane 1:4); m.p. 145 °C (from $CDCl_3$); FTIR: ν_{max} (thin film)/cm^{-1} 2978 (C-H, w), 1773 (C=O, m), 1730 (C=O, m), 1328 (C-O, s), 1125 (C-O, s).^{1}H NMR (500 MHz; $CDCl_3$) δ_H 8.67 (1H, dd, *J* 8.2, 1.5, H-9), 8.02 (1H, dd, *J* 8.3, 0.9, H-6), 7.64 (1H, ddd, *J* 8.2, 6.9, 0.9, H-8) 7.65 (1H, s, H-4), 7.59 (1H, ddd, *J* 8.3, 6.9, 1.5, H-7) 2.73 (3H, s, 5-CH_3), 1.63 (18H, s, C(CH_3)$_3$); ^{13}C NMR (125 MHz; $CDCl_3$) δ_C 156.8 (C-2), 150.0 (2C, 2 × C=O), 144.8 (C-1A), 131.7 (C-5 or C-5A), 131.6 (C-5 or C-5A), 129.6 (C-3A), 128.4 (C-9A), 126.6 (C-8), 126.1 (C-7), 124.8 (C-6), 124.5 (C-9), 119.0 (C-4), 85.2 (2C, 2 × *C*(CH$_3$)$_3$), 28.2 (6C, 6 × C(*C*H$_3$)$_3$), 20.3 (5-*C*H$_3$); HRMS *m/z* (ESI$^+$) [Found: 415.1684, $C_{22}H_{27}O_4N_2{}^{32}S$ requires [M+H$^+$], 415.1686]; LRMS *m/z* (ESI$^+$) 415; HPLC retention time 14.8 min*, >99% at 220 nm and 254 nm.

Di-*tert*-butyl (5-formylnaphtho[1,2-*d*]thiazol-2-yl)iminodicarboxylate (31)

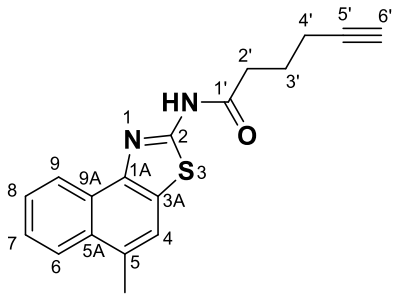


i) – 2,2′-Azobis(2-methylpropionitrile) (59 mg, 0.36 mmol, 0.3 eq) was added to a solution of the iminodicarboxylate **30** (500 mg, 1.21 mmol, 1.0 eq) and *N*-bromosuccinamide (431 mg, 2.42 mmol, 2.0 eq) in carbontetrachloride (5 mL). The reaction mixture was heated under reflux for 2 h allowed before being cooled to room temperature and then stirred for 12 h. The reaction mixture was diluted with ethyl acetate (15 mL) and quenched with HCl (4 × 20 mL, 1 M). The organic components were combined and dried over anhydrous magnesium sulfate, filtered, and concentrated under a stream of nitrogen to give di-*tert*-butyl (5-dibromomethylnaphtho[1,2-*d*]thiazol-2-yl)iminodicarboxylate (356 mg, 52%). The product was used in the next step (ii) without further characterisation due to gradual hydrolysis to **31**. R_f 0.29 (diethyl ether / pentane, 1:19); ^{1}H NMR (400 MHz, $CDCl_3$) δ_H 8.57–8.53 (1H, m), 8.21 (2H, bs), 7.60–7.50 (2H, m), 7.31 (1H, bs), 1.54 (18H, s).

ii) – Silver nitrate (447 mg, 2.63 mmol, 5 eq) was added to a solution of di-*tert*-butyl (5-dibromomethylnaphtho[1,2-d]thiazol-2-yl)iminodicarboxylate (300 mg, 526 µmol, 1.0 eq) in acetone and water (15 mL, 2:1). The reaction mixture was heated under reflux (65 °C) for 0.5 h. The reaction mixture was cooled to room temperature and extracted with ethyl acetate (15 mL). The organic components were washed with brine (15 mL), dried over anhydrous magnesium sulfate, filtered, and concentrated *in vacuo.* The

residue was purified by silica gel flash column chromatography (diethyl ether / pentane 1:19) to give **31** as colourless crystalline solid (96 mg, 43%): R_f 0.29 (diethyl ether / pentane, 1:19); m.p. 146-148 °C (from $CDCl_3$); FTIR: ν_{max} (thin film)/cm^{-1} 2980 (C-H, w), 1780 (C=O, m), 1731 (C=O, m), 1687 (C=O, m), 1328 (C-H, s); ^{1}H NMR (400 MHz, $CDCl_3$) δ_H 10.35 (1H, s, O=C-H), 9.28 (1H, dd, *J* 8.2, 1.4, H-9), 8.60 (1H, dd, *J* 7.6, 2.0, H-6), 8.30 (1H, s, H-4), 7.60 (1H, ddd, *J* 8.2, 7.2, 2.0, H-8) (1H, ddd, *J* 7.6, 7.2, 1.4, H-7), 1.66 (18H, s, C(C*H*$_3$)$_3$); ^{13}C NMR (101 MHz, $CDCl_3$) δ_C. 192.1 (*C*=O), 161.6 (C-2), 150.2 (C-1A), 149.1 (2C, 2 × O-*C*=O), 130.6 (C-4), 129.6 (C-5A), 128.4 (C-7), 128.1 (3A), 127.8 (C-5), 127.3 (C-8), 127.2 (C-9A), 125.2 (C-6), 124.2 (C-9), 85.9 (2C, 2 × *C*(CH$_3$)), 27.8 (6C. 6 × C(*C*H$_3$)); [Found: 429.1476, $C_{22}H_{25}O_5N_2{}^{32}S$ requires [M+H$^+$] 429.1479]; LRMS *m/z* (ESI$^+$) 429.

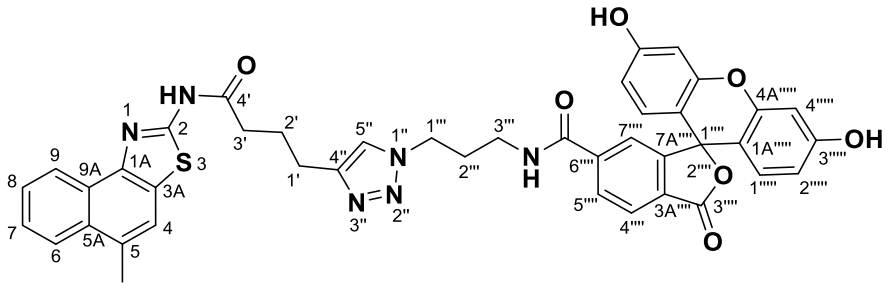
***N*-(5-Methylnaphtho[1,2-*d*]thiazol-2-yl)hex-5-ynamide (32)**



Hex-5-ynoyl chloride (20 mg, 0.15 mmol, 0.7 eq.) was added dropwise to a stirring solution of 5-methylnaphtho[1,2-*d*]thiazol-2-amine **5** (50 mg, 0.23 mmol, 1.0 eq.), 4-dimethylaminopyridine (15 mg, 0.12 mmol, 0.5 eq.) and triethylamine (96 µL, 0.69 mmol, 3.0 eq.) in anhydrous dichloromethane (1.5 mL) and anhydrous tetrahydrofuran (1.5 mL) at 4 °C. The reaction mixture was allowed to warm to room temperature, stirred over 2 h and then directly concentrated *in vacuo*. The residue was purified by silica gel flash column chromatography (dichloromethane, 0.1% triethylamine) to give **32** as a colourless solid (16 mg, 47%): R_f 0.32 (dichloromethane,

0.1% triethylamine); m.p. 139–141 °C (acetone); FTIR: ν_{max} (thin film)/cm^{-1}; 3304 (N-H, w), 2225 (C≡C, wb), 1692 (C-H, w), 1551 (C=C, s), 1273 (C-N, m); ^{1}H NMR (400 MHz; $CDCl_3$) δ_H 10.96 (1H, s, NH), 8.67–8.55 (1H, m, H-6), 8.12–8.07 (1H, m, H-9), 7.73 (1H, s, H-4), 7.61-7.49 (2H, m, H-7 and H-8), 2.79 (3H, s, 5-C*H*$_3$), 2.45 (2H, t, *J* 7.1, C-2′), 2.08 (2H, dt, *J* 7.1, 2.7, C-4′), 1.84 (2H, tt, *J* 7.1, C-3′), 1.76 (1H, t, *J* 2.7, H-6′); ^{13}C NMR (101 MHz; $CDCl_3$) δ_C 170.6 (C-1′), 157.3 (C-2), 142.8 (C-1A), 131.4 (C-5), 131.1 (C-5A), 125.7 (C-3A), 127.5 (C-9A), 127.0 (C-8), 126.2 (C-7), 124.7 (C-6), 123.3 (C-9), 118.8 (C-4), 82.5 (C-5′), 69.2 (C-6′), 34.5 (C-2′), 23.2 (C-3′), 19.8 (5-*C*H$_3$), 17.4 (C-4′); HRMS *m/z* (ESI$^+$) [Found: 309.1058, $C_{18}H_{17}N_2O^{32}S$ requires [M+H$^+$] 309.1056]; LRMS *m/z* (ESI$^+$) 309; HPLC retention time 9.6 min, 98% at 220 nm and 254 nm.

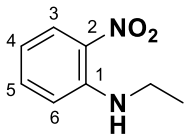
3'''',6''''-Dihydroxy-N-(3'''-(4''-(4'-((5-methylnaphtho[1,2-*d*]thiazol-2-yl)amino)-4'-oxobutyl)-1*H*-1'',2'',3''-triazol-1''-yl)propyl)-3''''-oxo-3*H*-spiro[isobenzofuran-1'''',9''''-xanthene]-6''''-carboxamide (33)



Sodium L-ascorbate (70 µL, 0.10 M in water, 7.0 µmol, 14 mol%) was added to a solution of *N*-(5-methylnaphtho[1,2-d]thiazol-2-yl)hex-5-ynamide **32** (16 mg, 50 µmol, 1.0 eq.), 4-((3-azidopropyl)carbamoyl)-2-(3,6-dihydroxy-9H-xanthen-9-yl)benzoic acid (23 mg, 50 µmol, 1.0 eq.), tris[(1-benzyl-1*H*-1,2,3-triazol-4-yl)methyl]amine (2 mg, 4 µmol, 7 mol%) and copper sulfate (83 µL, 0.1 M in water, 3.5 µmol, 7 mol%) in *tert*-butanol (314 µL), water (314 µL) and dimethylformamide (628 µL). The reaction mixture

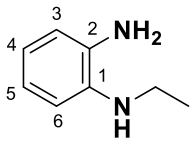
was stirred for 20 h and then extracted with ethyl acetate (3 × 10 mL). The combined organic components were dried over anhydrous magnesium sulfate, filtered, and concentrated *in vacuo*. The residue was purified silica gel flash column chromatography (dichloromethane / (dichloromethane, ethanol acetic, acid gradient 84:15:1) from 0 to 80%) to give **33** as an orange solid (25 mg, 66%): R_f 0.20 (ethanol / dichloromethane 1:9, 1% acetic acid); m.p. 113-115 °C (from ethanol); FTIR: ν_{max} (thin film)/cm^{-1} 3260 (O-H, bw), 2980 (N-H, s), 1757 (C=O, m), 1547 (C=C, s), 1453 (O-H, m), 1179 (C-N, s); ^{1}H NMR (400 MHz; (CD$_3$)SO) δ_H δ_H 8.75 (1H, t, *J* 5.6, 3′′′-NH), 8.53 (1H, dd, *J* 8.0, 1.7, H-6), 8.17 (1H, dd, *J* 8.3, 1.4, H-5′′′′), 8.09 (1H, d, *J* 6.8, H-9), 8.07 (1H, d, *J* 5.5, H-4′′′′), 7.90 (1H, s, H-5′′), 7.89 (1H, s, H-4), 7.70–7.60 (2H, m, H-7 and H-8), 7.67 (1H, s, H-7′′′′), 6.69 (2H, d, *J* 2.2, H-2′′′′′), 6.63–6.56 (4H, m, H-1′′′′′ and H-4′′′′′), 4.32 (2H, t, *J* 6.6, H-1′′′), 3.22 (2H, dt, *J* 6.6, 6.1, H-3′′′), 2.70 (s, 3H, 5-C*H*$_3$), 2.66 (2H, t, *J* 7.4, H-3′), 2.57 (2H, t, *J* 7.4, H-1′), 2.02 (2H, tt, *J* 6.6 H-2′′′), 1.95 (2H, tt, *J* 7.4, H-2′); ^{13}C NMR (101 MHz; (CD$_3$)SO) δ_C 171.7 (C-4′), 168.1 (C-3′′′′), 164.8 (6′′′′-C=O), 156.9 (C-2), 151.9 (4C, 2× C-3′′′′′ and 2 × C-4A′′′′′), 146.1 (C-4′′), 143.2 (C-1A), 140.6 (C-5), 130.9 (C-7A′′′′), 130.0 (2C, 2 × C-1′′′′′), 129.4 (C-5A), 129.3 (C-4), 126.9 (C-4′′′′), 126.8 (C-5′′′′), 126.3 (C-7), 125.8 (C-8), 125.0 (C-9A), 124.8 (C-9), 123.25 (C-6), 122.20 (C-3A), 122.1 (C-5′′), 119.3 (C-7′′′′), 112.8 (2C, 2 × C-2′′′′′), 109.2 (2C, 2 × C-1A′′′′′), 102.3 (2C, 2 × C-4′′′′′), 47.2 (C1′′′), 36.9 (C-3′′′), 34.5 (C-1′), 29.7 (C-2′′′), 24.50 (C-3′), 24.45 (C-2′), 19.4 (5-*C*H$_3$), fluorescein moiety carbons C-1′′′′, C-3A′′′′ and C-6′′′′ were not observed due to open and closed lactone equilibrium[15]; HRMS *m/z* (ESI$^+$) [Found: 767.2274, $C_{42}H_{35}O_7N_6{}^{32}S$ requires [M+H$^+$] 767.2282]; LRMS *m/z* (ESI$^+$) 767; HPLC retention time 9.1 min, 98% at 220 and 254 nm.

N-Ethyl-2-nitroaniline (35)[16,17]



Ethylamine (15.0 mL, 2 M in tetrahydrofuran, 30.0 mmol, 4.2 eq.) was added to a solution of 1,2-fluoronitrobenzene **34** (750 µL, 7.10 mmol, 1.0 eq.) in dimethyl formamide (15 mL) at room temperature. The solution turned from colourless to orange upon addition. The mixture was stirred for 22 h. Brine (25 mL) was added to the reaction mixture and was extracted with ethyl acetate (3 × 25 mL). The combined organic components were dried over anhydrous magnesium sulfate, filtered, and concentrated *in vacuo.* The residue was purified by silica gel flash column chromatography (ethyl acetate / pentane 1:19) to give **35** as a clear orange oil (1.179 g, 99%): R_f 0.40 (ethyl acetate / pentane 1:19); ^{1}H NMR (400 MHz; $CDCl_3$) δ_H 8.15 (1H, dd, *J* 8.5, 1.6, H-3), 7.97 (1H, br s, NH), 7.42 (1H, dddd, *J* 8.7, 6.9, 1.6, 0.7, H-5), 6.83 (1H, dd, *J* 8.7, 1.3, H-6), 6.62 (1H, ddd, *J* 8.5, 6.9, 1.3, H-4), 3.34 (2H, qd, *J* 7.2, 5.0, CH_2), 1.36 (3H, t, *J* 7.2, CH_3); ^{13}C NMR (101 MHz; $CDCl_3$) δ_C 145.6 (C-1), 136.3 (C-5), 131.8 (C-2), 127.0 (C-3), 115.2 (C-4), 113.8 (C-6), 37.8 (*C*H_2), 14.5 (*C*H_3); LRMS *m/z* (ESI$^+$) 189 [M+Na$^+$]. Data are consistent with literature values.[16]

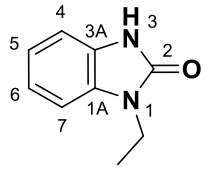
N-Ethylbenzene-1,2-diamine (36)[17]



Methanol (6.00 mL, 149 mmol, 19.3 eq.) was added dropwise over 1 h to a suspension of *N*-ethyl-2-nitroaniline **35** (1.28 g, 7.71 mmol, 1.0 eq.), sodium borohydride (585 mg, 15.3 mmol, 2.0 eq.) and 5% Pd/C (600 mg, 47%) in anhydrous tetrahydrofuran (15 mL). Effervescence was observed upon initial methanol addition and the reaction mixture

turned dark red from orange. After 0.5 h, the reaction mixture was judged to be complete by TLC analysis (visualised under U.V. light and stained with ninhydrin) and was directly concentrated *in vacuo*. The residue was purified by silica gel flash column chromatography (dichloromethane + 0.1% triethylamine) to give **36** as a dark red oil (847 mg, 81%): R_f 0.33 (dichloromethane + 0.1% triethylamine); ^{1}H NMR (400 MHz; $CDCl_3$) δ_H 7.13 (1H, ddd, *J* 7.6, 1.5, H-5), 6.98 (1H, ddd, *J* 7.7, 1.5, H-4), 6.92 (1H, dd, *J* 7.7, 1.5, H-3), 6.88 (1H, dd, *J* 7.6, 1.5, H-6), 3.57 (3H, br s, NH and NH_2), 3.33 (2H, q, *J* 7.1, CH_2), 1.48 (3H, t, *J* 7.1, CH_3); ^{13}C NMR (101 MHz; $CDCl_3$) δ_C 137.4 (C-1), 133.8 (C-2), 120.0 (C-5), 117.9 (C-4), 115.8 (C-6), 111.0 (C-3), 38.2 (*C*H_2), 14.4 (*C*H_3); LRMS *m/z* (ESI$^+$) 159 [M+Na$^+$].

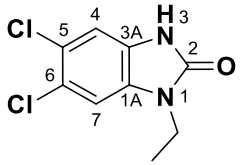
1-Ethyl-1,3-dihydro-2*H*-benzoimidazole-2-one (37) (*EBIO*)[17]



A solution of carbonyldiimidazole (1.20 g, 7.40 mmol, 1.3 eq.) in tetrahydrofuran (10 mL) was added dropwise over 0.5 h to a solution of *N*-ethylbenzene-1,2-diamine **36** (800 mg, 5.88 mmol, 1.0 eq.) in tetrahydrofuran (20 mL). The reaction mixture was stirred for 26 h and turned from dark red to colourless. The reaction mixture was quenched with sodium bicarbonate (50 mL, sat. aq.) and extracted with ethyl acetate (3 × 50 mL). The organic components were combined, dried over anhydrous magnesium sulfate, filtered, and concentrated *in vacuo*. The residue was purified by silica gel flash column chromatography (ethyl acetate / dichloromethane 1:9 + 0.1% triethylamine) to give **37** as a colourless solid (777 mg, 81%,): R_f 0.26 (ethyl acetate / dichloromethane 1:9 + 0.1% triethylamine); m.p. 117-118 °C (from $CDCl_3$); FTIR: ν_{max} (thin film)/cm^{-1} 3548 (N-H, w), 3066 (C-H, b), 1673 (C=O, sb), 1489 (C-H, m), 724 (s),

683 (s); ^{1}H NMR (400 MHz; $CDCl_3$) δ_H 10.62 (1H, br s, NH), 7.16 (1H, dd, *J* 7.2, 2.1, H-4), 7.09 (1H, ddd, *J* 7.2, 7.2, 1.6, H-5) 7.06 (1H, ddd, *J* 7.0, 7.2, 2.1, H-6), 7.01 (1H, dd, *J* 7.0, 1.9, H-7), 3.97 (2H, q, *J* 7.3, C*H*$_2$), 1.37 (3H, t, *J* 7.3, C*H*$_3$); ^{13}C NMR (101 MHz; $CDCl_3$) δ_C 155.8 (C-2), 130.0 (C-1A), 128.4 (C-3A), 121.5 (C-6), 121.3 (C-5), 110.0 (C-4), 107.8 (C-7), 35.7 (*C*H$_2$), 13.8 (*C*H$_3$); HRMS *m/z* (ESI$^+$) [Found: 163.0871, $C_9H_{10}N_2O$ requires [M+H$^+$] 163.0866.]; LRMS *m/z* (ESI$^+$) 163; HPLC retention time 6.6 min, 99% at 220 nm and 254 nm.

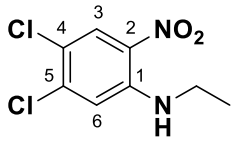
5,6-Dichloro-1-ethyl-1,3-dihydro-2*H*-benzoimidazole-2-one (38) (*DCEBIO*)[17]



A solution of carbonyldiimidazole (266 mg, 1.64 mmol, 1.4 eq.) in tetrahydrofuran (6.5 mL) was added dropwise over 0.5 h to a solution of diamine **41** (240 mg, 1.17 mmol, 1.0 eq.) in tetrahydrofuran (6.5 mL). The reaction mixture was stirred for 46 h before being diluted with water and extracted with ethyl acetate (3 × 10 mL). The organic components were combined, dried over anhydrous magnesium sulfate, filtered, and concentrated *in vacuo*. The residue was purified by silica gel flash column chromatography (ethyl acetate / dichloromethane 1:3) to give **38** as a colourless solid (177 mg, 70%): R_f 0.28 (ethyl acetate / dichloromethane 1:3); m.p. 173 °C (sublimation). (from $CDCl_3$); FTIR: ν_{max} (thin film)/cm^{-1} 2918 (N-H, w), 2849 (C-H, w), 2360 (C-H, w), 1699 (CO, s), 1491 (Ar-H, s); ^{1}H NMR (500 MHz; $(CD_3)SO$) δ_H 11.13 (1H, s, NH), 7.48 (1H, s, H-7), 7.15 (1H, s, H-4), 3.81 (2H, q, *J* 7.2, C*H*$_2$), 1.17 (3H, t, *J* 7.2, C*H*$_3$); ^{13}C NMR (125 MHz; $(CD_3)SO$) δ_C 153.9 (C-2), 130.0 (C-1A), 128.3 (C-3A), 122.7 (C-5 or C-6), 122.6 (C-5 or C-6), 109.9 (C-7), 109.2 (C-4), 35.0 (*C*H$_2$), 13.3 (*C*H$_3$); HRMS *m/z* (ESI$^+$)

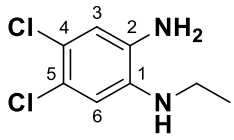
[Found: 231.0089. $C_9H_9ON_2{}^{35}Cl_2$ requires [M+H$^+$] 231.0086]; LRMS *m/z* (ESI$^+$) 231.0; HPLC retention time 8.7 min, >99% at 220 nm and 254 nm.

4,5-Dichloro-*N*-ethyl-2-nitroaniline (40)



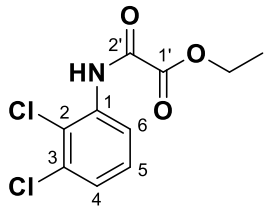
Ethylamine (3.30 mL, 3.80 mmol, 2 M in tetrahydrofuran, 1.6 eq.) was added to a solution of 1,2-dichloro-4-fluoro-5-nitrobenzene **39** (318 µL, 2.43 mmol, 1.0 eq.) in *N,N*-dimethylformamide (3 mL). The reaction mixture was stirred for 3 d and turned from colourless to orange. The reaction mixture was basified with potassium carbonate (5 mL, sat. aq.) and extracted with ethyl acetate (3 × 5 mL). The organic components were combined and dried over anhydrous magnesium sulfate, filtered, and concentrated under vacuum. The residue was purified using silica gel flash column chromatography (diethyl ether / pentane 1:19) to give **40** as a yellow solid (535 mg, 86%): R_f 0.59 (diethyl ether / pentane 1:19); m.p. 177 °C (from dichloromethane); FTIR: ν_{max} (thin film)/cm^{-1} 3379 (N-H, w), 3113 (C-H, w), 1569 (N=O, m), 1279 (N-C, m), 1257 (s); ^{1}H NMR (400 MHz; $CDCl_3$) δ_H 8.27 (1H, s, H-6), 7.88 (1H, br s, NH), 6.96 (1H, s, H-3), 3.32 (2H, dq, *J* 7.1, C*H*$_2$), 1.38 (3H, t, *J* 7.1, C*H*$_3$); ^{13}C NMR (101 MHz; $CDCl_3$) δ_C 144.1 (C-2), 141.3 (C-1), 130.5 (C-4), 127.8 (C-6), 118.7 (C-5), 115.1 (C-3), 38.2 (*C*H$_2$), 14.3 (*C*H$_3$); HRMS *m/z* (ESI$^+$) [Found: 235.0036, $C_8H_9N_2{}^{35}Cl_2$ requires [M+H$^+$] 235.0036]; LRMS *m/z* (ESI$^+$) Not found; HPLC retention time 11.8 min, >99% at 254 nm and 220 nm.

4,5-Dichloro-*N*-ethylbenzene-1,2-diamine (41)



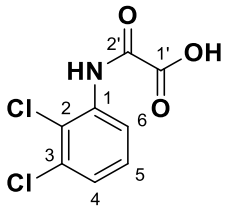
Activated iron powder (641 mg, 120%) was added to a solution of 4,5-dichloro-*N*-ethyl-2-nitroaniline **40** (535 mg, 2.29 mmol, 1 eq.) in acetic acid (8 mL). The reaction mixture was stirred at 100 °C for 1 h and judged to be complete by TLC analysis (visualised under U.V. light and stained with ninhydrin). The reaction mixture was cooled to room temperature, filtered through a pad of Celite® washed with methanol (30 mL) and concentrated *in vacuo*. The residue was resuspended in sodium carbonate (10 mL, sat. aq.) and extracted into ethyl acetate (3 × 5 mL). The organic components were combined, dried over anhydrous magnesium sulfate, filtered, and concentrated *in vacuo*. The residue was purified by silica gel flash column chromatography (diethyl ether / pentane 1:9) to give the **41** as an air sensitive, colourless oil (240 mg, 47%). The product was used in the next step without further characterisation due to facile decomposition in air: R_f 0.24 (diethyl ether / pentane 1:9); ^{1}H NMR (400 MHz; $CDCl_3$) δ_H 6.66 (1H, s, H-3), 6.59 (1H, s, H-6), 3.29 (3H, br s, NH_2 and NH), 3.02 (1H, q, *J* 7.3, C*H*$_2$), 1.25 (3H, t, *J* 7.3, C*H*$_3$); ^{13}C NMR (101 MHz; $CDCl_3$) δ_C 137.8 (C-1), 133.7 (C-2), 122.8 (C-5), 119.9 (C-4), 116.9 (C-3), 112.2 (C-6), 38.6 (*C*H$_2$), 14.6 (*C*H$_3$).

Ethyl-2′-((2,3-dichlorophenyl)amino)-2′-oxoacetate (43)



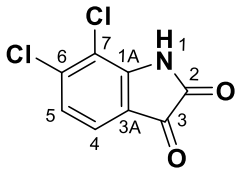
A solution of triethylamine (862 µL, 6.20 mmol, 2.0 eq.) in dichloromethane (7 mL) was added dropwise over 0.5 h to a solution of ethyl oxylyl chloride (370 µL, 3.26 mmol, 1.1 eq.) and 2,3-dichloro aniline **42** (500 mg, 3.11 mmol, 1.0 eq.) in dichloromethane (9 mL) at −14 °C (salted ice). The reaction mixture was stirred for 1 h then allowed to warm to room temperature over 12 h. The reaction mixture was quenched by the addition of sodium bicarbonate (25 mL, sat. aq.) and extracted with ethyl acetate (3 × 25 mL). The organic components were combined, dried over anhydrous magnesium sulfate, filtered, and concentrated *in vacuo*. The residue was purified by silica gel flash column chromatography (diethyl ether / pentane 1:19) to give **43** as a colourless solid (520 mg, 64%): R_f 0.14 (diethyl ether / pentane 1:19); m.p. 63–65 °C (from dichloromethane); FTIR: ν_{max} (thin film)/cm^{-1} 3373 (N-H, w), 1727 (C=O, mb), 1305 (N-C, m), 786 (C-Cl, s); ^{1}H NMR (500 MHz; $CDCl_3$) δ_H 9.56 (1H, s, NH), 8.39 (1H, dd, *J* 7.7, 2.1, H-4), 7.33–7.22 (2H, m, H-5 and H-6), 4.45 (2H, q, *J* 7.2, C*H*$_2$), 1.44 (3H, t, *J* 7.2, C*H*$_3$); ^{13}C NMR (125 MHz; $CDCl_3$) δ_C 160.3 (C-1′), 154.0 (C-2′), 134.9 (C-3), 133.1 (C-2), 128.0 (C-5), 126.5 (C-6), 122.2 (C-1), 119.1 (C-4), 64.1 (*C*H$_2$), 14.0 (*C*H$_3$); HRMS *m/z* (ESI$^+$) [Found: 283.9856, $C_{10}H_9Cl_2NO_3$ requires [M+Na$^+$], 283.9852]; LRMS *m/z* (ESI$^+$) 284 [M+Na$^+$]; HPLC retention time 10.2 min, 91% at 220 and 254 nm.

2′-((2,3-Dichlorophenyl)amino)-2′-oxoacetic acid (44)



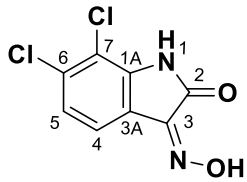
Ethyl-2-((2,3-dichlorophenyl)amino)-2-oxoacetate **43** (500 mg, 1.90 mmol, 1 eq.) was added to a solution of sodium hydroxide (230 mg, 5.70 mmol, 3 eq.) in ethanol (40 mL). The reaction mixture was stirred for 20 h, after which water was added. The precipitate suspension was filtered, the filter cake was acidified with several drops of hydrochloric acid (3 M, aq) and resuspended in ethyl acetate (100 mL). The solution was dried over anhydrous magnesium sulfate, filtered, and concentrated *in vacuo* to give **44** as a colourless solid (285 mg, 64%): R_f 0.29 (ethanol / ethyl acetate 1:9, 0.1% acetic acid); m.p. 140–142 °C (from MeOH); FTIR: ν_{max} (thin film)/cm^{-1} 3537 (O-H, w),3342 (N-H, w),1694 (C=O, s),1589 (C=C, m), 774 (C-Cl, w).^{1}H NMR (400 MHz; $(CD_3)SO$) δ_H 10.37 (1H, s, OH), 7.75 (1H, dd, *J* 8.1, 1.5, H-4), 7.55 (1H, dd, *J* 8.1, 1.5, H-6), 7.42 (1H, dd, *J* 8.1, H-5); ^{13}C NMR (101 MHz; $(CD_3)SO$) δ_C 161.5 (C-1′), 156.8 (C-2′), 135.6 (C-3), 132.1 (C-2), 128.4 (C-5), 127.8 (C-4), 125.9 (C-1), 24.3 (C-6); HRMS *m/z* (ESI$^-$) [Found: 231.9572, $C_8H_4O_3N^{35}Cl_2$ requires M$^-$ 231.9574]; LRMS *m/z* (ESI$^-$) 232; HPLC retention time 7.6 min, 99%.

6,7-Dichloroindoline-2,3-dione (46)



Hydrochloric acid (6.45 mL, 37% w/v, 77.4 mmol, 8.3 eq.) was added dropwise to a solution of 2,3-dichloroaniline **42** (1.50 g, 9.32 mmol, 1.0 eq.), chloral hydrate (1.68 g, 10.2 mmol, 1.1 eq.) and sodium sulfate (10.5 g, 74.0 mmol, 7.9 eq.) in water (20 mL). The reaction mixture was heated under reflux for 1 h, assessed by TLC analysis (visualised under U.V. light). The resulting yellow precipitate suspension was cooled to room temperature, filtered, and the filter cake was dried under suction before being added to preheated sulfuric acid (15 mL, 95% w/v) at 50 °C over 15 min. The mixture was heated to 65 °C and stirred for 1 h. The brick red precipitate suspension was filtered, and the filter cake was dried under suction before being purified by silica gel flash column chromatography (diethylether / pentane 3:7) to give **46** as an orange solid (586 mg, 29%): R_f 0.31 (diethylether / pentane 3:7); m.p. 184–185 °C (from methanol); FTIR: ν_{max} (thin film)/cm^{-1}; 3373 (N-H, w), 1727 (C=O, mb), 1305 (C-H, m), 786 (s); ^{1}H NMR (400 MHz; $(CD_3)SO$) δ_H 11.63 (1H, s, NH), 7.50 (1H, d, *J* 8.0, H-4), 7.32 (1H, d, *J* 8.0, H-5); ^{13}C NMR (101 MHz; $(CD_3)SO$) δ_C 182.5 (C-3), 159.8 (C-2), 149.4 (C-1A), 139.8 (C-6), 123.9 (C-4), 123.8 (C-5), 118.4 (C-7), 114.9 (C-3A); HRMS *m/z* (EI$^-$) [Found: 213.9470, $C_8H_2Cl_2NO_2$ requires M$^-$ 213.9468]; LRMS *m/z* (ESI$^+$) 238 [M+Na$^+$].

6,7-Dichloro-3-(hydroxyimino)indolin-2-one (47) (*NS309*)[18]



Hydroxylammonium chloride (82 mg, 1.2 mmol, 1.3 eq.) was added to a solution of 6,7-dichloroindoline-2,3-dione **46** (200 mg, 1.00 mmol, 1 eq.) in water (4 mL) and the reaction mixture was heated under reflux for 0.5 h. Sodium acetate (133 mg, 1.62 mmol, 1.8 eq.) was added to the reaction mixture. Heating under reflux was continued for a further 0.5 h. The reaction mixture was cooled to 4 °C and the resulting yellow precipitate suspension was filtered, and the filter cake was dried under vacuum. The precipitate was purified by silica gel flash column chromatography (diethyl ether / pentane 1:1) to give **47** as pale yellow solid (90 mg, 43%): R_f 0.33 (diethyl ether / pentane 1:1); m.p. 254 °C (sublimation) (from methanol); FTIR: ν_{max} (thin film)/cm^{-1} 3175 (O-H, b), 2360 (C=N, w), 1732 (C=O, s), 1609 (C=C, s), 1047 (s); ^{1}H NMR (400 MHz; $(CD_3)SO$) δ_H 13.69 (1H, s, OH), 11.32 (1H, s, NH), 7.87 (1H, d, *J* 8.1, H-4), 7.25 (1H, d, *J* 8.1, H-5); ^{13}C NMR (101 MHz; $CDCl_3$) δ_C 164.5 (C-2), 143.3 (C-3), 141.9 (C-1A), 134.0 (C-6), 126.0 (C-4), 123.4 (C-5), 115.9 (C-7), 113.2 (C-3A); HRMS *m/z* (ESI^+) [Found: 252.9543, $C_8H_4Cl_2N_2O_2$ requires [$M+Na^+$], 252.9542]; LRMS *m/z* (ESI^+) 231 [$M+H^+$], 253 [$M+Na^+$]; HPLC retention time 7.8 min, 99% at 220 nm and 254 nm.

6.4 Experimental Pharmacology Details

6.4.1 Animal Procedures and Isolated Tissue Preparation

Male Wistar rats (200-250g) were euthanised using procedures defined by the Animals (Scientific Procedures) Act 1986, UK (Schedule 1 procedure). Mesenteric tissue was excised from each rat and placed in ice cold (4 °C) 3-Morpholinopropane-1-

sulfonic acid (MOPS) buffered solution (MOPS (2 mM), NaCl (145 mM), KCl (4.7 mM), $CaCl_2$ (2 mM), $MgSO_4$ (1.17 mM), NaH_2PO_4 (1.2 mM), glucose (5 mM), pyruvate (2 mM), EDTA (0.02 mM) and NaOH (2.75 mM) adjusted to pH 7.4.). 2 mm ring segments of third-order mesenteric arteries (180–320 μm diameter) were dissected from the surrounding fat and cleaned of connective tissue. Isolated arteries were mounted on a multi myograph system 610M (Danish Myo Technology A/S) connected to a PowerLab 4/20 data acquisition system (AD instruments) and recorded using LabChart 7 software (AD instruments). Isolated arteries were mounted using 25 μm diameter gold plated tungsten wires connected to the myograph stage force transducer and a micrometer. Mounted arteries were submerged in Krebs (NaCl (118.0 mM), $NaCO_3$ (25 mM), KCl (3.6 mM), $MgSO_4 \cdot 7H_2O$ (1.2 mM), KH_2PO_4 (1.2 mM), glucose (11.0 mM), $CaCl_2$ (2.5 mM)) or MOPS buffered solutions (5 mL) in a temperature regulated chamber maintained at 37 °C. Krebs solutions were constantly gassed with a mixture of oxygen, carbon dioxide and nitrogen (21:5:74). The chamber solution was replaced 0.5 h. The endothelial nitric oxide synthase (eNOS) inhibitor L-N^{ω} - nitroarginine methyl ester (L-NAME) (100 μM) was present during all experiments to suppress nitric oxide (NO)–mediated relaxation.

Arteries were gradually set to a normalised resting tension equivalent to that generated at 90% of the diameter of the vessel at 70 mmHg. Only vessels with a functional endothelium were used in experiments; assessed by >95% relaxation in response to acetylcholine (ACh) (1 μM) pre-constricted with 10 μM phenylephrine (PE). The endothelium was removed with a human hair and denudation confirmed by <5% dilation to 1 μM Ach. Absolute maximal vessel constriction of all preparations was measured at the end of experimentation using PE (10 μM) in the presence of KCl (45 mM).

6.4.2 Assessment of Vasodilation to Novel and Published Small Molecule K_{Ca} Channel Modulators

Measurement of changes in wall tension (mN) was used to obtain dose response curves to ACh after submaximal pre-constriction to PE. In MOPS buffered solution, pre-constricted arteries were incrementally dilated with ACh before and after 0.5 h pre-incubation with SKA113 **4** (10 μM), SKA111 **5** (1 μM) or EBIO **37** (300 μM). Dose response curves of the synthesised test molecules were also collected after preconstruction with a submaximal concentration of PE. The effect of a single or combinations of multiple channel blockers; TRAM-34 (1 μM), apamin (100 nM) and either iberiotoxin (100 nM) or paxilline (100 nM), on observed test molecule direct dilation responses was investigated. The effect of endothelial denudation on observed test molecule direct dilation responses was also investigated.

6.4.3 Drugs and Solutions

All test molecules used were synthesised inhouse. All drugs were purchased from Sigma-Aldrich, except for, except iberiotoxin (Latoxan, Rosans, France). Inhibitors, ACh and PE stock solutions were prepared in MilliQ water, except TRAM34 which was dissolved in dimethylsulfoxide. Stock solutions of test compounds (200 mM) were made in dimethylsulfoxide. Stock solutions were serially diluted with physiological buffer to test concentrations immediately prior to experiments. The final dimethylsulfoxide concentration in the myograph chamber was maintained below 0.3% to avoid vehicle-associated artefacts. The inhibitors L-NAME (100 μM) was added to the incubation solution, and arterioles were equilibrated for at least 0.5 h prior to obtaining responses. Calcium activated potassium channel blockers; TRAM34 (1 μM), apamin (100 nM) and iberiotoxin (100 nM) were directly added to incubation solutions and equilibrated for at least 1 h prior to obtaining responses. Channel inhibitor and test compounds were added directly to the 5 mL incubation solution and mixed by gassing.

6.4.4 Data Analysis

Data sampling was performed using LabChart 7 and summarised as the mean ± SEM of n arterioles, where one n is equivalent to one animal. Constriction measurement samples were taken as 5 second windows of constriction plateau after each addition of vasoconstrictor or vasorelaxant. Data analysis, including non-linear sigmoidal line fitting and ACh EC_{50} calculation, was performed using Prism (GraphPad Software) software packages. Statistical comparisons were made using repeated measures two-way ANOVA with Bonferroni's post-test as appropriate, where $P < 0.05$ was considered significant. Dilation to each compound was expressed as the % of maximum artery contraction; 100% being the maximum diameter in each experiment.

Chapter 6 References

1. Zhang, M., Pascal, J. M., Schumann, M., Armen, R. S. & Zhang, J.-F. Identification of the functional binding pocket for compounds targeting small-conductance Ca^{2+}-activated potassium channels. *Nat. Commun.* **3,** 1021 (2012).

2. Chothia, C. & Lesk, A. M. The relation between the divergence of sequence and structure in proteins. *EMBO J.* **5,** 823–6 (1986).

3. Arnold, K., Bordoli, L., Kopp, J. & Schwede, T. The SWISS-MODEL workspace: A web-based environment for protein structure homology modelling. *Bioinformatics* **22,** 195–201 (2006).

4. Dunbrack, R. L. Rotamer libraries in the 21st century. *Curr. Opin. Struct. Biol.* **12,** 431–440 (2002).

5. Grosdidier, A., Zoete, V. & Michielin, O. Fast docking using the CHARMM force field with EADOCK DSS. *J. Comput. Chem.* **32,** 2149–2159 (2011).

6. Jakalian, A., Jack, D. B. & Bayly, C. I. Fast, efficient generation of high-quality atomic charges. AM1-BCC model: II. Parameterization and validation. *J. Comput. Chem.* **23,** 1623–1641 (2002).

7. Maier, J. A. *et al.* ff14SB: Improving the Accuracy of Protein Side Chain and Backbone Parameters from ff99SB. *J. Chem. Theory Comput.* **11,** 3696–3713 (2015).

8. Qiagen. CLC Drug Discovery Workbench User Manual. 1–367 (2014).

9. Vainio, M. J. & Johnson, M. S. Generating conformer ensembles using a multiobjective genetic algorithm. *J. Chem. Inf. Model.* **47,** 2462–2474 (2007).

10. Laforsh, C. & Tollrian, R. High efficiency transformation of *Escherichia coli* with plasmids. *Gene* **96,** 23–28 (1990).

11. Niesen, F. H., Berglund, H. & Vedadi, M. The use of differential scanning fluorimetry to detect ligand interactions that promote protein stability. *Nat. Protoc.* **2,** 2212–2221 (2007).

12. Clark, W., Still, W. C., Kahn, M. & Mitra, A. Rapid chromatographic technique for preparative separations with moderate resolution. *J. Org. Chem.* **43,** 2923–2925 (1978).

13. Sankaranarayanan, A. *et al.* Naphtho[1,2-*d*]thiazol-2-ylamine (SKA-31), a new activator of KCa2 and KCa3.1 potassium channels, potentiates the endothelium-derived hyperpolarizing factor response and lowers blood pressure. *Mol. Pharmacol.* **75,** 281–95 (2009).

14. Coleman, N. *et al.* New positive Ca^{2+} -activated K^{+} channel gating modulators with selectivity for KCa3.1. *Mol. Pharmacol.* **86,** 342–357 (2014).

15. Lavis, L. D. & Raines, R. T. Bright ideas for chemical biology. *ACS Chem. Biol.* **3,** 142–155 (2008).

16. Walczak, C. *et al.* The thermal instability of 2,4 and 2,6-*N*-alkylamino-disubstituted and 2-*N*-alkylamino-substituted nitrobenzenes in weakly alkaline solution: sec-amino effect. *J. Heterocycl. Chem.* **52,** 681–687 (2015).

17. Singh, S., Syme, C. A., Singh, A. K., Devor, D. C. & Bridges, R. J. Benzimidazolone activators of chloride secretion: potential therapeutics for cystic fibrosis and chronic obstructive pulmonary disease. *J.Pharmacol.Exp.Ther.* **296,** 600–611 (2001).

18. Strøbæk, D. *et al.* Activation of human IK and SK Ca^{2+}-activated K^+ channels by NS309 (6,7-dichloro-1H-indole-2,3-dione 3-oxime). *Biochim. Biophys. Acta* **1665,** 1–5 (2004).